Université de Montréal

Application de la mécanique quantique à la résolution de problèmes de spectroscopie : développement de méthodes pour le calcul de propriétés d'états métastables

par
Jean Christophe Tremblay

Département de chimie
Faculté des arts et des sciences

Thèse présentée à la Faculté des études supérieures
en vue de l'obtention du grade de Philosophiæ Doctor (Ph.D.)
en chimie

mars, 2007

Université de Montréal
Faculté des études supérieures

Cette thèse intitulée:

Application de la mécanique quantique à la résolution de problèmes de spectroscopie : développement de méthodes pour le calcul de propriétés d'états métastables

présentée par:

Jean Christophe Tremblay

a été évaluée par un jury composé des personnes suivantes:

Matthias Ernzerhof
président-rapporteur

Tucker Carrington Jr.
directeur de recherche

Radu Ion Iftimie
membre du jury

André Bandrauk
examinateur externe

Michel Delfour
représentant du doyen de la FES

Thèse acceptée le

RÉSUMÉ

L'objet de la présente thèse est le développement de méthodes de calcul permettant d'extraire l'information sur les propriétés d'états métastables. Un premier thème abordé est l'étude de molécules dans un champ électromagnétique fort, qui entraîne une molécule de HF de son état fondamental vibrationnel jusqu'à sa photodissociation. La solution de l'équation de Schrödinger dépendante du temps permet de caractériser cette réaction. Nous proposons ici un nouvel outil basé sur l'intégration directe de l'équation en utilisant un préconditionnneur efficace.

Un deuxième problème étudié est le calcul des énergies et fonctions d'onde des états métastables du système acétylène-vinylidène, qui représente une des plus simples réactions d'isomérisation. Les états vibrationnels métastables sont situés à très haute énergie (57 kcal/mol), ce qui a rendu leur calcul impossible jusqu'ici. Nous avons développé une méthode itérative basée sur l'algorithme de Lanczos et utilisant une base contractée pour obtenir à la fois les valeurs et fonctions propres de l'hamiltonien. Nous avons adapté et parallélisé une méthode récente en plus d'implémenter un schéma de réorthogonalisation locale. Nous avons obtenu les niveaux du vinylidène de plus grande durée de vie à précision spectroscopique.

Un autre volet de la présente thèse est l'étude des états résonants du HCO. Pour les calculer, on utilise normalement un potentiel complexe (CAP) pour éliminer la partie asymptotique des fonctions d'onde. Nous avons développé une approche qui permet d'éviter l'arithmétique complexe et rend le calcul efficace. À l'aide d'une variante de l'algorithme de Lanczos, on génère une base de vecteurs propres amortis qu'on utilise pour minimiser la perturbation due au CAP. L'approche est très robuste et une généralisation des idées pour rendre la méthode accessible sous une forme "boîte noire" est présentée.

Mots clés : Dynamique moléculaire, spectroscopie théorique, méthodes de calcul, état métastable, résonance, photodissociation, isomérisation.

ABSTRACT

In the present thesis we develop numerical methods to extract information on properties of metastable states. First, we study the photodissociation of gazeous HF in a strong, chirped electromagnetic field. The evolution of the system can be characterized by the time dependant Schrödinger equation. We propose here a novel scheme for solving the equation based on the direct numerical integration in the interaction representation using a cleverly defined preconditioner.

Second, we study the energies and wavefunctions of metastable states of the acetylene-vinylidene system, which is one of the simplest isomerization reaction. These vibrational metastable states are at very high energy (57 kcal/mol) and have therefore not yet been characterized exactly. We have developed a new iterative method based on the Lanczos algorithm in combination with a particular contracted basis in order to simultaneously obtain eigenvalues and eigenvectors of the Hamiltonian. We have adapted and parallelized a recently published method as well as implemented a local reorthogonalization scheme. The longest lived vinylidene states have been obtained at what is believed to be spectroscopic accuracy.

Third, we develop a method for studying resonance states of HCO. A complex absorbing potential (CAP) is usually needed in order to remove the asymptotic part of their wavefunction. We have developed, based on recently published ideas, a method that renders the calculation of resonance states efficient while avoiding complex arithmetic. A basis of damped eigenvectors is obtained from a variant of the Lanczos algorithm and used to minimize the perturbation of the Hamiltonian by the CAP. The new scheme is very robust and a "black box" generalization of the ideas is proposed for solving general real unsymmetric eigenproblems.

Keywords: Molecular dynamics, theoretical spectroscopy, method development, metastables state, resonance, photodissociation, isomerization.

TABLE DES MATIÈRES

LISTE DES TABLEAUX

LISTE DES FIGURES

LISTE DES APPENDICES

LISTE DES SIGLES

ARPACK	Arnoldi PACKage
BLAS	Basic Linear Algebra Subprograms
CAP	Complex Absorbing Potential
CPU	Central Processing Unit
CRP	Cumulative Reaction Probability
CW ou C&W	Cullum et Willoughby
DVR	Discrete Variable Representation
FBR	Finite Basis Representation
FD	Filter Diagonalization method
IR	Interaction Representation
KLTH	Kozin, Law, Tennison et Hudson
LAPACK	Linear Algebra PACKage
MCTDH	Multi Configuration Time-Dependant Hartree
MN	Mandelshtam et Neumaier
M&T	Mandelshtam et Taylor
NIST	National Institute of Standards and Technology
OSB	Optimal Separable Basis
OSB-W	Optimal Separable Basis preconditioner with Wyatt block
PIST	Preconditioned Inexact Spectral Transform method

PODVR ou PO-DVR	Potential Optimized Discrete Variable Representation
pRK4	intégrateur de type Runge-Kutta d'ordre 4 préconditionné
RK	intégrateur de type Runge-Kutta
RK4	intégrateur de type Runge-Kutta d'ordre 4
RULE	Refined Unsymmetric Lanczos Eigensolver
SIL	Short Iterative Lanczos algorithm
sine-DVR	Sinusoidal Discrete Variable Representation
SPO	SPlit Operator method
TDSE	Time-Dependant Schrödinger Equation
TISE	Time-Independant Schrödinger Equation
ULA	Unsymmetric Lanczos Algorithm
WKS	surface de potentiel Werner, Keller et Schinke
ZBB	Zou, Bowman et Brown

NOTATION

i	nombre imaginaire, $i = \sqrt{-1}$
$\hbar$	constante de Planck
$\|\alpha\|$	valeur absolue du nombre α
$\mathbf{v}$	vecteur quelconque
$\|\|\mathbf{v}\|\|$	norme euclidienne du vecteur $\mathbf{v}$
$\hat{O}$	opérateur quelconque
$\langle\hat{O}\rangle$	valeur attendue d'un opérateur $\hat{O}$

À ma famille

REMERCIEMENTS

Il me faut en premier lieu remercier mon directeur de recherche,Tucker Carrington Jr., pour la générosité dont il a fait preuve dans son enseignement durant ces longues années que j'ai passées à ses côtés, mais aussi pour sa compréhension, sa patience et son humanité. Je ne peux passer sous silence l'apport financier de certains organismes : le Conseil de Recherches en Sciences Naturelles et Génie ainsi que le Fonds Québécois de Recherche sur la Nature et les Technologies. Je tiens à remercier vivement mes collègues, Xiaogang "Doctor" Wang, Sergei "Sweet Russian Doll" Manzhos, Étienne "Titinne" Lanthier, François "Doudoune" Goyer, Richard "Manitoban Ogre" Dawes et Jason Richard Cooper, pour les nombreuses discussions scientifiques ainsi que pour les remarques peu pertinentes sur mon végétarisme à temps partiel. Que serais-je devenu sans le support moral de ma famille élargie, Suzanne Tremblay, Louis-Carl-Tremblay, Pierre Alexandre Tremblay, Claudine Levasseur, Maxime Levasseur, Édouard Levasseur, Louis Nicolas Tremblay, Justine Valence, Rosalie Tremblay et Joël Castongay-Bélanger ? Je vous remercie tous infiniment de votre simplicité et de votre amour inconditionnel. Finalement, j'aimerais remercier plus particulièrement Hilke Bahmann, aux côtés de laquelle j'ai pu découvrir la vraie nature du bonheur.

AVANT-PROPOS

La recherche en science a souvent pour but l'application directe de nouvelles solutions à des problèmes concrets. Un autre pan de la recherche touche le développement de nouvelles idées visant l'avancement des connaissances fondamentales. Dans les deux cas, la progression s'effectue généralement par résolution de problèmes, chaque problème représentant une petite étape d'un long chemin au dessein beaucoup plus grand. Afin de faire profiter la communauté scientifique de ses plus récentes découvertes, le chercheur se doit de publier ses résultats intermédiaires. Il apparaît donc tout naturel que le cours d'un doctorat en recherche soit jalonné de quelques publications qui marquent les grandes étapes de l'évolution du projet de l'étudiant. Le contenu de ces articles scientifiques, regroupés sous un thème unificateur, représente le corps de la thèse du doctorant.

Dans cette optique, j'ai choisi de présenter ma thèse comme une collection d'articles, publiés ou en cours de publication, afin de profiter du travail de synthèse que nous avons déjà fait, mon directeur de recherche et moi-même, pour rendre nos idées accessibles aux chercheurs de notre communauté. Il va sans dire que ce travail de collaboration mérite qu'on rende à mon directeur de recherche, Tucker Carrington Jr., tout les hommages qui lui sont dus. Aussi, je joins ici les références complètes des articles qui ont été utilisés pour la rédaction de la présente thèse. Suivra une déclaration signée par mon directeur autorisant l'utilisation desdits articles.

Bonne lecture !

Articles inclus dans la thèse :

JEAN CHRISTOPHE TREMBLAY ET TUCKER CARRINGTON JR., *Using preconditioned adaptive step size Runge-Kutta methods for solving the time-dependent Schroedinger equation*, J. Chem. Phys. **121**, (2004) 11535.

JEAN CHRISTOPHE TREMBLAY ET TUCKER CARRINGTON JR., *Calculating vibrational energies and wavefunctions of vinylidene using a contracted basis with a locally re-orthogonalized coupled two-term Lanczos eigensolver*, J. Chem. Phys. **125**, (2006) 094311.

JEAN CHRISTOPHE TREMBLAY ET TUCKER CARRINGTON JR., *Computing resonance energies, widths, and wavefunctions using a Lanczos method in real arithmetic*, J. Chem. Phys. **122**, (2005) 244107.

JEAN CHRISTOPHE TREMBLAY ET TUCKER CARRINGTON JR., *A refined unsymmetric Lanczos eigensolver for computing accurate eigentriplets of a real unsymmetric matrix*, Soumis à Electronic Transactions on Numerical Analysis.

À titre de coauteur des articles identifiés ci-dessus, je suis d'accord pour que Jean Christophe Tremblay inclue ces articles dans sa thèse de doctorat qui a pour titre "Application de la mécanique quantique à la résolution de problèmes de spectroscopie : développement de méthodes pour le calcul de propriétés d'états métastables".

Tucker Carrington Jr.

Coauteur Signature Date

CHAPITRE 1

INTRODUCTION

La chimie peut être définie comme l'étude de la composition, des propriétés ainsi que des transformations de la matière. Afin de comprendre ces phénomènes à l'échelle moléculaire, il est apparu très tôt au cours du XXe siècle que la description classique des atomes était inadéquate : le concept même d'atome, qui avait déjà bien changé au courant du siècle précédent, devait être redéfini une fois de plus. L'avènement de la mécanique quantique au cours des années 1920 a marqué un tournant dans l'interprétation des phénomènes chimiques, pavant la voie à la création d'une toute nouvelle branche de la chimie : la chimie théorique, dont l'objet d'étude est la caractérisation quantitative de propriétes atomiques et moléculaires. L'intérêt de la chimie théorique semblait à l'époque bien limité à cause de la difficulté associée à la résolution même des problèmes les plus simples. On se souviendra de la fameuse affirmation de Paul Dirac [1] :

> "*The fundamental laws necessary for the mathematical treatment of a large part of physics and the whole of chemistry are thus completely known, and the difficulty lies only in the fact that application of these laws leads to equations that are too complex to be solved.*"

Évidemment, Dirac ne pouvait pas prévoir la révolution informatique qui allait balayer le monde durant les décennies à venir et qui permettrait aux chimistes et aux physiciens de s'attaquer à des problèmes de plus en plus complexes.

Puisqu'il n'existe que très peu de systèmes quantiques dont la solution peut être obtenue analytiquement, le recours aux méthodes numériques pour la compréhension des systèmes chimiques est devenu un instrument important pour le chimiste théori-cien. Au cours des cinquante dernières années, l'évolution de la capacité de calcul des ordinateurs a été pour le moins ahurissante, ce qui a permis aux chi-

mistes d'expliquer dans le cadre de la mécanique quantique des phénomènes encore inabordés. Malgré les immenses progrès réalisés, de nombreux problèmes restent intraitables encore à ce jour. Les approches approximatives souvent utilisées représentent une voie commode pour l'étude qualitative de ces problèmes complexes mais elles présentent quelques fois d'importantes lacunes quant au traitement du caractère quantique des molécules. Il apparaît donc de mise de chercher à améliorer les méthodes de calcul numériquement exact afin, d'une part, d'exploiter au maximum les ressources informatiques disponibles et, d'autre part, de fournir une référence crédible pour la validation des schémas numériques approximatifs. Le développement de nouvelles approches pour la prédiction quantitative de propriétés chimiques représente un aspect majeur du travail du théoricien.

La spectroscopie a elle aussi grandement bénéficié des avancées en sciences numériques pour le traitement de systèmes obéissant à la mécanique quantique. La spectroscopie est avant tout une science expérimentale qui étudie les interactions entre la lumière et la matière, nommément l'absorbtion, l'émission et la diffusion de photons par les atomes et molécules. Elle demeure, en ce début de XXIe siècle, une des techniques les plus prisées pour sonder les entrailles de la matière afin d'extraire le maximum d'informations sur ses propriétés. L'analyse des résultats expérimentaux se fait à l'aide de modèles basés sur la mécanique quantique et permet l'interprétation des spectres obtenus en termes moléculaires. Les spectres à très haute résolution qu'il est possible d'obtenir aujourd'hui, grâce notamment à l'amélioration des sources laser continues, des composantes optiques ainsi que des techniques de refroidissement, nécessitent un traitement particulièrement soigné. Puisque les méthodes approximatives errent souvent dans leur interprétation des résultats de ces expériences, le recours au traitement exact des équations quantiques est impératif. Il convient donc de considérer les calculs quantitatifs de la spectroscopie théorique non seulement comme essentiels à une meilleure compréhension de la chimie, mais aussi comme des outils dont la valeur prédictive permet de guider

l'expérimentateur dans ses recherches.

Dans le cadre de l'approximation de Born-Oppenheimer, on considère qu'il est possible de séparer les mouvements des électrons et des noyaux. Cette approximation permet ainsi de s'intéresser uniquement à la dynamique moléculaire en traitant implicitement le déplacement des électrons. Les mouvements nucléaires revêtent une grande importance dans l'explication des phénomènes chimiques. Par exemple, l'étude des rotations peut donner de nombreuses informations sur la géométrie de la molécule étudiée, l'analyse des vibrations permet de connaître la force des liaisons entre atomes ainsi que leur réactivité, etc. Il apparaît donc essentiel de pouvoir interpréter théoriquement les résultats de ces expériences, non seulement d'un point de vue fondamental, mais aussi d'un point de vue pratique afin de confirmer et façonner l'intuition chimique. Ainsi, l'objet de la présente thèse s'inscrit dans cette lignée : le développement de méthodes numériques plus efficaces pour permettre la résolution de problèmes de dynamique moléculaire de plus en plus complexes. Avant d'entamer la suite, revenons d'abord sur les concepts qui permettront de bien comprendre les nouvelles approches proposées.

1.1 Quelques rudiments de mécanique quantique

Dans le cadre de la mécanique classique, le mouvement des particules d'un système donné peut être décrit à chaque instant par leur position $\mathbf{x}$ et leur vitesse $\mathbf{v}$ (ou leur quantité de mouvement $\mathbf{p}$) [2, 3]. Ainsi, les trajectoires de toutes les particules peuvent être connues explicitement et l'évolution du système peut être prédite. Ce modèle, quoique bien adapté à de nombreuses situations, ne peut représenter correctement le caractère ondulatoire des molécules qui, depuis l'avènement de la mécanique quantique, apparaît comme essentiel à la compréhension des phénomènes à l'échelle atomique. Un des postulats de cette nouvelle mécanique stipule que les fonctions classiques de position et de quantité de mouvement doivent être

remplacées par des opérateurs afin de tenir compte du caractère quantique des particules [4–6]. La conception déterministe de la position doit aussi être abandonnée. Quoiqu'il soit possible d'en mesurer la valeur exacte à un instant donné, il est impossible de prédire *a priori* quelle sera la position d'un corpuscule quantique ainsi que la trajectoire qu'il suivra. La probabilité de trouver une particule à l'intérieur d'un intervalle donné est ainsi décrite par une distribution qui dépend de la nature du système et des forces en présence. Comment peut-on, de cette façon, représenter un système quantique ? Par l'introduction d'un objet, appelé "fonction d'onde", qui permet de décrire l'état du système et de définir *toutes* les informations qu'on est susceptible d'en extraire. Nous dénoterons la fonction d'onde moléculaire totale $\chi_{n\alpha}(\mathbf{R}, \mathbf{r}, t)$, où $\mathbf{R}$ est un vecteur décrivant la position des noyaux, $\mathbf{r}$ est un vecteur décrivant la position de tous les électrons et t est le temps. Selon l'interprétation de Born, la distribution de probabilité est donnée par le carré de la fonction d'onde, $|\chi_{n\alpha}(\mathbf{R}, \mathbf{r}, t)|^2$. Conformément à cette interprétation probabiliste, on définit la valeur attendue d'un opérateur quelconque $\hat{O}$ pour un état donné comme une moyenne pondérée de l'opérateur sur tout l'espace, c'est-à-dire

$$\langle \hat{O} \rangle_{n\alpha}(t) = \int \chi^*_{n\alpha}(\mathbf{R}, \mathbf{r}, t) \hat{O} \chi_{n\alpha}(\mathbf{R}, \mathbf{r}, t) d\mathbf{R} d\mathbf{r} \quad , \tag{1.1}$$

où $\langle \hat{O} \rangle_{n\alpha}(t)$ est la valeur attendue à un temps t donné. L'approximation de Born-Oppenheimer permet de simplifier significativement le problème en permettant une séparation du traitement des mouvements nucléaires et électroniques [5–9]. Ainsi, on écrit

$$\chi_{n\alpha}(\mathbf{R}, \mathbf{r}, t) = \Psi_n(\mathbf{R}, t) \phi_\alpha(\mathbf{r}, t; \mathbf{R}) \quad , \tag{1.2}$$

où $\Psi_n(\mathbf{R}, t)$ est la n^{ieme} fonction d'onde nucléaire et $\phi_\alpha(\mathbf{r}, t; \mathbf{R})$ est la α^{ieme} fonction d'onde électronique qui dépend paramétriquement de $\mathbf{R}$. Pour l'étude de la dynamique moléculaire, seule la partie nucléaire reste d'intérêt et la partie électronique est considéré implicitement dans l'énergie potentielle du système.

Il existe une formulation alternative des équations classiques du mouvement, connue sous le nom de mécanique hamiltonienne, qui définit une fonction de l'énergie appelée "hamiltonien" (H) [3]. Il est possible de trouver les équations quantiques analogues aux équations hamiltoniennes du mouvement par l'introduction d'un opérateur quantique *hamiltonien*

$$\hat{H}(\mathbf{R}, t) = \hat{T}(\mathbf{R}) + \hat{V}(\mathbf{R}, t) \quad , \tag{1.3}$$

où $\hat{T}(\mathbf{R})$ est l'énergie cinétique du système étudié et $\hat{V}(\mathbf{R}, t)$ est son énergie potentielle, incluant toute contribution électronique [4–9]. L'opérateur quantique hamiltonien, ci-après simplement dénommé "hamiltonien", représente à la fois la molécule étudiée ainsi que son couplage à l'environnement. Par exemple, l'hamiltonien d'une molécule diatomique excitée par un champ laser comportera les termes d'énergie cinétique de vibration, de rotation et de translation de la molécule, l'énergie potentielle interne décrivant les interactions entre les atomes ainsi que, suivant une approximation semi-classique, l'énergie potentielle associée à la fluctuation du champ électromagnétique dans le temps. De façon générale, l'évolution de l'état d'une molécule décrite par un hamiltonien $\hat{H}(\mathbf{R}, t)$ sera régie par l'équation de Schrödinger dépendante du temps (TDSE),

$$\hat{H}(\mathbf{R}, t)\Psi_n(\mathbf{R}, t) = i\hbar\frac{\partial}{\partial t}\Psi_n(\mathbf{R}, t) \quad , \tag{1.4}$$

où $\hbar$ est la constante de Planck. Il arrive fréquemment que l'hamiltonien du système est lui-même indépendant du temps. En l'occurence, le déplacement, la déformation et les rotations de molécules isolées à l'état gazeux sont décrits par un hamiltonien indépendant du temps [7–9]. Dans un tel cas, il est possible d'effectuer la factorisation suivante

$$\Psi_n(\mathbf{R}, t) = \Theta(t)\psi_n(\mathbf{R}) \quad , \tag{1.5}$$

et de résoudre séparément, pour la partie spatiale et la partie temporelle, l'équation de Schrödinger [4–6]. La résolution de l'équation temporelle étant triviale et n'apportant aucun éclairage sur la dynamique des noyaux, on se concentre donc sur la partie spatiale de l'équation de Schrödinger obtenue par séparation des variables et par la simplification de TDSE (Eq. (1.4)) de sorte que

$$\hat{H}(\mathbf{R})\psi_n(\mathbf{R}) = E_n\psi_n(\mathbf{R}) \quad , \tag{1.6}$$

où E_n est l'énergie associée au n^{ieme} état du système. L'équation de Schrödinger indépendante du temps (TISE, Eq. (1.6)) est une équation centrale en dynamique moléculaire puisque sa résolution permet d'obtenir, entre autres choses, les énergies des états vibrationnels et rotationnels, les intensités des transitions spectroscopiques entre ceux-ci, la valeur attendue d'une foule d'observables, la probabilité réactionnelle à énergie donnée, etc [5–9]. Tout chimiste pourra se convaincre facilement de l'importance de tels calculs.

1.2 La méthode variationnelle linéaire

Comme nous l'avons dit précédemment, il n'existe que très peu de systèmes possédant des solutions analytiques et ces dernières sont généralement extrêmement difficiles à trouver. Très souvent, il est impossible de résoudre les équations 1.4 et 1.6 analytiquement et il faut avoir recours à des méthodes numériques pour extraire la fonction d'onde et les quantités désirées. Les approches les plus populaires en spectroscopie théorique sont certainement la méthode des perturbations et la méthode variationnelle linéaire [7–13]. Les deux voies possèdent certes des avantages mais la flexibilité de la seconde méthode la rend particulièrement attrayante. Nous ne nous attarderons donc que sur cette dernière.

Puisque la solution de TDSE ou TISE est inconnue, on remplace la fonction

d'onde par une combinaison linéaire de fonctions connues

$$\Psi_n(\mathbf{R}, t) = \sum_{j=1}^{N} C_j^n(t)\phi_j(\mathbf{R}) \quad , \tag{1.7}$$

advenant qu'on veuille résoudre TDSE, ou encore

$$\psi_n(\mathbf{R}) = \sum_{j=1}^{N} C_j^n \phi_j(\mathbf{R}) \quad , \tag{1.8}$$

dans le cas de TISE. L'ensemble des fonctions $\phi_j(\mathbf{R})$ est appelé "base" et ces fonctions de base sont connues *a priori*. On doit ensuite chercher les coefficients $C_j^n(t)$ (ou C_j^n, respectivement) permettant de représenter correctement les fonctions d'onde décrivant l'état de la molécule dans cette base. Les expansions 1.7 et 1.8 définissent exactement les fonctions d'onde dans la limite $N \to \infty$. En pratique, la valeur de N doit être grande même pour les problèmes de taille modeste et elle augmente typiquement de façon exponentielle avec la taille du système étudié. Pour cette raison, un effort particulier est fait par plusieurs groupes de recherche pour développer des fonctions plus efficaces permettant l'utilisation de bases plus compactes [14–21]. Une base dépendante du temps peut permettre, dans certains cas, de réduire la taille de la base nécessaire à la résolution de TDSE mais cela augmente significativement la complexité du calcul [22–27]. On s'en tiendra donc aux bases indépendantes du temps.

Comment doit-on choisir les fonctions de base pour minimiser simultanément la taille de la base et la complexité associée à leur calcul ? Afin de répondre à cette question, on doit connaître la forme exacte des équations à résoudre. En substituant les équations 1.7 et 1.8 dans TDSE (Eq. (1.4)) et TISE (Eq. (1.6)) respectivement,

on obtient

$$\hat{H}(\mathbf{R},t)\sum_{j=1}^{N}C_j^n(t)\phi_j(\mathbf{R}) = i\hbar\frac{\partial}{\partial t}\sum_{j=1}^{N}C_j^n(t)\phi_j(\mathbf{R}) \quad , \tag{1.9}$$

$$\hat{H}(\mathbf{R})\sum_{j=1}^{N}C_j^n\phi_j(\mathbf{R}) = E_n\sum_{j=1}^{N}C_j^n\phi_j(\mathbf{R}) \quad . \tag{1.10}$$

En multipliant à gauche les équations 1.9 et 1.10 par $\phi_i^*(\mathbf{R})$, une fonction quelconque de la base, et en intégrant sur tout l'espace, on obtient

$$\sum_{j=1}^{N}\left(\int\phi_i^*(\mathbf{R})\hat{H}(\mathbf{R},t)\phi_j(\mathbf{R})d\mathbf{R}\right)C_j^n(t) = i\hbar\frac{\partial}{\partial t}\sum_{j=1}^{N}C_j^n(t)\left(\int\phi_i^*(\mathbf{R})\phi_j(\mathbf{R})d\mathbf{R}\right) \quad ; \tag{1.11}$$

$$\sum_{j=1}^{N}C_j^n\left(\int\phi_i^*(\mathbf{R})\hat{H}(\mathbf{R})\phi_j(\mathbf{R})d\mathbf{R}\right) = E_n\sum_{j=1}^{N}C_j^n\left(\int\phi_i^*(\mathbf{R})\phi_j(\mathbf{R})d\mathbf{R}\right) \quad . \tag{1.12}$$

On peut choisir les fonctions de base de telle sorte qu'elles soient orthonormales, c'est-à-dire

$$\int\phi_i^*(\mathbf{R})\phi_j(\mathbf{R})d\mathbf{R} = \delta_{ij} \quad , \tag{1.13}$$

où δ_{ij} est connue sous le nom de "fonction delta de Kronecker", qui est égale à 1 si $i = j$ et 0 autrement. L'orthonormalité des fonctions de base permet de simplifier les équations 1.11 et 1.12 de la façon suivante

$$\sum_{j=1}^{N}\langle\phi_i(\mathbf{R})|\hat{H}(\mathbf{R},t)|\phi_j(\mathbf{R})\rangle C_j^n(t) = i\hbar\frac{\partial}{\partial t}C_i^n(t) \quad , \tag{1.14}$$

$$\sum_{j=1}^{N}C_j^n\langle\phi_i(\mathbf{R})|\hat{H}(\mathbf{R})|\phi_j(\mathbf{R})\rangle = E_nC_i^n \quad . \tag{1.15}$$

La notation de Dirac [4–6] a été utilisée pour représenter les intégrales sur l'espace de façon plus compacte en écrivant $\int\phi_i^*(\mathbf{R})\hat{O}\phi_j(\mathbf{R})d\mathbf{R} = \langle\phi_i(\mathbf{R})|\hat{O}|\phi_j(\mathbf{R})\rangle$, où $\hat{O}$ est un opérateur quelconque qui peut dépendre de la position $\mathbf{R}$ ou de la quantité de mouvement $\mathbf{p}$. On obtient ainsi un ensemble d'équations couplées qu'on peut

représenter plus efficacement sous forme matricielle

$$\mathbf{H}(t)\mathbf{C}_n(t) = i\hbar\frac{\partial}{\partial t}\mathbf{C}_n(t) \quad , \tag{1.16}$$

$$\mathbf{H}\mathbf{C}_n = E_n\mathbf{C}_n \quad . \tag{1.17}$$

Les éléments matriciels sont donnés par l'évaluation des intégrales des équations 1.14 et 1.15 et les coefficients $C_i^n(t)$ et C_i^n, contenus dans les vecteurs $\mathbf{C}_n(t)$ et $\mathbf{C}_n$, sont obtenus par la résolution des équations 1.16 et 1.17, respectivement.

Ayant établi les équations qu'on doit résoudre, on se trouve maintenant confronté au choix de la base. Rappelons d'abord les opérations qui devront être faites. En premier lieu, il est impératif de concevoir une base dont la taille est minimale afin de pouvoir traîter des problèmes de plus en plus complexes. De plus, il serait appréciable de savoir représenter simplement les opérateurs d'énergie cinétique et d'énergie potentielle de l'hamiltonien. Finalement, on souhaite pouvoir évaluer les intégrales efficacement. Le premier point dépend fortement du problème étudié et différentes solutions seront proposées dans les chapitres à venir. Afin d'illustrer une stratégie générale servant de fondement au développement de bases efficaces pour la représentation des opérateurs quantiques, admettons un hamiltonien vibrationnel indépendant du temps pour un problème modèle à 2 dimensions

$$\hat{H}(r_1, r_2) = \hat{T}_1(p_1) + \hat{T}_2(p_2) + \hat{V}(r_1, r_2) \quad , \tag{1.18}$$

où $\hat{T}_i(p_i)$ est l'opérateur d'énergie cinétique associé à la particule i et p_i est la quantité de mouvement de la particule i. Un choix judicieux serait de définir des fonctions de base sous forme de produit de fonctions unidimensionnelles orthogonales $\rho_{j_1}(r_1)$ et $\theta_{j_2}(r_2)$

$$\phi_{j_1 j_2}(r_1, r_2) = \rho_{j_1}(r_1)\theta_{j_2}(r_2) \quad . \tag{1.19}$$

Dans une telle base, les éléments matriciels de l'hamiltonien sont donnés par

$$\begin{aligned}\mathbf{H}_{i_1 j_1, i_2 j_2} =& \langle \rho_{i_1}(r_1)|\hat{T}_1(p_1)|\rho_{j_1}(r_1)\rangle \delta_{i_2 j_2} + \langle \rho_{i_2}(r_2)|\hat{T}_2(p_2)|\rho_{j_2}(r_2)\rangle \delta_{i_1 j_1} \\ &+ \langle \rho_{i_1}(r_1)\theta_{i_2}(r_2)|\hat{V}(r_1, r_2)|\rho_{j_1}(r_1)\theta_{j_2}(r_2)\rangle \quad .\end{aligned} \tag{1.20}$$

Les fonctions unidimensionnelles sont souvent des polynômes de différents types, p. ex. les polynômes associés de Legendre, les polynômes de Jacobi, les polynômes de Tchebychev du premier et deuxième type. Ces polynômes obéissent à un ensemble de relations de récurrence qui permettent souvent l'évaluation analytique des éléments matriciels de l'opérateur d'énergie cinétique [28]. Les éléments matriciels du potentiel doivent toutefois être évalués numériquement par quadrature, ce qui peut devenir très coûteux.

Il est aussi possible de définir un autre type de fonctions de base, dénommées "Discrete Variable Representation" (DVR) [29–37]. Ces fonctions sont choisies comme combinaisons linéaires de fonctions de base primitives unidimensionnelles, p. ex. un produit de polynômes orthogonaux et de fonctions de poids, qu'on appellera "Finite Basis Representation" (FBR). Les fonctions DVR sont des approximations aux fonctions propres de l'opérateur de position, dont les vraies solutions sont des fonctions delta de Dirac. La matrice d'énergie cinétique présente des singularités importantes dans cette base car les fonctions delta sont discontinues. La DVR est quant à elle constituée de fonctions continues et dérivables de sorte que la matrice représentant l'énergie cinétique est aussi bien définie dans la DVR que dans la FBR. Les fonctions DVR sont distribuées sur une grille. Elles ont une amplitude maximale à un point de la grille et sont nulles à tous les autres points, où sont centrées les autres fonctions de la base. La grille est définie par les points de la quadrature de Gauss associée aux fonctions primitives FBR, c'est-à-dire qu'elle représente le meilleur ensemble fini de points pour l'évaluation des intégrales sur ces fonctions de base. L'inconvénient majeur associé à la DVR est que la matrice

d'énergie cinétique est plus dense dans cette base. Puisqu'il existe une relation entre les fonctions FBR et DVR, il est possible d'évaluer efficacement les éléments de cette matrice en suivant une procédure toute simple. On obtient d'abord les représentations matricielles des opérateurs d'énergie cinétique et de position dans la base FBR (respectivement $\mathbf{T}_i^{FBR}$ et $\mathbf{R}_i^{FBR}$). Les intégrales définissant les éléments de la matrice de position sont aussi connues analytiquement dans le cas des polynômes orthogonaux. On calcule ensuite les valeurs et vecteurs propres de la matrice de position dans cette base pour obtenir une matrice de transformation unitaire $\mathbf{Z}_i$ qui diagonalise la coordonnée

$$\mathbf{R}_i^{FBR}\mathbf{Z}_i = \mathbf{Z}_i\mathbf{R}_i^{DVR} \quad . \tag{1.21}$$

$\mathbf{R}_i^{DVR}$ est une matrice diagonale dont les valeurs non nulles sont les points de quadrature. La matrice unitaire $\mathbf{Z}_i$ permet de transformer la matrice d'énergie cinétique de la FBR à la DVR

$$\mathbf{T}_i^{DVR} = \mathbf{Z}_i^{\mathbf{T}}\mathbf{T}_i^{FBR}\mathbf{Z}_i \quad . \tag{1.22}$$

On doit aussi représenter le potentiel dans la base DVR, ce qui est nécessaire car toutes les parties de l'opérateur hamiltonien doivent être définies dans une seule et même base afin que les valeurs propres qu'on en extrait possèdent une signification physique. On peut écrire toute fonction de la coordonnée r_i, comme par exemple un potentiel unidimensionnel $\hat{V}_i(r_i)$, à l'aide de l'équation

$$\hat{V}_i(r_i) = a_0 + a_1 r_i + a_2 r_i^2 + \ldots \ , \tag{1.23}$$

où $\{a_0, a_1, a_2, \ldots\}$ sont les coefficients du développement en série de puissances de

la fonction. On peut représenter ce développement dans la base FBR

$$\mathbf{V}_i^{FBR} = a_0\mathbf{I} + a_1\mathbf{R}_i^{FBR} + a_2\mathbf{R}_i^{FBR}\mathbf{R}_i^{FBR} + \dots \tag{1.24}$$

Il est important de noter que les différentes puissances de r_i sont toutes représentées comme produits de la matrice $\mathbf{R}_i^{FBR}$, pour laquelle les éléments sont connus analytiquement. La qualité de cette approximation diminue pour les puissances plus élevées. En transformant $\mathbf{V}_i^{FBR}$ dans la base DVR, on obtient

$$\begin{aligned}\mathbf{V}_i^{DVR} &= \mathbf{Z}_i^{\mathbf{T}}\mathbf{V}_i^{FBR}\mathbf{Z}_i \\ &= a_0\mathbf{I} + a_1\mathbf{R}_i^{DVR} + a_2\mathbf{R}_i^{DVR}\mathbf{R}_i^{DVR} + \dots\end{aligned} \tag{1.25}$$

Puisque la matrice $\mathbf{R}_i^{DVR}$ est diagonale et que la fonction $\hat{V}_i(r_i)$ est quelconque, il s'ensuit que la représentation de *toute fonction* de la coordonnée est diagonale dans la DVR. On peut ainsi complètement éviter l'évaluation du potentiel dans la FBR. Les éléments matriciels d'un potentiel 2D dans une base formée d'un produit tensoriel de fonctions DVR unidimensionnelles $\phi_\alpha(r_1)$ et $\phi_\beta(r_2)$ sont simplement donnés par

$$\langle\phi_\alpha(r_1)\phi_\beta(r_2)|\hat{V}(r_1,r_2)|\phi_{\alpha'}(r_1)\phi_{\beta'}(r_2)\rangle = V(r_1^\alpha, r_2^\beta)\delta_{\alpha\alpha',\beta\beta'} \quad , \tag{1.26}$$

c'est-à-dire que seuls les éléments diagonaux du potentiel sont non-nuls et leur valeur est donnée par l'évaluation du potentiel au point $\{r_1^\alpha, r_2^\beta\}$. Ceci simplifie grandement l'évaluation du potentiel, si compliqué soit-il.

Cette DVR étant une base orthogonale, on peut maintenant écrire la représentation matricielle de l'hamiltonien complet

$$\begin{aligned}\mathbf{H}_{\alpha\beta,\alpha'\beta'} =& \langle\phi_\alpha(r_1)|\hat{T}_1(p_1)|\phi_{\alpha'}(r_1)\rangle\delta_{\beta\beta'} + \langle\phi_\beta(r_2)|\hat{T}_2(p_2)|\phi_{\beta'}(r_2)\rangle\delta_{\alpha\alpha'} \\ &+ V(r_1^\alpha, r_2^\beta)\delta_{\alpha\alpha',\beta\beta'} \quad .\end{aligned} \tag{1.27}$$

Forts de cette représentation compacte et efficace, il nous reste maintenant à résoudre le problème d'algèbre linéaire afin d'en extraire les valeurs propres et vecteurs propres, représentant respectivement les énergies et les fonctions d'onde du système dans le cas de l'opérateur hamiltonien présenté ci-haut. Notons que l'équation 1.27 est aussi valide pour décrire les états continus, dont la fonction d'onde se développe jusqu'à l'infini. Le problème majeur est que la représentation d'une fonction d'onde infinie requiert un nombre *infini* de fonctions DVR. Plusieurs astuces ont été développées pour contourner ce problème [38–41]. Leur discussion sera reportée au chapitre 4.

1.3 Survol des méthodes numériques pour l'extraction des valeurs propres de représentations matricielles d'opérateurs quantiques indépendants du temps

Nous nous concentrerons dans cette section sur la solution de l'équation de Schrödinger indépendante du temps. La façon la plus simple de résoudre l'équation 1.17 est évidemment d'évaluer les intégrales comme définies dans la base désirée, de stocker les éléments dans la mémoire de l'ordinateur et d'utiliser une routine de diagonalisation directe telle la combinaison Householder/QR. Il existe plusieurs implémentations très efficaces de ces méthodes directes dans les librairies mathématiques de calcul [42–44]. La robustesse de ces méthodes numériques en fait encore à ce jour la référence pour l'extraction des valeurs propres et vecteurs propres de matrices de taille modérée. Toutefois, deux propriétés des méthodes directes en limitent l'usage pour les problèmes de plus grande taille. La première concerne le stockage de la matrice [44–46]. Choisissons d'abord une base sous forme de produit comme décrite dans l'équation 1.19. Admettons que n_b fonctions de bases orthogonales unidimensionnelles soient suffisantes pour représenter la distribution spatiale selon chaque coordonnée. Pour un système possédant f degrés de liberté, la taille totale de la

base sera n_b^f et le nombre d'éléments matriciels à stocker sera donc de n_b^{2f}. Concrètement, on peut estimer modestement que $n_b = 10$. Par conséquent, une matrice représentant l'hamiltonien vibrationnel d'une molécule triatomique sera composée de 10^6 éléments et nécessitera environ 8 mégaoctets de mémoire vive pour son stockage. Suivant les mêmes paramètres, une molécule tétraatomique possédant 6 degrés de libertés de vibration serait représentée par une matrice d'ordre $n_b = 10^6$ nécéssitant environ 7450 gigaoctets de stockage en mémoire vive. En comparant avec la mémoire typiquement disponible sur un ordinateur de bureau (environ 1 gigaoctet), on comprend l'étendue du problème.

La seconde limite majeure des méthodes directes est reliée au temps de calcul qui, pour ces méthodes, croît à une vitesse proportionnelle au *cube* de la taille de la base $N = n_b^f$ (pour un système à f dimensions) [44–46]. Ainsi, admettant que la diagonalisation de la matrice de l'hamiltonien vibrationnel d'une molécule triatomique prend 1 seconde, la résolution du même problème pour une molécule tétraatomique serait $\left(\frac{10^6}{10^3}\right)^3 = 10^9$ fois plus longue, soit de 10^9 secondes ou 11574 jours. Il va sans dire que cette approche ne peut être viable sans modification et plusieurs groupes de recherche ont poursuivi dans cette voie, tentant de remédier aux limites des méthodes directes par le développement de fonctions de base extrêmement compactes mais aussi infiniment complexes [14–21].

Une autre façon très efficace de contourner les problèmes susmentionnés est d'avoir recours aux méthodes itératives, telles l'algorithme de Lanczos, l'algorithme de Jacobi-Davidson, les iterations de sous-espace, etc [44–52]. Tous ces algorithmes sont basés sur l'idée centrale de projection de la matrice de l'opérateur sur un (ou des) vecteur(s), permettant ainsi d'éviter le stockage de la matrice. Ces méthodes exploitent le fait que seule une partie du spectre – c'est-à-dire l'ensemble des valeurs propres de l'opérateur – possède une signification physique et est donc désirable. En effet, il est bien connu que, suivant le principe variationnel, les solutions de TISE possédant les énergies les plus basses convergent les premières vers les valeurs

exactes lorsqu'on augmente la taille de la base utilisée dans l'expansion 1.7 (ou 1.8, selon le cas). Ainsi, seules les énergies les plus basses qu'on peut extraire de la matrice de l'hamiltonien sont physiquement intéressantes.

Outre la convergence variationnelle qui dépend de la taille de la base, il existe un autre phénomène de convergence associé à la méthode utilisée pour la résolution de l'équation 1.17. Dans le cas des méthodes directes, toutes les valeurs propres convergent simultanément après un nombre donné d'opérations. Ceci contraste avec le comportement des méthodes itératives, pour lesquelles la convergence est graduelle au fil des opérations, qui favorisent l'émergence précoce de certaines solutions au détriment des autres. Le figure 1.1 illustre schématiquement la différence entre ces deux comportements. La nature exacte de la convergence sélective varie subtile-

FIG. 1.1 – Représentation schématique de la convergence d'une valeur propre. Le trait plein représente le comportement associé à une méthode directe et le trait pointillé représente le comportement d'une méthode itérative typique.

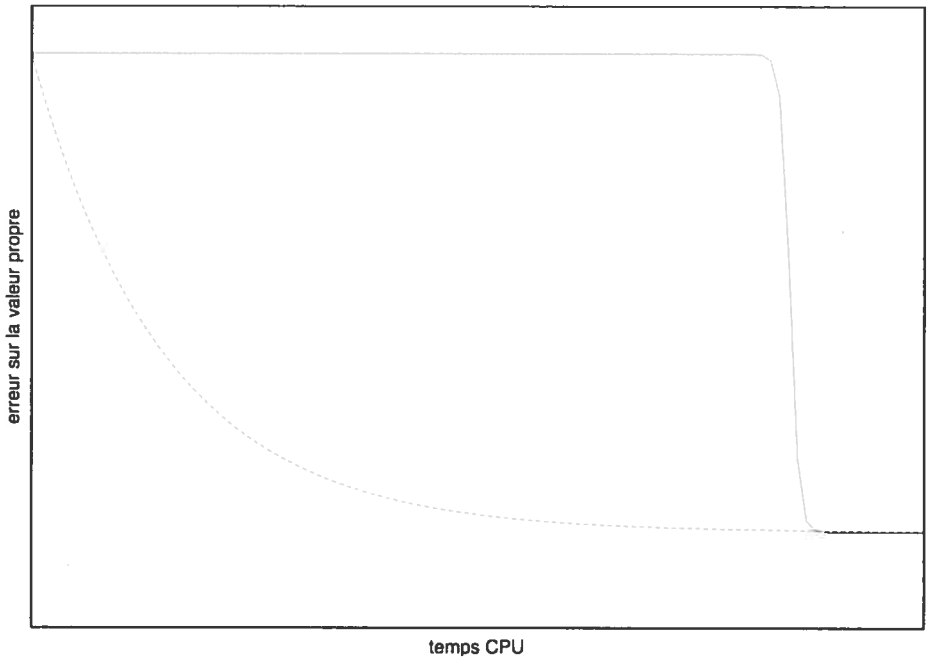

ment selon la méthode itérative utilisée et nous traiterons seulement des propriétés de l'algorithme de Lanczos, qui est au coeur de trois des méthodes développées

dans la présente thèse.

Comment les méthodes itérative font-elles pour extraire certaines valeurs propres sans stocker la matrice complète ? Les projections se font par le biais d'une opération centrale commune à toutes ces méthodes, le produit matrice-vecteur, pour laquelle il est essentiel de pouvoir exploiter la structure de la matrice. Prenons, encore une fois, notre hamiltonien vibrationnel modèle à 2 dimensions (Eq. (1.18)) décrit dans une base sous forme de produit (Eq. (1.19)) et définissons un vecteur $\mathbf{v}$ possédant deux indices $\{\alpha'\beta'\}$, un pour chaque coordonnée. Les éléments de la matrice dans la base DVR sont décrits par l'équation 1.27. On ne stocke en mémoire que les morceaux nécessaires pour pouvoir appliquer les éléments non-nuls de la matrice sur un vecteur. Ainsi, on peut multiplier efficacement la matrice $\mathbf{H}$ par le vecteur $\mathbf{v}$ en *simulant* l'utilisation d'une matrice pleine. On obtient chaque composante $\{\alpha\beta\}$ du nouveau vecteur $\mathbf{u}$ à l'aide de

$$\begin{aligned}\mathbf{u}_{\alpha\beta} = &\left(\sum_{\alpha'=1}^{n_1}\langle\phi_\alpha(r_1)|\hat{T}_1(p_1)|\phi_{\alpha'}(r_1)\rangle\mathbf{v}_{\alpha'\beta}\right)\delta_{\beta\beta'}+\\ &\left(\sum_{\beta'=1}^{n_2}\langle\phi_\beta(r_2)|\hat{T}_2(p_2)|\phi_{\beta'}(r_2)\rangle\mathbf{v}_{\alpha\beta'}\right)\delta_{\alpha\alpha'}+\\ &\left(V(r_1^\alpha, r_2^\beta)\mathbf{v}_{\alpha\beta}\right)\delta_{\alpha\alpha',\beta\beta'} \quad ,\end{aligned} \tag{1.28}$$

où n_1 et n_2 sont les nombres de fonctions de base pour décrire les coordonnées r_1 et r_2, respectivement. On voit clairement que, outre les 2 vecteurs, il n'est nécessaire de stocker que les éléments de petites matrices représentant les opérateurs unidimensionnels d'énergie cinétique en plus d'un vecteur supplémentaire pour le potentiel, ce qui donne un total de $(n_1^2+n_2^2+n_1n_2)$ éléments dans le cas présent. Le coût du produit matrice-vecteur peut ainsi être ramené à $n_1n_2(n_1+n_2+1)$ opérations en point flottant (flops) et se compare avantageusement à celui d'un produit matrice-vecteur direct, dont le coût s'élèverait à $(n_1n_2)^2$ flops. Non seulement cette façon de procéder permet-elle de sauver une grande quantité de mémoire mais elle

est aussi très efficace sur le plan du nombre de flops et donc du temps de calcul. De plus, ces économies augmentent exponentiellement avec le nombre de degrés de liberté du systéme étudié.

L'algorithme de Lanczos le plus général se sert de cette opération comme outil pour construire deux espaces de Krylov, c'est-à-dire des ensembles de vecteurs correspondant à diverses puissances de la matrice projetée sur deux vecteurs initiaux aléatoires

$$\begin{aligned} K_1^{(m)}\{\mathbf{H}, \mathbf{v}_1\} &= \{\mathbf{v}_1, \mathbf{H}\mathbf{v}_1, \cdots, \mathbf{H}^{\mathbf{m-1}}\mathbf{v}_1\} \ ; \\ K_2^{(m)}\{\mathbf{H}^{\mathbf{T}}, \mathbf{w}_1\} &= \{\mathbf{w}_1, \mathbf{H}^{\mathbf{T}}\mathbf{w}_1, \cdots, (\mathbf{H}^{\mathbf{T}})^{\mathbf{m-1}}\mathbf{w}_1\} \ , \end{aligned} \tag{1.29}$$

où $\mathbf{T}$ représente la transposée de la matrice et m est la taille de l'espace de Krylov [45, 46, 46, 49, 51]. Plus particulièrement, on génère deux espaces qui sont *biorthogonaux*, c'est-à-dire que les vecteurs obéissent à la relation

$$\mathbf{W}_m^{\mathbf{T}}\mathbf{V}_m = \mathbf{\Delta}_m \ , \tag{1.30}$$

où $\mathbf{V}_m$ et $\mathbf{W}_m$ sont des matrices dont les colonnes sont les vecteurs de Lanczos associés aux espaces de Krylov, un droit $K_1^{(m)}\{\mathbf{H}, \mathbf{v}_1\}$ et un gauche $K_2^{(m)}\{\mathbf{H}^{\mathbf{T}}, \mathbf{w}_1\}$, et $\mathbf{\Delta}_m = diag(\delta_1, \delta_2, \cdots, \delta_m)$ est la matrice diagonale des recouvrements entre les vecteurs gauches et droits. Les vecteurs gauches et droits sont générés par récurrence en respectant la condition de biorthogonalité. On peut ainsi obtenir, à chaque itération, de nouveaux vecteurs $\mathbf{v}_{k+1}$ et $\mathbf{w}_{k+1}$ à partir des des deux vecteurs précédents

$$\beta_{k+1}\mathbf{v}_{k+1} = \mathbf{r}_{k+1} = \mathbf{H}\mathbf{v}_k - \alpha_k\mathbf{v}_k - \gamma_k\mathbf{v}_{k-1} \ , \tag{1.31}$$

$$\xi_{k+1}\mathbf{w}_{k+1} = \mathbf{s}_{k+1} = \mathbf{H}^{\mathbf{T}}\mathbf{w}_k - \alpha_k\mathbf{w}_k - \frac{\beta_k\delta_k}{\delta_{k-1}}\mathbf{w}_{k-1} \ , \tag{1.32}$$

où $\gamma_k = \frac{\xi_k\delta_k}{\delta_{k-1}}$, $\delta_k = \mathbf{w}_k^{\mathbf{T}}\mathbf{v}_k$, $\alpha_k = \mathbf{w}_k^{\mathbf{T}}\mathbf{H}\mathbf{v}_k/\delta_k$, et β_k and ξ_k sont respectivement les facteurs de normalisation des vecteurs $\mathbf{r}_k$ et $\mathbf{s}_k$. L'algorithme est initialisé en

choisissant deux vecteurs aléatoires $\mathbf{v}_1$ et $\mathbf{w}_1$ et en posant $\gamma_1 = \beta_1 = 0$. Il existe une certaine flexibilité pour le choix des facteurs de normalisation, nous optons pour

$$\begin{aligned} \beta_k &= \sqrt{|\mathbf{s}_k^{\mathbf{T}} \mathbf{r}_k|} \quad , \\ \xi_k &= \frac{\mathbf{s}_k^{\mathbf{T}} \mathbf{r}_k}{\beta_k} \quad , \end{aligned} \tag{1.33}$$

ce qui permet de simplifier les équations puisque de cette façon $\delta_k = \mathbf{w}_k^{\mathbf{T}} \mathbf{v}_k = 1$. Ainsi, α, β et γ sont les éléments d'une matrice tridiagonale $\mathbf{T}_m$ qui représente la projection de la matrice $\mathbf{H}$ dans l'espace des vecteurs de Lanczos

$$\mathbf{T}_m = \mathbf{W}_m^{\mathbf{T}} \mathbf{H} \mathbf{V}_m = \begin{pmatrix} \alpha_1 & \gamma_2 & & & \\ \beta_2 & \alpha_2 & \gamma_3 & & \\ & \beta_3 & \alpha_3 & \ddots & \\ & & \ddots & \ddots & \gamma_m \\ & & & \beta_m & \alpha_m \end{pmatrix} \quad . \tag{1.34}$$

Il faut noter que la matrice $\mathbf{T}_m$ est généralement plusieurs ordres de grandeur plus petite que la matrice originale $\mathbf{H}$ [45, 46, 46, 49, 51]. De plus, il est très économique de stocker uniquement les éléments de $\mathbf{T}_m$ qui sont différents de 0 et plusieurs algorithmes existant permettent de trouver efficacement les valeurs propres d'une matrice tridiagonale. Quel est le lien entre les valeurs propres de $\mathbf{T}_m$ et celles de la matrice originale $\mathbf{H}$? Puisqu'il s'agit d'une méthode de projection, on trouvera dans l'ensemble des valeurs propres de $\mathbf{T}_m$ certaines des valeurs propres de la matrice originale (c.f. figure 1.2). Dans le cas de la méthode de Lanczos, les valeurs propres situées sur le pourtour convexe du spectre dans le plan complexe sont les premières à converger. L'augmentation de la densité du spectre et/ou du domaine spectral a pour effet de ralentir la convergence des valeurs propres. Puisqu'un opérateur hermitique, p. ex. l'hamiltonien, possède des valeurs propres réelles, les plus grandes et les plus petites de celles-ci seront bien entendu les premières à converger. C'est en

FIG. 1.2 – Représentation schématique des ensembles de valeurs propres pour une méthode de projection

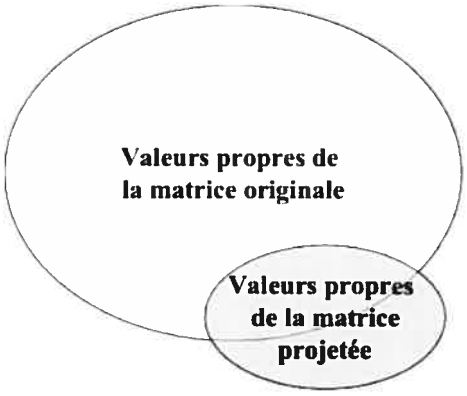

partie à cause de cette propriété fascinante que l'algorithme est si populaire pour l'extraction de certaines valeurs propres d'opérateurs quantiques. Il est à noter que le spectre de la matrice projetée contient généralement plusieurs copies des valeurs propres de la matrice originale ainsi qu'un ensemble de valeurs propres non-physiques. Ces artefacts de l'algorithme sont dus à la perte d'orthogonalité des vecteurs de Lanczos et ralentissent la convergence des autres valeurs propres de la matrice originale.

Advenant que l'opérateur étudié soit hermitique, l'algorithme de Lanczos permet une simplification qui le rend encore plus attrayant. D'abord, les vecteurs de départ sont choisis réels et égaux l'un à l'autre, $\mathbf{v}_1 = \mathbf{w}_1$. Ainsi, le second espace de Krylov $K_2^{(m)}\{\mathbf{H^T}, \mathbf{w}_1\}$ est strictement égal au premier et on peut simplement le considérer implicitement. Les équations 1.31 se réduisent à

$$\beta_{k+1}\mathbf{v}_{k+1} = \mathbf{r}_{k+1} = \mathbf{H}\mathbf{v}_k - \alpha_k\mathbf{v}_k - \beta_k\mathbf{v}_{k-1} \quad , \tag{1.35}$$

et la matrice tridiagonale devient symétrique puisque $\gamma_k = \beta_k$ pour tous les k. En évitant la seconde relation de récurrence, une projection tridiagonale de la matrice originale peut être obtenue en stockant deux fois moins de vecteurs durant la récursion et en effectuant deux fois moins d'opérations à chaque itération dans

le cas hermitique que dans le cas non-hermitique. Rappelons que les observables physiques sont définis par des opérateurs hermitiques, ce qui montre l'importance d'un tel résultat. Il arrive toutefois que la formulation de certains modèles nécessite la résolution de systèmes généralisés aux valeurs propres ou encore des problémes non-symétriques pour obtenir des quantités dérivées des observables quantiques. Le cas échéant, l'algorithme de Lanczos plus général et plus coûteux (Eq. (1.31)) doit être utilisé.

Les méthodes itératives possèdent de nombreux avantages sur les méthodes directes pour le calcul des valeurs propres de représentations matricielles d'opérateurs quantiques. Malgré cela, les limites actuelles des ordinateurs ne permettent d'extraire, par exemple, que quelques niveaux vibrationnels les plus bas de molécules à 5 ou 6 atomes. Dans ce cas, le temps de calcul est certainement le facteur limitant et certaines approches mixtes, cherchant le compromis entre le temps de calcul et l'utilisation de la mémoire vive, ont été développées afin de rendre les schémas numériques plus efficaces. Concernant les opérateurs non-hermitiques et la résolution des probèmes où l'hamiltonien dépend du temps, les mêmes limites que celles exposées plus haut pour les problèmes indépendants du temps se voient aussi exacerbées par la complexité des opérateurs étudiés.

1.4 Présentation des problèmes étudiés et des solutions proposées

Ayant rappelé quelques rudiments de la méthode variationnelle et les fondements des méthodes itératives nécessaires à sa résolution, on est maintenant en mesure de s'attaquer au corps de la présente thèse. L'organisation des prochains chapitres se fera par la présentation d'articles qui introduisent, expliquent et testent quatre nouvelles méthodes appliquées à différents problèmes de spectroscopie théorique et d'algèbre linéaire. Outre l'écriture des programmes informatiques pour la résolution des différents problèmes et les nombreux tests numériques qui ont été

nécessaires à la validation des approches développées, l'auteur de la thèse a écrit la version initiale de tous les articles qui seront reproduits ci-après. À la suite d'un processus itératif de rédaction-correction-échange entre les deux co-auteurs des articles, ceux-ci ont été soumis à des revues de premier plan dans le domaine de la chimie théorique et dans le domaine des mathématiques numériques afin d'en maximiser la visibilité dans la communauté scientifique.

Dans un premier temps, un nouvel intégrateur est proposé pour la résolution de TDSE. La solution exacte de l'équation de Schrödinger dépendante du temps peut être donnée par l'évolution dans le temps d'un paquet d'onde, c'est-à-dire une fonction qui décrit l'état de la particule à un temps t, par l'équation

$$\begin{aligned} \psi(\mathbf{R},t) &= \hat{U}(t)\psi(\mathbf{R},0) \\ &= \hat{T}e^{\int_0^t -i\hat{H}(\mathbf{R},t')dt'/\hbar}\psi(\mathbf{R},0) \quad , \end{aligned} \tag{1.36}$$

où $\hat{T}$ est un opérateur d'ordre temporel et $\psi(\mathbf{R},0)$ est le paquet d'onde à l'instant initial [4–6, 53–57]. Afin d'éviter l'évaluation de l'intégrale dans Eq. (1.36), l'opérateur d'évolution $\hat{U}(t)$ est généralement représenté approximativement comme un produit de propagateurs de courte durée pour lesquels l'hamiltonien est considéré indépendant du temps

$$\hat{U}(t) \simeq \prod_{k=0}^{N} e^{-i\hat{H}(t_k)\Delta t/\hbar} \quad , \tag{1.37}$$

où Δt est l'intervalle de temps sur lequel on considère l'opérateur constant [58–66]. L'erreur associée à cette approximation est de deuxième ordre en temps, $O(\Delta t^2)$. Plutôt que d'utiliser cette approximation, on peut transformer le paquet d'onde dans la représentation d'interaction [67–69], $\psi_I(\mathbf{R},t)$, c'est-à-dire en effectuant la transformation

$$\psi(\mathbf{R},t) = e^{-i\hat{H}_0(\mathbf{R},t)t/\hbar}\psi_I(\mathbf{R},t) \quad , \tag{1.38}$$

où $\hat{H}_0(\mathbf{R},t)$ est une approximation de l'hamiltonien. On substitue ensuite Eq. (1.38)

dans TDSE et on obtient

$$\frac{\partial \psi_I(\mathbf{R},t)}{\partial t} = \hat{H}_I(t)\psi_I(\mathbf{R},t) \quad , \tag{1.39}$$

où $\hat{H}_I(\mathbf{R},t) = e^{i\hat{H}_0(\mathbf{R},t)t/\hbar}\left(\frac{i(\hat{H}-\hat{H}_0)}{\hbar}\right)e^{-i\hat{H}_0(\mathbf{R},t)t/\hbar}$ est l'hamiltonien dans la représentation d'interaction. On verra au chapitre 2 comment il est possible de résoudre efficacement l'équation 1.39. Les tests numériques ont été effectués sur une molécule diatomique, HF, dans un champ laser intense [70]. Ce champ laser a été conçu pour maximiser le taux théorique de photodissociation du HF, représenté comme un oscillateur de Morse.

Dans un second temps, une étude de la réaction d'isomérisation entre l'acétylène et le vinylidène sera présentée. On qualifie de métastable un état dont la durée de vie possède une valeur finie. Dans le cas présent, le potentiel du système est liant et admet des états stationnaires, c'est-à-dire de durée de vie *infinie*, comme solution. Toutefois, on peut diviser le potentiel en différentes régions associées respectivement au vinylidène et à l'acétylène. Ainsi, on décrira la durée de vie d'un des isomères par la fraction de la fonction d'onde d'un état stationnaire qui se trouve localisée près de cette géométrie. La vérification de l'existence d'états du vinylidène de longues durées de vie, c'est-à-dire fortement localisés dans la région de l'espace associée à cet isomère, est une question brûlante que cette étude tentera de résoudre [71–83]. La surface d'énergie potentielle présente deux types de minima locaux, un situé près de la géométrie de l'actétylène et un, peu profond, situé à très haute énergie près de la géométrie du vinylidène [84–86]. Puisque le potentiel du système est liant et que son hamiltonien est indépendant du temps, il est possible d'étudier cette réaction d'isomérisation à l'aide des mêmes méthodes utilisées pour la caractérisation des vibrations d'une molécule.

L'acétylène possède 4 atomes et est excessivement stable dans sa configuration à l'equilibre. De ce fait, il est relativement aisé d'en calculer les quelques premiers

états vibrationnels à l'aide d'une méthode itérative utilisant une base sous forme de produit. Les états vibrationnels possédant des énergies inférieures à $13000cm^{-1}$ au-dessus de l'état fondamental ont d'ores et déjà été bien caractérisés [87]. Or, les états associés à l'espèce métastable vinylidène sont situés à des énergies significativement supérieures. La densité d'états est excessivement élevée autour de l'énergie d'isomérisation. On y trouve, d'un côté, les états localisés dans un puits de potentiel très peu profond correspondant au vinylidène et, de l'autre côté, une grande quantité d'états propres délocalisés associés à l'acétylène. Les limites de la méthode de Lanczos sont telles qu'il est impossible de calculer ces états sans le recours à une stratégie plus élaborée. Ainsi, une méthode mixte permettant le calcul et l'assignation des nombreux états dans la région d'intérêt du spectre sera décrite au chapitre 3. Un choix astucieux des coordonnées permettant une partition efficace des variables ainsi que l'utilisation d'une méthode itérative avec une base contractée sont au coeur de la nouvelle approche [88–95]. Une stratégie de réorthogonalisation locale est aussi mise de l'avant afin d'accélérer la convergence des états désirés.

Au chapitre 4, une nouvelle méthode pour l'étude des états résonants est présentée. La caractérisation des énergies et des durées de vie associées aux états résonants représente un défi pour les méthodes de calcul modernes. Les fonctions d'onde des états résonants se comportent comme des états vibrationnels liés dans une certaine région de l'espace de configuration mais possèdent aussi une queue infinie qu'il est impossible de caractériser à l'aide des bases conventionnelles décrite plus haut [96–105]. On procède généralement à l'absorption de l'onde sortante, la queue, par l'ajout d'un potentiel complexe $\hat{W}(r_1)$ qui perturbe l'Hamiltonien

$$\hat{H}'(r_1, r_2, \ldots, r_k) = \hat{H}(r_1, r_2, \ldots, r_k) + \eta \hat{W}(r_1) \quad , \tag{1.40}$$

où r_1 est la coordonnée dissociative et η est une constante déterminant la force de la perturbation [38, 39, 106–117]. On notera au passage que le potentiel absorbant

ne dépend que de la coordonnée de dissociation. On peut maintenant représenter l'hamiltonien perturbé 1.40 dans une base de notre choix, p. ex. la DVR. On doit, en arithmétique complexe, chercher à minimiser cette perturbation pour extraire les informations précises de l'équation. Une des principales difficultés est donc que toutes les opérations doivent être effectuées en arithmétique complexe et une autre est qu'il faille répéter le calcul plusieurs fois pour minimiser la perturbation. Le schéma numérique proposé au chapitre 4 permet premièrement d'éviter l'utilisation de l'arithmétique complexe en réécrivant le problème aux valeurs propres sous-tendu par l'opérateur 1.40 sous forme d'un problème non-symétrique réel [118,119]. L'algorithme de Lanczos de base (Eq. (1.31)) est utilisé pour extraire les valeurs propres du nouvel opérateur. Afin de rendre l'algorithme plus stable et d'en accélérer la convergence, une variante connue sous le nom de "coupled two-term Lanczos" est utilisée en lieu et place de la méthode standard [120–122]. De plus, la partie coûteuse du calcul, la projection de la matrice originale dans l'espace de Lanczos, n'est effectuée qu'une seule fois. À partir des deux espaces de Krylov obtenus pour un paramètre de force judicieusement sélectionné, un ensemble de vecteurs propres perturbés est généré et utilisé pour projeter la matrice de l'hamiltonien *non perturbé*. Ceci permet d'éviter la répétition du calcul pour minimiser la perturbation et limite l'utilisation de l'arithmétique complexe à la toute fin du calcul, une fois que la partie la plus coûteuse du calcul a déjà été effectuée. La méthode est testée sur un problème bien connu, la photodécomposition du HCO, dont le potentiel adiabatique présente un croisement évité et admet donc un ensemble de résonances de durées de vie fort variables comme solution [41, 123–128].

Le chapitre 5 présente une généralisation de l'algorithme introduit au chapitre précédent. L'algorithme de Lanczos dans sa version la plus primitive (Eq. (1.31)) comporte de sévères lacunes [45, 46, 51, 121, 129–134]. La plus importante est le manque de précision et d'exactitude des valeurs propres obtenues dans les cas où la matrice d'intérêt n'est ni symétrique ni hermitique. L'utilisation de la variante

"coupled two-term Lanczos" peut aider à contourner ce problème mais seulement en partie [120–122]. Certains auteurs ont proposé la réorthogonalisation complète ou partielle des vecteurs comme solution à ce problème mais cette solution ne peut pas être viable pour les problèmes de taille même modeste car il faudrait, pour ce faire, stocker tous les vecteurs dans la mémoire. Afin de contourner les limites de l'algorithme de Lanczos, une nouvelle stratégie inspirée de celle présentée pour les résonances est introduite. Ainsi, une projection de la matrice originale dans un espace de Krylov biorthogonal est générée à l'aide de Eq. (1.31) et des valeurs propres inexactes en sont extraites. Utilisant ces mêmes valeurs propres inexactes comme cibles, un ensemble de vecteurs de base est produit. Rappelons au passage que, contrairement au cas symétrique, une matrice non symétrique possède deux ensembles de vecteurs propres associés à chacune de ses valeurs propres. Ainsi, une matrice générale $\mathbf{G}$ satisfera aux équations

$$\begin{aligned} \mathbf{G}\mathbf{X}_{(R)} &= \mathbf{X}_{(R)}\mathbf{\Gamma} \quad , \\ \mathbf{X}_{(L)}^{\mathbf{T}}\mathbf{G} &= \mathbf{\Gamma}\mathbf{X}_{(L)}^{\mathbf{T}} \quad , \end{aligned} \tag{1.41}$$

où $\mathbf{X}_{(R)}$ est une matrice composée des vecteurs propres droits de la matrice $\mathbf{G}$ et $\mathbf{X}_{(L)}^{\mathbf{T}}$ est la matrice des vecteurs propres gauches associés [45, 46, 51]. La méthode proposée au chapitre 5 tient compte de cette réalité et cherche 2 ensembles de vecteurs de base représentant de bonnes approximations aux vrais vecteurs propres gauches et droits de la matrice générale $\mathbf{G}$. Un ensemble de filtres est utilisé pour restreindre la taille de la base. Par la suite, la matrice originale est projetée dans l'espace des vecteurs conservés en divisant le spectre désiré en plusieurs fenêtres afin d'éviter de stocker trop de vecteurs dans la mémoire de l'ordinateur. La précision et l'efficacité de la méthode sont démontrées par son application à un grand nombre de problèmes provenant de domaines variés. Les performances se comparent avantageusement à la méthode de référence [133, 135].

Bibliographie

[1] P. A. M. Dirac. Quantum mechanics of many-electron systems. *Proc. Roy. Soc. (London)*, 123 :714, 1929.

[2] K. R. Symon. *Mechanics.* Addison-Wesley, Menlo Park, California, 1971.

[3] H. Goldstein. *Classical Mechanics.* Addison-Wesley, Harvard University, Cambridge, MA, 1950.

[4] Claude Cohen-Tannoudji, Bernard Diu, and Franck Laloë. *Mécanique Quantique.* Hermann, éditeur des Sciences et des Arts, 1973.

[5] P. W. Atkins and R. S. Friedman. *Molecular Quantum Mechanics.* Oxford University Press Inc., New York, third edition, 1997.

[6] D. A. McQuarrie. *Quantum Chemistry.* University Science Books, Sausalito, California, 1983.

[7] J. M. Hollas. *Modern Spectroscopy.* John Wiley & Sons, Chichester, West Sussex, England, third edition, 1996.

[8] W. S. Struve. *Fundamentals of molecular spectroscopy.* John Wiley & Sons, New York, 1989.

[9] J. D. Graybeal. *Molecular Spectroscopy.* Mcgraw-Hill, 1993.

[10] E. B. Wilson Jr., J. C. Decius, and P. Cross. *Molecular Vibrations : The Theory of Infrared and Raman Vibrational Spectra.* McGraw-Hill Book Co., New-York, 1955.

[11] R. E. Wyatt and J. Z. H. Zhang, editors. *Dynamics of Molecules and Chemical Reactions.* Dekker, New York, 1996.

[12] J. Z. H. Zhang. *Theory and Application of Quantum Molecular Dynamics.* World Scientific Publishing Company, 1998.

[13] J.G.C. Booten and H.A. van der Vorst. Cracking large-scale eigenvalue computations, part i : Algorithms. *Computers in Physics*, 10 :239, 1996.

[14] S. Carter and N. C. Handy. The variational method for the calculation of rovibrational energy levels. *Comp. Phys. Rep.*, 5 :115, 1986.

[15] Z. Bačić and J. C. Light. Accurate localized and delocalized vibrational states of HCN/HNC. *J. Chem. Phys.*, 86 :3065, 1987.

[16] Z. Bačić and J. C. Light. Theoretical methods for rovibrational states of floppy molecules. *Annu. Rev. Phys. Chem.*, 40 :469, 1989.

[17] J. R. Henderson and J. Tennyson. All the vibrational bound states of H_3^+. *Chem. Phys. Lett.*, 173 :133, 1990.

[18] J. M. Bowman and B. Gazdy. A truncation/recoupling method for basis set calculations of eigenvalues and eigenvectors. *J. Chem. Phys.*, 94 :454, 1991.

[19] Y. Qiu, J. Z. H. Zhang, and Z. Bačić. Six-dimensional quantum calculations of vibration-rotation-tunneling levels of $\nu_1$and ν_2 HCl-stretching excited $(HCl)_2$. *J. Chem. Phys.*, 108 :4804, 1998.

[20] D. Luckhaus. 6D vibrational quantum dynamics : Generalized coordinate discrete variable representation and (a)diabatic contraction. *J. Chem. Phys.*, 113 :1329, 2000.

[21] M. Mladenović. Discrete variable approaches to tetratomic molecules. II : Application to H_2O_2 and H_2CO. *Spectrochim. Acta Part A*, 58 :809, 2002.

[22] H.-D. Meyer, U. Manthe, and L. S. Cederbaum. The multi-configurational time-dependent Hartree approach. *Chem. Phys. Lett.*, 165 :73, 1990.

[23] U. Manthe, H.-D. Meyer, and L. S. Cederbaum. Wave-packet dynamics within the multiconfiguration Hartree framework : General aspects and application to NOCL. *J. Chem. Phys.*, 97 :3199, 1992.

[24] U. Manthe, H.-D. Meyer, and L. S. Cederbaum. Multiconfigurational time-dependent Hartree study of complex dynamics : Photodissociation of NO_2. *J. Chem. Phys.*, 97 :9062, 1992.

[25] U. Manthe and A. D. Hammerich. Wavepacket dynamics in five dimensions. photodissociation of methyl iodide. *Chem. Phys. Lett. 211 (1993), 7.*, 211 :7, 1993.

[26] H.-D. Meyer, U. Manthe, and L. S. Cederbaum. *Numerical Grid Methods and their Application to Schrödinger's Equation*, chapter The multi-configuration Hartree approach., page 141. Kluwer Academic Publishers, Dordrecht, 1993.

[27] H.-D. Meyer and G. Worth. Quantum molecular dynamics : Propagating wavepackets and density operators using the multi-configuration time-dependent hartree (MCTDH) method. *Theor. Chem. Acc.*, 109 :251, 2003.

[28] G. B. Arfken and H. J. Weber. *Mathematical Methods for Physicists.* Academic Press, Boston, MA, sixth edition, 2005.

[29] J. C. Light, I. P. Hamilton, and J. V. Lill. Generalized discrete variable approximation in quantum-mechanics. *J. Chem. Phys.*, 82 :1400, 1985.

[30] J. T. Muckerman. Some useful discrete variable representations for problems in time-dependent and time-independent quantum mechanics. *Chem. Phys. Lett.*, 173 :200, 1990.

[31] C. Leforestier. Grid representation of rotating triatomics. *J. Chem. Phys.*, 94 :6388, 1991.

[32] D. T. Colbert and W. H. Miller. A novel discrete variable representation for quantum mechanical reactive scattering via the S-matrix Kohn method. *J. Chem. Phys.*, 96 :1982, 1992.

[33] J. Echave and D. C. Clary. Potential optimized discrete variable representation. *Chem. Phys. Lett.*, 190 :225, 1992.

[34] M. J. Bramley and T. Carrington Jr. A general discrete variable method to calculate vibrational energy levels of three- and four-atom molecules. *J. Chem. Phys.*, 99 :8519, 1993.

[35] H. Wei. Ghost levels and near-variational forms of the discrete variable representation : Application to H_2O. *J. Chem. Phys.*, 106 :6885, 1997.

[36] J. C. Light and T. Carrington Jr. Discrete variable representations and their utilization. *Adv. Chem. Phys.*, 114 :263, 2000.

[37] H.-G. Yu. A coherent discrete variable representation method for multidimensional systems in physics. *J. Chem. Phys.*, 122 :164107, 2005.

[38] G. Jolicard and E. Austin. Optical potential stabilisation method for predicting resonance levels. *Chem. Phys. Lett.*, 121 :106, 1985.

[39] G. Jolicard and E. Austin. Optical potential method of calculating resonance energies and widths. *Chemical physics*, 103 :295, 1986.

[40] H. W. Jang and J. C. Light. Artificial boundary inhomogeneity method for quantum scattering solutions in an Lt^2 basis. *J. Chem. Phys.*, 102 :3262, 1995.

[41] G. S. Whittier and J. C. Light. Calculation of resonances of HCO by the artificial boundary inhomogeneity method. *J. Chem. Phys.*, 107 :1816, 1997.

[42] E. Anderson, Z. Bai, C. Bischof, S. Blackford, J. Demmel, J. Dongarra, J. Du Croz, A. Greenbaum, S. Hammarling, A. McKenney, and D. Sorensen. *LAPACK Users' Guide.* Society for Industrial and Applied Mathematics, Philadelphia, PA, third edition, 1999.

[43] L. S. Blackford, J. Choi, A. Cleary, E. D'Azevedo, J. Demmel, I. Dhillon, J. Dongarra, S. Hammarling, G. Henry, A. Petitet, K. Stanley, D. Walker, and R. C. Whaley. *SCALAPACK Users' Guide.* Society for Industrial and Applied Mathematics, 1997.

[44] W. H. Press, S. A. S.A. Teukolsky, W. T. Vetterling, and B. P. Flannery. *Numerical Recipes in FORTRAN 77 The Art of Scientific Programming.* Cambridge University Press, 1986.

[45] G. H. Golub and C. F. Van Loan. *Matrix Computations.* John Hopkins University Press, Baltimore, 1989.

[46] L. N. Trefethen and D. Bau III. *Numerical Linear Algebra.* Society for Industrial and Applied Mathematics, Philadelphia, 1997.

[47] E. R. Davidson. The iterative calculation of a few of the lowest eigenvalues and corresponding eigenvectors of large real symmetric matrices. *J. Comput. Phys.*, 17 :87–94, 1975.

[48] F. Sartoretto, G. Gambpmato, and G. Pini. Accelerated simultaneous iterations for large finite element eigenvalues. *J. Comput. Phys.*, 81 :53, 1989.

[49] Y. Saad. *Iterative methods for sparse linear systems.* Society for Industrial and Applied Mathematics, Philadelphia, 2003.

[50] P. Arbenz, U. L. Hetmaniuk, R. B. Lehoucq, and R. S. S. Tuminaro. A comparison of eigensolvers for large-scale 3d modal analysis using AMG-preconditioned iterative methods. *Internat. J. Numer. Methods Engrg.*, 64 :204–236, 2005.

[51] Z. Bai, J. Demmel, J. Dongarra, A. Ruhe, and H. van der Vorst, editors. *Templates for the Solution of Algebraic Eigenvalue Problems : A Practical Guide.* Society for Industrial and Applied Mathematics, Philadelphia, 2000.

[52] G. W. Stewart. *Matrix Algorithms volume II : Eigensystems.* Society for Industrial and Applied Mathematics, Philadelphia, 2001.

[53] P. Pechukas and J. C. Light. On the exponential form of time-displacement operators in quantum mechanics. *J. Chem. Phys.*, 44 :3897, 1966.

[54] A. Askar and A. S. Cakmak. Explicit integration method for the time-dependent Schrödinger equation for collision problems. *J. Chem. Phys.*, 68 :2794, 1978.

[55] S. K. Gray and J. M. Verosky. Classical Hamiltonian structures in wave packet dynamics. *J. Chem. Phys.*, 100 :5011, 1994.

[56] D. E. Manolopoulos and S. K. Gray. Symplectic integrators for the multi-channel Schrödinger equation. *J. Chem. Phys.*, 102 :9214, 1995.

[57] S. K. Gray and D. E. Manolopoulos. Symplectic integrators tailored to the time-dependent Schrödinger equation. *J. Chem. Phys.*, 104 :7099, 1996.

[58] H. Tal-Ezer and R. Kosloff. An accurate and efficient scheme for propagating the time dependent Schrödinger equation. *J. Chem. Phys.*, 81 :3967, 1984.

[59] M.D. Feit and J.A. Fleck. Wave packet dynamics and chaos in the hénon-heiles system. *J. Chem. Phys.*, 80 :2578, 1984.

[60] T.J. Park and J.C. Light. Unitary quantum time evolution by iterative Lanczos reduction. *J. Chem. Phys.*, 85 :5870, 1986.

[61] R. Kosloff. Time-dependent quantum-mechanical methods for molecular dynamics. *J. Phys. Chem.*, 92 :2087, 1988.

[62] S. Das and D. J. Tannor. Time dependent quantum mechanics using picosecond time steps : Application to predissociation of HeI_2. *J. Chem. Phys.*, 92 :3403, 1990.

[63] Y. Shi and D. J. Tannor. Symmetry adapted Fourier solution of the time-dependent Schrödinger equation. *J. Chem. Phys.*, 92 :2517, 1990.

[64] C. Leforestier, R. Bisseling, C. Cerjan, M.D. Feit, R. Friesner, A. Guldberg, A. Hammerich, W. Jolicard, G. Karrlein, H.-D. Meyer, N. Lipkin, O. Roncero, and R. Kosloff. A comparison of different propagation schemes for the time dependent Schrödinger equation. *J. Comp. Phys.*, 94 :59, 1991.

[65] D. J. Tannor, A. Besprozvannaya, and C. J. Williams. Nested interaction representations in time dependent quantum mechanics. *J. Chem. Phys.*, 96 :2998, 1992.

[66] R. Kosloff. Propagation methods for quantum molecular dynamics. *Annu. Rev. Chem. Phys.*, 45 :145, 1994.

[67] J. Z. H. Zhang. New method in time-dependent quantum scattering theory : Integrating the wave function in the interaction picture. *J. Chem. Phys.*, 92 :324, 1990.

[68] J. Z. H. Zhang. Multichannel quantum wave packet propagation in the interaction picture : application to gas-surface scattering. *Comp. Phys. Comm.*, 63 :28, 1991.

[69] C. J. Williams, J. Qian, and D. J. Tannor. Dynamics of triatomic photodissociation in the interaction representation. I. methodology. *J. Chem. Phys.*, 95 :1721, 1991.

[70] S. Chelkowski, A. D. Bandrauk, and P. B. Corkum. Efficient molecular dissociation by a chirped ultrashort infrared laser pulse. *Phys. Rev. Lett.*, 65 :2355, 1990.

[71] C. E. Dykstra and H. F. Schaefer. The vinylidene-acetylene rearrangement. a self-consistent electron pairs study of a model unimolecular reaction. *J. Am. Chem. Soc.*, 100 :1378, 1978.

[72] S.M. Burnett, A. E. Stevens, C. S. Feigerle, and W. C. Lineberger. Observation of X^1A_1 vinylidene by photoelectron spectroscopy of the $C_2H_2^-$ ion. *Chem. Phys. Lett.*, 100 :124, 1983.

[73] T. Carrington Jr., L. M. Hubbard, H. F. Schaefer III, and W. H. Miller. Vinylidene : Potential energy surface and unimolecular reaction dynamics. *Chem. Phys.*, 80 :4347, 1984.

[74] K. M. Ervin, J. Ho, and W. C. Lineberger. A study of the singlet and triplet states of vinylidene by photoelectron spectroscopy of $H_2C{=}C^-$, $D_2C{=}C^-$, and $HDC{=}C^-$. vinylidene-acetylene isomerization. *J. Chem. Phys.*, 91 :5974, 1989.

[75] N.-Y. Chang, M.-Y. Shen, and C.-H. Yu. Extended ab initio studies of the vinylidene-acetylene rearrangement. *J. Chem. Phys.*, 106 :3237, 1997.

[76] T. C. Germann and W. H. Miller. Quantum mechanical calculation of resonance tunneling in acetylene isomerization via the vinylidene intermediate. *J. Chem. Phys.*, 109 :94, 1998.

[77] J. Levin, H. Feldman, A. Baer, D. Ben-Hamu, O. Heber, D. Zajfman, and Z. Vager. Study of unimolecular reactions by coulomb explosion imaging : The nondecaying vinylidene. *Phys. Rev. Lett.*, 81 :3347, 1998.

[78] R. Schork and H. Köppel. Barrier recrossing in the vinylidene-acetylene isomerization reaction : A five-dimensional ab initio quantum dynamical investigation. *J. Chem. Phys.*, 115 :7907, 2001.

[79] S. Zou and J. M. Bowman. Reduced dimensionality quantum calculations of acetylene $< -- >$ vinylidene isomerization. *J. Chem. Phys.*, 116 :6667, 2002.

[80] S. Zou and J. M. Bowman. Full dimensionality quantum calculations of acetylene/vinylidene isomerization. *J. Chem. Phys.*, 117 :5507, 2002.

[81] R. Prosmiti and S. C. Farantos. Periodic orbits and bifurcation diagrams of acetylene/vinylidene revisited. *J. Chem. Phys.*, 118 :8275, 2003.

[82] S. Zou, J. M. Bowman, and A. Brown. Full-dimensionality quantum calculations of acetylene–vinylidene isomerization. *J. Chem. Phys.*, 118 :10012, 2003.

[83] I. N. Kozin, M. M. Law, J. Tennyson, and J. M. Hutson. Calculating energy levels of isomerizing tetraatomic molecules : II. the vibrational states of acetylene and vinylidene. *J. Chem. Phys.*, 122 :064309, 2005.

[84] J. F. Stanton and J. Gauss. Vibrational structure in the vinylidene anion photoelectron spectrum : Closing the gap between theory and experiment. *J. Chem. Phys.*, 110 :6079, 1999.

[85] D. Xu, H. Guo, S. Zou, and J. M. Bowman. A scaled ab initio potential energy surface for acetylene and vinylidene. *Chem. Phys. Lett.*, 377 :582, 2003.

[86] S. Zou and J. M. Bowman. A new ab initio potential energy surface describing acetylene/vinylidene isomerization. *Chem. Phys. Lett.*, 368 :421, 2003.

[87] D. Xu, G. Li, D. Xie, and H. Guo. Full-dimensional quantum calculations of vibrational energy levels of acetylene (HCCH) up to 13000 cm^{-1}. *Chem. Phys. Lett.*, 365 :483, 2002.

[88] M. J. Bramley and T. Carrington Jr. Calculation of triatomic vibrational eigenstates : Product or contracted basis sets, lanczos or conventional eigensolvers ? what is the most efficient combination ? *J. Chem. Phys.*, 101 :8494, 1994.

[89] X. Wang and T. Carrington Jr. New ideas for using contracted basis functions with a Lanczos eigensolver for computing vibrational spectra of molecules with four or more atoms. *J. Chem. Phys.*, 117 :6923, 2002.

[90] H.-G. Yu. Two-layer Lanczos iteration approach to molecular spectroscopic calculation. *J. Chem. Phys.*, 117 :8190, 2002.

[91] X. Wang and T. Carrington Jr. A contracted basis-Lanczos calculation of vibrational levels of methane : Solving the Schrödinger equation in nine dimensions. *J. Chem. Phys.*, 119 :101, 2003.

[92] X. Wang and T. Carrington Jr. Using simply contracted basis functions with the Lanczos algorithm to calculate vibrational spectra. *Int. J. Quant. Chem.*, 99 :556, 2004.

[93] H.-G. Yu. Converged quantum dynamics calculations of vibrational energies of CH_4 and CH_3D using an ab initio potential. *J. Chem. Phys.*, 121 :6334, 2004.

[94] H.-G. Yu. Full-dimensional quantum calculations of vibrational spectra of six-atom molecules. I. theory and numerical results. *J. Chem. Phys.*, 120 :2270, 2004.

[95] X. Wang and T. Carrington Jr. Contracted basis Lanczos methods for computing numerically exact rovibrational levels of methane. *J. Chem. Phys.*, 121 :2937, 2004.

[96] A. F. J. Siegert. On the derivation of the dispersion formula for nuclear reactions. *Phys. Rev.*, 56 :750, 939.

[97] A. U. Hazi and H. S. Taylor. Stabilization method of calculating resonance energies : Model problem. *Phys. Rev. A*, 1 :1109, 1970.

[98] G. D. Doolen. A procedure for calculating resonance eigenvalues. *J. Phys. B*, 8 :525, 1975.

[99] B. Simon. The definition of molecular resonance curves by the method of exterior complex scaling. *Phys. Lett. A*, 71 :211, 1979.

[100] N. Moiseyev, S. Friedland, and P. R. Certain. Cusps, θ trajectories, and the complex virial theorem. *J. Chem. Phys.*, 74 :4739, 1981.

[101] W. P. Reinhardt. Complex coordinates in the theory of atomic and molecular structure and dynamics. *Ann. Rev. Phys. Chem.*, 33 :223, 1982.

[102] D.G. Truhlar, editor. *Resonances in Electron-Molecule Scattering, Van der Waals Complexes, and Reactive Chemical Dynamics.* Number 263 in Symposium Series. American Chemical Society, Washington, 1984.

[103] V. I. Kukulin, Krasnopol'ky, and J. Horáček. *Theory of Resonances.* Kluwer Academic Publisher, Dordrecht, 1989.

[104] O. Atabek and R. Lefebvre. Application of the complex coordinate method to the conical resonances of Jahn-Teller spectra. *J. Chem. Phys.*, 97 :3973, 1992.

[105] R. Schinke. *Photodissociation Dynamics.* Cambridge University Press, Cambridge, 1993.

[106] G. Jolicard, C. Leforestier, and E. Austin. Resonance states using the optical potential model. study of Feshbach resonances and broad shape resonances. *J. Chem. Phys.*, 88 :1026, 1988.

[107] D. Neuhauser and M. Baer. The time-dependent Schrödinger equation : Application of absorbing boundary conditions. *J. Chem. Phys.*, 90 :4351, 1989.

[108] M. S. Child. Analysis of a complex absorbing barrier. *Mol. Phys.*, 72 :89, 1991.

[109] G. Jolicard and G.D. Billing. Partial widths and time-dependent dissociation dynamics by the optical potential method. *J. Chem. Phys.*, 97 :997, 1992.

[110] T. Seideman and W.H. Miller. Calculation of the cumulative reaction probability via a discrete variable representation with absorbing boundary conditions. *J. Chem. Phys.*, 96 :4412, 1992.

[111] A. Vibok and G. G. Balint-Kurti. Parametrization of complex absorbing potentials for time-dependent quantum dynamics. *J. Phys. Chem.*, 96 :8712, 1992.

[112] D. Macias, S. Brouard, and J. G. Muga. Optimization of absorbing potentials. *Chem. Phys. Lett.*, 228 :672, 1994.

[113] U.V. Riss and H.-D. Meyer. Investigation on the reflection and transmission properties of complex absorbing potentials. *J. Chem. Phys.*, 105 :1409, 1996.

[114] J.Y Ge and J.Z.H. Zhang. Use of negative complex potential as absorbing potential. *J. Chem. Phys.*, 108 :1429, 1998.

[115] D. E. Manolopoulos. Derivation and reflection properties of a transmission-free absorbing potential. *J. Chem. Phys.*, 117 :9552, 2002.

[116] B. Poirier and T. Carrington Jr. Semiclassically optimized complex absorbing potentials of polynomial form. I. pure imaginary case. *J. Chem. Phys.*, 118 :17, 2003.

[117] B. Poirier and T. Carrington Jr. Semiclassically optimized complex absorbing potentials of polynomial form. II. complex case. *J. Chem. Phys.*, 119 :77, 2003.

[118] V. A. Mandelshtam and A. Neumaier. Pseudotime Schrödinger equation with absorbing potential for quantum scattering calculations. *Phys. Rev. Lett.*, 86 :5031–5034, 2001.

[119] V. A. Mandelshtam and A. Neumaier. Further generalization and numerical implementation of pseudotime Schrödinger equations for quantum scattering calculations. *J. Theor. Comput. Chem.*, 1 :1, 2002.

[120] R. W. Freund and N. M. Nachtigal. *Linear Algebra for Large Scale and Real-Time Applications.* Kluwer Academic Publishers, 1993.

[121] R. W. Freund and N. M. Nachtigal. Implementation details of the coupled QMR algorithm. *SIAM J. Sci. Stat. Comp.*, 15 :313, 1994.

[122] H. O. Karlsson and S. Holmgren. Cross correlation functions $c_{nm}(e)$ via lanczos algorithms without diagonalization. *J. Chem. Phys.*, 117 :9116, 2002.

[123] J. M. Bowman, J. S. Bittman, and L.B. Harding. Ab initio calculations of electronic and vibrational energies of HCO and HOC. *J. Chem. Phys.*, 85 :911, 1986.

[124] D. Wang and J. M. Bowman. L^2 calculations of resonances and final rotational distributions for HCO $--$ >H+CO. *J. Chem. Phys.*, 100 :1021, 1994.

[125] T. P. Grozdanov, V. A. Mandelshtam, and H. S. Taylor. Recursion polynomial expansion of the green's function with absorbing boundary conditions : Calculations of resonances of HCO by filter diagonalization. *J. Chem. Phys.*, 103 :7990, 1995.

[126] H.-M. Keller, A. J Floethmann, H. and. Dobbyn, R. Schinke, and H. J. Werner. The unimolecular dissociation of HCO. II. comparison of calculated resonance energies and widths with high-resolution spectroscopic data. *J. Chem. Phys.*, 105 :4983, 1996.

[127] B. Poirier and J. C. Light. Phase space optimization of quantum representations : Three-body systems and the bound states of HCO. *J. Chem. Phys.*, 114 :6562, 2001.

[128] B. Poirier and T. Carrington Jr. A preconditioned inexact spectral transform method for calculating resonance energies and widths, as applied to HCO. *J. Chem. Phys.*, 116 :1215, 2002.

[129] B. N. Parlett, D. R. Taylor, and Z. A. Liu. A look-ahead Lanczos algorithm for unsymmetric matrices. *Math. Comp.*, 44 :105, 1985.

[130] R. W. Freund and N. M. Nachtigal. An implementation of the look-ahead Lanczos algorithm for non-hermitian matrices. *SIAM J. Sci. Comput.*, 14 :137, 1993.

[131] Z. Bai. Error analysis of the lanczos algorithm for the nonsymmetric eigenvalue problem. *Math. Comp.*, 62 :209–226, 1994.

[132] D. Day. An efficient implementation of the nonsymmetric Lanczos algorithm. *SIAM J. Matrix Anal. Appl.*, 18 :566–589, 1997.

[133] Z. Bai, D. Day, and Q. Ye. ABLE : An adaptive block-lanczos method for non-hermitian eigenvalue problems. *SIAM J. Matrix Anal. Appl.*, 20 :1060–1082, 1999.

[134] M.-C. Kim and I.-W. Lee. Solution eigenproblems for non-proportional damping system by Lanczos method. *Earthquake Engng. Struct. Dyn.*, 28 :157, 1999.

[135] http ://www.caam.rice.edu/software/ARPACK/.

CHAPITRE 2

DE LA SOLUTION DE L'ÉQUATION DE SCHRÖDINGER POUR LES SYSTÈMES DÉCRITS PAR UN HAMILTONIEN DÉPENDANT EXPLICITEMENT DU TEMPS : DÉVELOPPEMENT D'UNE MÉTHODE DE PROPAGATION

Dans cette section, une méthode de propagation basée sur l'intégration directe de l'équation de Schrödinger dépendante du temps dans la représentation d'interaction est présentée. Le manuscrit a été soumis à la revue "Journal of Chemical Physics" le 24 août 2004 et accepté le 17 septembre 2004. La publication a eu lieu le 8 décembre 2004.

Using preconditioned adaptive step size Runge-Kutta methods for solving the time-dependent Schroedinger equation

Jean Christophe Tremblay[1] and Tucker Carrington Jr.[2]

Département de chimie, Université de Montréal,

C.P. 6128, succursale Centre-ville, Montréal (Québec) H3C 3J7, Canada

Abstract

If the Hamiltonian is time-dependent it is common to solve the time dependent Schroedinger equation by dividing the propagation interval into slices and using an (e.g., split operator, Chebyshev, Lanczos) approximate matrix exponential within each slice. We show that a preconditioned adaptive step size Runge-Kutta method can be much more efficient. For a chirped laser pulse designed to favour the dissociation of HF the preconditioned adaptive step size Runge-Kutta method is about an order of magnitude more efficient than the time sliced method.

[redacted]

Fax: 514-343-7586

2.1 Introduction

A great deal of effort has been devoted to the development of numerical methods for solving the time dependent Schroedinger equation (TDSE). If the Hamiltonian is time independent $\psi_S(T)$ can be obtained from the equation,

$$|\psi_S(T)\rangle = e^{-iTH/\hbar}|\psi_S(0)\rangle \ . \tag{2.1}$$

To use this equation one must be able to apply a matrix exponential to a vector. Many methods have been developed for this purpose and chemical physicists have played an important role in the development of some of them. [1–5] Leforestier *et al.* give a useful discussion of the advantages of several methods. [6] If the Hamiltonian is time dependent it is harder to compute $\psi_S(T)$; it is not sufficient to be able to apply a matrix exponential to a vector.

It is widely accepted that it is important to have good methods for solving the TDSE. Some time ago it was noticed that efficient methods for solving the TDSE with a time-independent Hamiltonian enable one to compute spectra, scattering cross sections, dissociation probabilities etc. without storing an $N \times N$ Hamiltonian matrix. [7] This was regarded as a key advantage of time-dependent methods. [8] It is now, however, well understood that iterative time-independent methods also enable one to compute spectra, scattering cross sections, dissociation probabilities etc., without storing (or computing) an $N \times N$ Hamiltonian matrix. [9–19] All iterative methods, immaterial of whether they are designed to solve the TDSE or the time-independent Schroedinger equation (TISE), build solutions by evaluating matrix-vector products. The time-independent methods are simpler because there is no need to transform or process a time-dependent solution to obtain frequency- (or energy-) dependent results. Much more importantly, if one uses a time-independent approach, it is straightforward to use preconditioning (a preconditioner for $\mathbf{H}$ is a matrix which in some sense is similar to $\mathbf{H}$ but for

which matrix-vector products are inexpensive) to drastically reduce the number of matrix-vector products required to obtain converged results. For example to compute photodissociation cross sections one needs to apply a matrix representation of the Green's operator to a vector. To do so one solves a system of linear equations. Many good iterative linear solvers and preconditions have been developed. [20] Using a preconditioner to reduce the number of matrix-vector products required to determine energy levels is not as easy but this can be done by using the preconditioned inexact spectral transform method. [21, 22] In contrast, the most popular computational methods used to solve the TDSE (the Chebyshev expansion method, the short iterative Lanczos (SIL) method, the split operator method, etc.) make no use of a preconditioner.

Would it be useful to have algorithms for solving the TDSE that take advantage of the fact that it often not hard to find a good preconditioner? Even if the Hamiltonian is time-independent it can sometimes be helpful to solve the TDSE because time-dependent methods often provide a means of combining numerically exact and approximate techniques. They also enable one to understanding energy redistribution etc. If the Hamiltonian is time-dependent the need for a preconditioned TDSE solver is more obvious. In the time-dependent case, one needs to solve the TDSE to compute observables and it would clearly be advantageous to have a preconditioned method. Of course it is always good to use an efficient method for solving the TDSE, but for problems whose solution requires solving the TDSE repeatedly this is especially true. This is the case for the optimal control problem. [23] The best method we test is almost an order of magnitude better than commonly used approaches. If the TDSE were to be solved many times to derive an optimal field, the reduction in the total CPU time achieved by using the preconditioned variable step size methods of section II would be very significant. If the Hamiltonian is time dependent there are essentially two strategies for obtaining $\psi_S(T)$. (1) If the solution is desired in the range (0,T) one can divide the range

into time slices of duration ΔT, propagate from 0 to ΔT, and then from ΔT to $2\Delta T$ etc., assuming that the Hamiltonian is time-independent within each slice. For each $n\Delta T$ to $(n+1)\Delta T$ propagation one can use any of the well established methods for solving the TDSE with a time-independent Hamiltonian (e.g. SIL or Chebyshev). (2) One abandons the idea of using tools developed to exponentiate a matrix and applies any of a large number of numerical intergration schemes developed to solve ordinary differential equations. The most popular of these techniques is the fourth-order Runge-Kutta method. [24] In chemical physics the first strategy is more popular.

Both of these strategies have serious disadvantages. The principal drawback of the first strategy is the fact that for many time-dependent Hamiltonians ΔT must be very small. Sometimes the split operator method is used for the $n\Delta T$ to $(n+1)\Delta T$ propagations of the first strategy. If ΔT is small enough that the error in $\psi_S(T)$ is less than some preselected tolerance then the $n\Delta T$ to $(n+1)\Delta T$ propagations can be done with one split operator step (it is not the split operator error but the ΔT discretization that determines the error in the final $\psi_S(T)$). If the Chebyshev method is used to do the $n\Delta T$ to $(n+1)\Delta T$ propagations then the total number of matrix-vector products required is large because with the Chebyshev method one needs a minimum number of polynomials, regardless of the length of the propagation. [6] The fact that ΔT must be small is therefore a problem if one employs the first strategy.

The Magnus expansion [25,26] offers a way around this problem but in practise it is messy and is seldom used. To use the Magnus expansion one must act on a vector with the exponential of a sum of operators. To propagate from 0 to T one divides the propagation range into intervals of duration ΔT_M. If, to attain some specified accuracy, ΔT is the size of the interval one must use with the simplest version of the first strategy and ΔT_M is the size of the Magnus interval one must use to achieve the same accuracy then $\Delta T < \Delta T_M$. If only the first term in the Magnus

expansion is retained and the time integral of the first term is approximated with a one-point quadrature then for the $n\Delta T_M$ to $(n+1)\Delta T_M$ interval the exponential one must apply to the vector is $e^{\frac{-i\Delta T_M \mathbf{H}(n\Delta T_M + \Delta T_M/2)}{\hbar}}$. To include the second term in the Magnus expansion one must evaluate a commutator of the Hamiltonian at two different times. If the size of the Hamiltonian matrix is large evaluating this commutator is expensive.

Just like the SIL, Chebyshev, and split operator methods, Runge-Kutta type methods build the solution of the Schroedinger equation by evaluating matrix-vector products. The principal drawback of the second strategy is that it is inefficient. For example we find that for the test problem of Table 2.1 105'000 matrix-vector products are sufficient with the split operator method but more than 800'000 are required if one uses the fourth-order Runge-Kutta method. This drawback of RK type methods is widely appreciated and they are not frequently used in chemical physics. The symplectic integration schemes of Gray and Manolopoulos, and of Sanz-Serna and Portillo are partitioned RK type methods. [27–30]

We can choose to solve the TDSE in any basis. It makes sense to choose the basis (representation) to make solving the differential equations as easy as possible. Zhang and Tannor *et al.* suggesting using the interaction representation. Both used the interaction representation to solve the TDSE for a time independent Hamiltonian. [31–36] If the Hamiltonian in the Schroedinger representation is time independent using the interaction representation complicates solving the TDSE because in the interaction representation the Hamiltonian is time dependent and this precludes the straightforward use of methods such as split operator and Chebyshev. If the Hamiltonian is already time dependent in the Schroedinger representation using the interaction representation does not introduce new time dependence. For the TDSE the use of the interaction representation is a means of preconditioning the problem. Williams *et al.* used the interaction representation and dealt with the time dependence of the Hamiltonian in the interaction representation by using the

Magnus expansion and the first strategy mentioned previously. [35] In this paper we use the interaction representation to precondition the TDSE but we apply it to a Hamiltonian that is time dependent in the Schroedinger representation (the interaction representation does not therefore convert the problem from one with a time independent Hamiltonian to one with a time dependent Hamiltonian) and we use the second strategy – a Runge-Kutta type integration scheme. We show that, at least in some cases, this yields a very efficient method.

2.2 Runge-Kutta methods

If the Hamiltonian is time independent it appears to be advantageous to exploit the fact that the formal solution is known, Eq. (2.1). In this case, one needs only to find a good means of evaluating matrix-vector products with $e^{\frac{-iT\mathbf{H}}{\hbar}}$. If the Hamiltonian is time dependent it is far from obvious that it is best to break the propagation interval into slices and use (within each slice) a matrix exponential approximation. The alternative is to use a general method that advances the solution step by step without breaking the entire interval into slices within which matrix exponential approximations are used. Most step by step methods use information computed at several values of t to build an approximate solution. Runge-Kutta methods use a Taylor series expansion to approximate the solution. Knowing $\psi_{\mathbf{S}}(t)$ the standard second (fourth) order Runge-Kutta method enables one to compute $\psi_{\mathbf{S}}(t+\delta t)$ by evaluating two (four) Hamiltonian matrix-vector products. If n is greater than four than n'th order Runge-Kutta methods require more than n Hamiltonian matrix-vector products to determine $\psi_S(t+\delta t)$. A simple fourth-order Runge-Kutta method for solving

$$i\hbar\frac{\partial\psi_S}{\partial t} = \hat{H}\psi_S \tag{2.2}$$

is

$$\mathbf{k_1} = \delta t \mathbf{A}(t)\psi_S(t) \tag{2.3}$$

$$\mathbf{k_2} = \delta t \mathbf{A}(t + \frac{\delta t}{2})(\psi_S(t) + \frac{\mathbf{k_1}}{2}) \tag{2.4}$$

$$\mathbf{k_3} = \delta t \mathbf{A}(t + \frac{\delta t}{2})(\psi_S(t) + \frac{\mathbf{k_2}}{2}) \tag{2.5}$$

$$\mathbf{k_4} = \delta t \mathbf{A}(t + \delta t)(\psi_S(t) + \mathbf{k_3}) \tag{2.6}$$

$$\psi_S(t + \delta t) = \psi_S(t) + \frac{\mathbf{k_1}}{6} + \frac{\mathbf{k_2}}{3} + \frac{\mathbf{k_3}}{3} + \frac{\mathbf{k_4}}{6} \ , \tag{2.7}$$

where

$$\mathbf{A}(t) = \frac{\mathbf{H}}{i\hbar} \tag{2.8}$$

All Runge-Kutta methods have a similar structure. [24]

Runge-Kutta methods work best if the solution can be pieced together from local low-order Taylor expansions. This means that they will work best if the absolute values of the largest eigenvalues of $\frac{\mathbf{H}}{\hbar}$ are small – i.e., if the solution is smooth. This in turn implies that it should be advantageous to work in the interaction representation (IR). We therefore solve

$$\frac{\partial \psi_I(t)}{\partial t} = \hat{H}_I(t)\psi_I(t) \ , \tag{2.9}$$

where $\hat{H}_I(t) = e^{i\hat{H}_0 t/\hbar}\left(\frac{i(H-H_0)}{\hbar}\right)e^{-i\hat{H}_0 t/\hbar}$ is the Hamiltonian in the IR and H_0 is some preconditioner. If the eigenvalues of $\left(\frac{H-H_0}{\hbar}\right)$ are small Runge-Kutta methods converge quickly. The wavefunction in the Schroedinger representation is easily obtained from the solution of Eq. (2.9)

$$\psi_S(t) = e^{-i\hat{H}_0 t/\hbar}\psi_I(t) \ . \tag{2.10}$$

Zhang and Tannor *et al.* have discussed the advantages of propagating in the IR. [31–36] In their work H (in the Schroedinger representation) is time indepen-

dent and they deal with the time dependence introduced by the interaction representation by dividing the propagation range into time slices and using approximate matrix exponentials within the slices. In contrast we use various Runge-Kutta methods to solve the TDSE in the IR. Castillo and Saad proposed several preconditioned integration schemes one of which is equivalent to a fourth-order fixed step size Runge-Kutta method applied to the TDSE in the IR. [37] Quack and Sutcliffe and Quack and Stohner have solved the TDSE in a quasiresonant basis which is related to an interaction representation. [38, 39]

Applied to the Schroedinger equation in the Schroedinger representation the fourth order Runge-Kutta method is not efficient. For the problem for which results are presented in Table 2.1, it is almost a factor of 8 more costly than using time slicing and the split operator method. However, in the interaction representation the fourth order Runge-Kutta method is almost a factor of two *more* efficient than using time slicing and the split operator method. This indicates that the interaction representation-Runge Kutta combination is worth considering. It is common to use time slicing because it is considered to be simple (especially true if it is used with the split operator method) but it is very easy to program a fourth-order Runge Kutta method and there is no reason not to consider it, if it is used in conjunction with the interaction representation.

In fact, more refined Runge Kutta methods are even more efficient. This extra efficiency is achieved by varying the step size (δt) which makes it possible to decrease the number of steps required to propagate from 0 to T. The step size is chosen to attain some specified local accuracy. By using larger step sizes where the solution is smoother the total number of steps can be reduced drastically. [24, 40] One begins with an initial step size and adjusts it after each step. After obtaining the solution at t_k by taking a step of size δt_k, one determines δt_{k+1} (the step used to compute $\psi(t_k + \delta t_{k+1})$) by comparing the desired local accuracy with an estimate of the local accuracy at t_k. If the desired accuracy is smaller than the estimate of the

local accuracy at t_k the solution at t_k is rejected and the step size is decreased. If the desired accuracy is larger than the estimate of the local accuracy at t_k, the step size is increased or decreased. The new step size is given by the equation [24, 40]

$$\delta t_{k+1} = s\delta t_k \left| \frac{A_d}{A_a} \right|^{0.2} , \tag{2.11}$$

where $s = 0.8$, A_d is the desired local accuracy, and A_a is the estimated attained local accuracy. Choosing $s < 1$ reduces the number of rejected steps and therefore improves the efficiency of the numerical scheme.

How does one estimate the attained local accuracy? We have used three different procedures for doing this. The first is called step doubling. The step doubling error estimate is determined from the difference between the solution at $t_k + \delta t_{k+1}$ obtained by taking one step of δt_{k+1} and the solution at $t_k + \delta t_{k+1}$ obtained by taking two steps of $\frac{\delta t_{k+1}}{2}$. [24] The second and third procedures use so-called embedded Runge Kutta methods. An embedded Runge Kutta methods takes advantage of the fact that, in some cases, from one set of matrix-vector products, it possible to determine two solutions $\psi_{\mathbf{S}}(t_k + \delta t_{k+1})$ one accurate to nth order and the other accurate to $(n-1)$th order. Again, the difference between these two solutions yields an error estimate. The first method of this kind was due to Fehlberg and is a $5^{th}(4^{th})$-order scheme requiring only 6 matrix-vector products per time step. [24] A more recent scheme that gives a somewhat better error estimate is the Dormand-Prince embedded method. [40]

2.3 Test calculations

As explained in the introduction, it is especially important to develop efficient propagation schemes if the Hamiltonian is time dependent. We have therefore decided to test the Runge Kutta - interaction representation (with and without adaptive step sizes) ideas by calculating populations of vibrational states of a di-

atomic molecule in a chirped laser field. Because the intensity is high and the dissociation time is much less than spontaneous emission lifetimes it is reasonable to treat the field classically. The chirped field proposed by Chelkowski *et al.* [41] has recently been used by Farnum and Mazziotti to test the usefulness of spectral difference methods for propagation. [42] The electric field of the chirped pulse is

$$E = E_M U(t) \cos[\omega(t)t] \ . \tag{2.12}$$

The time dependence of the pulse frequency is chosen to push population from the ground state of HF up the vibrational ladder. The field-free potential is a Morse potential and the full Hamiltonian is

$$\hat{H} = K + D[1 - e^{-ax}]^2 - \mu_1 x E_M U(t) \cos[\omega(t)t] \ , \tag{2.13}$$

where K is the kinetic energy operator, $x = r - r_e$, r is the bond length, r_e is the equilibrium bond length. Chelkowski *et al.* use $D = 0.225509$ hartree , $\mu_1 = 0.309$ e, $a = 1.17411$ bohr^{-1}, r_e= 1.7329 bohr, and $E_M = \sqrt{8\pi I/c}$ for a given intensity I. In Eq. (2.13) it has been assumed that the dipole is linear in x and the dipole moment at $r = r_e$ has been neglected because its effect on the computed populations is small and the chirped laser pulse has been optimized without it. $U(t)$ is the optimized pulse envelope and $\omega(t)$ is the chirped frequency, both of which are defined clearly in Ref. [41]. Chelkowski *et al.* did calculations for $I = 10^{13}\ Wcm^{-1}$ and $I = 10^{12}\ Wcm^{-1}$. These intensities are hereafter referred to as (respectively) the strong and weak field cases. This HF potential supports 24 bound states. Populations $P_n(t)$ and the dissociation probability $P_D(t)$ were calculated using the equations

$$P_n(t) = |\langle \psi_n | \psi_S(t) \rangle|, \quad P_D(t) = 1 - \sum_{n=0}^{23} P_n(t) \ . \tag{2.14}$$

Chelkowski *et al.* computed dissociation probabilities with the time slice strategy and used the split operator method within each slice. Figures 1 and 2 show, for the strong and weak field cases, that the populations of the higher levels increase as the propagation proceeds. Our calculations are done with a slightly modified dipole

Figure 2.1: Time dependence of the populations of the ground state (——), first excited state (— —), eighth excited state (– –), fourteenth excited state (- - -) and dissociation probability (— - — -) for HF in a chirped laser field of intensity $I = 10^{13} W cm^{-1}$.

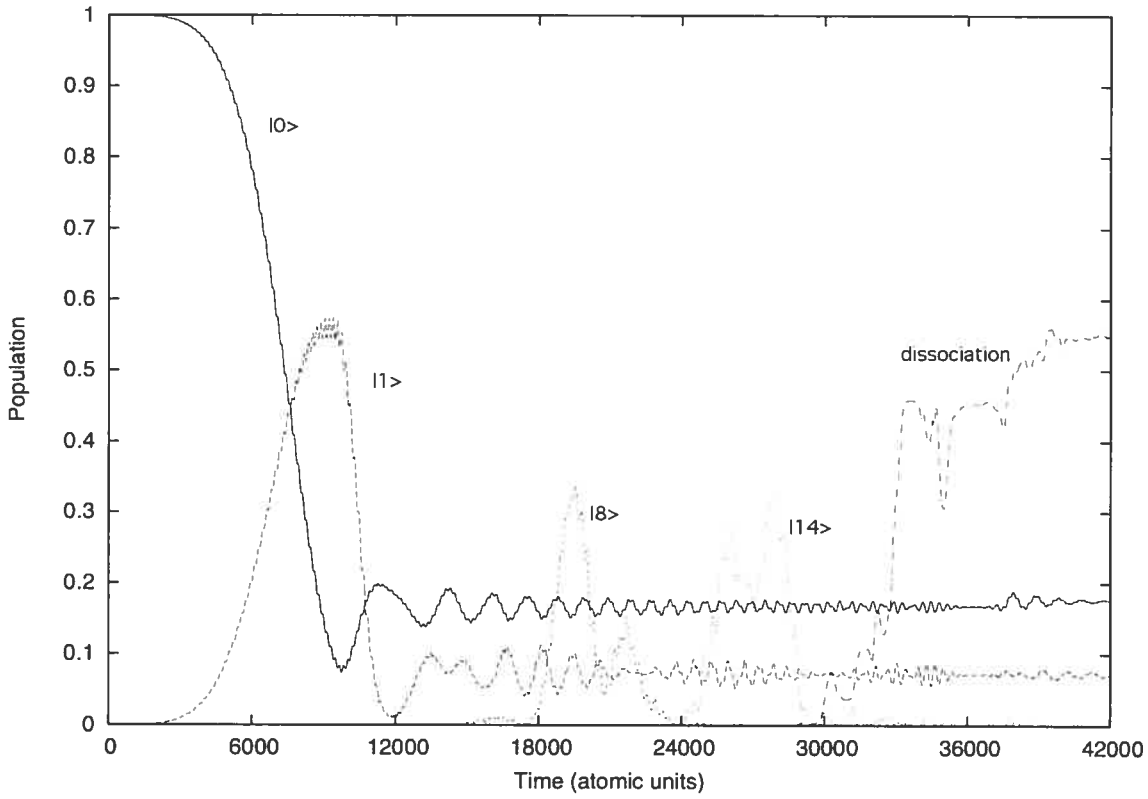

function: we set $\mu_1 = 0$ if $x > 10$ bohr. This has no effect on the populations (because the vibrational wavefunctions are all very small if $x > 10$ bohr) but it makes the dipole more physical and facilitates our calculations. The linear approximation is certainly reasonable close to $r = r_e$ but it is unphysical for large values of r. In addition, we used a 1024 point spatial grid from 0 to 65 bohr rather than the 2048 point grid employed by Chelkowski *et al.* as our goal is not to converge

populations to 10 digit accuracy but simply to demonstrate the efficiency of the new propagation schemes.

Figure 2.2: The same as figure 1 but for a laser field of intensity $I = 10^{12} W cm^{-1}$.

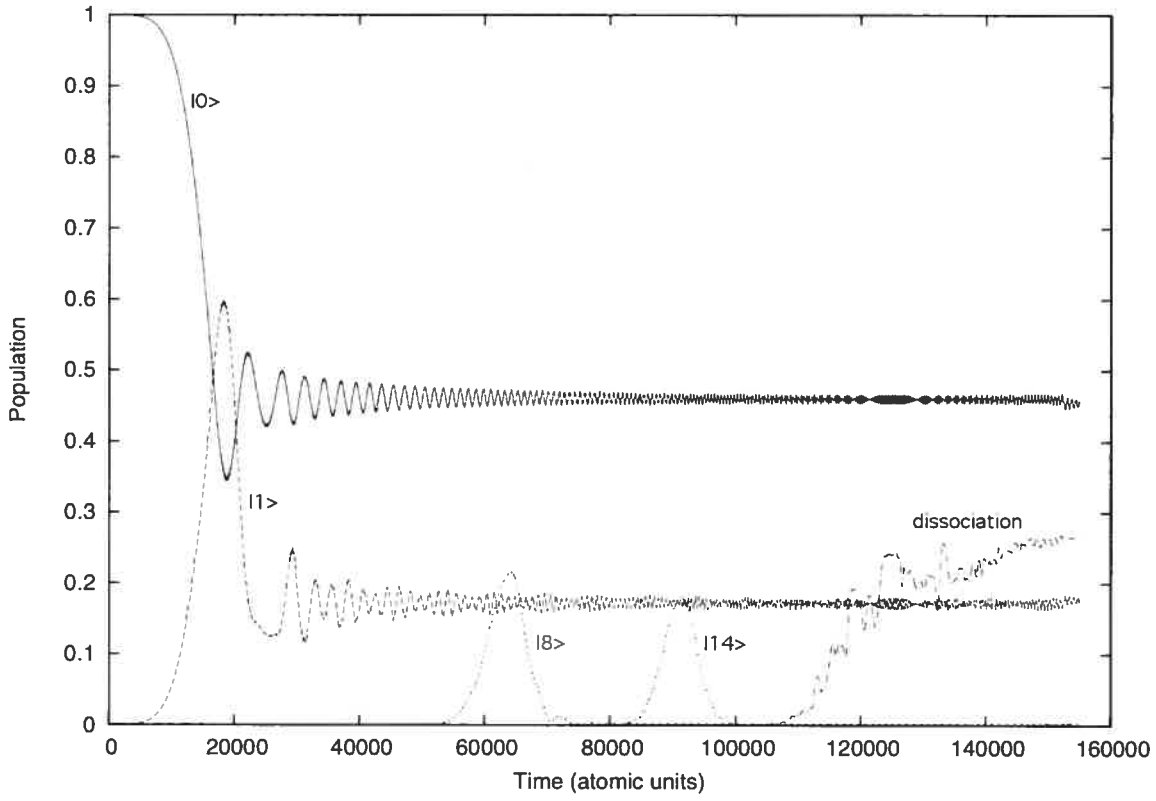

The field-free Hamiltonian,

$$\hat{H}_{ff} = K + D[1 - e^{-ax}]^2 \ , \tag{2.15}$$

is a natural choice for the preconditioner. It will be a better preconditioner for weaker fields. To calculate populations we need to compute eigenvectors of the field-free Hamiltonian. As the primary representation (the representation in which the wavefunction is propagated) we choose the basis of eigenvectors of $\mathbf{H_{ff}}$. To use the interaction representation Runge Kutta method one must evaluate matrix-vector products with $\mathbf{H_I}$. The three factors of $\mathbf{H_I}$ are applied sequentially. Matrix-

vector products with $e^{i\mathbf{H_0}t/\hbar}$ and $e^{-i\mathbf{H_0}t/\hbar}$ are trivial. Matrix-vector products for $\mathbf{H}-\mathbf{H_0}$ are done using

$$(\mathbf{H}-\mathbf{H_0})\mathbf{v} = -\mu_1 E_M U(t)\cos[\omega(t)t]\mathbf{T}^t\mathbf{x}\mathbf{T}\mathbf{v}\ , \tag{2.16}$$

where $\mathbf{T}$ is the matrix of eigenvectors of $\mathbf{H_{ff}}$ in a sine discrete variable representation (DVR) basis [43, 44] and $\mathbf{x}$ is a diagonal matrix whose diagonal elements are the DVR points. For a multidimensional problem one could choose a separable approximation for $\mathbf{H_{ff}}$ as the preconditioner. If the preconditioner were time dependent it would be necessary to diagonalise it at each time step and this would be costly. If we put $\mathbf{H_0} = \mathbf{H_{ff}}$ and do not truncate the dipole moment, $\mathbf{H}-\mathbf{H_0}$ is large when x is large and the preconditioner does not work as well.

In Table 2.1 we compare our strong field results with those obtained using the time slice strategy with the split operator method (time slicing with the SIL method is much less efficient than time slicing with the split operator method). We have used the split operator method with both the $[K, D[1-e^{-ax}]^2-\mu_1 x E_M U(t)\cos[\omega(t)t]]$ and the $[H_0, -\mu_1 x E_M U(t)\cos[\omega(t)t]]$ decompositions. The number of matrix-vector products required to obtain well-converged results is very similar in both cases. The results reported in Tables 2.1 and 2.2 are those obtained with the decomposition $[H_0, -\mu_1 x E_M U(t)\cos[\omega(t)t]]$. We use the $[H_0, -\mu_1 x E_M U(t)\cos[\omega(t)t]]$ decomposition in the basis of eigenvectors of $\mathbf{H_0}$ and compute the exponential of $\mu_1\mathbf{x}E_M U(t)\cos[\omega(t)t]$ using the eigenvectors of $\mathbf{H_0}$. Note that to propagate between $k\Delta T$ and $(k+1)\Delta T$ we use $e^{+i\Delta T\mu_1 x E_M U(t_m)\cos[\omega(t_m)t_m]/\hbar}$, where $t_m = \frac{k\Delta T+(k+1)\Delta T}{2}$, to approximate using the first term in the Magnus expansion. We choose to measure the cost of a RK propagation in terms of the number of $\mathbf{H_I}$ matrix-vector products and the cost of a split operator propagation in terms of the number of $e^{+i\Delta T\mu_1\mathbf{T^t}\mathbf{x}\mathbf{T}E_M U(t_m)\cos[\omega(t_m)t_m]/\hbar}$ matrix-vector products. Both involve transforming from the $\mathbf{H_0}$ eigenvector basis to the DVR, applying a diagonal operator, and trans-

Table 2.1: Comparison of costs for the dissociation of HF in a chirped LASER field of intensity $I = 10^{13} W cm^{-2}$. The initial wavefunction was propagated for 42000a.u.

Method	Successful steps	rejected steps	mtrx-vec
Split-operator	105000	-	105000
4th-order Runge-Kutta	200000	-	800000
preconditioned 4th-order Runge-Kutta	15000	-	60000
preconditioned 4th-order RK with step doubling	3818	44	23400
preconditioned embedded Fehlberg RK	2657	0	15943
preconditioned embedded Dormand-Prince RK	1977	19	11977

forming from the DVR to the $\mathbf{H_0}$ eigenvector basis. The number of matrix-vector products is given in the last column of the table. In all cases, the number of matrix-vector products is the number required to converge the dissociation probability at $t = 42000$ a.u. to within 5×10^{-5} of the exact result.

According to the results of Table 2.1, using RK4 in the Schroedinger representation is worse than time slicing and using the split operator method within each slice. A very small time step is required to achieve convergence with the RK4 method. This is due to the fact that the solution of the TDSE is highly oscillatory. RK4 routines are easy to program and good easily usable black-box codes are available but in the Schroedinger representation they are not efficient for most laser molecule problems. Preconditioning makes a huge difference: the preconditioned Runge-Kutta scheme (pRK4) is *more* efficient than the time sliced split operator method. Combining preconditioning with an adaptive step size algorithm yields an even more efficient method. The three adaptive step size methods (step doubling, Fehlberg and Dormand-Prince) are all very good. Dormand-Prince is about an order of magnitude better than the time sliced split operator method. The Fehlberg and Dormand-Prince embedded schemes are better than the step doubling method

because to obtain a step-doubling error estimate one must do two propagations (whose step sizes differ by a factor of two). The time-step convergence curve for

Figure 2.3: Convergence curves for the preconditioned fourth-order Runge-Kutta scheme without adaptive time steps (— —), for the split-operator technique (——) and for the Short Iterative Lanczos procedure (- - -) for HF in a chirped laser field of intensity $I = 10^{13} W cm^{-1}$.

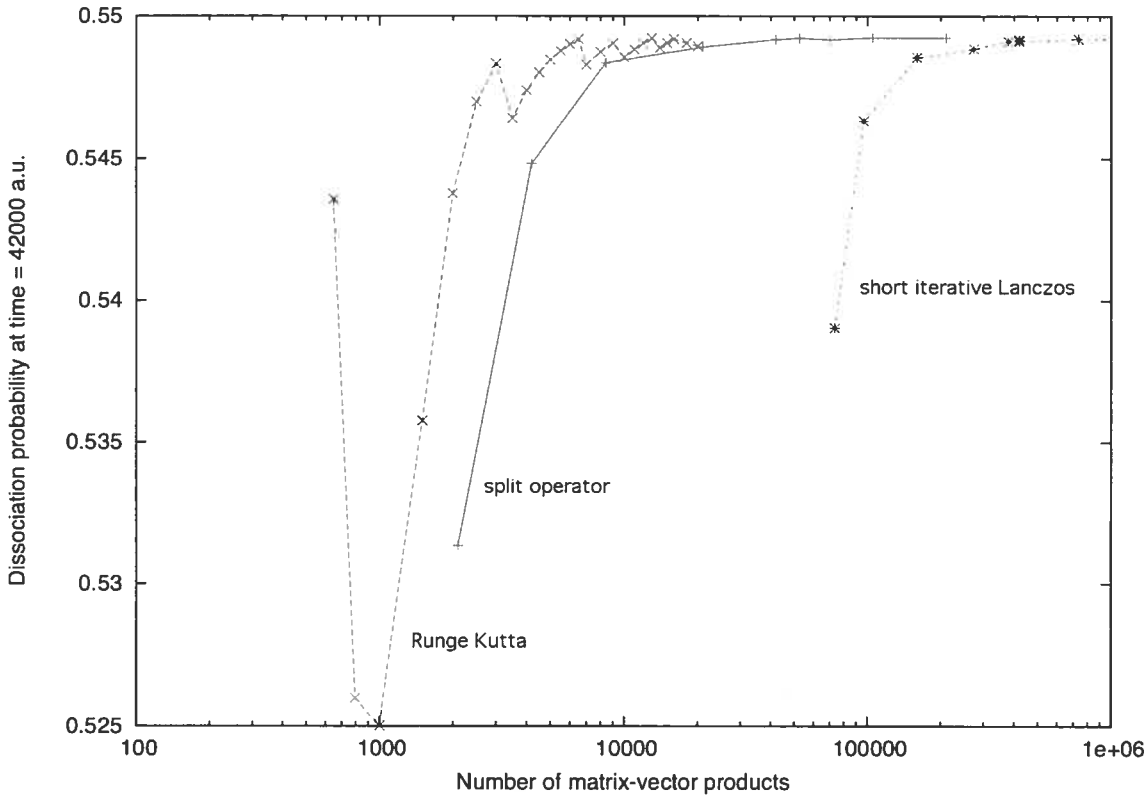

the SPO method is smooth but the curve for pRK4 oscillates; see figure 3. The amplitude of the oscillation decreases as the step size decreases.

The preconditioner we are using is good but it is not unrealistically good. The perturbation is quite large, due to the high intensity of the field. To precondition a time-dependent problem it is important to choose the preconditioner so that many of its eigenvalues are close to those of of the full Hamiltonian. In contrast, in the time-independent case it is possible to calculate a spectrum window by window and to choose a window-dependent preconditioner that is especially good

for one region of the spectrum. [22] The results of table 2.1 are computed with a preconditioner for which the ratio of the Frobenius norms of the perturbation and the total Hamiltonian is about 2 percent. The largest eigenvalue of the matrix is 0.0087081 a.u. Approximate Hamiltonian preconditioners of this quality can be obtained even for difficult problems. [45]

The local error for the time sliced split operator method is $O(\Delta T^2)$ (because the error is due to the slicing). The local error for the RK4 method is $O(\delta t^5)$. Although local error estimates are known, a global error estimate is difficult to obtain and it is therefore necessary to decrease ΔT and δt until the desired global accuracy is attained. We used a desired local error of 1×10^{-4} for the step-doubling scheme, 1×10^{-6} for the Fehlberg scheme, and 1×10^{-5} for the Dormand-Prince scheme. Another parameter that can influence the efficiency of the propagation is the size of the original time step. For the step-doubling and Fehlberg procedures, this parameter does not seem to play an important role. On the other hand, the number of matrix-vector products required with the Dormand-Prince procedure does significantly depend on the choice of the first step length. We have made no attempt to "optimize" the first step length but have observed that the number of matrix-vector products can be reduced from 11977 (reported in table 2.1) to 7243 by changing the initial step length. The initial step length we use is determined by taking a tenth of the maximum allowed time step, which is a tenth of the propagation interval.

We have done a similar set of calculations for the weak field case. The results are presented in Table 2.2. In general terms the relative efficiencies of the methods are similar in the weak- and strong-field cases. The weak field unpreconditioned to preconditioned ratio is larger than its strong-field counterpart. This is simply due to the fact that the weak-field preconditioner is better. Because the preconditioner is so good, the solution of the preconditioned problem is very smooth and switching from a fixed time step method to a variable time step method reduces the number

Table 2.2: Comparison of costs for the dissociation of HF in a chirped laser field of intensity $I = 10^{12} W cm^{-2}$. The initial wavefunction was propagated for 155000a.u.

Method	Successful steps	rejected steps	mtrx-vec
Split-operator	275000	-	275000
preconditioned 4th-order Runge-Kutta	24000	-	96000
preconditioned 4th-order RK with step doubling	11694	83	71100
preconditioned embedded Fehlberg RK	8116	0	48697
preconditioned embedded Dormand-Prince RK	6553	24	39463

of time steps less than in the high-field case. All the adaptive step size methods reduce the number of matrix-vector products somewhat and again the Dormand-Prince option is the most efficient (a factor of seven better than the time sliced split operator method). In both the strong- and weak-field cases with the Runge-Kutta-Fehlberg algorithm there are no rejected steps. This implies that s in the error estimate equation could be increased.

It is also interesting to compare the efficiencies of the time sliced split operator method and the RK4 methods when less accuracy is required. We have therefore done calculations to converge the strong-field dissociation probability to 10^{-3}. With the time sliced split operator method it was necessary to do 23000 matrix-vector products (or time steps); with the Dormand-Prince RK method and a desired local error of 3×10^{-4} 5839 matrix-vector products are required; with the Fehlberg RK method and a desired local error of 10^{-4} only 4567 matrix-vector products are required.

Without preconditioning the RK4 methods are poor. It is important to have some indication of how sensitive the preconditioned RK4 methods are to the quality of the preconditioner. In the strong field case preconditioning reduces the number of required matrix-vector products by a factor of about 13. The intensity of the

laser field is already fairly large but one might wonder what would happen if it were even larger. Another way to make the preconditioner poorer is to use a poor approximation for H_{ff} as the preconditioner.

How poor does the preconditioner have to be before the time sliced split operator method is better than the preconditioned RK4 methods? In figure 4 we show the number of required Dormand-Prince matrix-vector products as a function of the magnitude of the largest eigenvalue of $\frac{H_I}{\hbar}$ for the strong field case. In these calculations $\hat{H}_0 = K + \frac{D}{\sqrt{\alpha}}[1 - e^{-\alpha a x}]^2$, a Morse oscillator Hamiltonian with the same frequency as the Morse Hamiltonian that is H_{ff}. Increasing α increases the anharmonicity of the Morse potential without changing its frequency. The quality

Figure 2.4: Effect of the quality of the preconditioner on the efficiency of the preconditioned Runge-Kutta-Dormand-Prince method.

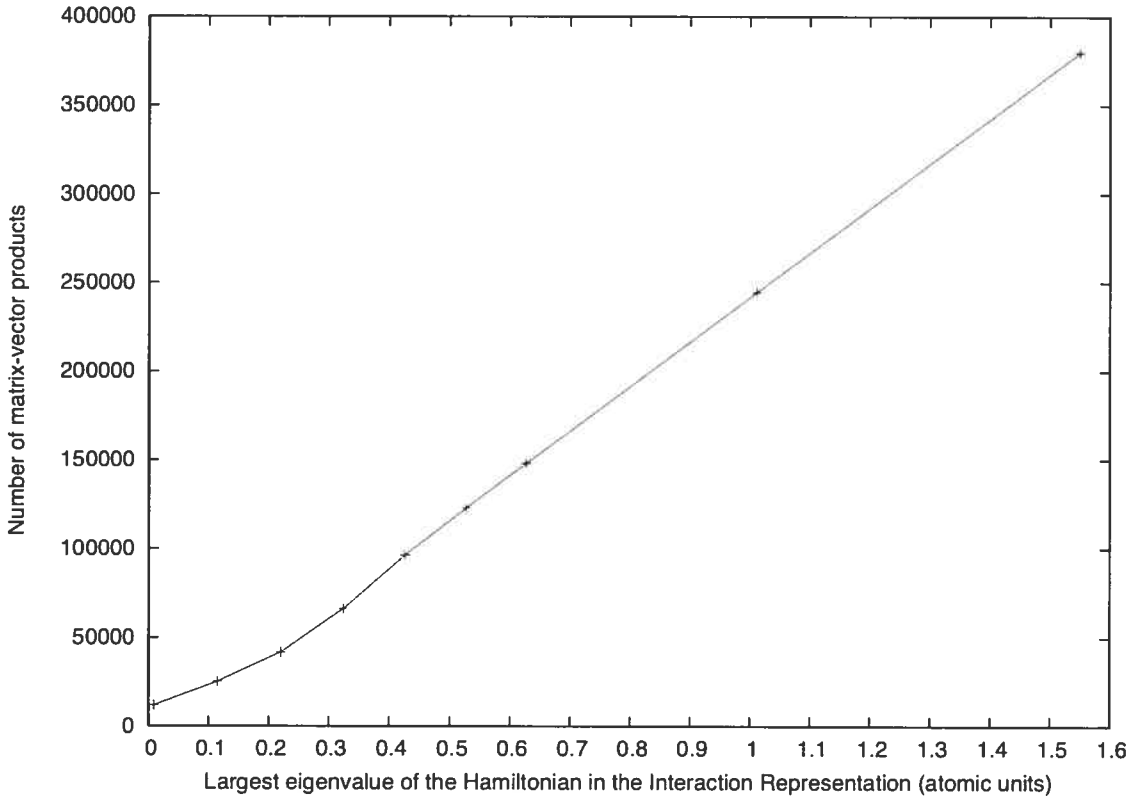

of this preconditioner is reasonably good for the whole spectrum. The number of

matrix-vector products increases approximately linearly with the magnitude of the largest eigenvalue of $\mathbf{H_I}/\hbar$. The time sliced split operator technique becomes more efficient if the largest eigenvalue of $\mathbf{H_I}/\hbar$ is greater than 0.46 a.u. This corresponds to a poor preconditioner. Effective preconditioners for molecular problems exist and we therefore believe that preconditioned adaptive step size RK4 methods should, for many important problems, be more efficient than time sliced methods.

2.4 Conclusion

Most propagation methods for time-dependent Hamiltonians can be classified as either time sliced methods, for which matrix exponential approximations are used within each slice, or RK-type methods that use local series approximations to determine a solution step by step. The time slice methods are more popular. They have the advantage that they enable use of familiar matrix exponential approximations (e.g., split operator, SIL, Chebyshev etc.) that are used if the Hamiltonian is time-independent. In this paper we point out that although RK-type methods are less efficient if no preconditioning is used, they are more efficient if preconditioning is used. As it is true that for many molecular problems a good preconditioner is available, preconditioned RK methods should be considered seriously. When the preconditioned RK method is combined with a variable step size algorithm a very efficient propagation method is obtained. In the strong-field case the preconditioned variable step size RK method is almost an order of magnitude better than the time sliced method. Note that using the SIL or Chebyshev method to propagate within each time slice cannot improve the efficiency of time-sliced method (because the size of the ΔT slices must be small to achieve good accuracy). We find that the quality of the preconditioner required to achieve superior performance is good but not unrealistically good.

To be sure that we thoroughly understand how the methods work we have

written our own Runge-Kutta codes but there is no reason not to use black-box RK codes. This is easy to do and at every step we have compared our codes to black-box programs. Even in the interaction representation it is very easy to use a black-box RK code, with or without the adaptive step size refinement. It is only necessary to couple the black-box program to an interaction representation Hamiltonian matrix-vector product routine. Although there is a tendency to think that time sliced methods are simple nothing could be simpler than using a black-box RK program. It is quite possible that other adaptive step size RK-type methods (perhaps the 8^{th}-order Dormand-Prince) used with preconditioning might be even more efficient.

Acknowledgements

This work has been supported by the Natural Sciences and Engineering Research Council of Canada (NSERC). We thank Martin Gander for useful discussions.

Bibliography

[1] A. Askar and A. S. Cakmak. Explicit integration method for the time-dependent Schrödinger equation for collision problems. *J. Chem. Phys.*, 68:2794, 1978.

[2] M.D. Feit and J.A. Fleck. Wave packet dynamics and chaos in the hénon-heiles system. *J. Chem. Phys.*, 80:2578, 1984.

[3] H. Tal-Ezer and R. Kosloff. An accurate and efficient scheme for propagating the time dependent Schrödinger equation. *J. Chem. Phys.*, 81:3967, 1984.

[4] T.J. Park and J.C. Light. Unitary quantum time evolution by iterative Lanczos reduction. *J. Chem. Phys.*, 85:5870, 1986.

[5] R. Kosloff. Propagation methods for quantum molecular dynamics. *Annu. Rev. Chem. Phys.*, 45:145, 1994.

[6] C. Leforestier, R. Bisseling, C. Cerjan, M.D. Feit, R. Friesner, A. Guldberg, A. Hammerich, W. Jolicard, G. Karrlein, H.-D. Meyer, N. Lipkin, O. Roncero, and R. Kosloff. A comparison of different propagation schemes for the time dependent Schrödinger equation. *J. Comp. Phys.*, 94:59, 1991.

[7] R. Kosloff. Time-dependent quantum-mechanical methods for molecular dynamics. *J. Phys. Chem.*, 92:2087, 1988.

[8] J. Z. H. Zhang. *Theory and Application of Quantum Molecular Dynamics.* World Scientific Publishing Company, 1998.

[9] H. Köppel, W. Domcke, and L. S. Cederbaum. Multimode molecular dynamics beyond the Born-Oppenheimer approximation. *Adv. Chem. Phys.*, 57:59, 1984.

[10] C. Iung and C. Leforestier. Accurate determination of a potential energy surface for CD_3H. *J. Chem. Phys.*, 90:3198, 1989.

[11] R. E. Wyatt. RRGM, recursive residue generation method. *Adv. Chem. Phys.*, 73:231, 1989.

[12] A. McNichols and T. Carrington Jr. Vibrational energy levels of formaldehyde calculated from an internal coordinate Hamiltonian using the Lanczos algorithm. *Chem. Phys. Lett.*, 202:464, 1993.

[13] M. J. Bramley and T. Carrington Jr. A general discrete variable method to calculate vibrational energy levels of three- and four-atom molecules. *J. Chem. Phys.*, 99:8519, 1993.

[14] M. R. Wall and D. Neuhauser. Extraction, through filter-diagonalization, of general quantum eigenvalues or classical normal mode frequencies from a small number of residues or a short-time segment of a signal. I. theory and application to a quantum-dynamics model. *J. Chem. Phys.*, 102:8011, 1995.

[15] V. A. Mandelshtam and H. S. Taylor. A low-storage filter diagonalization method for quantum eigenenergy calculation or for spectral analysis of time signals. *J. Chem. Phys.*, 106:5085, 1997.

[16] H.-G. Yu and S. C. Smith. The calculation of vibrational eigenstates by MINRES filter diagonalization. *Ber. Bunsenges Phys. Chem.*, 101:400, 1997.

[17] S. Y. Lin and H. Guo. Quantum wave packet study of reactive and inelastic scattering between $C(^1D)$ and H_2. *J. Chem. Phys.*, 119:11602, 2003.

[18] S. Y. Lin and H. Guo. Full-dimensional quantum wave packet study of rotationally inelastic transitions in $H_2 + H_2$ collision. *J. Chem. Phys.*, 117:5183, 2002.

[19] T. Seideman. A new method for the calculation of photodissociation cross sections. *J. Chem. Phys.*, 98:1989, 1993.

[20] Y. Saad. *Iterative methods for sparse linear systems.* Society for Industrial and Applied Mathematics, Philadelphia, 2003.

[21] S.-W. Huang and T. Carrington Jr. A new iterative method for calculating energy levels and wave functions. *J. Chem. Phys.*, 112:8765, 2000.

[22] B. Poirier and T. Carrington Jr. Accelerating the calculation of energy levels and wave functions using an efficient preconditioner with the inexact spectral transform method. *J. Chem. Phys.*, 114:9254, 2001.

[23] W. Warren, H. Rabitz, and M. Dahleh. Coherent control of quantum dynamics: The dream is alive. *Science*, 259:1581, 1993.

[24] W. H. Press, S. A. S.A. Teukolsky, W. T. Vetterling, and B. P. Flannery. *Numerical Recipes in FORTRAN 77 The Art of Scientific Programming.* Cambridge University Press, 1986.

[25] W. Magnus. On the exponential solution of differential equations for a linear operator. *Commun. Pure Appl. Math.*, 7:649, 1954.

[26] P. Pechukas and J. C. Light. On the exponential form of time-displacement operators in quantum mechanics. *J. Chem. Phys.*, 44:3897, 1966.

[27] S. K. Gray and J. M. Verosky. Classical Hamiltonian structures in wave packet dynamics. *J. Chem. Phys.*, 100:5011, 1994.

[28] S. K. Gray and D. E. Manolopoulos. Symplectic integrators tailored to the time-dependent Schrödinger equation. *J. Chem. Phys.*, 104:7099, 1996.

[29] D. E. Manolopoulos and S. K. Gray. Symplectic integrators for the multichannel Schrödinger equation. *J. Chem. Phys.*, 102:9214, 1995.

[30] J. M. Sanz-Serna and A. Portillo. Classical numerical integrators for wavepacket dynamics. *J. Chem. Phys.*, 104:2349, 1996.

[31] J. Z. H. Zhang. New method in time-dependent quantum scattering theory: Integrating the wave function in the interaction picture. *J. Chem. Phys.*, 92:324, 1990.

[32] J. Z. H. Zhang. Multichannel quantum wave packet propagation in the interaction picture: application to gas-surface scattering. *Comp. Phys. Comm.*, 63:28, 1991.

[33] S. Das and D. J. Tannor. Time dependent quantum mechanics using picosecond time steps: Application to predissociation of HeI_2. *J. Chem. Phys.*, 92:3403, 1990.

[34] Y. Shi and D. J. Tannor. Symmetry adapted Fourier solution of the time-dependent Schrödinger equation. *J. Chem. Phys.*, 92:2517, 1990.

[35] C. J. Williams, J. Qian, and D. J. Tannor. Dynamics of triatomic photodissociation in the interaction representation. I. methodology. *J. Chem. Phys.*, 95:1721, 1991.

[36] D. J. Tannor, A. Besprozvannaya, and C. J. Williams. Nested interaction representations in time dependent quantum mechanics. *J. Chem. Phys.*, 96:2998, 1992.

[37] P. Castillo and Y. Saad. Preconditioning the matrix exponential operator with applications. *J. of Sci. Computing*, 13:275, 1998.

[38] M. Quack and E. Sutcliffe. On the validity of the quasiresonant approximation for molecular infrared-multiphoton excitation. *J. Chem. Phys.*, 83:3805, 1985.

[39] M. Quack and J. Stohner. Femtosecond quantum dynamics of functional groups under coherent infrared multiphoton excitation as derived from the analysis of high-resolution spectra. *J. Phys. Chem.*, 97:12574, 1993.

[40] U. M. Ascher and L. R. Petzold. *Computer Methods for Ordinary Differential Equations and Differential-Agebraic Equations.* Society for Industrial and Applied Mathematics, Philadelphia, 1998.

[41] S. Chelkowski, A. D. Bandrauk, and P. B. Corkum. Efficient molecular dissociation by a chirped ultrashort infrared laser pulse. *Phys. Rev. Lett.*, 65:2355, 1990.

[42] J. D. Farnum and D. A. Mazziotti. Spectral difference Lanczos method for efficient time propagation in quantum control theory. *J. Chem. Phys.*, 120:5962, 2004.

[43] D. T. Colbert and W. H. Miller. A novel discrete variable representation for quantum mechanical reactive scattering via the S-matrix Kohn method. *J. Chem. Phys.*, 96:1982, 1992.

[44] J. C. Light and T. Carrington Jr. Discrete variable representations and their utilization. *Adv. Chem. Phys.*, 114:263, 2000.

[45] B. Poirier. Efficient preconditioning scheme for block partitioned matrices with structured sparsity. *Numer. Linear Algebra Appl.*, 7:715, 2000.

CHAPITRE 3

DE LA CARACTÉRISATION DES ÉTATS MÉTASTABLES DU SYSTÈME ACÉTYLÈNE-VINYLIDÈNE

Dans cette section, on présente une étude de la réaction d'isomérisation du système acétylène-vinylidène. L'article a été soumis à la revue "Journal of Chemical Physics" le 30 mai 2006 et accepté le 26 juin 2006. L'article est paru en version électronique le 5 septembre 2006.

Calculating vibrational energies and wavefunctions of vinylidene using a contracted basis with a locally re-orthogonalized coupled two-term Lanczos eigensolver

Jean Christophe Tremblay[1] and Tucker Carrington Jr.[2]

Département de chimie, Université de Montréal,

C.P. 6128, succursale Centre-ville, Montréal (Québec) H3C 3J7, Canada

Abstract

We use a contracted basis + Lanczos eigensolver approach to compute vinylidene-like vibrational states of the acetylene-vinylidene system. To overcome problems caused by loss of orthogonality of the Lanczos vectors we re-orthogonalize Lanczos vector and use a coupled two-term approach. The calculations are done in CC-HH diatom-diatom Jacobi coordinates which make it easy to compute states one irreducible representation at a time. The most costly parts of the calculation are parallelized and scale well. We estimate that the vinylidene energies we compute are converged to $\sim 1\text{cm}^{-1}$.

[redacted] Fax: 514-343-7586

3.1 Introduction

The vinylidene/acetylene system has intrigued scientists for many years. [1–7] Quantum chemistry calculations indicate that there is a shallow vinylidene well at high energies. [2, 3, 8–10] Is the vinylidene well deep enough and are the barriers separating it from acetylene-like geometries high and broad enough that it is legitimate to think of vinylidene as being a reactive intermediate? What consequences does the existence of the vinylidene well have for spectroscopic studies of C_2H_2? Are there high-lying levels of C_2H_2 that may be described as vinylidene-like?

In this paper we report calculations of highly excited states of C_2H_2 that have significant vinylidene character. We use a contracted basis designed to favor the convergence of vinylidene-like states and an iterative method to compute energies and wavefunctions. We confirm that vinylidene-like states do exist, but find that some of them are not well localized in the vinylidene well. Many previous calculations have been done. In Ref. [5] a multidimensional approximate Feshbach approach was used to compute vinylidene "lifetimes". The vinylidene-acetylene system is of course bound and has stationary states. Nonetheless, a linear combination of vinylidene-like states prepared by an experiment will evolve and it is the lifetime associated with this process that is referred to. Zou, Bowman, and Brown (ZBB) were the first to compute vinylidene-like states in six dimensions (6D). [11, 12] They convincingly showed that vinylidene-like states do exist, but the degree of localization of some of these states was in doubt because the computational methods they employed did not enable them to use very large basis sets. Kozin, Law, Tennyson, and Hutson (KLTH) have also done 6D calculations. [13] They found vinylidene-like states and speculated that some of the vinylidene-like states identified by ZBB might de-localize if the basis size is increased.

Both ZBB and KLTH used direct linear algebra methods to compute high-lying vibrational states. Straightforward use of such methods requires storing in memory

the matrix whose eigenvalues and eigenvectors are to be computed. This limits the size of the matrix one can use to about 50'000. The largest basis size used by ZBB is 33'840 and most of their vinylidene-like states were computed with a basis with only 21'600 functions. KLTH included more acetylene-like basis functions than did ZBB but they clearly explain that the accuracy of their vinylidene-like states is limited by fact that they discard basis functions that are probably important. They also suspect that one of their primitive one dimensional (1D) primitive basis sets is too small. Using modern methods and computers it is relatively straightforward to compute vibrational levels up to $\sim 13000\text{cm}^{-1}$ above the zero point energy. Even ro-vibrational calculations of low-lying levels were reported more than a decade ago. [14] However, computing high-lying levels of C_2H_2 requires a very large basis. This is due to the large amplitude motions of the atoms and to the importance of coupling. Some coordinate choices are better than others but coupling is important for all. Coordinates that make exploiting symmetry simple are not the least coupled.

Iterative methods are often used to alleviate the difficulty of using huge basis sets. [15–24] More than ten years ago the Lanczos algorithm was employed with basis sets of about a million functions to compute vibrational levels of a four-atom molecule. [19] It might therefore seem as if it should be easy to use Lanczos to compute vinylidene-like states. Previous direct diagonalization calculations used far fewer than a million functions. [12, 13] Nevertheless, using Lanczos to compute vinylidene-like states is not easy for two reasons. First, although Lanczos calculations with a direct product basis are simple, employing the Lanczos algorithm with a contracted basis is harder. The direct product basis required to converge vinylidene-like states would be much larger than the basis sets of ZBB and KLTH. Second, the density of states at energies at which vinylidene-like states occur is very large and the cost of a Lanczos calculation depends on the number of matrix-vector products required to converge the desired energy levels which in turn depends

on the density of states. [25] The first difficulty is overcome by using an efficient contracted iterative method similar to those suggested by Wang and Carrington and by Yu. [26–28] The number of required matrix-vector products depends not only on the density of states but also on the spectral range of the Hamiltonian matrix. The spectral range of the contracted-basis matrix is significantly smaller than its product-basis counterpart. Using a contracted basis therefore decreases the required number of matrix-vector products. To reduce problems caused by the density of states we use a coupled two-term Lanczos algorithm [29, 30] and local re-orthogonalization. [31] Details of the computational approach are presented in the next section.

3.2 Computational Method

It is only by means of basis set methods that one can compute high-lying levels and their associated wavefunctions. Because the size of the Hamiltonian matrix is often huge computing eigenvalues and eigenvectors of a large matrix is a difficult part of any such calculation. To obviate the need to store Hamiltonian matrices we use a Lanczos algorithm. As direct product functions would be poor we employ a contracted iterative method (see section II B). Our coordinate choice is explained in section II A. We use the *ab initio* potential of Zou and Bowman. [10] It appears to describe the vinylidene region quite well. A good potential is critical: without one it is obviously impossible to study the vinylidene-like states. Preliminary calculations, on a potential adjusted by Xu, Guo, Zou, and Bowman to reproduce better the experimental acetylene vibrational energy levels, indicate the vinylidene-like levels it supports are very close to those of the *ab initio* potential of Zou and Bowman. [32]

3.2.1 Coordinate system

The best coordinates would both minimize coupling and facilitate exploiting symmetry. For the acetylene-vinylidene system we would like to choose coordinates so that low-energy isomerization paths on the potential surface involve changing as few coordinates as possible. Motion along coordinates whose values at the acetylene and vinylidene geometries are similar will be small amplitude and the corresponding 1D basis sizes will be small. In general, large amplitude coordinates will require larger 1D basis sets. Important coupling also increases the size of the required 1D bases. Orthogonal satellite coordinates seem to minimize coupling. They consist of a R_{CC} distance, distances between the two H atoms and a canonical point and the associated angles. [33] All of the stretch coordinates and the dihedral angle exhibit small amplitude motion. KLTH use these coordinates. They were also used by Schork and Köppel. [34] We did some preliminary calculations using these coordinates and found that the bend basis needed to obtain convergence was quite large. The results presented below were all obtained using the CC-HH diatom-diatom Jacobi coordinates[1] suggested by Zou and Bowman. [35] The required bend basis is smaller. The CC-HH coordinates are r_{CC}, r_{HH}, the inter center of mass distance, R, and the associated angles, θ_1, θ_2, ϕ. At the acetylene geometry $R = 0$ and at the vinylidene geometry R is slightly larger than 2Å. r_{HH} is much smaller at the vinylidene geometry ($\sim$ 3.5Å) than at the acetylene geometry ($\sim$ 6.3Å). The biggest drawback of these coordinates is the fact that R, r_{HH}, θ_1, and θ_2 have large accessible domains and are strongly coupled. To deal with this coupling we use contracted basis functions. The most important advantage of the CC-HH coordinates is that they make symmetry exploitation trivial. When using an iterative method it is important to be able to exploit symmetry because doing so reduces the number of matrix-vector products required to converge levels. There are

[1] voir l'annexe I

two well-established ways of taking advantage of symmetry: either one uses a basis of symmetry adapted functions or the symmetry adapted Lanczos method (SAL) [36,37] with a basis whose functions do not transform like irreducible representation s. If a symmetry adapted basis is used not only does one reduce the number of matrix-vector products but one also decreases the size of the vectors which must be stored. It is common to use the SAL with full-length vectors. [24, 28, 38] The CC-HH coordinates have the important advantage that 6D basis functions that are products of functions of the 6 coordinates transform like irreducible representation s – no symmetry adaptation is necessary. This was realized and exploited by

Table 3.1: Effect of the symmetry operations of the $G8$ group on the *CC-HH* Jacobi coordinates and on the primitive angular basis functions.

Operation	$\{r_{HH}, r_{CC}, R, \theta_1, \theta_2, \phi\}$	$\|l_1, l_2, m_2\rangle$
E*	$\{r_{HH}, r_{CC}, R, \theta_1, \theta_2, -\phi\}$	$\|l_1, l_2, -m_2\rangle$
P_{HH}	$\{r_{HH}, r_{CC}, R, \pi - \theta_1, \theta_2, \phi + \pi\}$	$(-1)^{l_1}\|l_1, l_2, m_2\rangle$
P_{CC}	$\{r_{HH}, r_{CC}, R, \theta_1, \pi - \theta_2, \phi + \pi\}$	$(-1)^{l_2}\|l_1, l_2, m_2\rangle$

ZBB. [11, 12, 35] In this paper we exploit this simplicity with an iterative method. By computing levels for only a single irreducible representation we take advantage of the fact that the density of states of a matrix for a single irreducible representation is much smaller than the full density of states. The density of states in the vinylidene region of the spectrum is high enough that this advantage is important. The complete nuclear permutation and inversion group of C_2H_2 is $G8$. In table 3.1 we show the effect of the symmetry operations on the coordinates and primitive basis functions (see the next subsection).

The CC-HH coordinates have the disadvantage that they make it very hard to compute acetylene-like states. The kinetic energy operator singularity at $R = 0$ will significantly retard the converge of acetylene-like states. As our goal is to study the vinylidene-like states, and we bias our basis to favor the convergence of the vinylidene-like states, this is not an important problem.

3.2.2 Contracted-iterative procedure

It is clear that direct product bases are inefficient and contracted basis functions have therefore been used for many years. [39–45] All commonly used contraction schemes involve dividing coordinates into groups and solving sub-problems. "Optimally" contracted functions are obtained by computing eigenfunctions of reduced-dimension Hamiltonians, for one set of coordinates, labelled by basis labels for the other set of coordinates. KLTH use this sort of contraction scheme. The Bačić-Light ray eigenvector method [46] is a contraction scheme of this kind – for each bend discrete variable representation (DVR) [47, 48] index eigenvectors of a reduced dimension stretch Hamiltonian matrix are computed. "Simply" contracted functions are products of eigenfunctions sub-Hamiltonians. The sub-Hamiltonians are not labelled by basis labels for other coordinates. Wang and Carrington [26], Yu [27], and Bramley and Carrington [49] (who introduced the terms optimally and simply) have emphasized that the simply contracted scheme can be coupled efficiently with the Lanczos algorithm. The final contracted basis has an easily exploitable product structure. A key advantage of this sort of approach is that it obviates the need to solve a large number of reduced-dimension problems. Wang and Carrington use contracted functions for two groups of coordinates whereas Yu uses contracted functions for one group and uncontracted functions for the other group. In this paper we use a contraction procedure similar to Yu's.

One of the most important advantages of using the Lanczos algorithm with contracted basis functions is that the contracted basis reduces the *number* of matrix-vector products required to obtain converged energy levels. The rate of convergence (Lanczos convergence not basis set convergence) of an energy level depends on the energy gaps between it and its neighbors relative to the spectral range of the matrix. [25] Using contracted functions significantly reduces the spectral range and therefore accelerates convergence.

The contracted basis we use is very similar to that of ZBB. They use it with a direct eigensolver, whereas we use it with Lanczos. Using it with Lanczos enables us to take a much larger basis. The vibrational Hamiltonian in the CC-HH Jacobi coordinates is

$$\begin{aligned}\hat{H} = & \frac{-\hbar^2}{2\mu_{r_{HH}} r_{HH}^2}\left(\frac{\partial^2}{\partial\theta_1^2} + \cot\theta_1\frac{\partial}{\partial\theta_1} - \frac{1}{\sin\theta_1{}^2}l_{2z}^2\right) + \frac{\hbar^2}{2\mu_{r_{CC}} r_{CC}^2}l_2^2 \\ & + \frac{\hbar^2}{2\mu_R R^2}\left[l_2^2 - 2l_{2z}^2 - \left(\frac{\partial^2}{\partial\theta_1^2} + \cot\theta_1\frac{\partial}{\partial\theta_1} - \frac{1}{\sin\theta_1{}^2}l_{2z}^2\right)\right. \\ & \left. + l_{2-}\left(\frac{\partial}{\partial\theta_1} + \cot\theta_1 l_{2z}\right) + l_{2+}\left(\frac{-\partial}{\partial\theta_1} + \cot\theta_1 l_{2z}\right)\right] \\ & - \frac{\hbar^2}{2\mu_{r_{HH}}}\frac{\partial^2}{\partial r_{HH}^2} - \frac{\hbar^2}{2\mu_{r_{CC}}}\frac{\partial^2}{\partial r_{CC}^2} - \frac{\hbar^2}{2\mu_R}\frac{\partial^2}{\partial R^2} + V(r_{HH}, r_{CC}, R, \theta_1, \theta_2, \phi) \quad .\end{aligned} \tag{3.1}$$

where l_2^2, l_{2z}, l_{2+} and l_{2-} are angular momentum operators in terms of θ_2 and ϕ. [50] The reduced masses are defined elsewhere. [19,26,33,51] The basis functions we use are products of 4D contracted functions, 1D functions of r_{HH}, and 1D functions of r_{CC}. The 4D contracted functions are eigenfunctions of

$$\hat{H}_{4D} = T_{ang} - \frac{\hbar^2}{2\mu_R}\frac{\partial^2}{\partial R^2} + V_{4D}(R, \theta_1, \theta_2, \phi) \quad , \tag{3.2}$$

with

$$\begin{aligned}T_{ang} = & \frac{-\hbar^2}{2\mu_{r_{HH}} r_{HH;viny}^2}\left(\frac{\partial^2}{\partial\theta_1^2} + \cot\theta_1\frac{\partial}{\partial\theta_1} - \frac{1}{\sin\theta_1{}^2}l_{2z}^2\right) + \frac{\hbar^2}{2\mu_{r_{CC}} r_{CC;viny}^2}l_2^2 \\ & + \frac{\hbar^2}{2\mu_R R^2}\left[l_2^2 - 2l_{2z}^2 - \left(\frac{\partial^2}{\partial\theta_1^2} + \cot\theta_1\frac{\partial}{\partial\theta_1} - \frac{1}{\sin\theta_1{}^2}l_{2z}^2\right)\right. \\ & \left. + l_{2-}\left(\frac{\partial}{\partial\theta_1} + \cot\theta_1 l_{2z}\right) + l_{2+}\left(\frac{-\partial}{\partial\theta_1} + \cot\theta_1 l_{2z}\right)\right]\end{aligned} \tag{3.3}$$

where $V_{4D}(R, \theta_1, \theta_2, \phi)$ is determined by finding, for each set of $(R, \theta_1, \theta_2, \phi)$ coordinates, the values of r_{HH} and r_{CC} that minimize the potential. In the kinetic energy operator r_{HH} and r_{CC} have been set equal to the values they take at the vinyli-

dene geometry. Due to this choice, some of the 4D basis functions have significant amplitude in the vinylidene well. It is, however, also important that $\hat{H}_{4D}$ have eigenfunctions with significant amplitude and oscillatory structure in the acetylene region. The $\hat{H}_{4D}$ we use is the same as that of ZBB. It is a good 4D model of the isomerization. Because r_{HH} is quite different in vinylidene and acetylene coupling between the 6D basis functions is significant.

The eigenfunctions of $\hat{H}_{4D}$ are computed in a primitive basis composed of products of sine-DVR functions [52, 53] and parity adapted angular functions. The parity adapted functions are

$$u^P_{l_1,l_2,m_2}(\theta_1,\theta_2,\phi) = \frac{1}{2\sqrt{\pi(1+\delta_{m_2,0})}} \left(\Theta^{m_2}_{l_1}(\pi-\theta_1)\Theta^{m_2}_{l_2}(\theta_2)e^{im_2\phi} + (-1)^P\Theta^{-m_2}_{l_1}(\pi-\theta_1)\Theta^{-m_2}_{l_2}(\theta_2)e^{-im_2\phi}\right) \tag{3.4}$$

where $\Theta^{m_2}_l(\theta)$ is a normalized associated Legendre polynomials with the Condon-Shortley phase convention. [26] The eigenfunctions of $\hat{H}_{4D}$ are represented as

$$\psi^P_i = \sum_{\gamma,l_1,l_2,m_2} C^{(i)}_{\gamma,l_1,l_2,m_2}\Phi_\gamma(R)u^P_{l_1,l_2,m_2}(\theta_1,\theta_2,\phi) \quad . \tag{3.5}$$

The $\Phi_\gamma(R)$ are sine-DVR functions. We retain only N_{4D} 4D functions (see section IV) The effect of all symmetry operations of the $G8$ group on the primitive basis functions is easy to determine because the operations affect the coordinates in a simple fashion (See Table 3.1). [54] The evenness and oddness of l_1 and l_2 determine how a primitive basis function transforms. Eigenvalues and eigenvectors of the matrix representation of $\hat{H}_{4D}$ are computed using a coupled two-term Lanczos algorithm (see the next subsection). Matrix-vector products for the kinetic terms are simple because the matrices representing the angular momentum operators are banded and well known. [26, 50, 51] Matrix-vector products for V_{4D} are done by using Gauss quadrature for integrals over θ_1, θ_2, ϕ and doing sums sequentially in

the standard fashion. [23,26,55] The matrix-vector product is done in parallel. The 4D Hamiltonian matrix elements are

$$\begin{aligned}\langle\gamma' l_1' l_2' m_2'|\hat{H}_{4D}|\gamma l_1 l_2 m_2\rangle &= \langle\gamma' l_1' l_2' m_2'|T_{ang}|\gamma l_1 l_2 m_2\rangle\delta_{\gamma'\gamma} \\ &+ \langle\gamma'|T_R|\gamma\rangle\delta_{l_1' l_2' m_2' l_1 l_2 m_2} + \langle\gamma' l_1' l_2' m_2'|V_{4D}|\gamma l_1 l_2 m_2\rangle\delta_{\gamma'\gamma}\end{aligned} \tag{3.6}$$

Because there are more angular quadrature points than angular basis functions, matrix-vector products with V_{4D} are more costly than matrix-vector products with the other terms. The parallelization scheme is therefore chosen to spread the computation of the V_{4D} among several processors. This is easy to do because $T_{ang}+V_{4D}$ is diagonal in γ'. We need to do

$$\begin{aligned} &for \quad \gamma' = 1 : N_R \\ &for \quad k' = 1 : N_{ang} \\ &\qquad \mathbf{w}_{\mathbf{k}'\gamma'} = \quad \sum_k \langle k'|T_{ang}^{\gamma'} + V_{4D}^{\gamma'}|k\rangle \mathbf{v}_{\mathbf{k}\gamma'} \quad , \end{aligned} \tag{3.7}$$

where N_{ang} is the number of angular basis functions, and k is a composite index representing values of l_1, l_2, m_2. The inner loops can easily be done separately for different values of γ'. We do two γ' values on one processor and use $N_R/2$ processors. Having chosen to put different γ' on different processors the matrix-vector product with T_R cannot be efficiently parallelized but it is less costly. Eigenvectors are determined by transforming eigenvectors of the tridiagonal Lanczos matrix. The transformation is done using Lanczos vectors (stored on disk). The number of Lanczos vectors used to transform is the optimal iteration depth, which is chosen as in Ref. [28].

The final (6D) basis functions we use are products $\delta_\alpha(r_{HH})\Delta_\beta(r_{CC})\psi_i^P(R,\theta_1,\theta_2,\phi)$. $\Delta_\beta(r_{CC})$ is a PO-DVR basis function [56, 57]. For r_{HH} a set of evenly spaced sine-DVR functions is used. The reference potential used to make the PO-DVR

functions is obtained by fixing all other coordinates at their vinylidene values. In terms of H_{4D}

$$\hat{H} = \hat{H}_{4D} + \hat{T}_{HH} + \hat{T}_{CC} + \Delta G_{HH}(r_{HH})\hat{j_1}^2 + \Delta G_{CC}(r_{CC})\hat{j_2}^2 + \Delta V \quad , \tag{3.8}$$

where $\Delta G_j(r_j) = \frac{-\hbar^2}{2\mu_j}(r_j^{-2} - r_{j;viny}^{-2})$, $T_{HH} = -\frac{\hbar^2}{2\mu_{r_{HH}}}\frac{\partial^2}{\partial r_{HH}^2}$, $T_{CC} = -\frac{\hbar^2}{2\mu_{r_{CC}}}\frac{\partial^2}{\partial r_{CC}^2}$, and $\Delta V = V(r_{HH}, r_{CC}, R, \theta_1, \theta_2, \phi) - V_{4D}(R, \theta_1, \theta_2, \phi)$. Matrix elements of this operator in the final basis are

$$\begin{aligned} \langle \alpha'\beta'i'|\hat{H}|\alpha\beta i\rangle &= E_i\delta_{\alpha\alpha'}\delta_{\beta\beta'}\delta_{ii'} + \langle \alpha'|\hat{T}_{HH}|\alpha\rangle\delta_{\beta\beta'}\delta_{ii'} + \langle \beta'|\hat{T}_{CC}|\beta\rangle\delta_{\alpha\alpha'}\delta_{ii'} \\ &+ \Delta G_{HH}(\alpha)\langle i'|\hat{j}_1^2|i\rangle\delta_{\alpha\alpha'}\delta_{\beta\beta'} + \Delta G_{CC}(\beta)\langle i'|\hat{j}_2^2|i\rangle\delta_{\alpha\alpha'}\delta_{\beta\beta'} \\ &+ \langle i'|\Delta V_{\alpha\beta}|i\rangle\delta_{\alpha\alpha'}\delta_{\beta\beta'} \quad , \end{aligned} \tag{3.9}$$

where E_i is an eigenvalue of $\hat{H}_{4D}$. The resulting matrix representation has the following structure

$$\mathbf{H} = \tag{3.10}$$

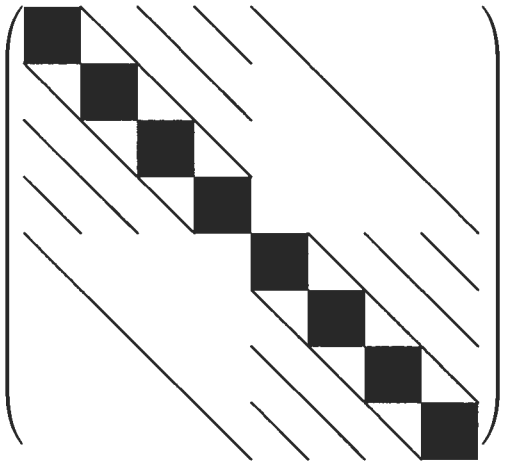

This matrix is not constructed, instead we assemble matrix-vector products by

doing sums sequentially. [19, 23, 26, 55, 58] A potential matrix element is written

$$\begin{aligned}\langle i'|\Delta V_{\alpha\beta}|i\rangle &= \sum_{\gamma' l_1' l_2' m_2'} \sum_{\gamma l_1 l_2 m_2} C^{i'}_{\gamma' l_1' l_2' m_2'} C^{i}_{\gamma l_1 l_2 m_2} \langle u^P_{l_1',l_2',m_2'} | \langle \gamma' | \Delta V_{\alpha\beta} | \gamma \rangle | u^P_{l_1,l_2,m_2} \rangle \\ &= \sum_{\gamma l_1' l_2' m_2' l_1 l_2 m_2} C^{i'}_{\gamma l_1' l_2' m_2'} C^{i}_{\gamma l_1 l_2 m_2} \langle u^P_{l_1',l_2',m_2'} | \Delta V_{\alpha\beta\gamma} | u^P_{l_1,l_2,m_2} \rangle \quad , \end{aligned} \tag{3.11}$$

and $\langle u^P_{l_1',l_2',m_2'} | \Delta V_{\alpha\beta\gamma} | u^P_{l_1,l_2,m_2} \rangle$ is evaluated using Gauss quadrature. The calculation of the $\mathbf{\Delta V}$ matrix is parallelized. Because $\mathbf{C}$ is too large to store in the memory of one processor we do not parallelize over $\alpha\beta$. Instead, for each $\alpha\beta$, we use the parallel LAPACK routine "dsyrk" to calculate all the $\langle i'|\Delta V_{\alpha\beta}|i\rangle$ matrix elements. The number of Gauss points is larger than the number of parity adapted basis functions. Equations for the matrix-vector product calculation are similar to those of Ref. [26] but slightly simpler because we contract only for one group of coordinates in this paper.

Eigenvalues and eigenvectors of the final matrix are computed with a coupled two-term Lanczos algorithm. For each eigenvector we determine an optimal depth. [28] The 6D matrix-vector product is costly and therefore it is worth parallelizing. Due to the direct product structure of the basis it can be can be easily parallelized with openMP. [59] A 6D matrix element is $\langle \alpha'\beta'i'|\hat{H}|\alpha\beta i\rangle$. To do the matrix-vector product one must evaluate

$$\mathbf{w}_{\alpha'\beta'\mathbf{i}'} = \sum_{\alpha\beta i} \langle \alpha'\beta'i'|\hat{H}_{4D}|\alpha\beta i\rangle \mathbf{v}_{\alpha\beta\mathbf{i}} \tag{3.12}$$

for each value of i', β', α'. The loops could be set up:

$$
\begin{aligned}
&for \quad i' = 1 : N_{4D} \\
&for \quad \beta' = 1 : N_{\beta} \\
&for \quad \alpha' = 1 : N_{\alpha} \\
&\qquad \mathbf{w}_{\alpha'\beta'\mathbf{i}'} = \quad \sum_{\alpha\beta i} \langle \alpha'\beta' i' | \hat{H}_{4D} | \alpha\beta i \rangle \mathbf{v}_{\alpha\beta\mathbf{i}}
\end{aligned}
\tag{3.13}
$$

We do loops for different i' on different processors. We use p processors and do N_{4D}/p values of i' with a single processor.

3.2.3 Coupled two-term Lanczos with Local Re-orthogonalization

The standard Lanczos recursion relation is

$$\beta_{m+1}\mathbf{q_{m+1}} = \mathbf{H}\mathbf{q_m} - \alpha_m \mathbf{q_m} - \beta_m \mathbf{q_{m-1}} \quad , \tag{3.14}$$

where $\mathbf{H}$ is the Hamiltonian matrix and $\mathbf{q_m}$ is a Lanczos vector. [60] The first Lanczos vector, $\mathbf{q_1}$, is the start vector and $\mathbf{q_0}$ is set to $\mathbf{0}$. In matrix form this is,

$$\mathbf{H}\mathbf{Q_M} = \mathbf{Q_{M+1}}\mathbf{T_{M+1}} \tag{3.15}$$

where $\mathbf{T_{M+1}}$ is the left $M+1 \times M$ part of a $M+1 \times M+1$ tridiagonal matrix whose diagonal elements are $\{\alpha_1, \alpha_2, \cdots, \alpha_{M+1}\}$ and whose subdiagonal elements are $\{\beta_2, \beta_3, \cdots, \beta_{M+1}\}$ and $\mathbf{Q_M}$ is the matrix whose M columns are the M Lanczos vectors. The Lanczos vectors are (formally) orthogonal and therefore $\mathbf{Q_M^T H Q_M} = \mathbf{T_M}$ with $\mathbf{T_M}$ being the matrix obtained from $\mathbf{T_{M+1}}$ by removing the last row. Among the eigenvalues of $\mathbf{T_M}$ are eigenvalues of $\mathbf{H}$. Extremal eigenvalues of $\mathbf{H}$ are obtained with small M but to compute closely spaced eigenvalues of $\mathbf{H}$ that are in the middle of the spectrum requires using a large value of M. This is true

even in exact arithmetic but the problem is exacerbated by round-off error. Due to round-off error the Lanczos vectors are not orthogonal and converged eigenvalues are copied. The greater the loss of orthogonality the larger the number of copies produced. Making copies of converged eigenvalues is wasteful and drastically slows the convergence of the vinylidene-like states. As a result, a very large number of matrix-vector products is required to converge vinylidene-like states. The calculation of vinylidene-like states is difficult not because the basis is large or because the matrix-vector products are costly but owing to the fact that a very large *number* of matrix-vector products must be computed. The number of required matrix-vector products is large because the vinylidene-like states are far from the lowest states and in a region of very high density. In previous calculations (see for example Refs. [18, 19, 24, 26, 28, 49, 61–63] we have used the Cullum and Willoughby (CW) Lanczos strategy in which nothing is done to minimize the effect of round-off error but accurate results are extracted. Using the CW Lanczos approach it would be extremely difficult to compute vinylidene-like states because of wasteful copying of the lowest eigenvalues. To facilitate the convergence of the vinylidene-like states we have modified the standard approach in two ways. Without these modifications the calculation would have been nearly impossible.

The first modification is the use of the coupled two-term procedure of Freund and Nachtigal. [29,30] Karlsson and Holmgren [64] have used it and we have used to compute resonance states [65]. The coupled two-term idea should slow the loss of orthogonality of the Lanczos vectors. [29,30] Rather than directly computing the elements of $\mathbf{T_{M+1}}$ one computes the elements of the $\mathbf{L_M}$ $(M+1 \times M)$ and $\mathbf{U_M}$

$(M \times M)$ factors of $\mathbf{T_{M+1}}$, where

$$\mathbf{T_{M+1}} = \mathbf{L_M U_M}$$

$$\begin{pmatrix} \alpha_1 & \beta_2 & 0 & 0 \\ \beta_2 & \alpha_2 & \beta_3 & 0 \\ 0 & \beta_3 & \alpha_3 & \ddots \\ 0 & 0 & \ddots & \ddots \end{pmatrix} = \begin{pmatrix} \gamma_1 & 0 & 0 & 0 \\ \beta_2 & \gamma_2 & 0 & 0 \\ 0 & \beta_3 & \gamma_3 & 0 \\ 0 & 0 & \ddots & \ddots \end{pmatrix} \begin{pmatrix} 1 & u_2 & 0 & 0 \\ 0 & 1 & u_3 & 0 \\ 0 & 0 & 1 & \ddots \\ 0 & 0 & 0 & \ddots \end{pmatrix} \tag{3.16}$$

This is done by defining a matrix $\mathbf{P_M}$ whose columns are the first M $\mathbf{p_m}$ vectors,

$$\mathbf{Q_M} = \mathbf{P_M U_M} \ . \tag{3.17}$$

In terms of vectors

$$\mathbf{p}_m = \mathbf{q}_m - u_m \mathbf{p}_{m-1} \ , \tag{3.18}$$

where $u_m = \beta_m / \gamma_{m-1}$. Substituting Eq. (3.17) and $\mathbf{T_{M+1}} = \mathbf{L_M U_M}$, into Eq. (3.15) one obtains

$$\mathbf{H P_M} = \mathbf{Q_{M+1} L_M} \ . \tag{3.19}$$

The $\mathbf{p}$ and $\mathbf{q}$ vectors are thus linked by the relations

$$\begin{aligned} \tilde{\mathbf{q}}_{m+1} &= \mathbf{H p}_m - \gamma_m \mathbf{q}_m \ ; \\ \beta_{m+1} &= \|\tilde{\mathbf{q}}_{m+1}\|_2 \ ; \ \ \mathbf{q}_{m+1} = \tilde{\mathbf{q}}_{m+1} / \beta_{m+1} \ . \end{aligned} \tag{3.20}$$

Orthonormality of the $\mathbf{q}_m$ and Eq. (3.20) imply that

$$\gamma_m = \mathbf{q}_m^t \mathbf{H p}_m \ . \tag{3.21}$$

Eq. (3.17) and Eq. (3.19) are two coupled two-term recursion relations (both $\mathbf{L_M}$ and $\mathbf{U_M}$ are bidiagonal because $\mathbf{T_{M+1}}$ is tridiagonal). The process is initiated by choosing $\mathbf{q_1}$ and setting $\mathbf{p_0}$ to $\mathbf{0}$. Diagonal matrix elements of $\mathbf{T_M}$ are computed from $\alpha_m = \beta_m u_m + \gamma_m$. The coupled two-term procedure reduces the number of matrix-vector products needed to converge the vinylidene-like states.

The second modification is the use of local re-orthogonalization. [31] We enforce *local* orthogonality by reorthogonalizing each $\mathbf{q}_{m+1}$ against the k vectors, $q_{m+1-k}, \cdots, q_m$. The k vectors required to do the re-orthogonalization are kept in memory. We use classical Gram-Schmidt re-orthogonalization. [66] This, of course, does not guarantee perfect orthogonality of the Lanczos vectors but it does greatly reduce the number of copies of converged (low-lying) eigenvalues and therefore accelerates the convergence of the vinylidene-like states. To parallelize the re-orthogonalization we use the SGI parallel level-2 BLAS routine "dgemv" to multiply the transpose of the matrix whose columns are the k previous Lanczos vectors and the vector to be re-orthogonalized. This vector of coefficients is multiplied by the matrix of Lanczos vectors and subtracted from the vector to be re-orthogonalized, again using "dgemv". The parallel BLAS routine works well but if k is larger than about 3000 it is not efficient to use more than about 4 processors. If k is less than about 3000 the scaling with respect to the number of processors is almost linear.

3.3 Computational parameters

3.3.1 Basis and quadrature parameters

We have calculated only totally symmetric states by including in our angular basis only even values of l_1 and l_2 and using $P = 0$ (c.f. Table 3.1). We must choose the number of primitive 4D functions (i.e., N_R, the number of $\delta_\gamma(R)$ sine-DVR functions, and the value for $l_{max} = m_{max}$) and also the number of Gauss-Legendre points for the two θ and Gauss-Chebyshev points of the first kind for the

ϕ integrals. Owing to the symmetry of the potential the integration range for ϕ is reduced to $[0, \pi]$. Having solved the 4D problem we need to choose basis sizes for r_{HH} and r_{CC} and the number of 4D functions to retain.

For the 4D problem we fix l_{max} at a fairly large value, $l_{max} = 31$, and vary N_R to determine the value that converges the 4D levels. The domain of the R sine-DVR functions is $[0, 5]a_0$, which covers the vinylidene and the acetylene geometries as well as the saddle point. We did calculations with $N_R = 24, 30, 32$ and 36. Even with $N_R = 32$ the acetylene ground state decreases by more than 1cm^{-1} when N_R is increased by 4. Nevertheless, the energies of four lowest states with wavefunctions almost perfectly localized in the vinylidene region vary less than 1cm^{-1}. The 4D vinylidene ground state changed by only 0.01cm^{-1}. All states more or less localized in the vinylidene region change by $\leq 1\text{cm}^{-1}$ when $N_R = 32$ is increased from 32 to 36 and we therefore use $N_R = 32$ to compute the 4D functions used in the final calculation. It is known that if wavefunctions have significant amplitude at $R = 0$ using the DVR to evaluate matrix elements of $1/R^2$ causes error. [67] This problem should not affect the vinylidene-like states but would certainly affect the acetylene-like states. To determine l_{max} we fix $N_R = 32$ and vary l_{max}. It is increased increased from 26 to 41 in increments of 5. $l_{max} = 31$ is large enough to converge the acetylene ground state and 4D vinylidene states to better than the 1cm^{-1}. With the $N_R = 32$, $l_{max} = 31$ basis we expect to be able to converge 6D vinylidene states to within 1cm^{-1}. Angular integrals were computed on a grid with $N_\theta = l_{max} + 11$ Gauss-Legendre points and $N_\phi = m_{max} + 11$ Gauss-Chebyshev points of the first kind. These grid sizes were selected by computing eigenvalues of the 4D Hamiltonian with $N_R = 24$ and $l_{max} = 26$ and increasing the number of points used to compute the integrals. We tried $l_{max} + 1$, $l_{max} + 5$ and $l_{max} + 11$. We observe that the 4D levels are well converged with $l_{max} + 11$ points for both θ and ϕ.

Using a small 4D primitive basis ($l_{max} = 14$ and $N_R = 24$) and retaining only

150 4D eigenfunctions we determine the number of r_{HH} and r_{CC} functions (denoted N_{CC} and N_{HH}) necessary to converge vinylidene-like states, that are *unconverged* with respect to l_{max}, N_R, and the number of retained 4D functions, and then use these values in our final calculation. The domains chosen for the sine-DVR basis for r_{HH} and the PO-DVR basis for r_{CC} are $[2.1, 8.5]a_0$ and $[1.8, 3.5]a_0$ respectively. These domains are chosen so that the saddle point and both the acetylene and vinylidene geometries are included. Fixing $N_{HH} = 24$, the value of N_{CC} was increased from 6 to 12 in increments of 2. With $N_{CC} = 10$ the vinylidene-like states change by less than 1cm^{-1} when N_{CC} is increased to 12. Similarly, we fixed $N_{CC} = 10$ and increased the value of N_{HH} from 24 to 30 in increments of 2. With $N_{HH} = 28$ the vinylidene-like states change by less than 1cm^{-1} when N_{HH} is increased to 30.

To confirm that $N_{CC} = 10$ and $N_{HH} = 30$ are large enough we compared 6D levels computed with the $N_{4D} = 331$ $N_{HH} = 30$ $N_{CC} = 10$ 6D basis, for which results are reported in Section IV, a $N_{4D} = 331$ $N_{HH} = 32$ $N_{CC} = 10$ basis, and a $N_{4D} = 331$ $N_{HH} = 30$ $N_{CC} = 12$ basis. When N_{HH} is increased from 30 to 32 all states below 25000cm^{-1} shift by less than 0.01cm^{-1}. When N_{CC} is increased from 10 to 12 the vinylidene ground state changes by 0.0001cm^{-1} and the excited vinylidene states change by less than 0.4cm^{-1}. We expect the energies of the vinylidene-like states computed with $l_{max} = 31$ $N_R = 32$, $N_{CC} = 10$ and $N_{HH} = 30$ to be within about 1cm^{-1} of the numerically exact energies.

3.3.2 Lanczos parameters

To solve the 4D problem we use local re-orthogonalization and the coupled two-term Lanczos algorithm. 75'000 matrix-vector products are required to converge the 640 $4D$-eigenfunctions with energies below 25000cm^{-1}. Each Lanczos vector is orthogonalized with respect to the previous 1500 vectors. A potential energy ceiling of $V_{cut} = 50000\text{cm}^{-1}$ is applied to reduce the spectral range of the Hamiltonian and

therefore to accelerate convergence of the Lanczos algorithm. [55] The solution of the 4D problem is the most expensive part of the whole calculation. After computing the 4D functions they are used to form the matrix representing ΔV in the final $\delta_\alpha(r_{HH})\Delta_\beta(r_{CC})\psi_i^P(R,\theta_1,\theta_2,\phi)$ basis. This matrix was stored on disk and the required piece of it is read into memory before doing the 6D Lanczos calculation.

The 6D Lanczos calculation is also done with the coupled two-term Lanczos algorithm. We have done five different 6D calculations with 5 different 4D bases. In calculations I, II, III, and IV we retain the 4D eigenfunctions with the lowest 500, 550, 600, and 640 (respectively) eigenvalues. In calculation V we omit the 169 4D eigenfunctions with the lowest eigenvalues and retain 20 4D eigenfunctions with eigenvalues smaller than the 4D vinylidene ground state and 310 4D eigenfunctions with eigenvalues larger than the 4D vinylidene ground state. For the largest basis 70′000 iterations, with re-orthogonalization with respect to 5000 Lanczos vectors, were required to converge 3388 eigenvalues below 25′000cm^{-1}. We made no attempt to optimize the number of vectors with respect to which we re-orthogonalize. A potential energy ceiling was set at 50′000cm^{-1}. Only eigenvectors associated with eigenvalues between 20400cm^{-1} and 23500cm^{-1} were constructed from the Lanczos vectors which were stored on disk.

3.4 Results and Discussion

In this section we present our results, discuss differences between our approach and the approaches of ZBB and KLTH, and consider possible implications of those differences. Our contraction scheme is essentially the same as that of ZBB. The main difference between their calculation and ours is the fact that we use iterative methods, to solve both the 4D and the 6D problems. This has two advantages. First, it enables us to use a larger primitive basis to solve the 4D problem. ZBB use $l_{max} = m_{max} = 26$ and we use $l_{max} = m_{max} = 31$. The size of the matrix

whose eigenvectors give us the 4D contracted functions is 87552. It is not possible to use a direct method with a matrix this large. Using a larger primitive 4D basis enables us to describe better the angular dependence of the 4D contracted functions. Second, use of iterative methods makes it possible to use a larger 6D basis and to thoroughly test the ZBB assumption that one may discard 4D functions with eigenvalues significantly below the 4D vinylidene eigenvalues. Owing to the fact that ZBB use direct diagonalization they are not able to incluce both all of the 4D states up to vinylidene region and a large number of 4D states in and above the vinylidene region. The Lanczos algorithm enables us to do this. The ZBB basis and the basis of this paper are designed to favor the convergence of vinylidene-like states. On the other hand, KLTH propose a contraction method that they hope will work well not only for vinylidene-like states but also for aceteylene-like states. Computing both is of course more difficult. KLTH state clearly in their paper that they must restrict the size of their contracted basis in order to obtain a final matrix small enough that its eigenvalues may be computed by direct diagonalization. They estimate the error caused by this restriction to be about 20 - 30cm^{-1}. However, having all of the 4D states up to the vinylidene region included in their basis is a clear advantage, an advantage shared by the method we use. Although we make no attempt to converge acetylene-like states we have 1147 6D states below 15000cm^{-1}. This compares reasonably well with KLTH who have $\sim$ 1350. In the 20000cm^{-1} - 22500cm^{-1} region we have one state every 2.7cm^{-1} whereas KLTH have one every 2.2cm^{-1} and ZBB have one state every 7cm^{-1}. Our density of states is higher than ZBB's because we use a larger primitive bend basis and a larger R basis.

A contraction scheme works well if only a small number of the reduced-dimension eigenfunctions need be retained. Imagine dividing the full 6D basis into two groups of functions. One group consists of 6D functions that are vinylidene-like (products of 4D vinylidene-like functions and DVR functions for r_{CC} and r_{HH}) and the other group consists of 6D functions that are acetylene-like. The 4D vinylidene-

like basis functions should be good for the purpose of computing 6D vinylidene-like states because they are designed (by using vinylidene values for r_{CC} and r_{HH} in the kinetic energy operator and a minimized V_{4D}) to favor their convergence. Matrix elements that couple functions in the two groups are small because ΔG_{HH} andΔG_{CC} (see Eq. (3.8)) and ΔV are small for 6D geometries close to vinylidene and the vinylidene-like 6D basis functions are small for 6D geometries far from vinylidene. As these matrix elements are small it should be a good approximation to retain only the vinylidene-like block of the full matrix. The coupling is nonetheless non-zero and the energies of vinylidene-like 6D states will shift somewhat if some acetylene-like basis functions are retained. 6D acetylene-like basis functions made from 4D acetylene-like functions with 4D energies close to the 4D vinylidene-like states are probably the most important. Adding such basis functions will delocalize the 6D vinylidene-like states. The acetylene-like functions may not be good enough to converge 6D acetylene-like states, but if enough of those that are most strongly coupled to the vinylidene-like functions are included in the final basis it should nevertheless be possible to compute accurate 6D vinylidene-like states. We have verified that the contracted basis program gives the same results as we obtain with a product basis if we retain all of the 4D eigenfunctions for a small test basis. This confirms that the eigenpairs of the 4D and 6D eigenproblems are calculated correctly.

From among the many high-lying states obtained from the final Lanczos calculation we wish to extract those that are vinylidene-like. Some states are well localized in the vinylidene regions of the surface and it is easy to identify them as vinylidene-like. Other states are clearly delocalized and are certainly not vinylidene-like. There are also states that are partially localized in the vinylidene regions of the surface and it is unclear to what extent they may be considered vinylidene-like. The partially localized states are most sensitive to the basis set choice. To identify vinylidene-like states we use three tools. As suggested by ZBB we look at plots of

Figure 3.1: Expectation values of r_{HH}, R and $\hat{X}_{viny}$ for the truncated $N_{4D} = 331$ basis (calculation V)

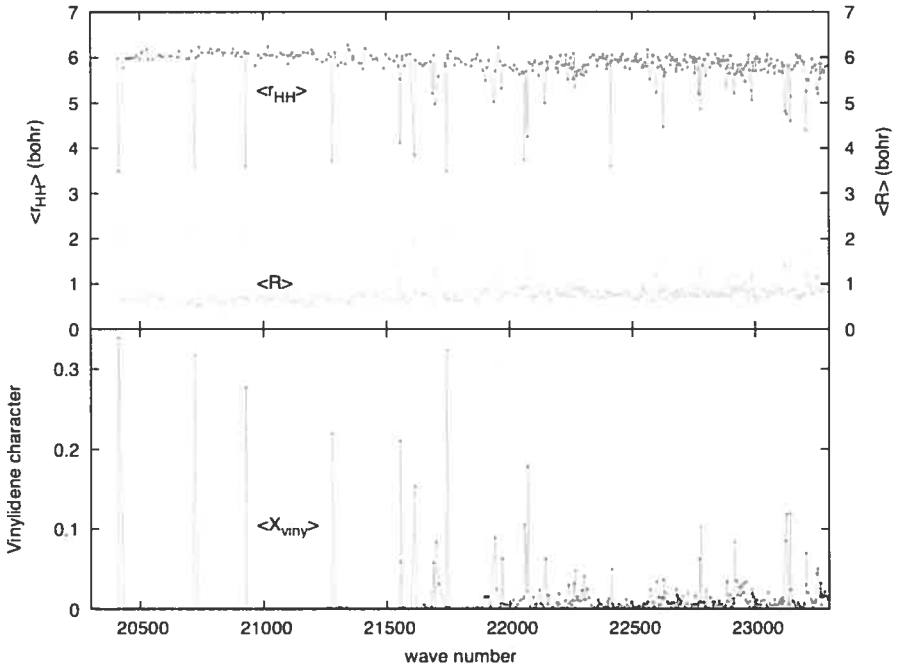

expectation values of R and r_{HH}. Plots of the expectation values of R and r_{HH} for different basis size are shown in the top panel of figures 3.1 to 3.4. R and r_{HH} are selected because their vinylidene and acetylene values are very different. We also make wavefunction plots similar to those of KLTH. In figure 3.5 we present plots of the R and θ_2 dependence of wavefunctions. The plotted functions are obtained by integrating the wavefunction over r_{HH}, r_{CC}, and θ_1 and setting $\phi = 0$. We cannot integrate over ϕ because doing so would give us zero. As $\phi = 0$ there is only one acetylene geometry. Wavefunctions are deemed vinylidene-like if there is significant amplitude in a region with $R \sim 2.2$ bohr and θ_2 close to either 0 or π. Acetylene-like wavefunctions have $R < 0.5$ bohr and θ_2 close to $\pi/2$. The nodal structure of wavefunctions is also used to assign states. Finally we look at expectation values

Figure 3.2: Expectation values of r_{HH}, R and $\hat{X}_{viny}$ for the $N_{4D} = 500$ basis (calculation I)

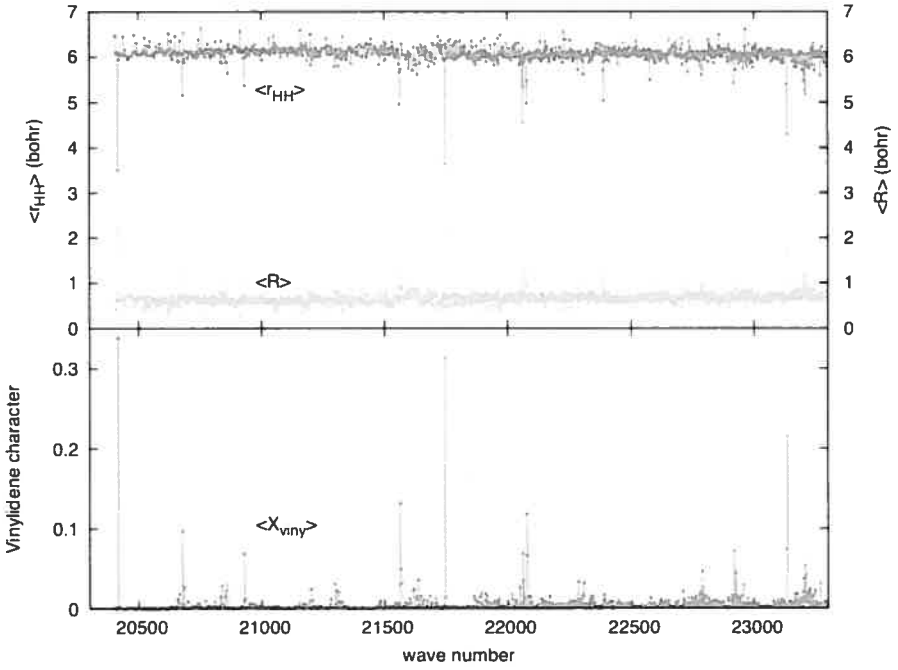

of a localization operator defined by

$$\hat{X}_{viny} = \begin{cases} 1 \quad \text{if} \quad 2.95a_0 \leq r_{HH} \leq 4.15a_0 \ , \\ \qquad\quad\ \ 2.40a_0 \leq r_{CC} \leq 2.50a_0 \ , \\ \qquad\quad\ \ 1.75a_0 \leq R \leq 2.75a_0 \ , \\ \qquad\quad\ \ |\cos(\theta_2)| \geq 0.848 \ ; \\ 0 \quad \text{otherwise} \end{cases}$$

which quantifies the vinylidene character of a wavefunction. The minimum and maximum values of Z, $Z = R, r_{HH}, r_{CC}$ of a vinylidene region (there is one for positive $\cos(\theta_2)$ and another for negative $\cos(\theta_2)$) are $Z_{viny} \pm \Delta_Z$ where Z_{viny} is a value of Z close to the vinylidene minimum and $\Delta_Z = |Z_{viny} - Z_{limit}|$. Z_{limit} is close to the saddle point. Expectation values of $\hat{X}_{viny}$ can be computed simply by

Figure 3.3: Expectation values of r_{HH}, R and $\hat{X}_{viny}$ for the $N_{4D} = 600$ basis (calculation III)

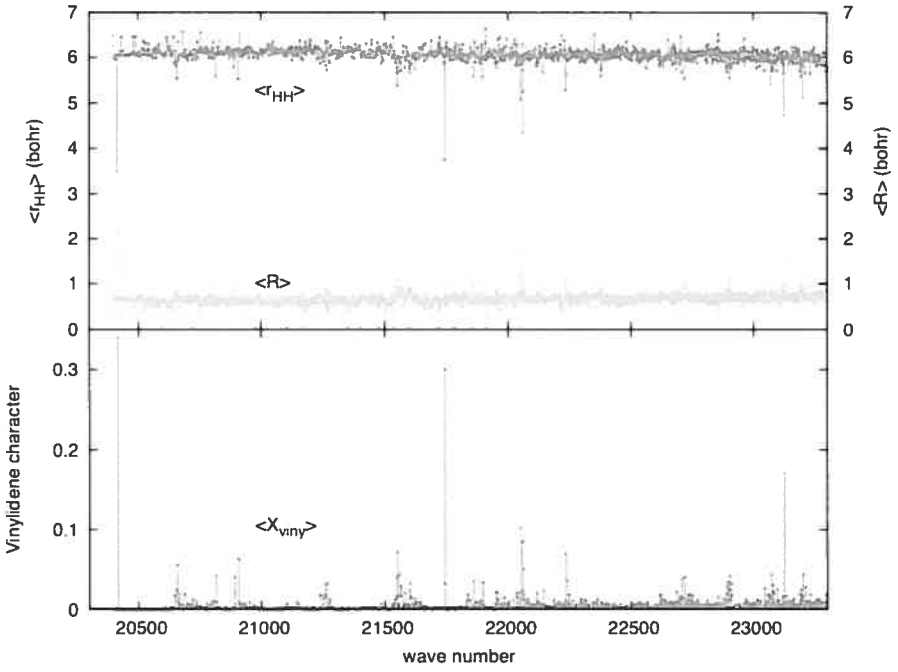

constraining the range of the sums involved in the calculation,

$$< \hat{X}_{viny} >= \sum_{\alpha=\alpha_{min}}^{\alpha_{max}} \sum_{\beta=\beta_{min}}^{\beta_{max}} \sum_{ii'} d^k_{\alpha\beta i} d^k_{\alpha\beta ip} f_{ii'} \quad , \tag{3.22}$$

where $d^k_{\alpha\beta i}$ are coefficients of the expansion of the k^{th} wavefunction in the 6D basis, and

$$f_{ii'} = \sum_{\gamma=\gamma_{min}}^{\gamma_{max}} \sum_{l_1 l_2 l_2' m_2} C^i_{\gamma l_1 l_2 m_2} C^{i'}_{\gamma l_1 l_2' m_2} \int_{|\cos(\theta_2)|=0.848}^{|\cos(\theta_2)|=1} \Theta^{m_2}_{l_2}(\theta_2) \Theta^{m_2}_{l_2'}(\theta_2) \sin(\theta_2) d\theta_2 \quad . \tag{3.23}$$

$\alpha_{min}, \beta_{min}, \gamma_{min}$ are the smallest DVR points included in the ranges of Eq. (3.22). $\alpha_{max}, \beta_{max}, \gamma_{max}$ are the largest DVR points included in the ranges of Eq. (3.22). The expectation values of $\hat{X}_{viny}$ for the different 4D bases are shown in the lower panel of figures 3.1 to 3.4.

Figure 3.4: Expectation values of r_{HH}, R and $\hat{X}_{viny}$ for the $N_{4D} = 640$ basis (calculation IV)

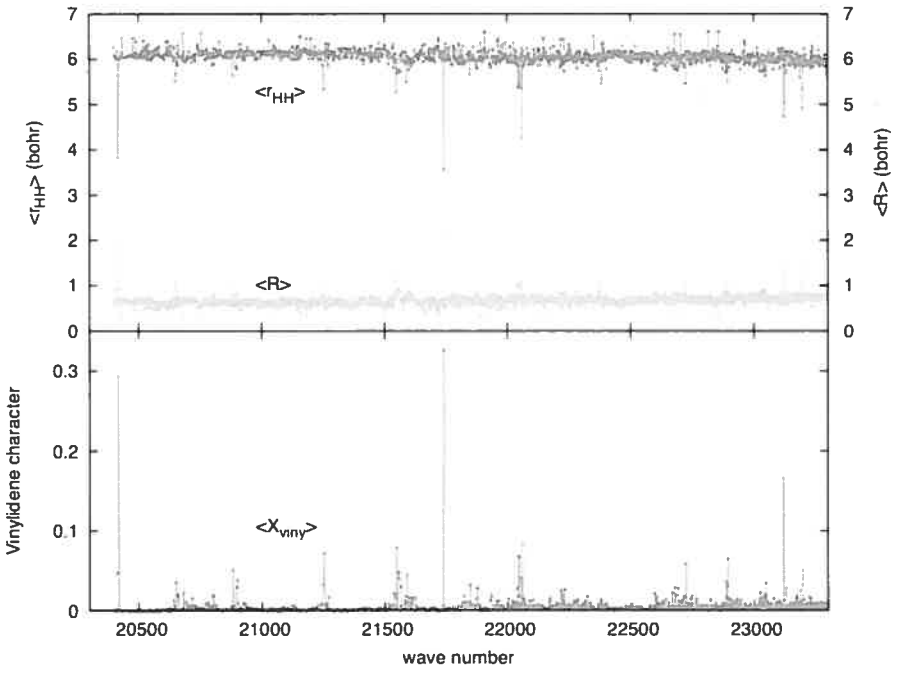

In table 3.2 we report the energy of the vinylidene ground state and differences of excited state energies and the ground state energy and compare with results of other papers. The ground state energy we compute is quite a bit lower than

Table 3.2: Comparison of the wavenumbers (in cm^{-1}) of vinylidene states

	Kozin	Zou	Present work; $4D$ states included in the basis				
Assignment	et al.	et al.	170-500	0-500	0-550	0-600	0-640
ZPE	20490	20424	20415.9	20415.8	20415.5	20414.8	20414.8
ν_3	1195	1179	1200.0	1148.7	1144.2	1137.5	1133.4
$2\nu_4$	—	—	1331.5	1331.3	1328.8	1327.8	1327.3
ν_2	1683	1654	1646.9	1646.0	1646.3	1645.7	1646.6
ν_1	2783	2783	2794.1	2795.2	2794.9	2786.5	2783.5

that of ZBB and KLTH but most of the energy differences are close to theirs. Our best (column 8) ν_2 and ν_1 energies are close to the values of ZBB and KLTH. Wavefunction plots for the ground state, ν_1, ν_2 and ν_3 states are in figure 3.5. On the other hand, the ν_3 we obtain is quite a bit lower than the results of both ZBB

Figure 3.5: Wavefunctions of selected vinylidene states computed with the $N_{4D} = 640$ basis

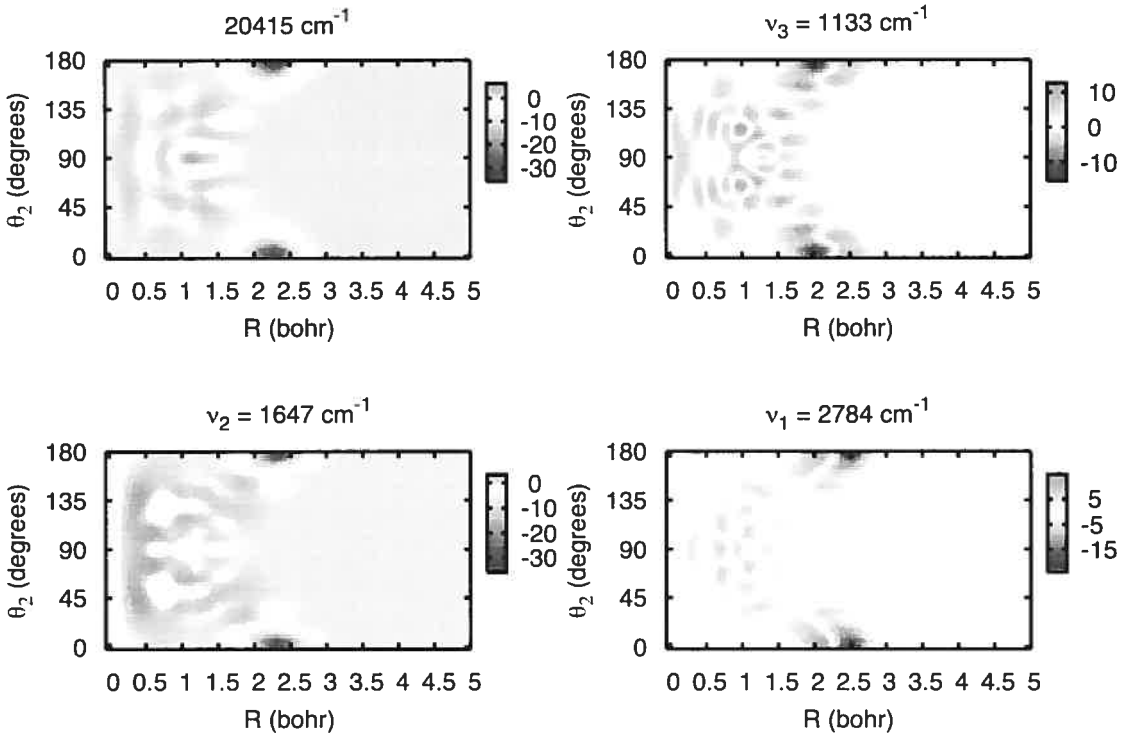

and KLTH (which differ from each other by 16cm^{-1}). The fundamental difference between the states that are close and the state that is further off is the degree of localization. The delocalized state is more sensitive to basis parameters and is therefore harder to compute accurately. Because it is not as well localized it is not possible to be certain of the assignment of the state we denote ν_3. To choose the state that we label as ν_3 we look for a nearly localized state (i.e., a state with a fairly large average R and a fairly small average r_{HH}), with an energy of about 1200cm^{-1} above the vinylidene ground state energy, with the right nodal structure. It is possible, but seems unlikely, that some other state might also be labelled ν_3. We have looked for states with energies closer to the ν_3 states found by ZBB, KLTH, and the experimental value of Ref. [68] but find nothing that

has significant localization and the right nodal structure. There is a well localized

Figure 3.6: Wavefunction of the $2\nu_4$ state computed with the $N_{4D} = 640$ basis

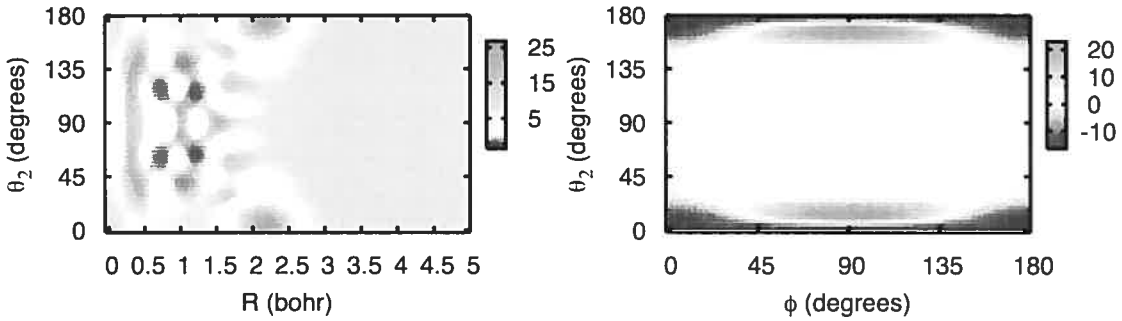

vinylidene-like state at $\sim 1327\text{cm}^{-1}$. If $\phi = 0$ it has no nodes along θ_2. For almost any other value of ϕ there is nodal structure. Plotting the wavefunction in the $\theta_2 - \phi$ plane we see a clear nodal structure located in the vinylidene well (c.f. figure 3.6). Therefore, we assign this state as $2\nu_4$, where ν_4 is the vinylidene wagging mode which involves motion that changes both ϕ and θ_2

One of the goals of this paper is to assess to what extent the localization of vinylidene-like states observed by ZBB is jeprodized by increasing the basis size. KLTH suggest that increasing the density of acetyelene-like basis functions might delocalize some of the vinylidene-like states. We find, see figures 3.2, 3.3, and 3.4, that with the exception of the vinylidene ground state, vinylidene-like states are only moderately localized. In many cases it is not possible to unambiguoulsy denote a state as vinylidene-like. Comparing with the figures of ZBB one sees that their vinylidene-like states are better localized. The better localization of calculations with a smaller basis is also clearly revealed by comparing figures 1 and 2. The basis of figure 3.1 is similar to the basis of ZBB. Truncating the 4D basis from below (column 4 of table 3.2) yields 6D wavefunctions that are more localized. Adding acetylene-like 4D basis functions therefore appears to delocalize vinylidene-

like 6D wavefunctions. If we include all the 4D functions up to a threshold value and increase the threshold we observe that the localization of some vinylidene-like states varies quite a bit. As the threshold is increased the localization (assessed both in terms of expectation values of R and r_{HH} and in terms of the expectation value of the localization operator) of some states decreases and then increases. This indicates that as the basis size is increased one adds some functions that are vinylidene-like and others that are acetylene-like but couple significantly with vinylidene-like basis functions. KLTH suggest that "increasing the density of the acetylenic states in the basis set could significantly reduce the localization of the $2\nu_6$ and $4\nu_6$ states in the vinylidene well." [13] They were not able to identify these states. We also find that these states are not well localized. There are several 6D energy levels near 238cm^{-1} and 468cm^{-1} that are somewhat localized in the vinylidene region and that appear to have the right nodal structure in the vinylidene region (and an oscillatory tail in the acetylene region) but these energies seems too low and the degree of localization is not really convincing.

The ground state, ν_1, and ν_2 are well localized. The energies of these states vary least as the basis size is changed. The energies of the ground state and ν_2 are almost unchanged by truncating the basis from below. Adding high-energy basis functions also has relatively little effect. On the other hand, the energies of the more delocalized states do depend on the basis size. In particular the energy of the ν_3 state changes appreciably, e.g., truncating the basis from below shifts its energy by about 51cm^{-1}. The less localized states are more senstive to basis size because they have more aceytlene character. This is confirmed by the fact that energies of the less localized states are changed significantly by adding acetylene-like basis functions with energies less than the 4D vinylidene energy, but energies of the better localized states (ground state, ν_1, and ν_2) are hardly affected by adding such basis functions. The energy of the ν_3 state changes by about 23cm^{-1} when the basis is enlarged from the smallest basis used (column 4) to the largest basis

used (column 8). On the basis of the numbers in table 3.2 we estimate that the better localized vinylidene-like states are converged to within about 1cm^{-1}. This is consistent with the convergence analysis of the primitive basis given in Section IIB.

Comparing the numbers in columns 5, 6, 7, and 8 of table 3.2 one observes that with only one exception energy levels decrease as high-energy functions are added to the basis. The exception is the ν_2 state for which the energy increases from column 7 to column 8. Comparing the numbers in columns 4 and 5 one observes that truncating the basis from below moves some levels up and others down.

3.5 Conclusion

For many years it has been known that a high-lying vinylidene local minimum exists on the C_2H_2 potential. It is nevertheless not clear to what extent vinylidene should be thought of as independent species. This depends on the localization of states that have significant vinylidene character. To compute these states one must solve a 6D vibrational Schrödinger equation (without imposing a complex absorbing potential). It is by now almost routine to compute 6D wavefunctions. This can be done either by using a direct eigensolver and a contracted basis or by using an iterative eigensolver (usually the Lanczos algorithm) and a direct product basis. Unfortunately, neither of these approaches is well suited to calculating high-lying vinylidene-like states. The applicability of the direct eigensolver + contracted basis approach is limited by the size of the basis required to converge the vinylidene-like states. With currently available computers it is not possible to use a basis large enough that one can be confident that the vinylidene-like levels are converged. The usefulness of the iterative eigensolver + product basis approach is limited not by the required basis size (becasue there is no need to store the Hamiltonian matrix) but by the *number* of matrix-vector products that must be evaluated. To compute

high-lying levels one would need a huge number of matrix-vector products.

In this paper we apply the Lanczos algorithm to obtain vinylidene-like levels. We estimate that the well-localized vinylidene-like states are converged to within $\sim 1\text{cm}^{-1}$. To do this we combine three tools. As suggested by Wang and Carrington and by Yu we use a contracted basis with the Lanczos method. The key idea of this approach is the use of contracted functions obtained by dividing the coordinates into two groups and computing eigenfunctions of either both [26] or one [27] of the groups. It was noticed years ago Ref. [49] that such "simplified" contracted functions, as opposed to the more commonly used "optimally" contracted functions were advantageous when an iterative approach is employed. Using contracted basis functions significantly decreases the spectral range of the Hamiltonian matrix and therefore the number of matrix-vector products necessary to obtain converged energy levels. Despite the advantages of the contracted basis it would be nearly impossible to compute vinylidene-like states using the usual CW Lanczos approach. This is due to wasteful copying of low-lying energies levels which is caused by loss of orthogonality of the Lanczos vectors. To reduce this copying we use a coupled two-term Lanczos scheme and local re-orthogonalization. The contractred basis + coupled two-term + local re-orthogonalization combination makes it possible to determine vinylidene-like states. The final basis we use is too big for a direct diagonalization approach.

We have also used the preconditioned inexact spectral transform (PIST) method [69] to calculate vinylidene-like states. PIST enables one to compute a group of high-lying levels without also converging many low-lying levels. PIST will work well only if a good preconditoiner is available. Fortunately, our final matrix, Eq. (3.10) has exactly the structure one needs to build the optimal separable basis + Wyatt (OSB+W) preconditioner of Ref. [70]. It has been demonstrated that for some problems the OSB+W preconditioner is very effective. [70, 71] It is only useful if Poirier's optimal separable basis [72, 73] (OSB) can be obtained efficiently and this

is always the case if the Hamiltonian matrix has the simple structure of Eq. (3.10). PIST with the OSB+W preconditioner works. The OSB+W preconditioner is good, i.e., it significantly reduces the number of matrix-vector products required to solve the linear equations to apply the spectral transform. However, the Jacobi iterations used to build the OSB are so costly that we did not pursue this approach.

Basis functions and coordinates are chosen so that it is easy to obtain a contracted basis with functions that transform like irreducible representation s. Using this basis and a coupled two-term re-orthogonalized Lanczos approach we compute (J=0) vinylidene-like states. Note that we calculate not only energy levels but also wavefunctions. Without 6D wavefunctions it would not be possible to assess the degree of vinylidene localization of the computed states. Although we definitely find states that can be described as vinylidene-like we also observe that there are few such states that are well localized and that energies of vinylidene-like states that are not well localized are sensitive to the basis we use. As the basis size is increased, and in particular, as the number of 4D acetylene-like functions in the basis is increased, the poorly localized levels shift. It appears that there are very few well-localized vinylidene-like states.

Acknowledgments

We are grateful to Joel Bowman for providing his potential. We thank Xiaogang Wang and Richard Dawes for stimulating discussions. This work has been supported by the Natural Sciences and Engineering Research Council of Canada. The calculations were done on the Altix computer of the Réseau québécois de calcul de haute performance.

Bibliography

[1] W. Lindinger, D. L. Albritton, F. C. Fehsenfeld, and E. E. Ferguson. Reactions of O^- with N_2, N_2O, SO_2, NH_3, CH_4, and C_2 H_4 and C_2 H_2^- with O_2 from 300 K to relative kinetic energies of 2 eV. *J. Chem. Phys.*, 63:3238, 1975.

[2] C. E. Dykstra and H. F. Schaefer. The vinylidene-acetylene rearrangement. a self-consistent electron pairs study of a model unimolecular reaction. *J. Am. Chem. Soc.*, 100:1378, 1978.

[3] Y. Osamura, H. F. Schaefer, Stephen K. Gray, and W. H. Miller. Tunneling in the unimolecular decomposition of formaldehyde, a more quantitative study. *J. Am. Chem. Soc.*, 103:1904, 1981.

[4] S.M. Burnett, A. E. Stevens, C. S. Feigerle, and W. C. Lineberger. Observation of X^1A_1 vinylidene by photoelectron spectroscopy of the $C_2H_2^-$ ion. *Chem. Phys. Lett.*, 100:124, 1983.

[5] T. Carrington Jr., L. M. Hubbard, H. F. Schaefer III, and W. H. Miller. Vinylidene: Potential energy surface and unimolecular reaction dynamics. *Chem. Phys.*, 80:4347, 1984.

[6] M. P. Jacobson and R. W. Field. Acetylene at the threshold of isomerization. *J. Phys. Chem. A*, 104:3073, 2000.

[7] J. Levin, H. Feldman, A. Baer, D. Ben-Hamu, O. Heber, D. Zajfman, and Z. Vager. Study of unimolecular reactions by coulomb explosion imaging: The nondecaying vinylidene. *Phys. Rev. Lett.*, 81:3347, 1998.

[8] N.-Y. Chang, M.-Y. Shen, and C.-H. Yu. Extended ab initio studies of the vinylidene-acetylene rearrangement. *J. Chem. Phys.*, 106:3237, 1997.

[9] J. F. Stanton and J. Gauss. Vibrational structure in the vinylidene anion photoelectron spectrum: Closing the gap between theory and experiment. *J. Chem. Phys.*, 110:6079, 1999.

[10] S. Zou and J. M. Bowman. A new ab initio potential energy surface describing acetylene/vinylidene isomerization. *Chem. Phys. Lett.*, 368:421, 2003.

[11] S. Zou and J. M. Bowman. Full dimensionality quantum calculations of acetylene/vinylidene isomerization. *J. Chem. Phys.*, 117:5507, 2002.

[12] S. Zou, J. M. Bowman, and A. Brown. Full-dimensionality quantum calculations of acetylene–vinylidene isomerization. *J. Chem. Phys.*, 118:10012, 2003.

[13] I. N. Kozin, M. M. Law, J. Tennyson, and J. M. Hutson. Calculating energy levels of isomerizing tetraatomic molecules: II. the vibrational states of acetylene and vinylidene. *J. Chem. Phys.*, 122:064309, 2005.

[14] M. J. Bramley and N. C. Handy. Efficient calculation of rovibrational eigenstates of sequentially bonded four-atom molecules. *J. Chem. Phys.*, 98:1378, 1993.

[15] H. Köppel, W. Domcke, and L. S. Cederbaum. Multimode molecular dynamics beyond the Born-Oppenheimer approximation. *Adv. Chem. Phys.*, 57:59, 1984.

[16] R. E. Wyatt. RRGM, recursive residue generation method. *Adv. Chem. Phys.*, 73:231, 1989.

[17] C. Leforestier. Grid representation of rotating triatomics. *J. Chem. Phys.*, 94:6388, 1991.

[18] A. McNichols and T. Carrington Jr. Vibrational energy levels of formaldehyde calculated from an internal coordinate Hamiltonian using the Lanczos algorithm. *Chem. Phys. Lett.*, 202:464, 1993.

[19] M. J. Bramley and T. Carrington Jr. A general discrete variable method to calculate vibrational energy levels of three- and four-atom molecules. *J. Chem. Phys.*, 99:8519, 1993.

[20] M. R. Wall and D. Neuhauser. Extraction, through filter-diagonalization, of general quantum eigenvalues or classical normal mode frequencies from a small number of residues or a short-time segment of a signal. I. theory and application to a quantum-dynamics model. *J. Chem. Phys.*, 102:8011, 1995.

[21] T. P. Grozdanov, V. A. Mandelshtam, and H. S. Taylor. Recursion polynomial expansion of the green's function with absorbing boundary conditions: Calculations of resonances of HCO by filter diagonalization. *J. Chem. Phys.*, 103:7990, 1995.

[22] H.-G. Yu and S. C. Smith. The calculation of vibrational eigenstates by MIN-RES filter diagonalization. *Ber. Bunsenges Phys. Chem.*, 101:400, 1997.

[23] R. Chen and H. Guo. Discrete energy representation and generalized propagation of physical systems. *J. Chem. Phys.*, 108:6068, 1998.

[24] X. Wang and T. Carrington Jr. Six-dimensional variational calculation of the bending energy levels of HF trimer and DF trimer. *J. Chem. Phys.*, 115:9781, 2001.

[25] J. K. Cullum and R. A. Willoughby. *Lanczos algorithms for large symmetric eigenvalue computations.* Birkhäuser, Boston, 1985.

[26] X. Wang and T. Carrington Jr. New ideas for using contracted basis functions with a Lanczos eigensolver for computing vibrational spectra of molecules with four or more atoms. *J. Chem. Phys.*, 117:6923, 2002.

[27] H.-G. Yu. Two-layer Lanczos iteration approach to molecular spectroscopic calculation. *J. Chem. Phys.*, 117:8190, 2002.

[28] X. Wang and T. Carrington Jr. A contracted basis-Lanczos calculation of vibrational levels of methane: Solving the Schrödinger equation in nine dimensions. *J. Chem. Phys.*, 119:101, 2003.

[29] R. W. Freund and N. M. Nachtigal. *Linear Algebra for Large Scale and Real-Time Applications.* Kluwer Academic Publishers, 1993.

[30] R. W. Freund and N. M. Nachtigal. Implementation details of the coupled QMR algorithm. *SIAM J. Sci. Stat. Comp.*, 15:313, 1994.

[31] Beresford N. Parlett. *The Symmetric Eigenvalue Problem.* Society for Industrial and Applied Mathematics, Philadelphia, 1998.

[32] D. Xu, H. Guo, S. Zou, and J. M. Bowman. A scaled ab initio potential energy surface for acetylene and vinylidene. *Chem. Phys. Lett.*, 377:582, 2003.

[33] M. Mladenović. Rovibrational Hamiltonians for general polyatomic molecules in spherical polar parametrization: I. orthogonal representations. *J. Chem. Phys.*, 112:1070, 2000.

[34] R. Schork and H. Köppel. Barrier recrossing in the vinylidene-acetylene isomerization reaction: A five-dimensional ab initio quantum dynamical investigation. *J. Chem. Phys.*, 115:7907, 2001.

[35] S. Zou and J. M. Bowman. Reduced dimensionality quantum calculations of acetylene $< -- >$ vinylidene isomerization. *J. Chem. Phys.*, 116:6667, 2002.

[36] X. Wang and T. Carrington Jr. A symmetry-adapted Lanczos method for calculating energy levels with different symmetries from a single set of iterations. *J. Chem. Phys.*, 114:1473, 2001.

[37] R. Chen and H. Guo. A single lanczos propagation method for calculating transition amplitudes. II. Modified QL and symmetry adaptation. *J. Chem. Phys.*, 114:1467, 2001.

[38] X. Wang and T. Carrington Jr. A finite basis representation Lanczos calculation of the bend energy levels of methane. *J. Chem. Phys.*. 118:6946, 2003.

[39] S. Carter and N. C. Handy. The variational method for the calculation of rovibrational energy levels. *Comp. Phys. Rep.*, 5:115, 1986.

[40] Z. Bačić and J. C. Light. Theoretical methods for rovibrational states of floppy molecules. *Annu. Rev. Phys. Chem.*, 40:469, 1989.

[41] J. R. Henderson and J. Tennyson. All the vibrational bound states of H_3^+. *Chem. Phys. Lett.*, 173:133, 1990.

[42] J. M. Bowman and B. Gazdy. A truncation/recoupling method for basis set calculations of eigenvalues and eigenvectors. *J. Chem. Phys.*, 94:454, 1991.

[43] Y. Qiu, J. Z. H. Zhang, and Z. Bačić. Six-dimensional quantum calculations of vibration-rotation-tunneling levels of $\nu_1$and ν_2 HCl-stretching excited $(HCl)_2$. *J. Chem. Phys.*, 108:4804, 1998.

[44] D. Luckhaus. 6D vibrational quantum dynamics: Generalized coordinate discrete variable representation and (a)diabatic contraction. *J. Chem. Phys.*, 113:1329, 2000.

[45] M. Mladenović. Discrete variable approaches to tetratomic molecules. II: Application to H_2O_2 and H_2CO. *Spectrochim. Acta Part A*, 58:809, 2002.

[46] Z. Bačić and J. C. Light. Accurate localized and delocalized vibrational states of HCN/HNC. *J. Chem. Phys.*, 86:3065, 1987.

[47] J. C. Light, I. P. Hamilton, and J. V. Lill. Generalized discrete variable approximation in quantum-mechanics. *J. Chem. Phys.*, 82:1400, 1985.

[48] J. C. Light and T. Carrington Jr. Discrete variable representations and their utilization. *Adv. Chem. Phys.*, 114:263, 2000.

[49] M. J. Bramley and T. Carrington Jr. Calculation of triatomic vibrational eigenstates: Product or contracted basis sets, lanczos or conventional eigensolvers? what is the most efficient combination? *J. Chem. Phys.*, 101:8494, 1994.

[50] Claude Cohen-Tannoudji, Bernard Diu, and Franck Laloë. *Mécanique Quantique.* Hermann, éditeur des Sciences et des Arts, 1973.

[51] R. Chen, G. Ma, and H. Guo. Six-dimensional quantum calculations of highly excited vibrational energy levels of hydrogen peroxide and its deuterated isotopomers. *J. Chem. Phys.*, 114:4764, 2001.

[52] J. T. Muckerman. Some useful discrete variable representations for problems in time-dependent and time-independent quantum mechanics. *Chem. Phys. Lett.*, 173:200, 1990.

[53] D. T. Colbert and W. H. Miller. A novel discrete variable representation for quantum mechanical reactive scattering via the S-matrix Kohn method. *J. Chem. Phys.*, 96:1982, 1992.

[54] X. Wang. Vibrational levels of Ar_4. *Unpublished*, 2006.

[55] M. J. Bramley, J. W. Tromp, T. Carrington Jr., and G. C. Corey. Efficient calculation of highly excited vibrational energy levels of floppy molecules: The band origins of H_3^+ up to 35 000 cm^{-1}. *J. Chem. Phys.*, 100:6175, 1994.

[56] J. Echave and D. C. Clary. Potential optimized discrete variable representation. *Chem. Phys. Lett.*, 190:225, 1992.

[57] H. Wei and T. Carrington Jr. The discrete variable representation of a triatomic Hamiltonian in bond length-bond angle coordinates. *J. Chem. Phys.*, 97:3029, 1992.

[58] U. Manthe and H. Köppel. New method for calculating wave packet dynamics: Strongly coupled surfaces and the adiabatic basis. *J. Chem. Phys.*, 93:345, 1990.

[59] R. Chandra, R. Menon, L. Dagum, D. Kohr, D. Maydan, and J. McDonald. *Parallel Programming in OpenMP.* Elsevier, 2000.

[60] G. H. Golub and C. F. Van Loan. *Matrix Computations.* John Hopkins University Press, Baltimore, 1989.

[61] N. M. Poulin, M. J. Bramley, T. Carrington Jr., H. G. Kjaergaard, and B. R. Henry. Calculation of vibrational (J=0) excitation energies and band intensities of formaldehyde using the recursive residue generation method. *J. Chem. Phys.*, 104:7807, 1996.

[62] P. Sarkar, N. Poulin, and T. Carrington Jr. Calculating rovibrational energy levels of a triatomic molecule with a simple Lanczos method. *J. Chem. Phys.*, 110:10269, 1999.

[63] P.-N. Roy and T. Carrington Jr. An evaluation of methods designed to calculate energy levels in a selected range and application to a (one-dimensional) Morse oscillator and (three-dimensional) HCN/HNC. *J. Chem. Phys.*, 103:5600, 1995.

[64] H. O. Karlsson and S. Holmgren. Cross correlation functions $c_{nm}(e)$ via lanczos algorithms without diagonalization. *J. Chem. Phys.*, 117:9116, 2002.

[65] J. C. Tremblay and T.. Carrington Jr. Computing resonance energies, widths, and wave functions using a Lanczos method in real arithmetic. *J. Chem. Phys.*, 122:244107:1–11, 2005.

[66] W. H. Press, S. A. S.A. Teukolsky, W. T. Vetterling, and B. P. Flannery. *Numerical Recipes in FORTRAN 77 The Art of Scientific Programming.* Cambridge University Press, 1986.

[67] J. R. Henderson, J. Tennyson, and B. T. Sutcliffe. All the bound vibrational states of H_3^+: A reappraisal. *J. Chem. Phys.*, 98:7191, 1993.

[68] K. M. Ervin, J. Ho, and W. C. Lineberger. A study of the singlet and triplet states of vinylidene by photoelectron spectroscopy of $H_2C{=}C^-$, $D_2C{=}C^-$, and $HDC{=}C^-$. vinylidene-acetylene isomerization. *J. Chem. Phys.*, 91:5974, 1989.

[69] S.-W. Huang and T. Carrington Jr. A new iterative method for calculating energy levels and wave functions. *J. Chem. Phys.*, 112:8765, 2000.

[70] B. Poirier and T. Carrington Jr. Accelerating the calculation of energy levels and wave functions using an efficient preconditioner with the inexact spectral transform method. *J. Chem. Phys.*, 114:9254, 2001.

[71] B. Poirier and T. Carrington Jr. A preconditioned inexact spectral transform method for calculating resonance energies and widths, as applied to HCO. *J. Chem. Phys.*, 116:1215, 2002.

[72] B. Poirier. Optimal separable bases and series expansions. *Phys. Rev. A*, 56:120, 1997.

[73] B. Poirier. Efficient preconditioning scheme for block partitioned matrices with structured sparsity. *Numer. Linear Algebra Appl.*, 7:715, 2000.

CHAPITRE 4

DU CALCUL DES ÉNERGIES ET DURÉES DE VIE DES ÉTATS RÉSONANTS : NOUVELLE APPROCHE BASÉE SUR L'UTILISATION D'UN OPÉRATEUR NON-SYMÉTRIQUE EN ARITHMÉTIQUE RÉELLE

On propose dans cette section une nouvelle méthode permettant le calcul de propriétés des états Siegert ou états résonants. L'approche est appliquée à la détermination des durées de vie et énergies des états résonants du radical HCO. L'article a été soumis à la revue "Journal of Chemical Physics" le 30 mai 2006 et accepté le 26 juin 2006. L'article est paru en version électronique le 5 septembre 2006.

Computing resonance energies, widths, and wavefunctions using a Lanczos method in real arithmetic

Jean Christophe Tremblay[1] and Tucker Carrington Jr.[2]

Département de chimie, Université de Montréal,

C.P. 6128, succursale Centre-ville, Montréal (Québec) H3C 3J7, Canada

Abstract

We introduce new ideas for calculating resonance energies and widths. It is shown that a non-hermitian Lanczos approach can be used to compute eigenvalues of $H + W$ where H is the Hamiltonian and W is a complex absorbing potential (CAP), without evaluating complex matrix-vector products. This is done by exploiting the link between a CAP-modified Hamiltonian matrix and a real but nonsymmetric matrix $\mathbf{U}$ suggested by Mandelshtam and Neumaier and using a coupled two-term Lanczos procedure. We use approximate resonance eigenvectors obtained from the nonhermitian Lanczos algorithm and a very good CAP to obtain very accurate energies and widths without solving eigenvalue problems for many values of the CAP strength parameter and searching for cusps. The method is applied to the resonances of HCO. We compare properties of the method with those of established approaches.

[redacted]

Fax: 514-343-7586

4.1 Introduction

Resonances are important in atomic and molecular physics. [1–8] They play a key role in processes such as autoionization, photodissociation, reaction dynamics, electron-molecule scattering etc. [9–11] Sometimes resonance energies and widths are computed from the energy dependence of cross sections or phase shifts. In most cases, however, it is easier to determine complex-energy solutions of Schrödinger's equation (called Siegert states) for which the corresponding wavefunctions satisfy outgoing boundary conditions and to associate the real part of the complex energy with the resonance energy and the negative imaginary part with the resonance width. [12] Because of the outgoing boundary conditions the resonance wavefunctions, that correspond to complex energies $E = E_r - iE_i$ with $E_i > 0$, diverge asymptotically. The outgoing boundary conditions make it difficult to use matrix methods. Nonetheless several methods have been developed that enable one to calculate these complex-energy solutions with techniques very similar to those used to calculate bound state energies. This is usually done by modifying the Hamiltonian operator so that resonance wavefunctions are unaffected in the interaction region where they resemble bound states but damped in the asymptotic region. Because eigenfunctions of the modified operator are damped they may be computed with standard matrix methods. Two means of modifying the Hamiltonian are popular: the complex scaling method [13–17] and the absorbing potential method [18–23]. In the complex scaling method R, the dissociative coordinate, in the Hamiltonian operator is changed to $Re^{i\theta}$ where θ is a scaling angle. To use the absorbing potential method the Hamiltonian, H, is replaced with $H - i\eta W'$, where W' is a complex absorbing potential (CAP). Both approaches require computing eigenvalues of a complex-symmetric Hamiltonian matrix.

4.2 Established methods for computing resonances

The two most popular methods for studying resonances are the CAP-Lanczos approach [24–26] and the filter diagonalization (FD) procedure [27–29]. There are other methods [30–32] but these are common workhorses. Both the CAP-Lanczos and the FD methods have the advantage that they may be used without storing a Hamiltonian matrix. It is necessary only to compute matrix-vector products which may be evaluated by applying the Hamiltonian matrix to a vector term by term and, for each term, factor by factor. [33] In this section these methods are briefly reviewed and we identify aspects of both methods which can be improved.

4.2.1 The CAP-Lanczos approach

Jolicard and coworkers proposed using a CAP to compute resonances. [18] Their idea is attractive because it enables one to use a great deal of what has been learned about solving bound state problems to solve the resonance problem. The CAP added to the Hamiltonian must be chosen so that it is zero in the interaction region, absorbs outgoing flux from the interaction region and does not lead to spurious incoming flux (towards the interaction region). There has been considerable work done on designing optimal CAPs. [34–43] Once a CAP has been selected it is necessary to choose basis functions and calculate eigenvalues (and eigenvectors if one is interested in understanding the motions of the atoms and attributing zeroth order quantum numbers) of a matrix representation of the Hamiltonian. Unless the CAP is very good eigenvalues of a complex-symmetric matrix must be computed for many values of η. To compute the eigenvalues one may choose either a direct or an iterative eigensolver. [44] Iterative methods have the important advantage that they make it possible to use very large basis sets. The most obvious iterative method is the complex-symmetric Lanczos algorithm without reorthogonalization. To use this Lanczos approach one must store (in memory) only two vectors. The

number of matrix-vector products required to converge a particular complex energy depends on the local density of the complex eigenvalues and how far the complex energy is from the outside edge of the set that contains all the complex eigenvalues (how close it is to the convex hull). The CAP-Lanczos combination has been used by many groups. [24–26,45] We have used it with an inexact spectral transform. [46]

The CAP-Lanczos approach works well but we have identified two aspects that can be improved. (1) To extract eigenvalues from a Krylov space with M vectors one must do M matrix-vector products. Owing to the fact that the operator is complex the matrix-vector products are complex. This increases their cost. If a discrete variable representation (DVR) [47,48] basis is used the CAP is diagonal and matrix-vector products with the CAP are therefore inexpensive. The costly matrix-vector product is the one for $\mathbf{H}$. Because $\mathbf{H}$ is real but the vectors are complex the cost of the $\mathbf{H}$ matrix-vector product is about a factor of two larger than it would be without a CAP. In this paper we demonstrate that it is possible to use a CAP and a Lanczos eigensolver without doing complex matrix-vector products. This reduces the cost of matrix-vector products by about a factor of two. (2) Although it is not difficult to do, it is rare that Lanczos is used to compute both eigenvalues and eigenvectors. The best way to compute eigenvectors is to store Lanczos vectors on disk and to compute optimal iteration depths for each eigenvalue. Modified versions of the original approach of Cullum and Willoughby [49] have been used recently. [50] In this paper we compute resonance wavefunctions from eigenvectors obtained with a Lanczos method.

4.2.2 FD procedures

By combining a damped Chebyshev recursion [51,52] with the filter diagonalisation idea [53], Mandelshtam and Taylor devised an effective means of computing resonances. [27–29] They apply Chebyshev polynomials of the unmodified Hamiltonian operator to a vector to generate a "signal". The signal is used to com-

pute Hamiltonian and overlap matrices in a filtered space from which one obtains complex resonance energies. [29] If the recursion relation is damped the Chebyshev identity used to reduce the number of required matrix-vector products in the bound state case is formally invalid. As explained in Ref. [27] one must compute K matrix-vector products to generate a signal of length K with which one extracts eigenvalues from a Krylov space of $K/2$ vectors. The size of the Krylov space required to converge the resonances of interest is about the same whether one uses FD or Lanczos. [26, 54] In the FD case, the number of matrix-vector products required to extract eigenvalues from this subspace is a factor of two larger. A simple comparison of the number of required matrix-vector products is, however, misleading because the FD matrix-vector products are real and the Lanczos matrix-vector products are complex. These issues have been thoroughly discussed by Xie, Chen, and Guo who point out that the factor of two one saves because the FD approach uses real arithmetic is compensated for by the necessity of computing a factor of 2 more matrix-vector products. [26]

FD methods that enable one to generate a signal of length K, with which one extracts the eigenvalues associated with a Krylov space of size $K/2$, from $K/2$ matrix-vector products have been developed. These methods have the advantage of real matrix-vector products (which the standard FD method also has) and the advantage of being able to obtain the eigenvalues associated with a Krylov space of size $K/2$ from only $K/2$ matrix-vector products (which the complex-symmetric Lanczos method also has). Li and Guo, reasoning that the damping (CAP) should have little influence on wavefunctions in the interaction region, simply used the Chebyshev identity despite the fact that formally it does not hold. [55] Although using the Chebyshev identity is an approximation (and one whose quality is somewhat hard to assess and control) they observe that for some resonances it works very well. In very impressive papers Mandelshtam and Neumaier (MN) have introduced a rigorously justified FD scheme that allows one to both use real arithmetic

and to compute eigenvalues extracted from a $K/2$ dimensional Krylov subspace by computing only $K/2$ matrix-vector products. [56,57] This method appears promising.

The method we suggest in this paper is based on MN's observation that the CAP-modified Hamiltonian can be written as a quadratic eigenvalue problem. Our method differs from theirs in four aspects: 1) We use a Lanczos algorithm whereas they use Chebyshev polynomials. 2) We compute not only eigenvalues but also eigenvectors. 3) We use only double precision. In contrast, MN use quadruple precision to process their signal. 4) We use a different CAP. [42] Our CAP is a high degree polynomial chosen to minimize reflection and transmission. It has a very small real part. We highly recommend the method of MN and do not wish to imply that the Lanczos approach we propose is necessarily better.

In summary, in this paper we propose a Lanczos-based method that has the same advantages as MN's method (real matrix-vector products, no doubling of the number of required matrix-vector products) and use it with a very good CAP. Our computational scheme for computing resonances is based on the idea of moving the damping from the operator to the basis.

4.3 The eigenvalue problem for the Hamiltonian with a CAP can be written as a quadratic eigenvalue problem

MN [57] write the eigenvalue problem for the Hamiltonian with a CAP as

$$(\mathbf{H} + \mathbf{W})\mathbf{x}_k = E_k \mathbf{x}_k \ . \tag{4.1}$$

In this equation $\mathbf{H}$ is a matrix representation of the Hamiltonian scaled so that its eigenvalues are between -1 and +1 and $\mathbf{W}$ is a matrix representation of the CAP $W(R)$, which a function of the dissociative coordinate R. $W(R) = -i\eta W'$ (see for example Eq. (4.8)). Boldface symbols are matrix representations of operators or

kets. MN noticed that if one chooses an energy-dependent CAP

$$W(R) = \frac{u_k}{2}\left(1 - D_1(R)\right) + \frac{1}{2u_k}\left(1 - D_2(R)\right) \ , \tag{4.2}$$

where u_k is defined by $E_k = \left(\frac{u_k}{2} + \frac{1}{2u_k}\right)$, then Eq. (4.1) becomes

$$\mathbf{H}\mathbf{x}_k = \left(\frac{u_k}{2} + \frac{1}{2u_k}\right)\mathbf{x}_k - \mathbf{W}\mathbf{x}_k \tag{4.3}$$

or

$$\mathbf{H}\mathbf{x}_k = \frac{u_k}{2}\mathbf{D_1} + \frac{1}{2u_k}\mathbf{D_2} \tag{4.4}$$

which is the quadratic eigenvalue problem

$$(u_k^2\mathbf{D}_1 - 2\mathbf{H}u_k + \mathbf{D_2})\mathbf{x}_k = 0 \ . \tag{4.5}$$

$\mathbf{D_1}$ and $\mathbf{D_2}$ are real matrices. It is crucial that $W(R)$ and the relationship between E_k and u_k be chosen so that (1) by properly defining D_1 and D_2, W can be made a good CAP and (2) the convergence of the eigenvalues of the quadratic eigenvalue problem that correspond to the desired E_k is facilitated. For more detail the reader is referred to the papers of MN. [56,57] After transforming the quadratic eigenvalue problem in the standard fashion [44] one obtains the linearized eigenvalue problem,

$$\mathbf{U}\hat{\mathbf{x}}_k = u_k\hat{\mathbf{x}}_k \ , \tag{4.6}$$

where

$$\mathbf{U} = \begin{pmatrix} \mathbf{0} & \mathbf{I} \\ -\mathbf{D}_1^{-1}\mathbf{D_2} & 2\mathbf{D}_1^{-1}\mathbf{H} \end{pmatrix} \tag{4.7}$$

and $\hat{\mathbf{x}}_k = \begin{pmatrix} \mathbf{x_k} \\ \mathbf{x_k'} \end{pmatrix}$. The key advantage of Eq. (4.6) is the fact that $\mathbf{U}$ is real. The eigenvalues of a real matrix can be computed by doing real matrix-vector products.

Because we use the DVR, $\mathbf{D_1}$ and $\mathbf{D_2}$ are diagonal and matrix-vector products with $\mathbf{U}$ are therefore almost as inexpensive as matrix-vector products with $\mathbf{H}$. One computes eigenvalues of $\mathbf{U}$ and from them obtains eigenvalues of $\mathbf{H}+\mathbf{W}$. It is better to work with $\mathbf{U}$ than with $\mathbf{H}+\mathbf{W}$ not only because $\mathbf{U}$ is real but also because the eigenvalues of $\mathbf{U}$ that correspond to desired complex resonance energies converge more favourably. In the upper half plane they are just inside the unit disk ($\mathbf{H}$ is scaled so that its eigenvalues are between -1 and +1) and in the lower half plane they are not far from (but below) the unit disk. Eigenvalues in both the lower and upper half planes are close to the convex hull of the spectrum, the former being closer than the latter.

In this paper we use the matrix $\mathbf{U}$ proposed by MN but we choose $D_1(R)$ and $D_2(R)$ differently. The E_k obtained from the u_k are only useful if $W(R)$ is a good CAP. If $W(R)$ is a poor CAP then being able to compute eigenvalues of $\mathbf{H}+\mathbf{W}$ easily from those of $\mathbf{U}$ is not very useful. A good CAP is one which is zero in the interaction region and turns on smoothly at some selected left edge. Its imaginary part should be negative and much larger than its real part. There is some evidence that it is good to have a small negative real part (which serves to decrease the de Broglie wavelength and therefore the width of the required absorbing region). [58] To ensure that the CAP has these properties we use $D_1(R) = (1+\eta W_{14}(R))$ and $D_2(R) = (1-\eta W_{14}(R))$ where $W_{14}(R) = w((R-R_0)/(R_{max}-R_0))$ and $w(z)$ is the fourteenth order optimal absorbing potential derived in Ref. [43]. R_0 is the point at which the CAP turns on and R_{max} is the largest R DVR point. This choice yields the CAP

$$W(R) = -i\eta\sqrt{(1-E_k^2)}W_{14}(R)\ . \tag{4.8}$$

The optimal CAP would be $W_{opt}(R) = E_k W_{14}(R)$. [43] The energy dependence of $W(R)$ is therefore not ideal but its dependence on the dissociative coordinate is. For a given energy if we choose η so that $\eta\sqrt{(1-E_k^2)} = E_k$ we obtain an optimal

CAP. The only consequence of using $W(R)$ rather than the optimal CAP is that the best value of the parameter η is a function of energy (and not necessarily close to one).

4.4 Lanczos-based methods for computing the eigenvalues of U

U is real but it is not symmetric. Because **U** is square it can be factorized $\mathbf{U} = \mathbf{B^{-1}A}$, where both **A** and **B** are symmetric. The asymmetric eigenvalue problem $\mathbf{UX} = \mathbf{Xu}$, where **X** is the matrix of right eigenvectors and **u** is the diagonal eigenvalue matrix, is therefore equivalent to the symmetric generalized eigenvalue problem $\mathbf{AX} = \mathbf{BXu}$. If **A** or **B** is positive definite all of the eigenvalues are real and there exist good numerical algorithms that exploit the symmetry of **A** and **B** for computing the eigenvales. For our problem $\mathbf{A} = \hat{\mathbf{D}}\mathbf{U}$ and $\mathbf{B} = \hat{\mathbf{D}}$, where

$$\hat{\mathbf{D}} = \begin{pmatrix} \mathbf{D_2} & \mathbf{0} \\ \mathbf{0} & -\mathbf{D_1} \end{pmatrix} . \tag{4.9}$$

Neither $\hat{\mathbf{D}}\mathbf{U}$ nor $\hat{\mathbf{D}}$ is positive definite. One way to compute the eigenvalues of **U** is to solve the $(\hat{\mathbf{D}}\mathbf{U})\mathbf{X} = \hat{\mathbf{D}}\mathbf{X}\mathbf{u}$ eigenproblem using a Lanczos algorithm based on the $\hat{\mathbf{D}}$ inner product. Various versions of this 'symmetric indefinite Lanczos method' are explained in articles and books. [44, 59–62] Two vectors **x** and **y** are orthogonal with respect to the $\hat{\mathbf{D}}$ inner product if $\mathbf{x^t}\hat{\mathbf{D}}\mathbf{y} = \mathbf{0}$. Unfortunately, if $\hat{\mathbf{D}}$ is not positive definite, Lanczos vectors that are othogonal with respect to the $\hat{\mathbf{D}}$ inner product may not even be linearly independent because of cancellation error. We have applied the 'symmetric indefinite Lanczos method' [44] to $(\hat{\mathbf{D}}\mathbf{U})\mathbf{X} = \hat{\mathbf{D}}\mathbf{X}\mathbf{u}$ and found that it works poorly.

4.4.1 The nonhermitian Lanczos method

Instead, we use the nonhermitian Lanczos method and create two sets of of bi-orthogonal Lanczos vectors. There are different ways to normalize the vectors and the accuracy of the computed eigenvalues depends on how the Lanczos vectors are normalized. [63,64] We follow the procedure of Freund and Nachtigal. [64] The Lanczos vectors are generated from three-term recurrence relations

$$\tilde{\mathbf{v}}_{\mathbf{n+1}} = \mathbf{U}\mathbf{v}_n - \mu_n \mathbf{v}_n - \nu_n \mathbf{v}_{n-1} \tag{4.10}$$

$$\tilde{\mathbf{w}}_{\mathbf{n+1}} = \mathbf{U}^{\mathbf{t}}\mathbf{w}_n - \mu_n \mathbf{w}_n - (\nu_n \rho_n / \xi_n)\mathbf{w}_{n-1} \tag{4.11}$$

where $\mu_n = \mathbf{w}_n^t \mathbf{U}\mathbf{v}_n/\delta_n$, $\nu_n = \xi_n \delta_n/\delta_{n-1}$, with $\rho_{n+1} = \|\tilde{\mathbf{v}}_{n+1}\|$, $\xi_{n+1} = \|\tilde{\mathbf{w}}_{n+1}\|$, $\mathbf{v_{n+1}} = \tilde{\mathbf{v}}_{\mathbf{n+1}}/\rho_{n+1}$, and $\mathbf{w}_{n+1} = \tilde{\mathbf{w}}_{\mathbf{n+1}}/\xi_{n+1}$. Formally, if $k \neq j$ $\mathbf{w}_k^t \mathbf{v}_j = 0$ and we define δ_k such that $\delta_k = \mathbf{w}_k^t \mathbf{v}_k$. The process is initiated with two arbitrary normalized vectors $\mathbf{v}_1$ and $\mathbf{w}_1$. Note that matrix-vector products with both $\mathbf{U}$ and $\mathbf{U^t}$ are necessary. The n columns of the matrices $\mathbf{V}_n$ and $\mathbf{W}_n$ are the first n Lanczos vectors. The recursion relations Eqs. (4.11) can be written in matrix form,

$$\mathbf{U}\mathbf{V}_M = \mathbf{V}_{M+1}\mathbf{T}_{M+1} \tag{4.12}$$

$$\mathbf{U}^{\mathbf{t}}\mathbf{W}_M = \mathbf{W}_{M+1}\mathbf{\Gamma}^{-1}{}_{M+1}\mathbf{T}_{M+1}\mathbf{\Gamma}_M \tag{4.13}$$

where $\mathbf{\Gamma}_M$ is a diagonal matrix whose diagonal elements are $(\mathbf{\Gamma}_M)_{11} = \gamma_1 = 1$, $(\mathbf{\Gamma}_M)_{kk} = \gamma_k = \gamma_{k-1}\rho_k/\xi_k$, and $\mathbf{T}_{M+1}$ is the $(M+1) \times M$ upper left corner of a

$(M+1)\times(M+1)$ tridiagonal matrix,

$$(\mathbf{W^t}_{M+1}\mathbf{V}_{M+1})^{-1}(\mathbf{W^t}_{M+1}\mathbf{U}\mathbf{V}_M) = \mathbf{T}_{M+1} = \begin{pmatrix} \mu_1 & \nu_2 & 0 & \cdots & 0 \\ \rho_2 & \mu_2 & \ddots & & \vdots \\ 0 & \ddots & \ddots & \ddots & \\ \vdots & & \ddots & \mu_{M-1} & \nu_M \\ 0 & \cdots & & \rho_M & \mu_M \\ 0 & \cdots & & 0 & \rho_{M+1} \end{pmatrix} \tag{4.14}$$

Multiplying Eq. (4.12) on the left by $\mathbf{W^t}_M$ and using the bi-orthogonality of the vectors one obtains

$$\mathbf{W^t}_M\mathbf{U}\mathbf{V}_M = \mathbf{\Delta}_M\mathbf{T}_M \tag{4.15}$$

where $\mathbf{T}_M$ is obtained from $\mathbf{T}_{M+1}$ by removing the last row and $\mathbf{\Delta}_M$ is an $M\times M$ diagonal matrix whose diagonal elements are the δ_M values. The matrix eigenvalue problem we wish to solve is $\mathbf{UX} = \mathbf{Xu}$. Multiplying on the left by $\mathbf{W^t}_M$ and introducing $\mathbf{X} = \mathbf{V}_M\mathbf{R}$ we find $\mathbf{\Delta}_M\mathbf{T}_M\mathbf{R} = \mathbf{\Delta}_M\mathbf{R}\mathbf{u}$ or $\mathbf{T}_M\mathbf{R} = \mathbf{R}\mathbf{u}$. One hopes that some of the eigenvalues of $\mathbf{T}_M$ will be very close to eigenvalues of $\mathbf{U}$ even if M is much smaller than the size of $\mathbf{U}$.

Cullum & Willoughby [65] propose using recursion relations that generate a symmetric tridiagonal matrix. This has the disadvantage that it requires doing complex matrix-vector products but the advantage that it helps to limit the nefarious effect numerical error can have on results obtained with the nonhermitian Lanczos algorithm. We use the recursion relations of Freund and Nachtigal (and real matrix-vector products) but after calculating the Lanczos vectors we compute eigenvalues of a complex-symmetric tridiagonal matrix $\tilde{\mathbf{T}}_M = \mathbf{G}^{-1}\mathbf{T}_M\mathbf{G}$ where $\mathbf{G}$ is a diagonal matrix chosen so that $\mathbf{G}^{-1}\mathbf{T}_M\mathbf{G}$ is symmetric. The complex-symmetric

matrix whose eigenvalues we compute is,

$$\tilde{\mathbf{T}}_M = \begin{pmatrix} \mu_1 & \sqrt{\rho_2\nu_2} & 0 & \cdots & 0 \\ \sqrt{\rho_2\nu_2} & \mu_2 & \ddots & & \vdots \\ 0 & \ddots & \ddots & \ddots & \\ \vdots & & \ddots & \mu_{M-1} & \sqrt{\rho_M\nu_M} \\ 0 & \cdots & & \sqrt{\rho_M\mu_M} & \mu_M \end{pmatrix}. \tag{4.16}$$

Because the tridiagonal matrix is symmetric there is no need to balance [44] it before computing its eigenvalues and there is no need to compute both right and left eigenvectors (they are identical). Using the CMTQL routine [49] to extract the eigenvalues of the complex-symmetric matrix $\tilde{\mathbf{T}}_M$ also renders the algorithm more efficient.

4.4.2 Coupled two-term variant

We would like to use the nonhermitian Lanczos algorithm the same way one commonly uses the Hermitian Lanczos algorithm: without reorthogonalization and assuming that copied eigenvalues are good. In the Hermitian case eigenvalue copies are accurate to machine precision. [49] In the nonhermitian case this is not true. *Near* copies *are* produced but as we augment the number of iterations, the norm of the difference of the copied eigenvalues with the largest and smallest norms increases. Due to this spread, we do not know what to take as the best estimate of an eigenvalue. After doing many iterations the clump of $\mathbf{T}$ eigenvalues associated with one eigenvalue of $\mathbf{U}$ overlaps with the clump of $\mathbf{T}$ eigenvalues associated with one another eigenvalue of $\mathbf{U}$. To some extent these problems can be alleviated by using the coupled two-term Lanczos approach. [64] A set of $\mathbf{p}_k$ vectors that spans the same space as the $\mathbf{v}_k$ vectors and a set of $\mathbf{q}_k$ vectors that spans the same space as the $\mathbf{w}_k$ vectors are generated with the $\mathbf{v}_k$ and $\mathbf{w}_k$. The M columns of the matrix

$\mathbf{P}_M$ ($\mathbf{Q}_M$) are the first M $\mathbf{p}_k$ ($\mathbf{q}_k$ vectors). Start with Eq. (4.12) and replace $\mathbf{T}_{M+1}$ with its LU factorization, $\mathbf{T}_{M+1} = \mathbf{L}_M \mathbf{U}'_M$ (the upper triangular matrix is denoted $\mathbf{U}'_M$ to avoid confusing it with $\mathbf{U}$ the matrix whose eigenvalues are sought),

$$\mathbf{U}\mathbf{V}_M = \mathbf{V}_{M+1}\mathbf{L}_M\mathbf{U}'_M \ . \tag{4.17}$$

If $\mathbf{P}_M$ is defined so that $\mathbf{V}_M = \mathbf{P}_M\mathbf{U}'_M$ we obtain

$$\mathbf{U}\mathbf{P}_M = \mathbf{V}_{M+1}\mathbf{L}_M \ . \tag{4.18}$$

If $\mathbf{Q_M}$ is defined so that $\mathbf{W}_M = \mathbf{Q}_M{\mathbf{\Gamma}^{-1}}_M\mathbf{U}'_M\mathbf{\Gamma}_M$, then

$$\mathbf{U}^{\mathbf{t}}\mathbf{Q}_M = \mathbf{W}_{M+1}{\mathbf{\Gamma}^{-1}}_{M+1}\mathbf{L}_M\mathbf{\Gamma}_M \ . \tag{4.19}$$

Note that both $\mathbf{L}_M$ and $\mathbf{U}'_M$ are bidiagonal because $\mathbf{T}_M$ is tridiagonal. Owing to this bidiagonality the four recursion relations used to generate the four sets of vectors involve only two vectors (see appendix A for the full algorithm):

$$\mathbf{p}_n = \mathbf{v}_n - \frac{\xi_n\delta_k}{\epsilon_{n-1}}\mathbf{p}_{n-1} \tag{4.20}$$

$$\mathbf{q}_n = \mathbf{w}_n - \frac{\rho_n\delta_k}{\epsilon_{n-1}}\mathbf{q}_{n-1} \tag{4.21}$$

$$\tilde{\mathbf{v}}_{n+1} = \mathbf{U}\mathbf{p}_n - \beta_k\mathbf{v}_n \tag{4.22}$$

$$\tilde{\mathbf{w}}_{n+1} = \mathbf{U}^{\mathbf{t}}\mathbf{q}_n - \beta_k\mathbf{w}_n \tag{4.23}$$

where $\epsilon_n = {\mathbf{q}^{\mathbf{t}}}_n\mathbf{U}\mathbf{p}_n$ and $\beta_n = \epsilon_n/\delta_n$. It has been argued that this coupled-two-term variant of the Lanczos algorithm is more stable. [64] The stability is achieved at the expense of updating a couple of constants at each iteration and storing one more vector. The non-zero elements of the symmetric complex tridiagonal matrix $\tilde{\mathbf{T}}_M$

are found by combining the elements of the LU factorization

$$\mu_n = \beta_n + \rho_n \xi_n \delta_n / \epsilon_{n-1} \tag{4.24}$$

$$\chi_n = \sqrt{\rho_n \nu_n} = \sqrt{\beta_{n-1} \rho_k \xi_n \delta_n / \epsilon_{n-1}} \tag{4.25}$$

where χ_n are the offdiagonal elements.

4.4.3 All of the required vectors can be generated from one set of matrix-vector products

The coupled two-term variant of the nonhermitian Lanczos algorithm does appear to be numerically more stable than its three-term counterpart but by itself it is not an attractive approach for computing resonances because $2M$ matrix-vector products (M with $\mathbf{U}$ and M with $\mathbf{U^t}$) are necessary to extract eigenvalues associated with a Krylov space of size M. It is possible to reduce the number of matrix-vector products by a factor of two by exploiting the fact that $\mathbf{U^t}\hat{\mathbf{D}} = \hat{\mathbf{D}}\mathbf{U}$. [57] It is easy to verify that the $\mathbf{w}_k$ computed from

$$\tilde{\mathbf{w}}_{k+1} = \theta_k \hat{\mathbf{D}} \tilde{\mathbf{v}}_{\mathbf{k+1}} \tag{4.26}$$

satisfy the recursion relation Eq. (4.22) if $\theta_k = \theta_{k-1}\rho_k/\xi_k$ where $\theta_0 = 1$. The new vectors $\mathbf{q}_k$ are obtained from

$$\mathbf{q}_k = \theta_k \hat{\mathbf{D}} \mathbf{p}_k \ . \tag{4.27}$$

Since the matrix $\hat{\mathbf{D}}$ is diagonal, the cost of a $\hat{\mathbf{D}}$ matrix-vector product is negligible compared to the cost of a $\mathbf{U}$ matrix-vector product. This refinement therefore reduces the cost of each nonhermitian Lanczos iteration by about a factor of two.

4.5 Accurate resonance eigenvalues

Using the coupled two-term variant of the nonhermitian Lanczos algorithm and exploiting the fact that $\mathbf{U}$ is symmetric with respect to the $\hat{\mathbf{D}}$ inner product it is in principle possible to compute complex resonance energies from a single set of matrix-vector products without using complex arithmetic. Despite the advantages of the coupled two-term variant it is not, however, possible to obtain accurate eigenvalues of $\mathbf{U}$ by increasing the size of $\mathbf{T}_M$ and hoping that nearly perfect numerical copies will indicate that an eigenvalue of $\mathbf{T}_M$ is also an eigenvalue of $\mathbf{U}$. The quality of the copies, though better than with the three-term variant, is just not good enough.

4.5.1 Accurate eigenvalues and eigenvectors

We first outline a procedure for computing accurate eigenvalues and eigenvectors of $\mathbf{U}$ for a particular value of η for which we have computed a $\mathbf{T}_M$ matrix. We are interested only in the resonance eigenpairs. The resonance eigenvalues correspond to eigenvalues of $\mathbf{U}$ whose magnitudes are close to one. The $\mathbf{U}$ matrix of MN has been constructed to facilitate the convergence of these eigenvalues. We make a list of $\mathbf{T}_M$ eigenvalues ordering them according to their real part. Focusing only on eigenvalues with norms close to one, we identify groups for which the norm of the differences and the difference of the norms of neighbouring eigenvalues in the list are less than 10^{-4}. The average of the eigenvalues in a group is denoted $\tilde{u}$. $\tilde{u}$ is an approximate eigenvalue of $\mathbf{U}$. As $\mathbf{U}$ is not symmetric it has right and left eigenvectors. Approximate right eigenvectors of $\mathbf{T}_M$ are computed by inverse iteration (see Appendix B) using the LU decomposition of $(\tilde{u}\mathbf{I} - \mathbf{T}_M)$. The matrix of approximate right eigenvectors of $\mathbf{T}_M$ is denoted $\tilde{\mathbf{R}}$. Approximate right eigenvectors of $\mathbf{U}$ are obtained from approximate right eigenvectors of $\mathbf{T}_M$ by $\mathbf{X}^R_{Lan} = \mathbf{V}_{ID}\tilde{\mathbf{R}}$ where ID is the optimal iteration depth. [49, 50] We store the Lanczos vectors on

disk. It is straightforward to show that the left eigenvectors can be obtained from the right eigenvectors by using the relation

$$\mathbf{X}_{Lan}^{L} = \hat{\mathbf{D}}\mathbf{X}_{Lan}^{R} \ . \tag{4.28}$$

Due to the fact that the cluster of eigenvalues centered at $\tilde{u}$ is fairly large, $\tilde{u}$ is only a good approximation for an eigenvalue of $\mathbf{U}$ but it is not itself accurate. Similarly, the approximate right and left eigenvectors $\mathbf{X}_{Lan}^{R}$ and $\mathbf{X}_{Lan}^{L}$ are good approximations but not accurate.

When obtaining an eigenvector of $\mathbf{U}$ from the corresponding eigenvector of $\mathbf{T}_M$ it is important to use the right iteration depth, i.e., the right number of Lanczos vectors. Cullum & Willoughby provide a scheme for determining the optimal iteration depth in the complex-symmetric case. [49] They indicate that, for a given eigenvalue, it is between the number of iterations at which the first copy appears (m_{k1}) and the number at which the second copy appears (m_{k2}). To find the optimal iteration depth we compute eigenvectors $\tilde{\mathbf{r}}_{Lan}$ of $\mathbf{T}_K$ for 20 values of K between m_{k1} and m_{k2} and choose the value which minimizes $\|\rho_{K+1}\tilde{r}_{Lan}^{(K)}\|$, where $\tilde{r}_{Lan}^{(K)}$ is the K^{th} component of the computed vector.

To obtain accurate eigenvalues and eigenvectors of $\mathbf{U}$ we might implement further refinements of the nonhermitian Lanczos method (local re-bi-orthogonalization of Lanczos vectors, look-ahead Lanczos, etc.). [44] Instead, we use the approximate right and left eigenvectors computed using the nonhermitian Lanczos method to obtain accurate eigenvalues and eigenvectors. If the right and left eigenvectors we obtain from the nonhermitian Lanczos method are good approximations for the true right and left eigenvectors of $\mathbf{U}$ they should be excellent for the purpose of computing accurate eigenvalues and eigenvectors. To solve $\mathbf{UX} = \mathbf{Xu}$ we first set $\mathbf{X} = \mathbf{X}_{Lan}^{R}\mathbf{Z}$, then mutliply on the left by $(\mathbf{X}_{Lan}^{L})^t$ and finally solve the eigenvalue problem $(\mathbf{X}_{Lan}^{L})^t\mathbf{U}\mathbf{X}_{Lan}^{R}\mathbf{Z} = (\mathbf{X}_{Lan}^{L})^t\mathbf{X}_{Lan}^{R}\mathbf{Z}\mathbf{u}$. $(\mathbf{X}_{Lan}^{L})^t\mathbf{X}_{Lan}^{R}$ is nearly diagonal. By

using the approximate right and left eigenvectors, obtained from the nonhermitian Lanczos method, in this way we greatly increase the accuracy of the final eigenvalues and the stability of the algorithm. We obtain not only accurate complex energies but also accurate eigenvectors from which we can obtain accurate resonance wavefunctions. Methods that do not construct an explicit basis [27, 57] cannot obtain wavefunctions directly. One has to either re-evaluate all the matrix-vector products or read from disk the stored Chebyshev vectors (the way we read the stored Lanczos vectors) to get wavefunctions.

4.5.2 Using damped basis functions

The ultimate goal of most methods for determining resonance energies and widths is the computation of complex Siegert eigenvalues. Due to the fact that the Siegert functions that correspond to resonances diverge exponentially this cannot be done by diagonalizing the Hamiltonian operator in a basis suitable for computing bound states. However, matrix methods are the best for the purpose of computing many states. The usual solution to this quandary is to modify H so that it *can* be used with a basis suitable for computing bound states in order to compute resonance states. The most common modifications are a rotation in the complex plane of the dissociative coordinate [13,14] and the addition of a CAP [18,21,23]. In this subsection we advocate choosing the basis so that complex resonance energies may be obtained from the *unmodified* operator.

Although in this paper we work with $\mathbf{U}$ the idea will be explained first as it would be applied to H. As basis functions for H we suggest using functions that are similar to the Siegert functions (i.e. they diverge exponentially) we wish to calculate but are damped far from the interaction region that determines both the energy and the width of the resonances. The particular basis functions we suggest for use with H are those associated with the resonance eigenvectors of $\mathbf{H} - i\eta\mathbf{W}'$ for some appropriate value of $\eta = \eta_{guide}$. Because the exponential

divergence is built into the basis functions eigenvalues are good approximations for the Siegert energies. The accuracy of the eigenvalues depends on the quality of the CAP. If both transmission and reflection error are small, eigenvalues in the damped basis are very close to Siegert energies. Note that it is important to use *only* the resonance eigenvectors. If eigenvectors that correspond to non-resonance eigenvalues are included in the basis the method will be less accurate. This is due to the fact that non-resonance eigenfunctions do not have outgoing boundary conditions, are therefore not damped, and are thus not small where the CAP is large. Define the projectors $P = \sum_k |\phi_k\rangle\langle\phi_k^*|$ and $Q = 1 - P$ (P and Q here are not to be confused with the matrix of Lanczos vectors), where the $|\phi_k\rangle$ are resonance eigenfunctions of $H - i\eta_{guide}W'$. It is easy to show that the complex energy E_j, where $H\psi_j = E_j\psi_j$, is an eigenvalue of the matrix whose elements are $\langle\phi_k^*|H|\phi_{k'}\rangle$ if the ϕ_k are orthogonal, $\langle\phi_k^*|H|Q\psi_j\rangle = 0$ and $\langle\phi_k^*|Q\psi_j\rangle = 0$. The last two conditions are nearly fulfilled if all of the $|\phi_k\rangle$ are small where W' is large. Using resonance eigenfunctions for $\eta = \eta_{guide}$ as basis functions works for exactly the same reason that it is possible to compute complex resonance energies by adding a CAP to the Hamiltonian.

We could apply the idea of using approximate resonance eigenfunctions as basis functions to compute eigenvalues of H. Instead we have used it in conjunction with $\mathbf{U}$. We do this because $\mathbf{U}$ matrix-vector products are real and because the eigenvalues of $\mathbf{U}$ that correspond to resonance eigenvalues converge preferentially. Eigenvalues of $\mathbf{U}(\eta = 0)$ that correspond to resonance states are computed by using the $\mathbf{X}^L_{Lan}$ and $\mathbf{X}^R_{Lan}$ eigenvector matrices computed for some reasonable choice of η_{guide}. Because the $\mathbf{U}(\eta = \eta_{\mathbf{guide}})$ matrix used to create the basis is not symmetric we must use both the right and the left eigenvectors. Also in this case, it is important to include only resonance basis functions. From the computed eigenvalues of $\mathbf{U}(\eta = 0)$ we obtain the corresponding H eigenvalues. The final eigenvalue problem

we solve is $\mathbf{U}^0_{LR}\mathbf{M} = \mathbf{S}_{LR}\mathbf{M}\mathbf{F}$ where

$$\mathbf{U^0_{LR}} = (\mathbf{X}^R_{Lan})^t \hat{\mathbf{D}} \mathbf{U}_{\eta=0} \mathbf{X}^R_{Lan} \tag{4.29}$$

$$= (\mathbf{X}^R_{Lan})^t \begin{pmatrix} \mathbf{D_{2,guide}} & \mathbf{0} \\ \mathbf{0} & -\mathbf{D}_{1,guide} \end{pmatrix} \begin{pmatrix} \mathbf{0} & \mathbf{I} \\ -\mathbf{I} & 2\mathbf{H} \end{pmatrix} \mathbf{X}^R_{Lan} \tag{4.30}$$

$$\mathbf{S}_{LR} = (\mathbf{X}^R_{Lan})^t \hat{\mathbf{D}} \mathbf{X}^R_{Lan} \tag{4.31}$$

$$= (\mathbf{X}^R_{Lan})^t \begin{pmatrix} \mathbf{D}_{2,guide} & \mathbf{0} \\ \mathbf{0} & -\mathbf{D}_{1,guide} \end{pmatrix} \mathbf{X}^R_{Lan} \, . \tag{4.32}$$

To avoid storing a large number of vectors we compute eigenvalues in groups (for HCO (see the next section) we use four groups). For each group a different subset of the approximate nonhermitian Lanczos eigenvectors is used. We group together eigenvectors for which the corresponding eigenvalues have similar imaginary parts. This is done because the amelioration we achieve by solving $\mathbf{U}^0_{LR}\mathbf{M} = \mathbf{S}_{LR}\mathbf{M}\mathbf{F}$ is most important for the imaginary parts of the eigenvalues. The real parts of the diagonal elements of $\mathbf{F}$ are close to the real parts of the appropriate eigenvalues of $\mathbf{T}_M$. It is clear that for the purposes of calculating a Siegert wavefunction that diverges slowly it is better to take basis functions that are also diverge slowly. Including basis functions that diverge more rapidly would degrade the quality of the computed complex resonance energy.

If our basis set is good enough the diagonal elements of $\mathbf{F}$ are good numerical approximations for the Siegert energies. There is no error caused by modifying the operator. The only error is due to the failings of the basis set. Reflection from and transmission through the CAP will influence the basis functions. Varying η_{guide} reveals cusps but because the CAP is excellent the region of stability is very broad. For HCO we need only one η_{guide} to compute all of the resonances.

4.6 Resonance calculation for HCO

To demonstrate that the proposed Lanczos procedure works and is efficient we have computed $J = 0$ resonances for HCO. As there are many previous calculations of these resonances we can use HCO to show that with the Lanczos procedure of this paper one can obtain very accurate results. HCO is a popular test molecule in part because energies and widths of many states have been measured. These calculations show that the method works and is efficient but we have made no attempt to choose a particularly good primitive basis set. Several good potential surfaces exist. [66–68] We have chosen to use the WKS surface of Floethmann, Dobbyn, Werner, Keller and Schinke. [68]. We use Jacobi coordinates: r is the distance between the carbon and the oxygen atoms; R is the distance between H and the center of mass of CO; and γ is the angle between the r and R vectors, with $\gamma = \pi$ corresponding to the linear H-C-O configuration. R and γ are strongly coupled. Owing to the strong coupling a large basis is required to obtain converged results. We use the same masses as in Ref. [46] and the energy conversion factors on the NIST website. [69] Following Mandelshtam and Neumaier, we choose a simple direct-product DVR basis. [57] For the r coordinate we used 160 sine-DVR basis functions [70] in the interval $[1.8, 3.5]a_0$ to make $N_r = 16$ potential optimized DVR (PODVR) functions from eigenfunctions of a 1D Hamiltonian, $H^r_{1D}(r) = T_{1D}(r) + V(R_{min}(r), r, \gamma_{min}(r))$, where $V(R, r, \gamma)$ is the full 3D HCO potential and $R_{min}(r)$ and $\gamma_{min}(r)$ are minimum values of R and γ for each value of r. [71–77] Powell's method is used for the minimization procedure. [78] For the R coordinate, we use 400 sine-DVR functions in the range $[2, 8]a_0$ to make $N_R = 40$ PODVR functions from eigenfunctions of a 1D Hamiltonian, $H^R_{1D}(R) = T_{1D}(R) + V_(r_{min}(R), R, \gamma_{min}(R))$. $N_\gamma = 46$ Legendre DVR functions were used for γ. To reduce the spectral range ΔH and thereby reduce the number of matrix-vector products required [49], a potential energy ceiling [79] of $25000 cm^{-1}$ is imposed. As a result, $\Delta H \cong 45000 cm^{-1}$. The convergence of the

eigenvalues obtained with this basis was accessed by adding four basis functions for each coordinate and recomputing eigenvalues. Both the real and imaginary parts of the eigenvalues with real parts below $9000cm^{-1}$ change by less than $0.01cm^{-1}$ The change in the eigenvalues produced by changing the CAP used to generate the basis of approximate eigenvectors is larger.

The number of digits presented in Table I is a measure of our confidence in the accuracy of the results. To determine which digits are uncertain we do calculations with five different CAPs. We use: (1) the CAP defined in Eq. (4.8) with $R_0 = 5a_0$ (and absorbing width of $3a_0$) and $\eta_{guide} = 0.040913$; (2) the CAP defined in Eq. (4.8) with $R_0 = 5.5a_0$ (and absorbing width of $2.5a_0$) and $\eta_{guide} = 0.040913$; (3) the M&T CAP [57] with $R_0 = 5a_0$ (and absorbing width of $3a_0$) and $\eta_{guide} = 0.129378$; (4) the 5^{th}-order polynomial of Ref. [42] with $R_0 = 5a_0$ (and absorbing width of $3a_0$) and $\eta_{guide} = 0.0129378$); and (5) the 5^{th}-order polynomial of Ref. [42] with $R_0 = 5.25a_0$ (and absorbing width of $2.75a_0$) and $\eta_{guide} = 0.0129378$). Resonance energies obtained with these CAPs were all very close. The last digit of the numbers reported in the table depends on the CAP. The numbers reported are for CAP (1).

8000 Lanczos iterations (and thus 8000 matrix-vector products) were needed to obtain all resonance and bound states with energies lower than $9000cm^{-1}$. The number of required iterations depends slightly on the CAP used (8000 is for CAP (1)). MN use a similar number of matrix-vector products for a single value of η. [57] After having computed the approximate eigenvectors we calculate the complex resonance energies in groups. We divide the approximate right eigenvectors into four groups: one group for resonances with small widths, two for resonances with medium widths, and another for resonances with large widths. The parameters of the groups are listed in Table 4.2. Each group contains eigenvectors whose eigenvalues have similar imaginary parts and therefore basis functions with similar outgoing boundary conditions. It is also important to include enough eigenvectors in each group to make it possible to represent accurately the resonance wavefunc-

tions.

In Table 4.1 energies and widths of resonance states computed using our method and other methods [46, 57] are compared. The state labels are those given in Ref. [68]. In general, the resonance energies and widths agree very well. The calculation of precise widths is notoriously difficult. For some states our widths are larger or smaller than those of both the previous accurate calculations but for many states our widths are between those of the the previous calculations. The accuracy of our results is very good for resonances with widths whose magnitude is greater than than 10^{-6} (included in window I). The width of the first resonance, which is extremely narrow, is different for different CAPs and we are therefore only able to provide an upper bound for its width. Using $\mathbf{U}$ makes the width of the narrowest resonances especially sensitive to the choice of the CAP. This is due to the fact that the mapping between the eigenvalues of $\mathbf{U}$ and those of $\mathbf{H}+\mathbf{W}$ magnifies error (when computing the imaginary part of E_k from u_k a lot of of cancellation occurs). This is a disadvantage of using $\mathbf{U}$ (with a Lanczos-based method or a FD method). $\mathbf{U}$ has the advantage of favoring convergence of resonance eigenvalues but it does make computing eigenvalues of $\mathbf{H}+\mathbf{W}$ with very small widths difficult.

Our goal is to compute resonances with widths less than $105cm^{-1}$ and we therefore include in our basis only approximate eigenvectors with widths less than $105cm^{-1}$. Nevertheless, one state with $\Gamma = 106cm^{-1}$ appears when we compute eigenvalues using the basis functions with the largest widths. Our basis functions are all obtained with a single CAP (associated with a value of η_{guide}). It is not surprising that although none of the basis functions does a good job of representing a state with $\Gamma = 106cm^{-1}$ it is possible to obtain the state from a linear combination of them. This is another demonstration of the usefulness of the approximate eigenvector basis idea.

Table 4.1: Resonance energies and widths of HCO.[†]

Keller et al.	Present results		Poirier & Carrington		Mandelshtam & Neumaier	
State	E_{res}	Γ_{res}	E_{res}	Γ_{res}	E_{res}	Γ_{res}
|013 >	1098.7931	<2E-7	1098.7934	<1E-6	1098.7963	3E-8
|005 >	1251.1494	1.7E-6	1251.148	2E-6	1251.1525	1.8E-6
|111 >	1386.8741	0.00103	1386.88	0.00105	1386.877	0.00105
|103 >	1512.9827	0.0130	1512.993	0.0128	1512.986	0.0126
|030 >	1595.9671	3.3E-6	1595.972	4E-6	1595.9708	3.2E-6
|201 >	1633.5154	0.0564	1633.526	0.0558	1633.518	0.0572
|022 >	1897.2437	7.57E-4	1897.242	7.5E-4	1897.247	7.6E-4
|300 >	2069.0924	30.06	2069.6	29.5	2069.2	30.3
|014 >	2105.5321	0.7334	2105.537	0.741	2105.536	0.737
|006 >	2208.1948	0.0414	2208.16	0.0412	2208.198	0.0411
|120 >	2223.815	3.270	2223.85	3.265	2223.83	3.274
|202 >	2352.39	5.81	2352.47	5.75	2352.38	5.77
|112 >	2460.104	2.313	2460.12	2.28	2460.11	2.32
|210 >	2550.722	10.65	2550.78	10.54	2550.71	10.63
|104 >	2604.42	15.9	2604.3	15.7	2604.4	15.93
|031 >	2660.6367	0.0984	2660.63	0.09753	2660.64	0.0981
|023 >	2923.5512	0.1886	2923.556	0.1881	2923.554	0.1888
|015 >	3077.53	5.031	3077.5	5.04	3077.53	5.03
|007 >	3132.989	0.814	3132.82	0.8077	3132.991	0.814
|121 >	3232.32	7.36	3232.32	7.3	3232.327	7.31
|203 >	3251.29	67.4	3251.1	68.6	3251.3	67.5
|040 >	3388.1956	0.0782	3388.21	0.0786	3388.2	0.0782

Continued on next page

$\|113>$	3409.659	17.2	3409.6	17.17	3409.66	17.18
$\|211>$	3512.29	22.41	3512.31	22.43	3512.29	22.39
$\|105>$	3565.6	57.7	3566.1	57.8	3565.6	57.9
$\|032>$	3704.864	0.238	3704.872	0.238	3704.866	0.24
$\|024>$	3921.763	4.8	3921.77	4.677	3921.77	4.687
$\|130>$	3999.84	19.7	3999.9	18.9	3999.84	19.8
	3999.22	32.82			3999.2	32.8
$\|016>$	4036.63	9.96	4036.49	10.03	4036.63	9.94
$\|220>$	4084.73	20.2	4084.6	19.5	4084.71	20.25
$\|122>$	4214.48	23.1	4214.7	23.4	4214.49	23.12
$\|114>$	4345.8	23.82	4345.8	23.68	4345.79	23.8
$\|041>$	4436.597	10.07	4436.7	9.9	4436.61	10.03
	4463.67	12.46	4463.8	12.45	4463.7	12.44
$\|212>$	4514.18	47.9	4514.2	47.65	4514.1	47.8
$\|033>$	4725.7651	0.7259	4726.773	0.728	4725.768	0.727
$\|017>$	4885.81	9.99	4885.6	10.4	4885.78	9.98
	4887.7	64.62			4887.8	65.6
$\|131>$	5057.74	17.09	5057.9	17	5057.81	17.12
$\|213>$	5143.5	73	5143.5	73.2	5143.6	73.5
$\|050>$	5155.9330	0.0545	5156.2	0.054	5155.939	0.0544
$\|123>$	5275.69	32.5	5275.7	32.1	5275.8	32.3
$\|221>$	5400.5	46.6	5400.2	46.8	5400.5	46.6
$\|042>$	5492.9	6.03	5492.86	6.08	5492.91	6
$\|034>$	5717.82	5.22	5717.85	5.245	5717.82	5.23
	5752.59	21.14	5756	20.85	5752.56	21.13
$\|140>$	5823.011	9.3	5823.12	9.22	5823.02	9.29
$\|026>$	5845.5	61.8	5846.5	62.6	5845.4	62

Continued on next page

	5872.8	48.8	5872	49.8	5872.7	48.5
$\|230>$	5976.3	46.7	5976.83	45.9	5976.3	46.7
$\|132>$	6049.6	35.9	6049.7	36.2	6049.3	35.6
	6201.9	41.8	6201.9	42.1	6201.8	41.8
$\|051>$	6209.06	2.11	6209.04	2.079	6209.07	2.21
	6299.5	104.2			6299.7	104.2
$\|320>$	6343.83	31.1	6343.3	31.4	6343.9	31.2
$\|222>$	6402.2	81.8	6402.7	82.01	6402.3	81.7
$\|043>$	6507.59	3.11	6507.64	3.09	6507.59	3.1
$\|019>$	6652.98	27.0	6650.3	26.32	6652.99	26.96
$\|035>$	6679.815	37.8	6680	38.6	6679.8	37.9
	6718.0	106.5			6717.6	106.8
$\|027>$	6759.60	34.9	6759.11	35	6759.6	34.8
$\|141>$	6867.7	33.3	6867.6	34	6867.6	33.5
$\|060>$	6899.106	0.592	6899.15	0.6	6899.107	0.594
$\|223>$	6987.0	86	6987	85.8	6986.8	85.7
$\|125>$	7124.08	71.4	7124.2	71.7	7124.2	71.7
$\|052>$	7233.24	18.4	7233.1	18.2	7233.23	18.26
	7281.05	74.4	7281	74	7281.1	74.1
$\|044>$	7493.84	8.69	7493.83	8.73	7493.84	8.68
	7563.6	52.3	7568	50.3	7563.4	52.2
	7587	69	7585.8	74.8	7587.2	68.6
$\|150>$	7602.61	7.29	7602.67	7.31	7602.63	7.29
$\|036>$	7656.65	29.66	7656.7	29.56	7656.64	29.68
$\|142>$	7812.9	47.8	7813.3	47	7813.1	48.1
$\|240>$	7884.85	66.47	7884.9	66.6	7884.9	66.2
$\|061>$	7952.2875	5.526	7952.3	5.53	7952.29	5.52

Continued on next page

	8030.7	74.4			8030.7	74.3
|224 >	8170.7	105.2	8171.1	105	8170.6	105.1
|151 >	8233.02	29.2	8232	30.3	8233.06	29.48
|053 >	8236.6	96.4	8237.3	94	8236.6	96.1
	8287.15	66.3	8287.1	68.2	8287.2	66.9
|045 >	8444.9	37.9	8445.08	37.92	8444.9	37.9
	8486.6	37.2	8488	41	8486.7	37.5
	8557.58	52.68	8556.2	53	8557.5	52.6
|151 >	8557.68	39.00	8558	38	8557.7	39
|070 >	8616.4132	0.7170	8616.5	0.728	8616.421	0.717
|241 >	8688.0	76.5	8684	77	8687.8	76.3
|143 >	8801.8	88.7	8802.3	90	8801.8	88.6
	8921.5	90.9	8921.4	90.9	8921.4	90.9
|062 >	8973.25	8.22	8973.7	7.7	8973.27	8.28

† all energies and widths in cm^{-1}

Table 4.2: Parameters defining the groups used to compute the resonance states.†

Group	$Im(E)_{max}$	$Im(E)_{min}$	Number of basis vectors
I	0	-1	34
II	-1	-10	24
III	-10	-25	25
IV	-25	-55	22

† imaginary parts of energies in cm^{-1}.

4.7 Conclusion

In this paper we propose a new method for computing resonance energies and widths. We demonstrate that with a CAP of the form of Eq. (4.2) it is possible

to use Lanczos-based ideas to compute complex resonance energies without doing complex matrix-vector products or doubling the number of real matrix-vector products; The usual way to use the Lanczos algorithm to determine resonance widths requires adding a CAP to the Hamiltonian and computing eigenvalues of a complex-symmetric matrix. This entails doing complex matrix-vector products. This works, but it would be nice to avoid doing complex matrix-vector products. It is natural to suspect that this must be possible because in many ways FD and Lanczos are very similar and it *is* possible to use FD to get resonance widths without doing complex matrix-vector products. By exploiting the link between the $H + W$ eigenvalue problem, the quadratic eigenvalue problem of Eq. (4.4), and the doubled-size eigenvalue problem of Eq. (4.6) revealed by MN it is immediately obvious that one should be able to use Lanczos type methods to obtain resonance widths without doing complex matrix-vector products. However, Lanczos methods for nonsymmetric problems are difficult to use. Owing to finite computer precision the relationship between the eigenvalues of the tridiagonal matrix and the eigenvalues of the original matrix is lost. The eigenvalues and (right and left) eigenvectors that can be obtained with Lanczos methods are good but their precision is not nearly good enough for the purpose of determining resonance widths. We deal with this problem by using the eigenvectors we get from the Lanczos calculation as basis vectors, a bit like using approximate Lanczos vectors as a basis in the preconditioned inexact spectral transform (PIST) method. [46, 80, 81] This works very well. We do not need quadruple precision. We observe that we can accurately compute resonance energies and widths for resonances for which the approximate eigenvectors in the basis are poor. This clearly implies that the quality of our results is not determined by the error of the individual approximate eigenvectors. To use this idea we must store Lanczos vectors on disk. Note however that it is not necessary to read in the Lanczos vectors during the Lanczos iteration. We read the Lanczos vectors only when we compute approximate eigenvectors. Our method au-

tomatically provides not only complex energies but also wavefunctions. With one CAP (and therefore one set of matrix-vector products) we are able to obtain all of the resonances of HCO below $9000cm^{-1}$. In some cases our resonance energies and widths could be very slightly improved by adjusting η_{guide} or otherwise improving the basis but the range of η_{guide} values for which eigenvalues are stable appears to be very broad. It might be argued that a disadvantage of our approach is the need to compute (approximate) eigenvectors using a Lanczos approach but eigenvectors give us wavefunctions, which enable us to assign and interpret a resonance spectrum.

Acknowledgements

We are grateful to Bill Poirier for providing the WKS potential routine and to Vladimir Mandelshtam for helpful comments. This work has been supported by the Natural Sciences and Engineering Research Council of Canada. Some of the calculations were done on a computer of the Réseau québécois de calcul de haute performance.

4.8 Appendix A

In this appendix we give a pseudocode for the coupled two-term nonhermitian Lanczos algorithm including all constants and vectors updates. Boldface quantities are vectors and matrices.

$\mathbf{p_0} = \mathbf{0}$; $\mathbf{q_0} = \mathbf{0}$; $\theta_0 = 1$; $\epsilon_0 = 1$;

$\tilde{\mathbf{v}}_\mathbf{1}$ = random vector of length N;

$\tilde{\mathbf{w}}_\mathbf{1} = \theta_0 \hat{\mathbf{D}} \tilde{\mathbf{v}}_\mathbf{1}$;

$\mathbf{v_1} = \tilde{\mathbf{v}}_\mathbf{1}/\rho_1$; $\quad \rho_1 = \|\tilde{\mathbf{v}}_\mathbf{1}\|$;

$\mathbf{w_1} = \tilde{\mathbf{w}}_\mathbf{1}/\xi_1$; $\quad \xi_1 = \|\tilde{\mathbf{w}}_\mathbf{1}\|$;

for $k = 1, 2, \ldots, M$

$\theta_k = \frac{\theta_{k-1}\rho_k}{\xi_k}$;

$\delta_k = \mathbf{w_k^t v_k}$;

$\mathbf{p_k} = \mathbf{v_k} - \frac{\xi_k \delta_k}{\epsilon_{k-1}} \mathbf{p_{k-1}}$;

$\mathbf{q_k} = \mathbf{w_k} - \frac{\rho_k \delta_k}{\epsilon_{k-1}} \mathbf{q_{k-1}} = \theta_k \hat{\mathbf{D}} \mathbf{p_k}$;

$\epsilon_k = \mathbf{q_k^t U p_k}$;

$\beta_k = \frac{\epsilon_k}{\delta_k}$;

$\tilde{\mathbf{v}}_\mathbf{k+1} = \mathbf{U p_k} - \beta_k \mathbf{v_k}$;

$\tilde{\mathbf{w}}_\mathbf{k+1} = \mathbf{U^t q_k} - \beta_k \mathbf{w_k} = \theta_k \hat{\mathbf{D}} \tilde{\mathbf{v}}_\mathbf{k+1}$;

$\mathbf{v_{k+1}} = \tilde{\mathbf{v}}_\mathbf{k+1}/\rho_{k+1}$; $\quad \rho_{k+1} = \|\tilde{\mathbf{v}}_\mathbf{k+1}\|$;

$\mathbf{w_{k+1}} = \tilde{\mathbf{w}}_\mathbf{k+1}/\xi_{k+1}$; $\quad \xi_{k+1} = \|\tilde{\mathbf{w}}_\mathbf{k+1}\|$;

end

where ϵ_k, β_k, ξ_{k+1} and ρ_{k+1} are factors of the elements of the matrix $\mathbf{T_M}$.

4.9 Appendix B

The k^{th} approximate right and left eigenvectors of the submatrice $\mathbf{T_{ID}}$ of size $ID \times ID$ are computed using a generalization of the well-known Inverse Iteration algorithm

$$\mathbf{LU}' = (\tilde{u_k}\mathbf{I} - \mathbf{T}_{ID})$$

for $i = 1, 2, \ldots$

$$\mathbf{LU}'\tilde{\mathbf{z}} = \mathbf{z}_R^{(i-1)} \; ; \; \mathbf{z}_R^{(i)} = \tilde{\mathbf{z}}/\|\tilde{\mathbf{z}}\|$$

$$\mathbf{U}'^t\mathbf{L}^t\tilde{\mathbf{z}} = \mathbf{z}_L^{(i-1)} \; ; \; \mathbf{z}_L^{(i)} = \tilde{\mathbf{z}}/\|\tilde{\mathbf{z}}\|$$

$$\lambda_k^{(i)} = \frac{\mathbf{z_L^{(i)t} T_k z_R^{(i)}}}{\mathbf{z_L^{(i)t} z_R^{(i)}}}$$

end

where $\tilde{u}_k$ is the approximate eigenvalue obtained from the diagonalisation of $\tilde{\mathbf{T}}_{\mathbf{M}}$, and $\mathbf{z_R}$ and $\mathbf{z_L}$ are right and left eigenvectors. The Ritz value $\lambda_k^{(i)}$ is used to monitor the convergence of the k^{th} pair of eigenvectors.

Bibliography

[1] D.G. Truhlar, editor. *Resonances in Electron-Molecule Scattering, Van der Waals Complexes, and Reactive Chemical Dynamics.* Number 263 in Symposium Series. American Chemical Society, Washington, 1984.

[2] J. R. Taylor. *Scattering Theory.* Wiley, New York, 1972.

[3] J. C. Polanyi and A. H. Zewail. Direct observation of the transition state. *Acc. Chem. Res.*, 119:28, 1995.

[4] R. E. Wyatt and J. Z. H. Zhang, editors. *Dynamics of Molecules and Chemical Reactions.* Dekker, New York, 1996.

[5] V. I. Kukulin, Krasnopol'ky, and J. Horáček. *Theory of Resonances.* Kluwer Academic Publisher, Dordrecht, 1989.

[6] Q. Wei, A. W. Jasper, and D. G. Truhlar. Narrow subthreshold quantum mechanical resonances in the Li + HF $->$ H + LiF reaction. *J. Phys. Chem. A*, 107:7236, 2003.

[7] F. Fernandez-Alonso and R. N. Zare. Scattering resonances in the simplest chemical reaction. *Annu. Rev. Phys. Chem.*, 53:67, 2002.

[8] M. Thachuk, C. E. Chuaqui, and R. J. Le Roy. Linewidths and shifts of very low temperature CO in He: A challenge for theory or experiment? *J. Chem. Phys.*, 105:4005, 1996.

[9] J. M. Bowman. Resonances: Bridge between spectroscopy and dynamics. *J. Phys. Chem. A*, 102:3006, 1998.

[10] R. Schinke, H.-M. Keller, H. Floethmann, M. Stumpf, C. Beck, D. H. Mordaunt, and A. J. Dobbyn. Resonances in unimolecular dissociation: From mode-specific to statistical behaviour. *Adv. Chem. Phys.*, 101:745, 1997.

[11] R. Schinke. *Photodissociation Dynamics.* Cambridge University Press, Cambridge, 1993.

[12] A. F. J. Siegert. On the derivation of the dispersion formula for nuclear reactions. *Phys. Rev.*, 56:750, 939.

[13] W. P. Reinhardt. Complex coordinates in the theory of atomic and molecular structure and dynamics. *Ann. Rev. Phys. Chem.*, 33:223, 1982.

[14] see for example in. *Int. J. Quantum Chem.*, 14, special issue, 1978.

[15] O. Atabek and R. Lefebvre. Application of the complex coordinate method to the conical resonances of Jahn-Teller spectra. *J. Chem. Phys.*, 97:3973, 1992.

[16] G. D. Doolen. A procedure for calculating resonance eigenvalues. *J. Phys. B*, 8:525, 1975.

[17] N. Moiseyev, S. Friedland, and P. R. Certain. Cusps, θ trajectories, and the complex virial theorem. *J. Chem. Phys.*, 74:4739, 1981.

[18] G. Jolicard and E. Austin. Optical potential stabilisation method for predicting resonance levels. *Chem. Phys. Lett.*, 121:106, 1985.

[19] G. Jolicard and E. Austin. Optical potential method of calculating resonance energies and widths. *Chemical physics*, 103:295, 1986.

[20] G. Jolicard, C. Leforestier, and E. Austin. Resonance states using the optical potential model. study of Feshbach resonances and broad shape resonances. *J. Chem. Phys.*, 88:1026, 1988.

[21] D. Wang and J. M. Bowman. L^2 calculations of resonances and final rotational distributions for HCO $--$ >H+CO. *J. Chem. Phys.*, 100:1021, 1994.

[22] G. Jolicard and G.D. Billing. Partial widths and time-dependent dissociation dynamics by the optical potential method. *J. Chem. Phys.*, 97:997, 1992.

[23] U.V. Riss and H.-D. Meyer. Calculation of resonance energies and widths using the complex absorbing potential method. *J. Phys. B*, 26:4503, 1993.

[24] C. Leforestier and N. Yamashita, K.and Moiseyev. Transition state resonances by complex scaling: A three-dimensional study of ClHCl. *J. Chem. Phys.*, 103:8468, 1995.

[25] N. Lipkin, N. Moiseyev, and C. Leforestier. A three-dimensional study of NeICl predissociation resonances by the complex scaled discrete variable representation method. *J. Chem. Phys.*, 98:1888, 1993.

[26] D. Xie, R. Chen, and H. Guo. Comparison of Chebyshev, Faber, and Lanczos propagation-based methods for calculating resonances. *J. Chem. Phys.*, 112:5263, 2000.

[27] V. A. Mandelshtam and H. S. Taylor. Harmonic inversion of time signals and its applications. *J. Chem. Phys.*, 107:6756, 1997.

[28] V. A. Mandelshtam and H. S. Taylor. Spectral analysis of time correlation function for a dissipative dynamical system using filter diagonalization: Application to calculation of unimolecular decay rates. *Phys. Rev. Lett.*, 78:3274, 1995.

[29] M. R. Wall and D. Neuhauser. Extraction, through filter-diagonalization, of general quantum eigenvalues or classical normal mode frequencies from a small number of residues or a short-time segment of a signal. I. theory and application to a quantum-dynamics model. *J. Chem. Phys.*, 102:8011, 1995.

[30] B. Simon. The definition of molecular resonance curves by the method of exterior complex scaling. *Phys. Lett. A*, 71:211, 1979.

[31] H. W. Jang and J. C. Light. Artificial boundary inhomogeneity method for quantum scattering solutions in an Lt^2 basis. *J. Chem. Phys.*, 102:3262, 1995.

[32] G. S. Whittier and J. C. Light. Calculation of resonances of HCO by the artificial boundary inhomogeneity method. *J. Chem. Phys.*, 107:1816, 1997.

[33] M. J. Bramley and T. Carrington Jr. A general discrete variable method to calculate vibrational energy levels of three- and four-atom molecules. *J. Chem. Phys.*, 99:8519, 1993.

[34] S. Brouard, D. Macédas, and J. G. Muga. Perfect absorbers for stationary and wavepacket scattering. *J. Phys. A*, 27:L439–L445, 1994.

[35] U.V. Riss and H.-D. Meyer. Investigation on the reflection and transmission properties of complex absorbing potentials. *J. Chem. Phys.*, 105:1409, 1996.

[36] T. Seideman and W.H. Miller. Calculation of the cumulative reaction probability via a discrete variable representation with absorbing boundary conditions. *J. Chem. Phys.*, 96:4412, 1992.

[37] A. Vibok and G. G. Balint-Kurti. Parametrization of complex absorbing potentials for time-dependent quantum dynamics. *J. Phys. Chem.*, 96:8712, 1992.

[38] D. Neuhauser and M. Baer. The time-dependent Schrödinger equation: Application of absorbing boundary conditions. *J. Chem. Phys.*, 90:4351, 1989.

[39] M. S. Child. Analysis of a complex absorbing barrier. *Mol. Phys.*, 72:89, 1991.

[40] D. E. Manolopoulos. Derivation and reflection properties of a transmission-free absorbing potential. *J. Chem. Phys.*, 117:9552, 2002.

[41] D. Macias, S. Brouard, and J. G. Muga. Optimization of absorbing potentials. *Chem. Phys. Lett.*, 228:672, 1994.

[42] B. Poirier and T. Carrington Jr. Semiclassically optimized complex absorbing potentials of polynomial form. I. pure imaginary case. *J. Chem. Phys.*, 118:17, 2003.

[43] B. Poirier and T. Carrington Jr. Semiclassically optimized complex absorbing potentials of polynomial form. II. complex case. *J. Chem. Phys.*, 119:77, 2003.

[44] Z. Bai, J. Demmel, J. Dongarra, A. Ruhe, and H. van der Vorst, editors. *Templates for the Solution of Algebraic Eigenvalue Problems: A Practical Guide.* Society for Industrial and Applied Mathematics, Philadelphia, 2000.

[45] W. Bian and B. Poirier. Accurate and highly efficient calculation of the highly excited pure OH stretching resonances of $O(^1D)HCl$, using a combination of methods. *J. Chem. Phys.*, 121:4467, 2004.

[46] B. Poirier and T. Carrington Jr. A preconditioned inexact spectral transform method for calculating resonance energies and widths, as applied to HCO. *J. Chem. Phys.*, 116:1215, 2002.

[47] J. C. Light, I. P. Hamilton, and J. V. Lill. Generalized discrete variable approximation in quantum-mechanics. *J. Chem. Phys.*, 82:1400, 1985.

[48] J. C. Light and T. Carrington Jr. Discrete variable representations and their utilization. *Adv. Chem. Phys.*, 114:263, 2000.

[49] J. K. Cullum and R. A. Willoughby. *Lanczos algorithms for large symmetric eigenvalue computations.* Birkhäuser, Boston, 1985.

[50] X. Wang and T. Carrington Jr. A contracted basis-Lanczos calculation of vibrational levels of methane: Solving the Schrödinger equation in nine dimensions. *J. Chem. Phys.*, 119:101, 2003.

[51] V. A. Mandelshtam and H. S. Taylor. A simple recursion polynomial expansion of the Green's function with absorbing boundary conditions. application to the reactive scattering. *J. Chem. Phys.*, 103:2903, 1995.

[52] V. A. Mandelshtam, T. P. Grozdanov, and H. S. Taylor. Bound states and resonances of the hydroperoxyl radical HO_2: An accurate quantum mechanical calculation using filter diagonalization. *J. Chem. Phys.*, 103:10074, 1995.

[53] D. Neuhauser. Bound state eigenfunctions from wave packets: Time $--> $ energy resolution. *J. Chem. Phys.*, 93:2611, 1990.

[54] S.-W. Huang and T. Carrington Jr. A comparison of filter diagonalisation methods with the Lanczos method for calculating vibrational enery levels. *Chem. Phys. Lett.*, 312:311, 1999.

[55] G. H. Li and H. Guo. Doubling of Chebyshev correlation function for calculating narrow resonances using low-storage filter diagonalization. *Chem. Phys. Lett.*, 336:143, 2001.

[56] V. A. Mandelshtam and A. Neumaier. Pseudotime Schrödinger equation with absorbing potential for quantum scattering calculations. *Phys. Rev. Lett.*, 86:5031–5034, 2001.

[57] V. A. Mandelshtam and A. Neumaier. Further generalization and numerical implementation of pseudotime Schrödinger equations for quantum scattering calculations. *J. Theor. Comput. Chem.*, 1:1, 2002.

[58] J.Y Ge and J.Z.H. Zhang. Use of negative complex potential as absorbing potential. *J. Chem. Phys.*, 108:1429, 1998.

[59] B. N. Parlett and H. C. Che. Use of indefinite pencils for computing damped natural modes. *Linear Algebra Appl.*, 140:53, 1990.

[60] H.-D. Meyer, J. Horacek, and L. S. Cederbaum. Schwinger and anomaly-free Kohn variational principles and a generalized Lanczos algorithm for nonsymmetric operators. *Phys. Rev. A.*, 43:3587, 1991.

[61] M.-C. Kim and I.-W. Lee. Solution eigenproblems for non-proportional damping system by Lanczos method. *Earthquake Engng. Struct. Dyn.*, 28:157, 1999.

[62] T. Ericsson. *Large Scale Eigenvalue Problems.* Elsevier Scientific Publishers B.V., Amsterdam, 1985.

[63] G. H. Golub and C. F. Van Loan. *Matrix Computations.* John Hopkins University Press, Baltimore, 1989.

[64] R. W. Freund and N. M. Nachtigal. Implementation details of the coupled QMR algorithm. *SIAM J. Sci. Stat. Comp.*, 15:313, 1994.

[65] J. K. Cullum and R. A. Willoughby. *Large Scale Eigenvalue Problems.* Elsevier Scientific Publishers B.V., Amsterdam, 1985.

[66] H. Romanowski, K.T. Lee, J.M. Bowman, and L.B. Harding. Coupled channel calculation of resonances in H+CO. *J. Chem. Phys.*, 84:4888, 1986.

[67] J. M. Bowman, J. S. Bittman, and L.B. Harding. Ab initio calculations of electronic and vibrational energies of HCO and HOC. *J. Chem. Phys.*, 85:911, 1986.

[68] H.-M. Keller, A. J Floethmann, H. and. Dobbyn, R. Schinke, and H. J. Werner. The unimolecular dissociation of HCO. II. comparison of calculated resonance energies and widths with high-resolution spectroscopic data. *J. Chem. Phys.*, 105:4983, 1996.

[69] B. N. Mohr, P. J.and Taylor. *CODATA Recommended Values of the Fundamental Physical Constants: 1998.* National Institute of standards and Technology, 1998.

[70] D. T. Colbert and W. H. Miller. A novel discrete variable representation for quantum mechanical reactive scattering via the S-matrix Kohn method. *J. Chem. Phys.*, 96:1982, 1992.

[71] H. Wei and T. Carrington Jr. The discrete variable representation of a triatomic Hamiltonian in bond length-bond angle coordinates. *J. Chem. Phys.*, 97:3029, 1992.

[72] J. Echave and D. C. Clary. Potential optimized discrete variable representation. *Chem. Phys. Lett.*, 190:225, 1992.

[73] H. Wei. Ghost levels and near-variational forms of the discrete variable representation: Application to H_2O. *J. Chem. Phys.*, 106:6885, 1997.

[74] R. Meyer. Flexible models for intramolecular motion, a versatile treatment and its application to glyoxal. *J. Molec. Spec.*, 76:266, 1979.

[75] W. Bian and B. Poirier. Accurate and highly efficient calculation of the $O(^1D)HCl$ vibrational bound states, using a combination of methods. *J. Theo. Comp. Chem.*, 2:583, 2003.

[76] H.-S. Lee and J. C. Light. Iterative solutions with energy selected bases for highly excited vibrations of tetra-atomic molecules. *J. Chem. Phys.*, 120:4626, 2004.

[77] H.-S. Lee and J. C. Light. Molecular vibrations: Iterative solution with energy selected bases. *J. Chem. Phys.*, 118:3458, 2003.

[78] W. H. Press, S. A. S.A. Teukolsky, W. T. Vetterling, and B. P. Flannery. *Numerical Recipes in FORTRAN 77 The Art of Scientific Programming.* Cambridge University Press, 1986.

[79] M. J. Bramley, J. W. Tromp, T. Carrington Jr., and G. C. Corey. Efficient calculation of highly excited vibrational energy levels of floppy molecules: The band origins of H_3^+ up to 35 000 cm^{-1}. *J. Chem. Phys.*, 100:6175, 1994.

[80] S.-W. Huang and T. Carrington Jr. A new iterative method for calculating energy levels and wave functions. *J. Chem. Phys.*, 112:8765, 2000.

[81] B. Poirier and T. Carrington Jr. Accelerating the calculation of energy levels and wave functions using an efficient preconditioner with the inexact spectral transform method. *J. Chem. Phys.*, 114:9254, 2001.

CHAPITRE 5

GÉNÉRALISATION DE L'ALGORITHME D'EXTRACTION DES VALEURS PROPRES D'UN OPÉRATEUR NON SYMÉTRIQUE

Dans cette section, une généralisation de la méthode présentée au chapitre précédent. Le manuscrit a été soumis à la revue "Electronic Transactions on Numerical Analysis" le 23 décembre 2006 et est actuellement en traitement.

A refined unsymmetric Lanczos eigensolver for computing accurate eigentriplets of a real unsymmetric matrix

Jean Christophe Tremblay[1] and Tucker Carrington Jr.[2]

Département de chimie, Université de Montréal,

C.P. 6128, succursale Centre-ville, Montréal (Québec) H3C 3J7, Canada

Abstract

For most unsymmetric matrices it is difficult to compute many accurate eigenvalues using the primitive form of the unsymmetric Lanczos algorithm (ULA). In this paper we propose a modification of the ULA. It is related to ideas used in J. Chem. Phys. **122** (2005), p. 244107:1-11 to compute resonance lifetimes. Using the refined ULA we suggest, the calculation of accurate extremal and interior eigenvalues is feasible. The refinement is simple: approximate right and left eigenvectors computed using the ULA are used to form a small projected matrix whose eigenvalues and eigenvectors are easily computed. There is no re-biorthogonalization of the Lanczos vectors and no need to store large numbers of vectors in memory. The method can therefore be used to compute eigenvalues of very large matrices. The idea is tested on several matrices.

[redacted]

Fax: 514-343-7586

5.1 Introduction

Scientists and engineers frequently need to compute many eigenvalues of large real matrices, i.e. to solve

$$\mathbf{G}\mathbf{X}_{(R)} = \mathbf{X}_{(R)}\mathbf{\Lambda} \quad , \tag{5.1}$$

where $\mathbf{X}_{(R)}$ is a matrix of right eigenvectors, $\mathbf{x}_{(R)}$, and $\mathbf{\Lambda}$ is a diagonal matrix whose diagonal elements are eigenvalues; see for example [1–5]. They prefer eigensolvers that require little memory and are simple to implement. Of course, an eigensolver that is CPU efficient is also advantageous. For symmetric matrices the Lanczos procedure without re-orthogonalization is often the best choice, see [6–13]. Using this procedure it is possible to compute eigenvalues by storing only two vectors. Eigenvectors can be obtained either by re-generating the Lanczos vectors or by storing them on disk. The method is simple and easy to use. For unsymmetric matrices, on the other hand, the known eigensolvers have important deficiencies. For the purpose of computing many eigentriplets (eigenvalues, right eigenvectors $\mathbf{x}_{(R)}$, and left eigenvectors $\mathbf{x}_{(L)}$), the best unsymmetric matrix eigensolvers are based either on the Arnoldi algorithm or on the unsymmetric Lanczos algorithm. In this paper we assume that $\mathbf{G}$ always has a complete set of eigenvectors.

The Arnoldi algorithm is an orthogonal Krylov projection method [14, 15]. It has the important disadvantage that it requires storing many vectors in memory. Vectors must be stored in memory because every Arnoldi vector is orthogonalized against *all* of the previous computed Arnoldi vectors. It would be very costly to orthogonalize by reading previous Arnoldi vectors from disk because the orthogonalization is done at each iteration. The CPU cost of the orthogonalization also increases with the number of iterations. These problems are to some extent mitigated by using the implicitly restarted Arnoldi (IRA) technique [16]. It is implemented in the ARPACK code which is widely used and appreciated [17, 18].

The unsymmetric Lanczos algorithm (ULA) is an oblique projection method

that uses two Krylov spaces, one for $\mathbf{G}$ and one for $\mathbf{G}^*$, where $*$ denotes the conjugate transpose [14, 19]. The ULA has the advantage that its use requires the storage of only 4 vectors, but the important disadvantage that in its primitive form it does not always yield accurate eigenvalues. The formal memory advantage of the ULA is, of course, useless if one is not able to compute accurate eigentriplets.

Due in part to the inaccuracy of the ULA, the most popular approach for solving the unsymmetric eigenproblem is the Implicitly Restarted Arnoldi (IRA) idea and the ARPACK program [16, 18]. A cleverly designed restarting algorithm contracts a Krylov subspace with p vectors to a Krylov subspace with $k < p$ vectors. The contraction can be done to facilitate the convergence of eigenvalues whose magnitude, or real part, or imaginary part, is largest or smallest [17, 18]. The algorithm is repeatedly restarted until the desired eigenvalues are converged. ARPACK is robust and stable. The memory cost of the method is determined by the need to store p Arnoldi vectors in memory to perform the orthogonalization. Increasing p increases both the memory cost and the CPU cost of the orthogonalization, but decreases the number of necessary restarts. ARPACK has been widely applied and is considered a method of choice [20–22]. For extremal eigenvalues its most important disadvantage is the need to store p vectors in memory. If the size of $\mathbf{G}$ is large one requires a lot of memory in order to use ARPACK. In addition, to reliably obtain interior eigenvalues with ARPACK one must either use a large p (which is usually impractical) or a spectral transform. The use of ARPACK for interior eigenvalues is discussed in [23, 24]. Using a spectral transform is costly, especially if the matrix is so large that it cannot be factorized.

To compute (interior or extremal) eigenvalues of a very large matrix with ARPACK one requires a prohibitive amount of memory and it is therefore tempting to endeavor to improve the ULA. Modifying the ULA, without losing its memory advantage, so that accurate eigenvalues and eigenvectors can be computed, would drastically reduce the memory cost of eigencomputations with very large matrices

possible. The ULA (see section 2) uses two sets of biorthogonal vectors. Several authors have proposed modifications of the ULA. Conceptually, the simplest way to use the ULA to determine accurate eigenvalues is to re-biorthogonalize the two sets of Lanczos vectors. However, it is difficult to achieve biorthogonality that is good enough to ensure accurate eigenvalues. In addition, re-biorthogonalization significantly increases the CPU cost and negates the anticipated memory advantage of the ULA. The look-ahead modification is designed to deal with problems introduced by small normalizing factors [25, 26]. It does improve the accuracy of ULA eigenvalues and can be used with any of the other modifications described below. Day [27] has proposed a scheme for maintaining semi-biorthogonality. He shows that using this approach it is possible to compute eigenvalues accurate to "from full to half relative precision" but, to make the method work, all Lanczos vectors must either be stored in memory or read from disk at each re-biorthogonalization step. This significantly increases the memory cost or the calculation time. In [28], Cullum and Willoughby show that if the coefficients of the recursion relations are chosen so that the tridiagonal matrix is symmetric (but complex) accurate eigenvalues can be computed for some test problems. This is a low-memory method and it is simple to use but requires complex arithmetic. Using complex Lanczos vectors increases the memory and CPU costs by about a factor of two.

In this paper we show that it is possible to use Lanczos vectors to compute accurate eigenvalues and eigenvectors without storing vectors spanning Krylov space(s) in memory (we do no re-biorthogonalization of the Lanczos vectors). It is also possible to compute interior eigenvalues. To compute eigenvalues of a real matrix, we evaluate matrix-vector products in real arithmetic. The new idea is simple: we use approximate right and left eigenvectors obtained from the ULA to build a projected matrix which we diagonalize using a standard method. In effect we are using the ULA to compute vectors that have large components along the eigenvector directions. The eigenvectors obtained from the ULA are not accurate but they can

be used to compute accurate eigenvalues and eigenvectors. We dub this approach the refined unsymmetric Lanczos eigensolver (RULE). Although the word refined occurs in the name, the method is not directly related to that of [29].

The RULE's principle advantage is that it enables one to compute many eigenvalues of a large matrix without storing more than about a dozen vectors in memory. The number of eigenvalues (and eigenvectors) one can compute, from one tridiagonal matrix, is much larger than the number of vectors that one must store in memory. The RULE is a good alternative to ARPACK if the matrix for which eigenvalues are desired is so large that it is not possible to store many vectors in memory, or if one wishes interior eigenvalues. It makes it possible to extract accurate eigenvalues from large Krylov spaces. Although our numerical experiments show that the RULE works well for many difficult problems it is not backward stable. Nevertheless, it provides a means of computing eigentriplets of matrices for which the memory ARPACK requires exceeds that of the computer.

5.2 The standard unsymmetric Lanczos algorithm

The unsymmetric Lanczos algorithm is an iterative process for generating two sets of biorthogonal vectors, $\{\mathbf{v}_j\}_{j=1}^m$ and $\{\mathbf{w}_j\}_{j=1}^m$, which span two Krylov subspaces [14, 19],

$$K^{(m)}\{\mathbf{G}, \mathbf{v}_1\} = \{\mathbf{v}_1, \mathbf{G}\mathbf{v}_1, \cdots, \mathbf{G}^{\mathbf{m-1}}\mathbf{v}_1\} \text{ , and} \tag{5.2}$$

$$K^{(m)}\{\mathbf{G}^*, \mathbf{w}_1\} = \{\mathbf{w}_1, \mathbf{G}^*\mathbf{w}_1, \cdots, (\mathbf{G}^*)^{\mathbf{m-1}}\mathbf{w}_1\} \ . \tag{5.3}$$

The two sets of Lanczos vectors may be obtained from the two three-term recurrence relations

$$\rho_{k+1}\mathbf{v}_{k+1} = \mathbf{r}_{k+1} = \mathbf{G}\mathbf{v}_k - \alpha_k\mathbf{v}_k - \gamma_k\mathbf{v}_{k-1} \ , \tag{5.4}$$

$$\xi^*_{k+1}\mathbf{w}_{k+1} = \mathbf{s}_{k+1} = \mathbf{G}^*\mathbf{w}_k - \alpha^*_k\mathbf{w}_k - \frac{\rho^*_k\delta_k}{\delta_{k-1}}\mathbf{w}_{k-1} \ , \tag{5.5}$$

where $\gamma_k = \frac{\xi_k \delta_k}{\delta_{k-1}}$, $\delta_k = \mathbf{w}_k{}^* \mathbf{v}_k$, $\alpha_k = \mathbf{w}_k{}^* \mathbf{G} \mathbf{v}_k / \delta_k$, and ρ_k and ξ_k normalize $\mathbf{r}_k$ and $\mathbf{s}_k$, respectively. The procedure is started by choosing two random starting vectors ($\mathbf{v}_1$ and $\mathbf{w}_1$) and by setting $\gamma_1 = \rho_1 = 0$. In matrix form these relations are written

$$\mathbf{G}\mathbf{V}_m = \mathbf{V}_m \mathbf{T}_m + \rho_{m+1} \mathbf{v}_{m+1} \mathbf{e}_m^* \tag{5.6}$$

$$\mathbf{G}^* \mathbf{W}_m = \mathbf{W}_m \mathbf{\Delta}_m^{-1} \mathbf{T}_m^* \mathbf{\Delta}_m + \xi_{m+1}^* \mathbf{w}_{m+1} \mathbf{e}_m^* \quad , \tag{5.7}$$

where $\mathbf{V}_m$ and $\mathbf{W}_m$ are matrices whose columns are the first m vectors $\mathbf{v}_k$ and $\mathbf{w}_k$, respectively, and $\mathbf{\Delta}_m = diag(\delta_1, \delta_2, \cdots, \delta_m)$. The scalars α_k, ρ_k, and γ_k are elements of the tridiagonal matrix $\mathbf{T}_m = \mathbf{\Delta}_m^{-1} \mathbf{W}_m^* \mathbf{G} \mathbf{V}_m$,

$$\mathbf{T}_m = \begin{pmatrix} \alpha_1 & \gamma_2 & & & \\ \rho_2 & \alpha_2 & \gamma_3 & & \\ & \rho_3 & \alpha_3 & \ddots & \\ & & \ddots & \ddots & \gamma_m \\ & & & \rho_m & \alpha_m \end{pmatrix} . \tag{5.8}$$

Eigenvalues of $\mathbf{T}_m$ are computed by solving

$$\mathbf{T}_m \mathbf{Z} = \mathbf{Z} \mathbf{\Theta}_m \quad . \tag{5.9}$$

Some of the eigenvalues of $\mathbf{T}_m$ approximate eigenvalues of $\mathbf{G}$. There is some flexibility in the definition of ρ_k and ξ_k. We choose to normalize so that $\delta_k = \mathbf{w}_k{}^* \mathbf{v}_k = 1$ and $\mathbf{\Delta}_m^{-1} \mathbf{T}_m^* \mathbf{\Delta}_m = \mathbf{T}_m^*$. This choice will be assumed for the remainder of the paper. In pseudo-code the algorithm is:

Algorithm 1. Unsymmetric Lanczos

Choose $\mathbf{v}_1$ and $\mathbf{w}_1$ such that $\mathbf{w}_1^* \mathbf{v}_1 = 1$;

$\mathbf{r} = \mathbf{G}\mathbf{v}_1$;

$\mathbf{s} = \mathbf{G}^* \mathbf{w}_1$;

for $k = 1, 2, \ldots, m$

$\alpha_k = \mathbf{w}_k^* \mathbf{r}$;
$\mathbf{r} = \mathbf{r} - \alpha_k \mathbf{v}_k$;
$\mathbf{s} = \mathbf{s} - \alpha_k^* \mathbf{w}_k$;
$\mathbf{r} = \mathbf{r} - (\mathbf{r}^* \mathbf{w}_k)\, \mathbf{v}_k$;
$\mathbf{s} = \mathbf{s} - (\mathbf{s}^* \mathbf{v}_k)\, \mathbf{w}_k$;
if ($\|\mathbf{r}\| = 0$ or $\|\mathbf{s}\| = 0$), stop;
$\tilde{\delta}_k = \mathbf{r}^* \mathbf{s}$;
if ($\tilde{\delta}_k = 0$), stop;
$\rho_{k+1} = |\tilde{\delta}_k|^{1/2}$;
$\gamma_{k+1} = \tilde{\delta}_k^{\,*} / \rho_{k+1}$;
$\mathbf{v}_{k+1} = \mathbf{r} / \rho_{k+1}$;
$\mathbf{w}_{k+1} = \mathbf{s} / \gamma_{k+1}^*$;
$\mathbf{r} = \mathbf{G}\mathbf{v}_{k+1} - \gamma_{k+1} \mathbf{v}_k$;
$\mathbf{s} = \mathbf{G}^* \mathbf{w}_{k+1} - \rho_{k+1}^* \mathbf{w}_k$;

end

Breakdown or near breakdown can occur when $\tilde{\delta}_k \simeq 0$. However, in our experience, it never occurred and we shall not discuss it further. Breakdown can be dealt with using look-ahead methods [25, 26].

As the number of iterations increases, roundoff errors will ineluctably lead to loss of biorthogonality of the Lanczos vectors. When an eigenvalue converges, the corresponding eigenvectors will contaminate successive Lanczos vectors and near copies of converged eigenvalues will be generated. Increasing the size of the Krylov subspace will increase the number of near copies. For the Hermitian case this phenomenon was first explained by Paige [10–12]. In that case, if nothing is done to minimize the loss of orthogonality, multiple copies of converged eigenvalues appear.

Cullum and Willoughby denoted unconverged eigenvalues of $\mathbf{T}_m$ "spurious" eigenvalues and developed a practical procedure for identifying the spurious eigenvalues of an Hermitian $\mathbf{T}_m$ [7, 8]. Copies of converged eigenvalues are equal to machine precision and cause no problem. For non-Hermitian matrices the "copies" are not nearly as close and it is harder to distinguish between spurious and good eigenvalues. To a large degree this problem can be overcome by choosing the coefficients in the recursion relations so that the tridiagonal matrix is complex symmetric [28], but to minimize CPU and memory costs we wish to use real arithmetic. In real arithmetic and using the ULA: (1) in general, it is not possible, for a particular eigenvalue of $\mathbf{G}$, to find a Krylov subspace size m for which an eigenvalue of $\mathbf{T}_m$ accurately approximates an eigenvalue of $\mathbf{G}$; (2) for each nearly converged eigenvalue of $\mathbf{G}$ there is a cluster of closely spaced eigenvalues of $\mathbf{T}_m$, but the norm of differences between eigenvalues in the cluster may be so large that it is difficult to identify the cluster and impossible to determine an accurate value for the eigenvalue; (3) the width of the clusters increases with m; and (4) it is not possible to use the Cullum and Willoughby procedure to remove spurious eigenvalues from clumps of eigenvalues. The inadequacy of the ULA is well known [19, 30–32].

Consider the following example. We use Matlab 7 to create a random matrix of size $N = 300$

$$\text{RAND('SEED',0);} \tag{5.10}$$

$$\mathbf{G}_{ext} = \text{RAND}(N). \tag{5.11}$$

Eigenvalues computed with Matlab's EIG routine are shown in figure 5.1. One eigenvalue is well isolated. It is the eigenvalue of largest magnitude and is real. Its condition number,

$$c_\lambda = \frac{1}{|\mathbf{x}_{(L)}{}^* \mathbf{x}_{(R)}|} \quad , \tag{5.12}$$

Figure 5.1: Distribution of eigenvalues of G_{ext}

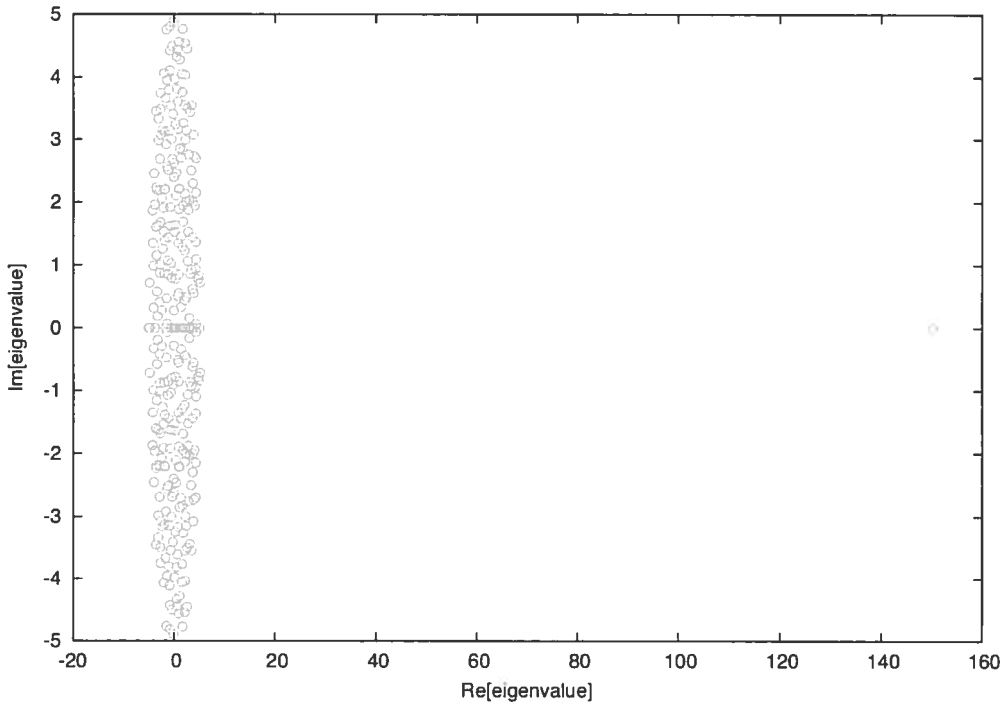

is 1.001. The ULA with $m = 300$ produces many approximate copies of this eigenvalue, see Table 5.1. Even for the isolated well-conditioned eigenvalue, the imperfect copies makes it hard to extract accurate eigenvalues from a large tridiagonal matrix.

Figure 5.2 shows the evolution of the error associated with the isolated eigenvalue. The error is defined as the the norm of the difference between the exact (computed with Matlab's EIG) eigenvalue and the average of the near copies in a cluster generated by the ULA. Two eigenvalues θ_j and θ_k are deemed to be in a cluster if $|\theta_k - \theta_j| \leq \eta \max(|\theta_k|, |\theta_j|)$ where η is chosen to be the square root of the machine precision [31]. For $\mathbf{G}_{ext}$, with the best possible value of m, the eigenvalue

Table 5.1: Selected eigenvalues of the 300×300 tridiagonal matrix that correspond to the isolated eigenvalue and an interior eigenvalue of $\mathbf{G}_{ext}$. The $\mathbf{G}_{ext}$ eigenvalues obtained with Matlab's EIG are $\lambda_1 =$
150.234556208130 and $\lambda_2 = 3.609257224171 + 3.069961788177i$

Approximate eigenvalue	error
150.234556208117	1.2989E-11
150.234556208121	8.9813E-12
150.234556208126	3.9790E-12
150.234556208129	9.9476E-13
150.234556208129	9.9476E-13
150.234556209596	1.4660E-09
150.234556220968	1.2838E-08
150.234556241745	3.3615E-08
150.234556268333	6.0203E-08
150.234556296133	8.8003E-08
150.234556320339	1.1221E-07
150.234556336769	1.2864E-07
$3.609257227317 + 3.069961798318i$	1.0617E-08
$3.609257246703 + 3.069961858171i$	7.3531E-08
$3.609256887624 + 3.069962297111i$	6.1014E-07
$3.609254779439 + 3.069965061303i$	4.0854E-06

accuracy is quite good (14 significant digits). The best possible value of m can be determined by using the procedure outlined by Cullum and Willoughby for the complex symmetric Lanczos algorithm [8]. The error associated with the average of the eigenvalues of the cluster eigenvalues for $m = 300$ is quite large. Nevertheless with some effort (i.e., by finding the right m) the ULA can be used to compute an isolated extremal eigenvalue.

Unfortunately, it is much harder to compute an eigenvalue that is not isolated (cf. Table 5.1). For interior eigenvalues all of the copies are further than 10^{-8} from the exact eigenvalues and it is impossible to find a tridiagonal matrix for which eigenvalues are very close to the desired exact eigenvalues of $\mathbf{G}_{ext}$ We find that using a simple Gram-Schmidt re-biorthogonalization is not good enough to

Figure 5.2: Error in an extremal extremal, isolated eigenvalue of $\mathbf{G}_{ext}$ computed with the ULA (see the text)

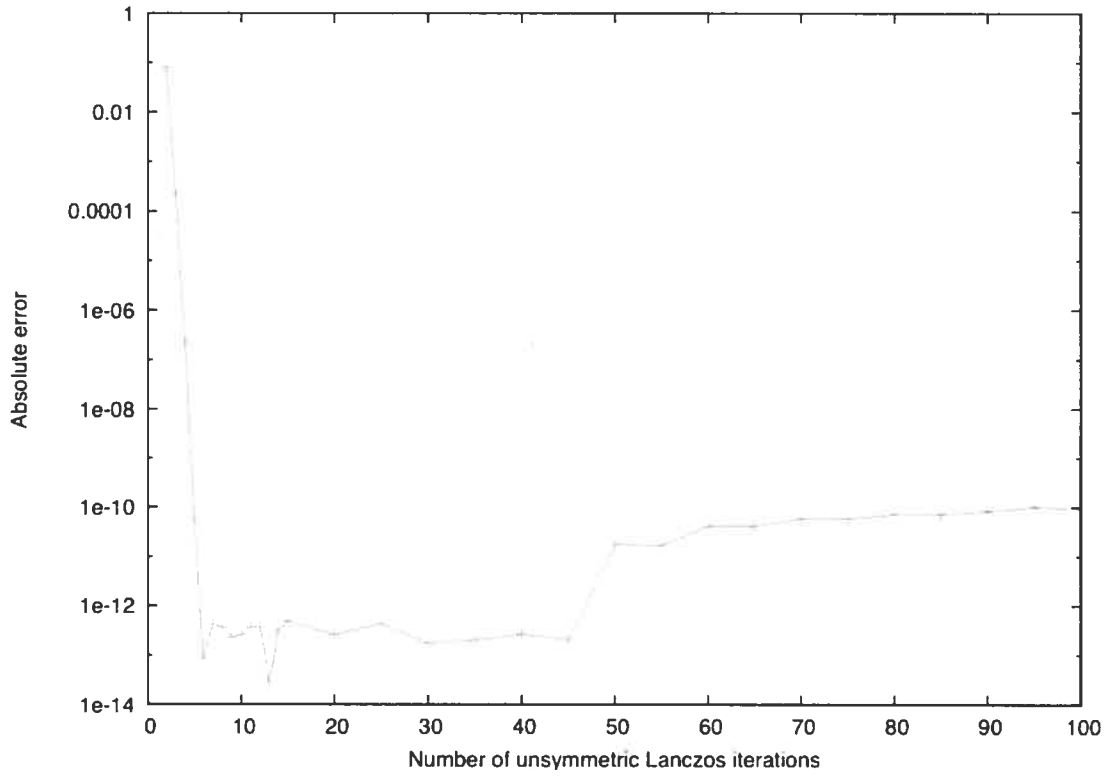

get accurate interior eigenvalues (although it does reduce the number of matrix-vector products required to achieve an error of $\sim 10^{-8}$). We shall now show that approximate right and left eigenvectors, obtained from the ULA with a single value of m, *can* be used to obtain many accurate eigenvalues.

5.3 Refined unsymmetric Lanczos eigensolver

As explained at the end of the introduction we use approximate right and left eigenvectors obtained from the ULA to determine accurate eigenvalues and eigenvectors of $\mathbf{G}$. To do this we must store Lanczos vectors on disk (they are not accessed during the iteration and we do not re-biorthogonalize them) and calculate eigenvalues in groups. Because one typically needs only a small fraction of the

eigenvalues of a huge matrix a small number of groups will be required. Although the RULE is designed for computing only a small fraction of the total number of eigenvalues, it may easily be used to calculate hundreds of eigenvalues. If a smaller number of eigenvalues is desired a Jacobi-Davidson algorithm would be a good alternative [33, 34].

We use the ULA with $v_1 = w_1 =$ a "random" vector to compute an unsymmetric tridiagonal matrix $\mathbf{T}_m$ for a large value of m. We transform $\mathbf{T}_m$ to obtain a complex symmetric tridiagonal with the same eigenvalues,

$$\hat{\mathbf{T}}_m = \mathbf{\Omega}^{-\frac{1}{2}} \mathbf{T}_m \mathbf{\Omega}^{\frac{1}{2}} \tag{5.13}$$

$$= \begin{pmatrix} \alpha_1 & (\rho_2\gamma_2)^{\frac{1}{2}} & & & \\ (\rho_2\gamma_2)^{\frac{1}{2}} & \alpha_2 & (\rho_3\gamma_3)^{\frac{1}{2}} & & \\ & (\rho_3\gamma_3)^{\frac{1}{2}} & \alpha_3 & \ddots & \\ & & \ddots & \ddots & (\rho_m\gamma_m)^{\frac{1}{2}} \\ & & & (\rho_m\gamma_m)^{\frac{1}{2}} & \alpha_m \end{pmatrix}. \tag{5.14}$$

where $\Omega = \mathrm{diag}(1, \frac{\rho_2\omega_1}{\gamma_2}, \frac{\rho_3\omega_2}{\gamma_3}, \cdots, \frac{\rho_m\omega_{m-1}}{\gamma_m})$ and ω_j is the j'th diagonal element of $\mathbf{\Omega}$. The matrix $\mathbf{\Omega}$ is obtained recursively. In a FORTRAN implementation of the RULE, eigenvalues of $\hat{\mathbf{T}}_m$ are computed using the CMTQL1 routine Cullum and Willoughby employ in their complex symmetric and unsymmetric Lanczos procedures [8]. We prefer to use $\hat{\mathbf{T}}_m$ and CMTQL1 because CMTQL1 exploits the symmetry to reduce both the CPU cost and the memory cost of calculating the eigenvalues. Our Matlab RULE routine simply uses EIG to diagonalize $\hat{\mathbf{T}}_m$. In a region of the spectrum in which we wish eigenvalues of $\mathbf{G}$ we form $\hat{\mathbf{T}}_m$ eigenvalue clusters. To do so we build a list of the $\theta_i, i = 1, \cdots, m$ eigenvalues. For one eigenvalue in the list, θ_k, we compute $|\theta_k - \theta_j|$ for all other eigenvalues in the list. θ_j for which $|\theta_k - \theta_j| \leq \eta \max(|\theta_k|, |\theta_j|)$, where η is a user-defined tolerance, are considered as being in the cluster associated with θ_k and removed from the list

before making the cluster associated with another eigenvalue in the list. Clusters with more than one eigenvalue contain near copies introduced by round-off error. If there are no near copies a cluster will contain only one eigenvalue; many clusters do only have one eigenvalue. A procedure for identifying spurious eigenvalues in the symmetric case was developed by Cullum and Willoughby [7, 8]. We use it to identify spurious eigenvalues. A complex symmetric tridiagonal matrix $\mathbf{T}_2$ is formed by removing the first column and the first row of $\hat{\mathbf{T}}_m$. $\mathbf{T}_2$ is then diagonalized to obtain its eigenvalues, $\tilde{\theta}_i$. Isolated eigenvalues (i.e. one-eigenvalue clusters) of $\hat{\mathbf{T}}_m$ that differ from isolated eigenvalues of $\mathbf{T}_2$ by less than $\eta \max(|\tilde{\theta}_i|, |\theta_j|)$ are identified as spurious. Doing the Cullum and Willoughby spurious test enables us to avoid calculating approximate eigenvectors that correspond to $\mathbf{T}_m$ eigenvalues that are not close to any of the eigenvalues of $\mathbf{G}$, without excluding vectors whose eigenvalues are close to those of $\mathbf{G}$. For each non-spurious cluster we compute an average eigenvalue. These average eigenvalues are used as shifts with inverse iteration [35], pages 619-633, to determine approximate right and left eigenvectors of $\mathbf{T}_m$ (one pair for each cluster). The inverse iteration algorithm we use is:

Algorithm 2.Two-sided inverse iteration

Choose random starting vectors $\mathbf{z}_r^j$ and $\mathbf{z}_l^j$

Factorize $\mathbf{LU} = (\hat{\lambda}_j \mathbf{I} - \mathbf{T}_m)$

for $i = 1, 2, \ldots$

Solve $\mathbf{LU}\tilde{\mathbf{z}} = \mathbf{z}_r^j$

$\mathbf{z}_r^j = \tilde{\mathbf{z}}/\|\tilde{\mathbf{z}}\|$

Solve $\mathbf{U}^*\mathbf{L}^*\tilde{\mathbf{z}} = \mathbf{z}_l^j$

$\mathbf{z}_l^j = \tilde{\mathbf{z}}/\|\tilde{\mathbf{z}}\|$

Evaluate $\theta_j^{(i)} = \frac{\mathbf{z}_l^{j\,*}\mathbf{T}_m\mathbf{z}_r^j}{\mathbf{z}_l^{j\,*}\mathbf{z}_r^j}$

Exit if converged

end

Here, $\hat{\lambda}_j$ is an approximate eigenvalue or average eigenvalue obtained from the diagonalization of $\hat{\mathbf{T}}_m$, and $\mathbf{z}_r^j$ and $\mathbf{z}_l^j$ are the associated right and left eigenvectors of matrix $\mathbf{T}_m$. The Ritz value $\theta_j^{(i)}$ is used to monitor the convergence of the j^{th} pair of eigenvectors. Inverse iteration is terminated at $i = m_j$ if $\theta_j^{(i)}$ and $\theta_j^{(i-1)}$ differ by less than $10^{-13}|\hat{\lambda}_j|$. Typically five or fewer inverse iteration steps are required for each converged $\{\mathbf{z}_r^j, \mathbf{z}_l^j\}$ pair. There are alternatives to inverse iteration. Any method with which one can exploit the tridiagonal structure of $\mathbf{T}_m$ could be used, e.g., shift and invert Arnoldi could be used because the factorization of a tridiagonal matrix can be easily computed and stored.

After having computed, for each eigenvalue or average value, eigenvectors of $\mathbf{T}_m$ we determine approximate left and right eigenvectors of $\mathbf{G}$ by reading Lanczos vectors $\mathbf{v}_k$ and $\mathbf{w}_k$ from disk and combining them according to

$$\mathbf{r}_j = \sum_{k=1}^{m} \mathbf{z}_r^j(k)\mathbf{v}_k \quad ; \quad \mathbf{l}_j = \sum_{k=1}^{m} \mathbf{z}_l^j(k)\mathbf{w}_k \tag{5.15}$$

where $\mathbf{r}_j$ and $\mathbf{l}_j$ are approximate jth right and left eigenvectors of $\mathbf{G}$, and $\mathbf{z}_r^j(k)$ ($\mathbf{z}_l^j(k)$) is the kth component of $\mathbf{z}_r^j$ ($\mathbf{z}_l^j$). If η is small it can happen that several $\mathbf{r}_j$ and $\mathbf{l}_j$ vectors are nearly parallel. This occurs if several of the clusters contain $\mathbf{T}_m$ eigenvalues associated with one exact $\mathbf{G}$ eigenvalue. To minimize the near linear dependance of the $\mathbf{r}_j$ and $\mathbf{l}_j$ and to reduce the number of the $\{\mathbf{z}_r^j, \mathbf{z}_l^j\}$ pairs we retain only pairs for which Ritz values obtained from inverse iteration differ by more than $\eta \max(|\theta_j^{m_j}|, |\theta_k^{m_k}|)$. The $\mathbf{r}_j$, $j = 1, \cdots, k$, where k is the number of retained approximate eigenvectors, are the columns of a matrix we denote $\mathbf{R}_k$. The $\mathbf{l}_j, j = 1, \cdots, k$ are the columns of a matrix we denote $\mathbf{L}_k$. One might also avoid nearly parallel vectors by increasing η, but if η is too large $\mathbf{T}_m$ eigenvalues associated with two or more exact eigenvalues will be lumped into a single cluster and one will miss eigenvalues. One could actually use the RULE with $\eta = 0$ (i.e. cluster width of zero). This would eliminate any possibility of missing closely-

spaced eigenvalues, but it would increase the number of $\{\mathbf{z}_r^j, \mathbf{z}_l^j\}$ pairs to compute, and increase the number of $\mathbf{r}_j$ and $\mathbf{l}_j$ to assemble and therefore make the calculation more costly.

To numerically solve 5.1 we replace

$$\mathbf{X}_{(R)} \simeq \hat{\mathbf{X}}_{(R)} = \mathbf{R}_k \mathbf{Y}_{(R)} \quad . \tag{5.16}$$

This yields,

$$\mathbf{G}\mathbf{R}_k \mathbf{Y}_{(R)} = \mathbf{R}_k \mathbf{Y}_{(R)} \tilde{\mathbf{\Lambda}} \quad , \tag{5.17}$$

where $\tilde{\mathbf{\Lambda}}$ is an approximation for $\mathbf{\Lambda}$ in 5.1. After multiplying both sides from the left by the conjugate transpose of $\mathbf{L}_k$ we obtain the generalized eigenvalue problem,

$$\mathbf{G}_k \mathbf{Y}_{(R)} = \mathbf{S}_k \mathbf{Y}_{(R)} \tilde{\mathbf{\Lambda}} \quad , \tag{5.18}$$

where $\mathbf{G}_k = \mathbf{L}_k^* \mathbf{G} \mathbf{R}_k$ and $\mathbf{S}_k = \mathbf{L}_k^* \mathbf{R}_k$. The matrix $\mathbf{S}_k$ is an overlap matrix of two sets of vectors. This oblique Rayleigh-Ritz-type procedure works because the better the approximate eigenvector spaces the better the eigenvalues obtained from the projected matrix [36], pages 280-289. For experiments we have done, the eigenvalues of 5.18 are accurate eigenvalues of $\mathbf{G}$ and accurate right eigenvectors can be obtained using 5.16. A matrix of approximate left eigenvectors, $\mathbf{X}_{(L)}$, is obtained from

$$\mathbf{X}_{(L)}^* \simeq \hat{\mathbf{X}}_{(L)}^* = \mathbf{Y}_{(L)}^* \mathbf{L}_k^* \quad , \tag{5.19}$$

where $\mathbf{Y}_{(L)}$ is defined by

$$\mathbf{Y}_{(L)}^* \mathbf{G}_k = \tilde{\mathbf{\Lambda}} \mathbf{Y}_{(L)}^* \mathbf{S}_k \quad , \tag{5.20}$$

and is computed simultaneously with $\mathbf{Y}_{(R)}$. If one wishes more eigenvalues it is necessary to compute additional approximate eigenvectors (from the same Lanczos vectors) and to form another $\mathbf{G}_k$ matrix. Using the approximate eigenvectors to

build $\mathbf{G}_k$ enables us to extract accurate eigenvalues from the Krylov spaces, but it does not change the subspaces themselves. The convergence rate of the RULE will be determined by the Krylov subspaces of the ULA which are to some extent affected by roundoff error.

The new method can be summarized as follows:

Algorithm 3. Refined Unsymmetric Lanczos Eigensolver (RULE)

1. Compute m steps of the Unsymmetric Lanczos Algorithm 1;
2. Form $\hat{\mathbf{T}}_m$ and compute its eigenvalues;
3. Form clusters of eigenvalues of $\hat{\mathbf{T}}_m$ and for each cluster compute an average;
4. Identify clusters with only one eigenvalue that are spurious;
5. Select shifts for non-spurious eigenvalue clusters in the spectral region of interest;
6. For each shift compute right and left eigenvectors of $\mathbf{T}_m$ using inverse iteration Algorithm 2;
7. Keep only eigenvectors of $\mathbf{T}_m$ with distinct Ritz values;
8. Assemble approximate left and right eigenvectors of $\mathbf{G}$ according to 5.15;
9. Project matrix $\mathbf{G}$ onto these vectors according to 5.18;
10. Solve the complex generalized eigenvalue problem using the QZ algorithm [19].

We choose a value of m and generate Lanczos vectors. If the associated $\hat{\mathbf{T}}_m$ has eigenvalues in the spectral region of interest, $\mathbf{G}_k$ is formed and 3.6 is solved. If $\hat{\mathbf{T}}_m$ does not have eigenvalues in the spectral region of interest or if the eigenvalues computed with the RULE are not converged, we increase m and calculate more Lanczos vectors. Increasing m cannot ruin the approximate eigenvectors so there is no need to carefully search for the best m. To obviate the need to store a large number of approximate eigenvectors in memory, eigenvalues are calculated in groups by repeating steps 5 to 10 of Algorithm 3. To compute eigenvalues with the largest/smallest,

real/imaginary part/norm we use approximate eigenvectors whose corresponding eigenvalues are those with the largest/smallest, real/imaginary part/norm. To calculate interior eigenvalues close to a target value we use approximate eigenvectors associated with the eigenvalues close to the target.

5.4 Numerical experiments

Many numerical experiments were done using both Matlab and FORTRAN programs. With Matlab we have computed extremal eigenvalues of "random" and Riemann matrices generated using Matlab routines and of Tolosa matrices from the Matrix Market [37]. Also using Matlab we have computed interior eigenvalues of PDE matrices from the Matrix Market. Eigentriplets of the AIRFOIL matrix, available from Matrix Market, and a matrix we constructed to determine energies and lifetimes of metastable states of the HCO radical were computed using a FORTRAN implementation of the RULE. In all cases η was chosen to be the square root of the machine precision.

5.4.1 Random matrix generated with 5.10

The random matrices of different size, obtained using 5.10, all had one isolated, extremal eigenvalue. In section 2 it is mentioned that it is possible to use the ULA to obtain a good approximation for the isolated eigenvalue if and only if a tridiagonal matrix of the optimal size is used. The smallest error that can be achieved, by choosing the best possible value of m, with the ULA is of the order of 10^{-13}. For other (non isolated) eigenvalues ULA does poorly. Interior eigenvalue errors are of the order of 10^{-8}. Both ARPACK and our implementation of the RULE yield non-extremal eigenvalues with absolute errors less than 10^{-13}.

Figure 5.3: ULA convergence and cluster width of an extremal eigenvalue of RIEMANN5000

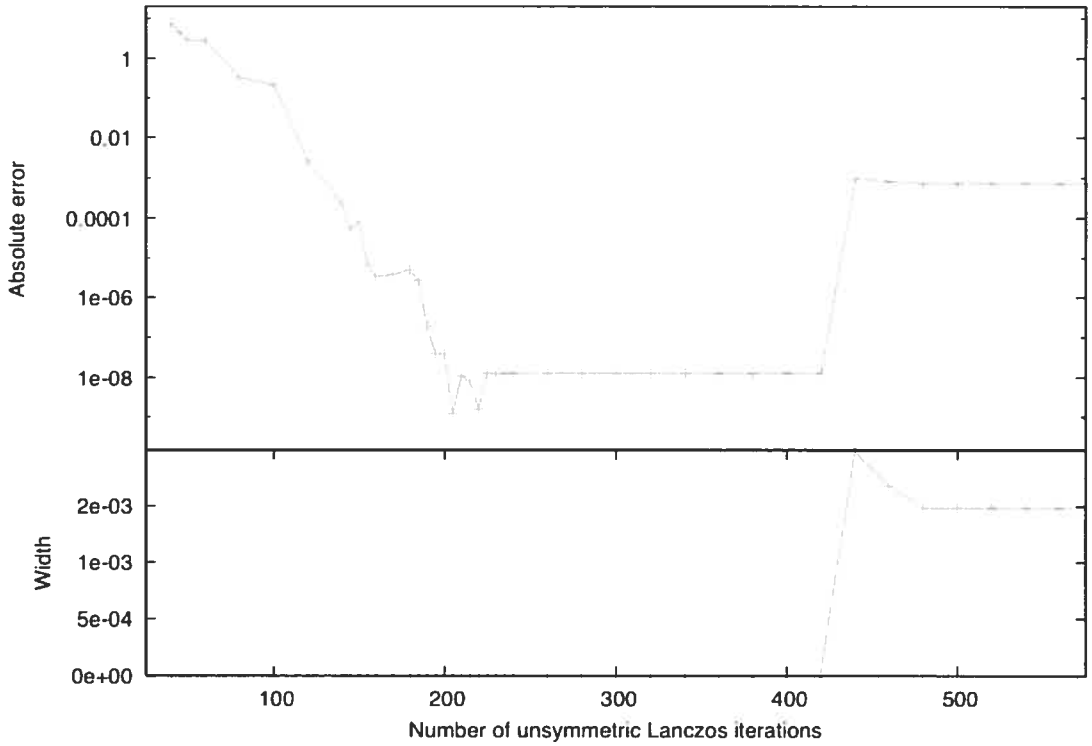

5.4.2 Riemann matrices

We have computed eigenvalues of different Riemann matrices. Results for the largest matrix studied, of size $N = 5000$, are presented in figure 5.3 and Table 5.2. The matrices are associated with the Riemann hypothesis and can be generated with Matlab using the function

$$\mathbf{G}_{rie} = \text{GALLERY('RIEMANN',}N\text{).} \tag{5.21}$$

For more details, the reader is referred to the Matrix Computation Toolbox available on the website of Professor N. Higham [38]. The complex eigenvalue distribution for the matrix is shown in figure 5.4. We decided to focus on eigenvalues with

Figure 5.4: Distribution of eigenvalues of the RIEMANN5000 matrix

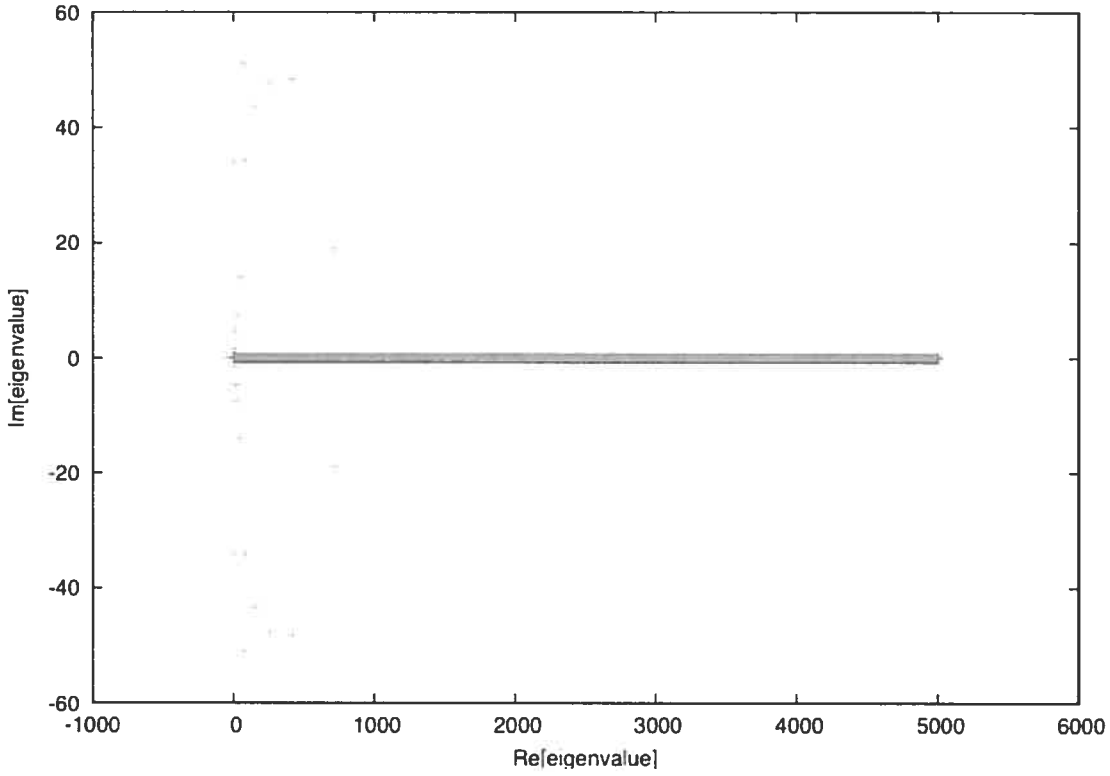

large imaginary parts since they are located near the convex hull of the spectrum but do not have the largest norms. Due to the fact that the desired eigenvalues with large imaginary parts are close to the convex hull the ULA should work fairly well [19]. The ULA convergence of a representative eigenvalue of matrix RIEMANN5000 is depicted in the top panel of figure 5.3. Although the ULA is expected to work well the minimum error is about $\sim 10^{-9}$ (the error is much larger for some eigenvalues). As m is increased the error decreases and reaches a plateau. The error, defined as the norm of the difference between the average of the nearly degenerate copies and the eigenvalue computed with Matlab's EIG, increases as m is increased further. It increases significantly when the first copy appears. As more copies accumulate the width of the cluster of nearly degenerate copies increases, as shown in the lower panel of figure 5.3. The 12 eigenvalues with the largest absolute

imaginary parts computed with the RULE are presented in Table 5.2. Note that the refinement decreases the eigenvalue error by many orders of magnitude. Some errors are reduced by 4 orders of magnitude.

In the fourth column of table 5.2 we report results obtained with ARPACK. ARPACK eigenvalues are also accurate. For some matrices RULE eigenvalues will be more accurate than ARPACK eigenvalues, for others the reverse will be true. We do not claim that RULE eigenvalues will always be more accurate. Nonetheless the RULE has the important advantage that it requires much less memory. Is this advantage obtained by sacrificing efficiency (i.e. increased CPU cost)? The

Table 5.2: Error in selected eigenvalues of the RIEMANN5000 matrix

Eigenvalue	ULA*	RULE**	ARPACK†	$\lvert \mathbf{x}^*_{(L)} \mathbf{x}_{(R)} \rvert$
$2.024454 - 34.08310i$	3.3E-9	4.5E-11	7.4E-11	5.9558E-03
$2.024454 + 34.08310i$	3.3E-9	4.2E-11	7.4E-11	5.9558E-03
$84.80854 - 34.24698i$	9.4E-8	1.3E-10	9.0E-11	9.2899E-03
$84.80854 + 34.24698i$	9.4E-8	1.5E-10	9.0E-11	9.2899E-03
$76.12058 - 51.07108i$	1.5E-8	3.0E-10	2.3E-10	5.7480E-03
$76.12058 + 51.07108i$	1.5E-8	2.9E-10	2.3E-10	5.7480E-03
$152.9928 - 43.53188i$	4.3E-8	4.5E-11	2.4E-11	4.1720E-02
$152.9928 + 43.53188i$	4.3E-8	4.6E-11	2.4E-11	4.1720E-02
$257.0954 - 47.71716i$	6.4E-7	3.4E-11	3.0E-11	8.9580E-02
$257.0954 + 47.71716i$	6.4E-7	3.2E-11	3.0E-11	8.9580E-02
$417.5244 - 48.37068i$	4.5E-8	3.3E-11	2.3E-11	1.5945E-01
$417.5244 + 48.37068i$	4.5E-8	3.5E-11	2.3E-11	1.5945E-01

* 475 Lanczos iterations; 950 matrix-vector products

** 475 Lanczos iterations; 962 matrix-vector products

† ARPACK parameters: k = 12, p=150, 7 restarts, 1116 matrix-vector products

efficiency of the RULE can be assessed on the basis of the number of matrix-vector products required to determine accurate eigenvalues (doing the matrix-vector products is the most time-consuming part of the calculation). Although the RULE requires matrix-vector products with both $\mathbf{G}^*$ and $\mathbf{G}$ and ARPACK needs only matrix-vector products with $\mathbf{G}$ the number of RULE matrix-vector products (962)

required is similar to the number of required ARPACK matrix-vector products (1116). Over and above those required to do the 475 Lanczos iterations the RULE requires only 12 matrix-vector products. The additional 12 are necessary for building $\mathbf{G}_k$. The cost of an ARPACK calculation includes not only the cost of doing the matrix-vector products but also the cost of the orthogonalization. We have chosen the ARPACK parameter p to approximately minimize the number of matrix-vector products. With this choice the number of ARPACK and RULE matrix-vector products is similar but the memory cost of the RULE is much less. It would have been possible to choose a smaller p to reduce the memory cost of ARPACK, but this would increase the number of restarts and the number of matrix-vector products (increasing p decreases the CPU cost but increases the memory cost). These results show that, for this problem, the RULE is not only accurate but also efficient in terms of CPU time.

5.4.3 TOLOSA matrices

The TOLOSA matrices were used in the stability analysis of an airplane in flight. The eigenvalues of interest are the three with largest imaginary parts. For more detail we refer the reader to the Matrix Market [37]. The desired eigenvalues are located on the convex hull of the spectrum (cf. Figure 5.5). Matrices of size 90, 340, 1090 and 2000 were studied. Using both the RULE and ARPACK it is easy to converge many eigenvalues of the three smaller matrices. We therefore focus on the largest matrix. Table 5.3 shows eigenvalue errors. The accuracy of the ULA eigenvalues for TOLS2000 is poor. The ULA convergence behavior for the eigenvalue of TOLS2000 with the third largest imaginary part is presented in the top panel of figure 5.6. The associated cluster width is shown in the lower panel. As was also true for the RIEMANN matrices, the width of the cluster increases as the number of copies grows. The ULA is indeed poor, for example, the absolute error is never less than 10^{-5} for the eigenvalue shown in figure 5.6. In contrast,

Figure 5.5: Distribution of eigenvalues of the TOLS2000 matrix

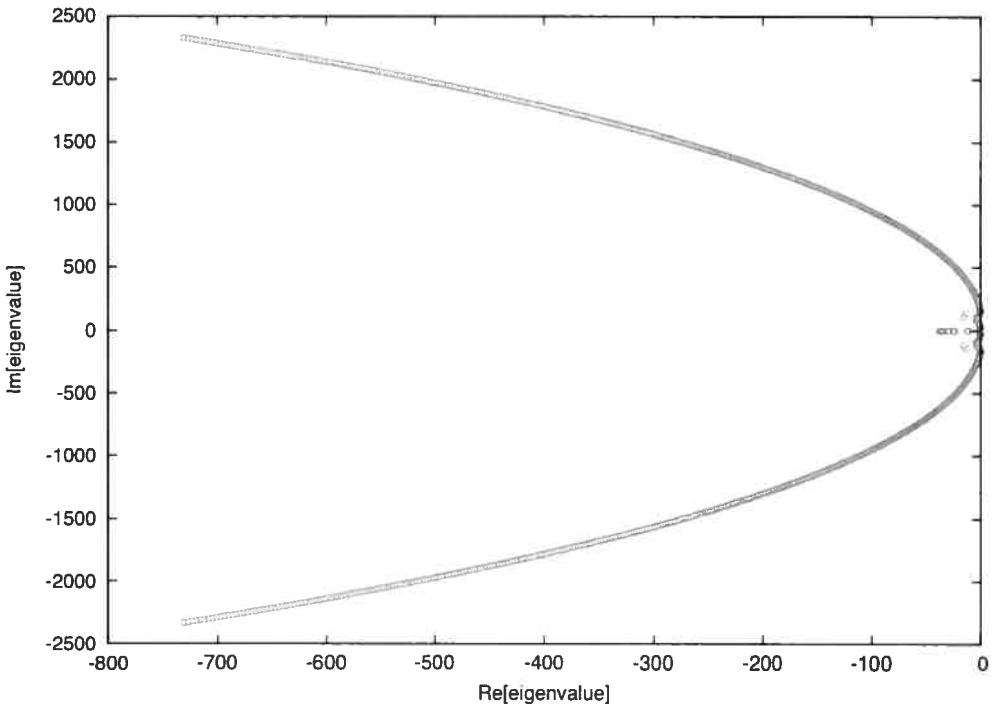

eigenvalues obtained with the RULE are quite accurate (and about as accurate as those computed with ARPACK).

5.4.4 PDE matrices

In this subsection we show that it is possible to use the RULE to compute interior eigenvalues. Without using a spectral transform one can do this by using the SM option of ARPACK, but this requires storing many vectors in memory. To test the computation of interior eigenvalues with the RULE we have used matrices obtained by discretizing a 2-D elliptic differential equation with a five-point central finite difference scheme. On Matrix Market the matrix we use is called PDE2961

Table 5.3: Error in extremal eigenvalues of the TOLS2000 matrix

Eigenvalue	ULA*	RULE**	ARPACK†	$\lvert\mathbf{x}^*_{(L)}\mathbf{x}_{(R)}\rvert$
$-723.2940 - 2319.859i$	5.4E-05	6.3E-07	2.5E-09	7.8574E-04
$-723.2940 + 2319.859i$	5.4E-05	6.3E-07	2.5E-09	7.8574E-04
$-726.9866 - 2324.992i$	4.8E-06	8.8E-11	1.4E-07	7.8360E-04
$-726.9866 + 2324.992i$	4.8E-06	8.5E-11	1.4E-07	7.8360E-04
$-730.6886 - 2330.120i$	6.7E-07	1.2E-11	4.6E-08	7.8148E-04
$-730.6886 + 2330.120i$	6.7E-07	1.2E-11	4.6E-08	7.8148E-04

* 170 Lanczos iterations; 340 matrix-vector products

** 170 Lanczos iterations; 346 matrix-vector products

† ARPACK parameters: k = 6, p=300, 2 restarts, 888 matrix-vector products

[37]. In figure 5.7 we show the spectrum of the matrix of size $N = 2961$. The approximate eigenvectors we use are those whose corresponding eigenvalues lie in a rectangular box of width 0.5 and height $0.1i$ centered at a target value of $8.3 + 0.35i$. Errors for eigenvalues close to the target are reported in Table 5.4 and figure 5.8 shows the typical convergence behavior of an eigenvalue computed with ULA. It is clear that the ULA is poor and that refinement improves the eigenvalues significantly. Although only eigenvalues close to the target are shown, all extremal eigenvalues are *also* well converged. An advantage of the RULE is that one does

Table 5.4: Interior eigenvalues of the PDE2961 matrix. The chosen target is $8.3 + 0.35i$. The error is defined as the norm of the difference between computed and exact values.

Refined eigenvalue	ULA*	RULE**	$\lvert\mathbf{x}^*_{(L)}\mathbf{x}_{(R)}\rvert$
$7.831661 + 0.3970848i$	7.4E-09	2.4E-12	3.0064E-02
$7.928410 + 0.2564949i$	3.3E-07	3.0E-11	2.0611E-03
$8.130354 + 0.4211668i$	1.0E-08	6.3E-14	5.3381E-02
$8.240396 + 0.2678090i$	3.8E-08	3.0E-13	3.8846E-03
$8.465128 + 0.4423992i$	2.7E-09	1.4E-14	8.1620E-02
$8.600357 + 0.2746980i$	9.4E-08	1.1E-13	6.3615E-03

* 450 Lanczos iterations; 900 matrix-vector products

** 450 Lanczos iterations; 906 matrix-vector products

Figure 5.6: ULA convergence and cluster width of an extremal eigenvalue of TOLS2000.

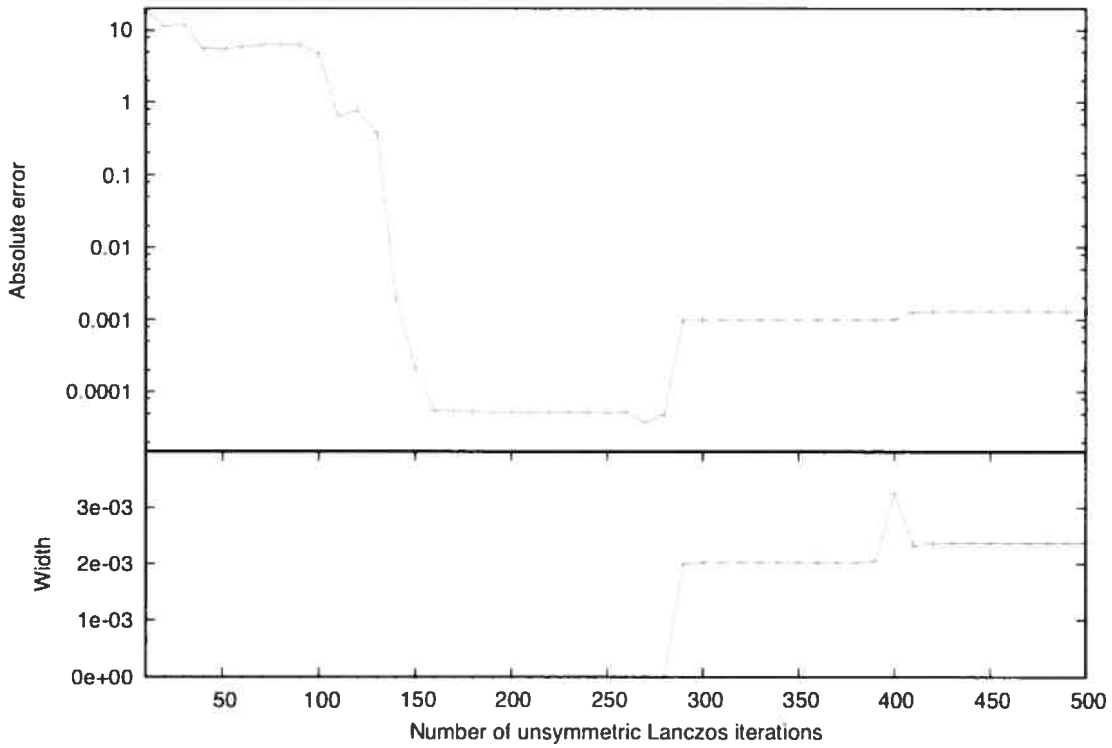

not need tridiagonal matrices of different size for different eigenvalues. All of the eigenvalues are extracted from one large tridiagonal matrix. This makes the method simple to use.

It is possible to compute the eigenvalues in Table 5.4 by applying ARPACK to $(\mathbf{G}-\sigma\mathbf{I})$, choosing σ to be in the centre of the desired spectral region, and using the SM option to extract eigenvalues with the smallest magnitude. Increasing p and therefore increasing the number of vectors stored in memory decreases the number of required matrix-vector products. We find that if $p = 100$ and $k = 50$ the number of vectors is not too large and 1385 matrix-vector products is enough to converge the eigenvalues in Table 5.4. Note also that because σ is complex, the cost of each ARPACK matrix-vector product, the cost of the ARPACK re-orthogonalisation,

Figure 5.7: Distribution of eigenvalues of the PDE2961 matrix

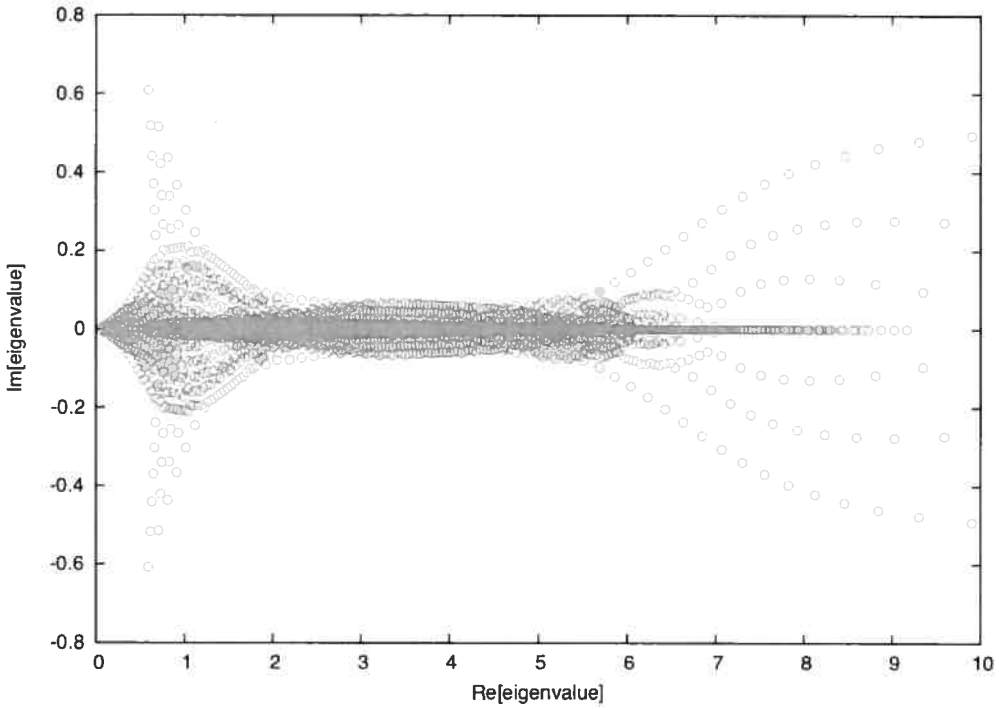

and the memory required to store the Arnoldi vectors are approximately doubled.

5.4.5 AIRFOIL matrix

The AIRFOIL matrix of matrix market is a good test as the matrix is large (23 560), but small enough that benchmark eigenvalues can be computed with a direct method. The matrix is obtained by modeling flow over airfoils with a finite difference representation of the Navier-Stokes equations. More details can be found on the Matrix Market [37]. We focus on the eigenvalues of largest magnitude for which both ARPACK and the RULE should work well. The spectral distribution is depicted in figure 5.9. As can be seen from table 5.5 accurate eigenvalues are

Figure 5.8: ULA convergence and cluster width of an interior eigenvalue of PDE2961.

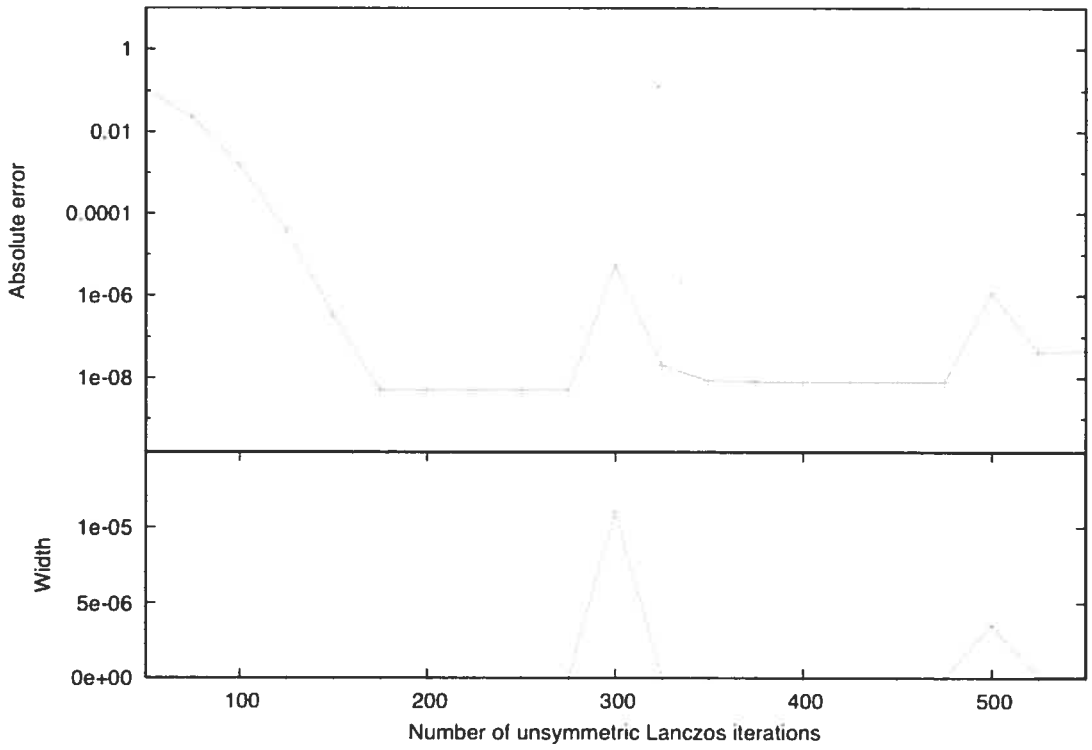

indeed obtained using both the RULE and ARPACK with a fairly small number of iterations. The error is defined as the absolute difference between an eigenvalue computed with Householder/QR [19] and either the RULE or ARPACK. The residuals are right eigenvector residuals defined by [31]

$$residual = \frac{||\mathbf{G}\mathbf{x}_j - \tilde{\lambda}_j \mathbf{x}_j||_2}{||\mathbf{G}||_1} \quad . \tag{5.22}$$

The matrix-vector product count slightly favours ARPACK in this case. The ARPACK results were obtained with a residual tolerance parameter equal to the machine precision.

Figure 5.9: Distribution of eigenvalues of the AF23560 matrix

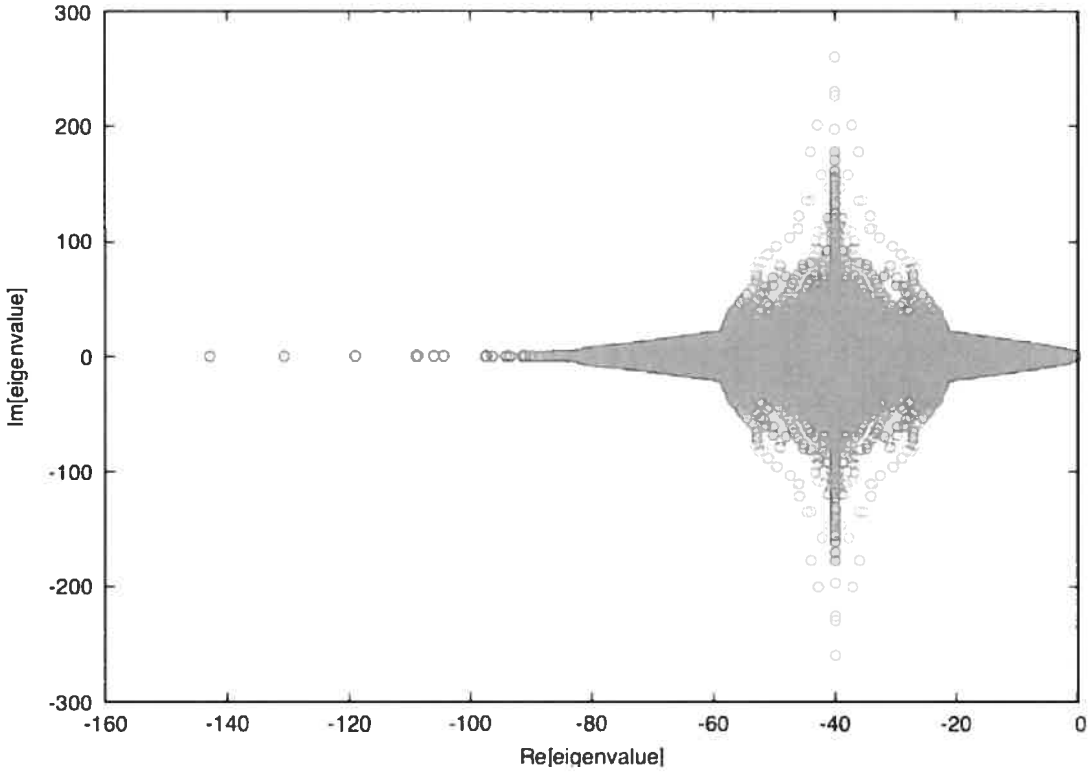

5.4.6 Lifetimes of states of HCO

The imaginary part of the complex energy of a resonance state is related to the lifetime of the state [39, 40]. The most popular approach for computing resonance states uses a complex absorbing potential (CAP) to enforce appropriate boundary conditions. The operator equation to be solved is,

$$\left(\hat{H} + u_k \hat{W}(r)\right) \psi_k = E_k \psi_k \quad , \tag{5.23}$$

where $\hat{H}$ is a Hamiltonian operator, $\hat{W}(r)$ is a CAP depending on the dissociation coordinate r, and E_k is the complex resonance energy; u_k is a function of E_k. If u_k is chosen appropriately and the operators are represented in a discrete variable representation (DVR) basis [41], 5.23 may be written as a quadratic matrix eigen-

Table 5.5: Error in extremal eigenvalues of the AF23560 matrix.

Eigenvalue	ULA*	RULE**	ARPACK†	RULE Residual	$\lvert\mathbf{x}^*_{(L)}\mathbf{x}_{(R)}\rvert$
$-37.18288 + 200.1360i$	1.1E-08	7.1E-13	2.3E-07	3.3E-08	0.21239
$-37.18288 - 200.1360i$	1.1E-08	4.3E-13	2.3E-07	3.5E-08	0.21239
$-37.14444 + 200.2190i$	3.8E-09	7.4E-13	4.8E-07	1.1E-07	0.21716
$-37.14444 - 200.2190i$	3.8E-09	5.8E-13	4.8E-07	9.1E-08	0.21716
$-42.81924 + 200.1356i$	7.5E-08	1.1E-12	1.9E-07	1.2E-07	0.21236
$-42.81924 - 200.1356i$	7.5E-08	7.0E-13	1.9E-07	7.0E-08	0.21236
$-42.85767 + 200.2186i$	9.0E-08	9.5E-13	3.5E-07	8.3E-08	0.21713
$-42.85767 - 200.2186i$	9.0E-08	5.5E-13	3.5E-07	8.9E-08	0.21713
$-40.00075 + 225.7328i$	1.2E-08	6.5E-13	8.6E-07	4.7E-08	0.26668
$-40.00075 - 225.7328i$	1.2E-08	3.7E-13	8.6E-07	2.2E-08	0.26668
$-40.00074 + 225.7714i$	3.4E-09	7.4E-13	8.4E-07	2.9E-08	0.26530
$-40.00074 - 225.7714i$	3.3E-09	1.1E-12	8.4E-07	2.8E-08	0.26530
$-40.00010 + 229.5187i$	1.1E-08	3.1E-13	6.2E-07	3.9E-08	0.22165
$-40.00010 - 229.5187i$	1.1E-08	1.1E-13	6.2E-07	3.3E-08	0.22165
$-40.00095 + 229.5291i$	1.2E-08	5.7E-13	8.0E-07	7.7E-08	0.22236
$-40.00095 - 229.5291i$	1.2E-08	1.5E-13	8.0E-07	2.9E-08	0.22236
$-40.00045 + 259.5435i$	1.2E-10	1.0E-12	4.8E-07	2.2E-07	0.41406
$-40.00045 - 259.5435i$	1.4E-10	7.6E-13	4.8E-07	8.7E-08	0.41406
$-40.00041 + 259.5534i$	9.0E-11	6.9E-13	1.6E-06	1.9E-07	0.41406
$-40.00041 - 259.5534i$	1.6E-10	4.1E-13	1.6E-06	6.2E-08	0.41406

* 125 Lanczos iterations; 250 matrix-vector products

** 125 Lanczos iterations; 270 matrix-vector products

† ARPACK parameters: k = 20, p=50, 6 restarts, 172 matrix-vector products

value problem. There is some freedom in the choice of u_k; different choices yield different quadratic eigenvalue problems. We choose $u_k = i\sqrt{(\sigma - E_k)}$ so that after linearizing the quadratic eigenvalue problem in the standard fashion [19], we obtain an unsymmetric eigenvalue problem,

$$\mathbf{G}\mathbf{x}_k = u_k\mathbf{x}_k \ , \tag{5.24}$$

where

$$\mathbf{G} = \begin{pmatrix} \mathbf{0} & \mathbf{I} \\ \mathbf{H} - \sigma\mathbf{I} & \mathbf{W} \end{pmatrix} \tag{5.25}$$

is a *real* matrix and $\mathbf{x}_k = \begin{pmatrix} \psi_k \\ u_k\psi_k \end{pmatrix}$. To obtain accurate resonance lifetimes one usually premultiplies the CAP by a parameter δ_{cap} and computes eigenvalues for several values of δ_{cap} to find the optimal absorbing potential. We choose σ large enough to ensure that for many states the E_k computed from the eigenvalues of $\mathbf{G}$ are close to the actual resonance energies. For more detail the reader is referred to [42–44].

The physically interesting eigenvalues, i.e. the bound states and the resonances, are located on and close to the imaginary axis, respectively. Because they are not extremal eigenvalues and because their condition numbers are large, it is difficult to compute them accurately. The DVR basis necessary to converge all low-lying resonance states of the HCO molecule gives rise to a real unsymmetric matrix $\mathbf{G}$ of size 184000, which is far too big to be diagonalized with direct methods on the computers we use. Table 5.6 shows some eigenvalues for HCO in the region $\mathrm{Im}[\lambda] \geq 55$ and $|\mathrm{Re}[\lambda]| \leq 0.1$, associated with narrow resonances and bound states. Because the RULE is a two-sided method we obtain simultaneously right and left eigenvectors. This makes it straightforward to compute condition numbers (last column).

To test the quality of the RULE results, we compute right eigenvector residuals. The accuracy of the RULE eigenvalues is good. With 3000 Lanczos iterations it is possible to compute not only the eigenvalues in Table 5.6 but also many others. The eigenvalues reported in Table 5.6 can be computed with fewer than 3000 iterations. Increasing the number of iterations does not adversely affect the quality of the eigenvalues. In constrast, the accuracy of ULA eigenvalues deteriorates as the number of iterations is increased (cf. figures 5.2, 5.3, and 5.6). Figure 5.10 shows the convergence of the residual, computed with the RULE, for the eigenvalue $\tilde{\lambda} =$

Table 5.6: Selected narrow resonance states of the HCO molecule. The residual error is defined as the norm of the residual vectors.

Refined eigenvalue	RULE Residual	$\lvert\mathbf{x}^*_{(L)}\mathbf{x}_{(R)}\rvert$
$0.000000000001608 + 99.63317i$	4.3E-09	2.007E-02
$0.000000000423172 + 94.06122i$	4.3E-09	2.126E-02
$-0.000000000030880 + 89.78747i$	2.0E-07	2.227E-02
$0.000000000017839 + 88.24727i$	7.6E-08	2.266E-02
$0.000000000000180 + 86.54286i$	1.3E-08	2.311E-02
$0.000000000000180 + 86.54286i$	1.9E-09	2.392E-02
$0.000000000013164 + 82.15547i$	1.9E-07	2.434E-02
$-0.000000000000079 + 80.30376i$	1.6E-08	2.490E-02
$-0.000000000003208 + 78.87198i$	2.0E-08	2.535E-02
$0.000000000002248 + 77.02845i$	8.2E-09	2.596E-02
$-0.000000000000226 + 75.73480i$	2.5E-09	2.640E-02
$-0.000000000000173 + 75.02610i$	9.3E-09	2.665E-02
$-0.000000000046711 + 73.83727i$	3.4E-08	2.708E-02
$-0.000000000044467 + 73.27523i$	1.8E-08	2.729E-02
$0.000000000000506 + 71.77733i$	3.2E-09	2.786E-02
$-0.000000000001369 + 70.00861i$	2.3E-09	2.856E-02
$-0.001503206670272 + 69.62269i$	1.2E-08	2.872E-02
$-0.001616758817681 + 69.28458i$	1.1E-07	2.886E-02
$-0.001799287965362 + 68.97843i$	7.1E-07	2.899E-02
$0.000000192654410 + 68.91187i$	1.1E-06	2.902E-02
$-0.001958836517186 + 68.69687i$	4.1E-06	2.910E-02

Number of unsymmetric Lanczos iterations: 3000

$-0.000000000001 + 70.00861i$. The condition number of this eigenvalue is $\sim 10^2$. Despite the large condition number, the residual is less than $\sim 10^{-9}$ with 2200 Lanczos iterations. If the number of Lanczos iterations is increased the residual oscillates about an average value of $\sim 10^{-8}$. Similar oscillations are observed for most of the residuals. The oscillations appear to be due to fluctuations in the quality of the basis vectors $\mathbf{r}_j, \mathbf{l}_j$ used to form $\mathbf{G}_k$. The quality of the $\mathbf{r}_j, \mathbf{l}_j$ depends on the size of the Krylov subspaces used to compute them. The fluctuations do not significantly affect the accuracy of the eigenvalues since to eleven significant digits they do not depend on the number of Lanczos iterations.

Figure 5.10: Residual of an eigenvalue associated with a resonance of HCO.

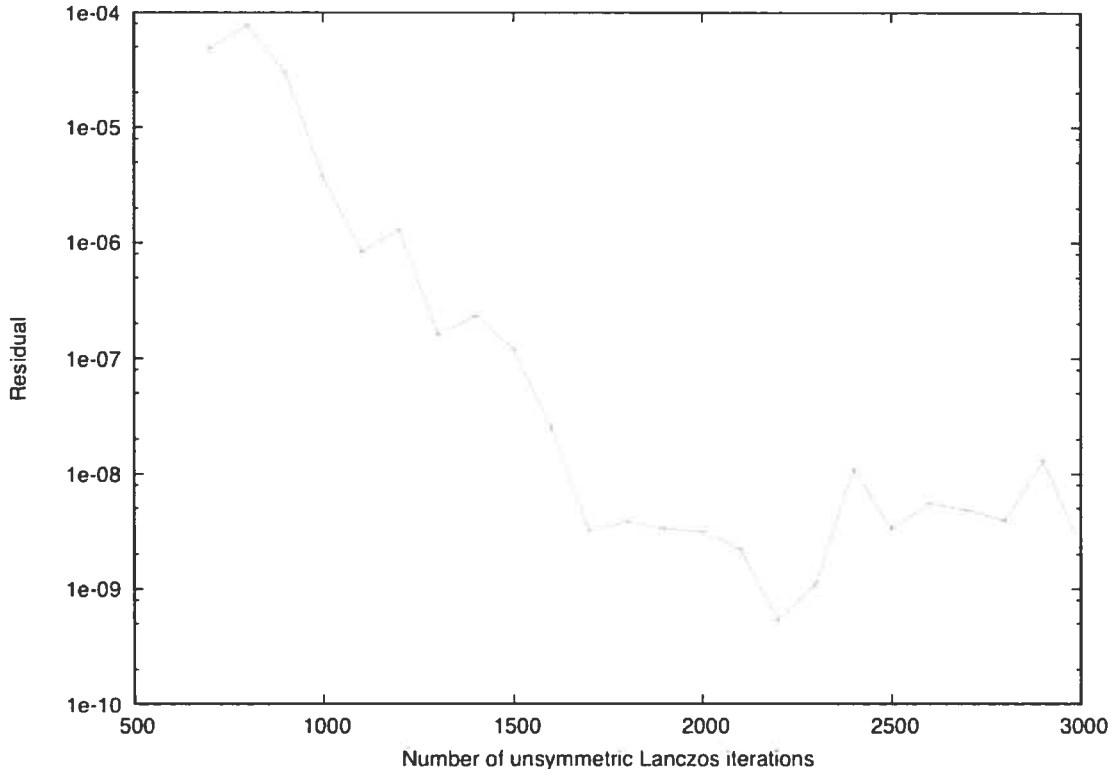

5.5 Conclusion

In a previous paper [44] we used the idea of projecting onto approximate eigenvectors, computed from the ULA, to determine lifetimes of metastable states by calculating many eigentriplets. In this paper we have generalized the approach and made it more robust. In [44] we did not project a matrix onto its own approximate eigenspaces, instead we projected one matrix onto approximate eigenspaces of another, related, matrix. Other important differences between the approach of the this paper and the method used in [44] are: (1) In [44] approximate eigenvectors were obtained by searching for the best value of m for each eigenvalue; we have found that this is not necessary. (2) In [44] we solved a special (factorizable) generalized eigenvalue problem and in this paper we solve the unsymmetric

eigenproblem. (3) We have modified the way clusters are defined and approximate eigenvectors are retained to ensure that we do not miss eigenvalues.

In this paper we show that a simple refinement makes it possible to extract accurate eigenvalues from the Krylov subspaces obtained from the ULA. We call the procedure the RULE. Using several test matrices we have shown that the RULE yields accurate extremal and interior eigenvalues. For all the eigenvalues in the tables we have computed eigenvectors and residuals. To use the RULE there is no need to store a large number of vectors in memory and no need to re-biorthogonalize Lanczos vectors. This makes it possible to use the RULE with very large matrices to compute large numbers of eigenvalues. One of the key advantages of the RULE is its ability to make use of large Krylov subspaces. The CPU cost of the RULE is close to or less than that of ARPACK. To use the RULE one must store vectors on disk but reading them from disk does not take significant computer time because they are only used *after* the tridiagonal matrix has been generated. It is important to stress that the refinement we propose is very inexpensive. We typically compute eigenvalues in groups of about 20 or less. For each group of 20 the cost of the refinement is only 20 additional matrix-vector products.

Acknowledgments

This work has been supported by the Natural Sciences and Engineering Research Council of Canada. We thank Rich Lehoucq, Chris Paige, Andreas Stathopoulos, Michiel Hochstenbach, Yvan Notay, and a referee who made suggestions for improving the manuscript.

Bibliography

[1] P. Arbenz, U. L. Hetmaniuk, R. B. Lehoucq, and R. S. S. Tuminaro. A comparison of eigensolvers for large-scale 3d modal analysis using AMG-preconditioned iterative methods. *Internat. J. Numer. Methods Engrg.*, 64:204–236, 2005.

[2] J.G.C. Booten and H.A. van der Vorst. Cracking large-scale eigenvalue computations, part i: Algorithms. *Computers in Physics*, 10:239, 1996.

[3] T. Carrington Jr. Methods for calculating vibrational energy levels. *Can. J. Chem.*, 82:900–914, 2003.

[4] E. R. Davidson. The iterative calculation of a few of the lowest eigenvalues and corresponding eigenvectors of large real symmetric matrices. *J. Comput. Phys.*, 17:87–94, 1975.

[5] F. Sartoretto, G. Gambpmato, and G. Pini. Accelerated simultaneous iterations for large finite element eigenvalues. *J. Comput. Phys.*, 81:53, 1989.

[6] M. J. Bramley and T. Carrington Jr. A general discrete variable method to calculate vibrational energy levels of three- and four-atom molecules. *J. Chem. Phys.*, 99:8519, 1993.

[7] J. K. Cullum and R. A. Willoughby. Computing eigenvalues of very large symmetric matrices-an implementation of a lanczos algorithm with no reorthogonalization. *J. Comput. Phys.*, 44:329–358, 1981.

[8] J. K. Cullum and R. A. Willoughby. *Lanczos algorithms for large symmetric eigenvalue computations.* Birkhäuser, Boston, 1985.

[9] U. Elsner, V. Mehrmann. F. Milde, R. Rmer, and M. Schreiber. The anderson model of localization: A challenge for modern eigenvalue methods. *SIAM J. Sci. Comput.*, 20:2089–2102, 1999.

[10] C. C. Paige. *The Computation of Eigenvalues and Eigenvectors of Very Large Sparse Matrices.* PhD thesis, University of London, 1971.

[11] C. C. Paige. Computational variants of the Lanczos method for the eigenproblem. *J. Inst. Math. Appl.*, 10:373, 1972.

[12] C. C. Paige. Error analysis of the Lanczos algorithm for tridiagonalizing symmetric matrix. *J. Inst. Math. Applic.*, 18:341–349, 1976.

[13] P.-N. Roy and T. Carrington Jr. An evaluation of methods designed to calculate energy levels in a selected range and application to a (one-dimensional) Morse oscillator and (three-dimensional) HCN/HNC. *J. Chem. Phys.*, 103:5600, 1995.

[14] G. H. Golub and C. F. Van Loan. *Matrix Computations.* John Hopkins University Press, Baltimore, 1989.

[15] L. N. Trefethen and D. Bau III. *Numerical Linear Algebra.* Society for Industrial and Applied Mathematics, Philadelphia, 1997.

[16] D. C. Sorensen. Implicit application of polynomial filters in a $k-$step Arnoldi method. *SIAM J. Matr. Anal. Appl.*, 13:357, 1992.

[17] R.B. Lehoucq, D.C. Sorensen, and C. Yang. *ARPACK Users' Guide: Solution of Large-Scale Eigenvalue Problems with Implicitly Restarted Arnoldi Methods.* Society for Industrial and Applied Mathematics, Philadelphia, 1998.

[18] http://www.caam.rice.edu/software/ARPACK/.

[19] Z. Bai, J. Demmel, J. Dongarra, A. Ruhe, and H. van der Vorst, editors. *Templates for the Solution of Algebraic Eigenvalue Problems: A Practical Guide.* Society for Industrial and Applied Mathematics, Philadelphia, 2000.

[20] R.B. Lehoucq, S.K. Gray, D.H. Zhang, and J.C. Light. Vibrational eigenstates of four-atom molecules: A parallel strategy employing the implicitly restarted Lanczos method. *Comput. Physics Comm.*, 109:15–26, 1998.

[21] R. B. Lehoucq and J. A. Scott. An evaluation of software for computing eigenvalues of sparse nonsymmetric matrices. Preprint MCS-P547-1195, Argonne National Laboratory.

[22] J. S. Warsa, T. A. Wareing, J. E. Morel, J. M. McGhee, and R. B. Lehoucq. Krylov subspace iterations for deterministic k-eigenvalue calculations. *Nucl. Sci. Eng.*, 147:26, 2004.

[23] J. Baglama, D. Calvetti, and L. Reichel. Iterative methods for the computation of a few eigenvalues of a large symmetric matrix. *BIT*, 36:400, 1996.

[24] S.-W. Huang and T. Carrington Jr. Calculating interior eigenvalues and eigenvectors with an implicitly restarted and a filter diagonalization method. *Appl. Numer. Math.*, 37:307, 2001.

[25] R. W. Freund and N. M. Nachtigal. An implementation of the look-ahead Lanczos algorithm for non-hermitian matrices. *SIAM J. Sci. Comput.*, 14:137, 1993.

[26] B. N. Parlett, D. R. Taylor, and Z. A. Liu. A look-ahead Lanczos algorithm for unsymmetric matrices. *Math. Comp.*, 44:105, 1985.

[27] D. Day. An efficient implementation of the nonsymmetric Lanczos algorithm. *SIAM J. Matrix Anal. Appl.*, 18:566–589, 1997.

[28] Jane K. Cullum and Ralph A. Willoughby. *Large Scale Eigenvalue Problems*, chapter A practical procedure for computing eigenvalues of large sparse nonsymmetric matrices. North-Holland, Amsterdam, 1986.

[29] Z. Jia. Refined iterative algorithms based on arnoldi's process for large unsymmetric eigenproblems. *Linear Algebra Appl.*, 259:1–23, 1997.

[30] Z. Bai. Error analysis of the lanczos algorithm for the nonsymmetric eigenvalue problem. *Math. Comp.*, 62:209–226, 1994.

[31] Z. Bai, D. Day, and Q. Ye. ABLE: An adaptive block-lanczos method for non-hermitian eigenvalue problems. *SIAM J. Matrix Anal. Appl.*, 20:1060–1082, 1999.

[32] H. I. van der Veen and K. Vuik. Bi-Lanczos with partial orthogonalization. *Comput. & Structures*, 56:605, 1995.

[33] D.R. Fokkema, G.L.G Sleijpen, and H.A. van der Vorst. Jacobi-davidson style QR and QZ algorithms for the partial reduction of matrix pencils. *SIAM J. Sci. Comput.*, 20:94–125, 1998.

[34] M.E. Hochstenbach and G.L.G. Sleijpen. Two-sided and alternating jacobi–davidson. *Linear Algebra Appl.*, 358:145–172, 2003.

[35] J.H. Wilkinson. *The algebraic eigenvalue problem.* Oxford University Press Inc., New York, 1988.

[36] G. W. Stewart. *Matrix Algorithms volume II: Eigensystems.* Society for Industrial and Applied Mathematics, Philadelphia, 2001.

[37] http://math.nist.gov/MatrixMarket/.

[38] http://www.ma.man.ac.uk/~higham/mctoolbox/.

[39] J. R. Taylor. *Scattering Theory.* Wiley, New York, 1972.

[40] D.G. Truhlar, editor. *Resonances in Electron-Molecule Scattering, Van der Waals Complexes, and Reactive Chemical Dynamics.* Number 263 in Symposium Series. American Chemical Society, Washington, 1984.

[41] J. C. Light and T. Carrington Jr. Discrete variable representations and their utilization. *Adv. Chem. Phys.*, 114:263, 2000.

[42] V. A. Mandelshtam and A. Neumaier. Further generalization and numerical implementation of pseudotime Schrödinger equations for quantum scattering calculations. *J. Theor. Comput. Chem.*, 1:1, 2002.

[43] V. A. Mandelshtam and A. Neumaier. Pseudotime Schrödinger equation with absorbing potential for quantum scattering calculations. *Phys. Rev. Lett.*, 86:5031–5034, 2001.

[44] J. C. Tremblay and T.. Carrington Jr. Computing resonance energies, widths, and wave functions using a Lanczos method in real arithmetic. *J. Chem. Phys.*, 122:244107:1–11, 2005.

CHAPITRE 6

DISCUSSION

Au cours des chapitres précédents, quelques schémas numériques pour l'étude et la caractérisation d'états métastables ont été présentés. Dans ce chapitre, les détails des différentes méthodes seront rappelés en mettant l'accent sur les nouveautés qu'elles contiennent. Les conclusions des quatre articles reproduits seront revues et approfondies dans l'espoir d'offrir au lecteur une meilleure compréhension des innovations proposées par les nouvelles approches numériques.

6.1 Un nouvel intégrateur pour l'équation de Schrödinger dépendante du temps

Dans un premier temps, nous avons considéré la photodissociation du HF gazeux dans un champ laser intense [1]. Afin de caractériser l'évolution du système, on doit résoudre l'équation de Schrödinger dépendante du temps (TDSE) car l'hamiltonien est fonction du temps. Nous avons proposé une approche basée sur la partition de l'hamiltonien de sorte qu'il soit possible de définir un nouvel opérateur pour lequel l'intégration directe de TDSE à l'aide de méthodes établies, tel l'algorithme de Runge-Kutta ici employé, est efficace. Comment peut-on définir un tel opérateur ? On sait qu'une molécule isolée est décrite par un hamiltonien indépendant du temps [2–4]. Ainsi, les solutions admises par l'équation de Schrödinger indépendante du temps (TISE) décriront un ensemble d'états stationnaires qui, comme leur nom l'indique, sont stables indéfiniment. Lorsqu'une dépendance en temps est ajoutée à l'hamiltonien, p. ex. on illumine la molécule avec un laser à impulsions de fréquence modulée, le système est maintenant décrit par TDSE et les solutions stationnaires de TISE ne sont plus valables. Toutefois, on peut alternativement interpréter l'interaction entre le champ laser et la molécule comme une perturba-

tion au système d'états stationnaires supportés par l'hamiltonien indépendant du temps, auquel cas le champ laser aura simplement pour effet de favoriser les transitions entre ces états [5–7]. On peut ainsi tirer profit de l'information disponible par la résolution de TISE en transformant la fonction d'onde dans la représentation d'interaction [2,8–10]. Cette idée est la base de la méthode proposée au chapitre 2. Nous avons d'abord séparé l'hamiltonien en deux parties, $\hat{H} = \hat{H}_0 + \Delta$, où $\hat{H}_0$ est une approximation de $\hat{H}$ qui est *indépendante* du temps. En transformant ensuite la fonction d'onde dans la représentation d'interaction (Eq. (1.38)) et en définissant ainsi un nouvel opérateur (Eq. (1.39)), nous avons démontré que le nombre d'opérations pour l'intégration directe de TDSE dans la représentation d'interaction pouvait être réduit jusqu'à 10 fois par rapport à l'intégration directe de TDSE avec l'opérateur non modifié. Ceci représente un des principaux avantages de la méthode proposée au chapitre 2. Dans le cas de la molécule de HF dans un champ électromagnétique fort, la méthode dans sa forme primitive s'est montrée deux fois plus efficace que la méthode la plus populaire pour résoudre TDSE [11,12].

Il apparaît évident que l'efficacité de la méthode variera en fonction de la qualité de la partition de l'hamiltonien. Les méthodes d'intégration directe appartenant à la famille Runge-Kutta génèrent une approximation du comportement de la fonction à intégrer sur un intervalle de temps δT [13,14]. Pour ce faire, la fonction est évaluée à un ensemble de points dans l'intervalle. Il est bien connu que l'approximation est d'autant meilleure que le domaine spectral de l'opérateur servant à la propagation est petit [13,14]. Dans le cas de notre nouvelle méthode, $\hat{H}_0$ sert de préconditionneur pour l'hamiltonien. Sa tâche est de réduire le domaine spectral de l'opérateur pour la propagation [14–19], dont nous rappelons ici la forme

$$\hat{H}_I = e^{i\hat{H}_0 t/\hbar} \left(\frac{i(\hat{H} - \hat{H}_0)}{\hbar} \right) e^{-i\hat{H}_0 t/\hbar} \quad . \tag{6.1}$$

Les facteurs exponentiels représentent une transformation unitaire de l'opérateur

$\left(\frac{i(\hat{H}-\hat{H}_0)}{\hbar}\right)$ et n'influencent donc pas le domaine spectral de $\hat{H}_I$ [2–4]. Ainsi, on voit facilement que le domaine spectral sera d'autant petit que $\hat{H}_0$ sera une bonne approximation pour $\hat{H}$. Nous avons exploré cette tendance et ainsi déterminé que l'efficacité de la nouvelle méthode de propagation dans la représentation d'interaction est assez sensible au choix du préconditionneur. C'est assurément la plus sérieuse limite de l'algorithme proposé. Quoiqu'il en soit, les exigences en matière de qualité du préconditionneur sont assez faciles à satisfaire [16–19]. De plus, si le préconditionneur choisi est indépendant du temps, le calcul nécessaire à sa construction ne doit être effectué qu'une fois avant le début de la propagation. C'est un avantage important que le présent schéma numérique peut exploiter à bon escient. Ainsi, un bon préconditionneur, qu'il est souvent coûteux de construire, rendra la propagation plus efficace sans augmenter significativement le temps de calcul. Notons qu'il n'existe pas de préconditionneur universel et qu'il incombe donc à l'utilisateur de créer le préconditionneur qui convient à chaque problème [14–19]. Notre étude de la molécule de HF dans un champ laser de fréquence variable permet toutefois de guider le choix de ce préconditionneur et suggère une approximation indépendante du temps pour maximiser l'efficacité de notre nouvelle méthode.

Un raffinement supplémentaire à la représentation d'interaction a aussi été introduit au chapitre 2. L'idée est basée sur le fait que la fonction d'onde n'évolue pas toujours rapidement dans certaines régions où, par exemple, le potentiel est relativement plat [2,8–10]. Il est possible d'exploiter ce comportement pour diminuer la charge de travail de l'intégrateur en variant le pas de temps au fur et à mesure que la propagation avance [13,14]. Il existe plusieurs stratégies de ce type qui sont toutes basées sur des estimations de l'erreur locale produite par l'intégrateur pour un pas de temps donné. Nous avons exploré les avenues les plus courantes dans ce domaine et nous avons observé qu'il était possible d'améliorer significativement les performances de la nouvelle méthode. Dans le meilleur cas, le nombre d'opérations coûteuses, tel qu'évalué par le nombre de produits matrice-vecteur nécessaire à la

propagation jusqu'au temps final, a été réduit d'un facteur 5 supplémentaire. Ainsi, la variante "Dormand-Prince" de l'intégrateur Runge-Kutta pour résoudre TDSE dans la représentation d'interaction s'est avérée la plus efficace. Dans sa version finale, notre nouveau schéma de propagation a supplanté par un facteur d'environ 10 la méthode la plus populaire en dynamique moléculaire, connue sous le nom de "split operator" [11, 12]. Le plus grand avantage de notre nouveau schéma numérique réside dans sa simplicité. En définissant une approximation raisonnable pour l'hamiltonien, il est possible d'utiliser les algorithmes d'intégration disponibles afin d'obtenir une méthode de type "boîte noire" excessivement efficace pour laquelle l'intuition chimique n'est nécessaire que pour définir le préconditionneur et l'opérateur dans la représentation d'interaction. Il existe toutefois un risque inhérent à notre schéma d'intégration directe de l'équation de Schrödinger car l'algorithme de Runge-Kutta n'est pas unitaire. L'utilisation d'une telle méthode peut entraîner une accumulation d'erreurs lorsque le temps d'intégration devient long. En observant la norme du vecteur propagé, il est possible de contrôler la qualité de l'intégration à long terme. Les tests numériques effectués montrent clairement que la méthode est stable pour les temps d'intégration nécessaires pour extraire l'information sur la dynamique des systèmes que nous avons étudiés.

6.2 L'étude de la réaction d'isomérisation

Le but de l'étude reportée au chapitre 3 était de mieux comprendre la réaction d'isomérisation du système acétylène-vinylidène. On souhaitait ainsi démontrer de façon claire l'existence d'états associés au vinylidène. Puisque ce dernier est un diradical, il est raisonnable de douter de sa stabilité et il est aussi discutable de le considérer comme intermédiaire réactionnel. Tout dépend de la durée de vie des états du vinylidène, s'ils existent, telle que caractérisée par le degré de localisation de leur fonction d'onde dans le puits de potentiel du vinylidène. Notons au passage

que le degré de localisation ne permet qu'une description *qualitative* de la durée de vie des différents états. Les approches approximatives jusqu'alors utilisées n'ont pas permis de répondre à ces questions [20, 21]. Dans certains cas, la déformation hors plan a été mise de côté pour réduire le nombre de degrés de liberté du système [22, 23]. D'un autre côté, d'autres auteurs ont suggéré un schéma numérique basé sur l'utilisation d'une méthode directe et d'une base judicieusement sélectionnée pour décrire les six degrés de liberté du système [24, 25]. Les fonctions de base possédant un caractère "acétylénique" trop fort ont été éliminées de la base afin de permettre de garder la matrice de l'hamiltonien suffisamment petite pour pouvoir la diagonaliser directement. En jetant les fonctions localisées dans le puits de l'acétylène, les auteurs de cette étude ont introduit un biais dans leur base et ont ainsi faussé le degré de localisation des états propres du vinylidène [26].

Nous avons proposé une nouvelle méthode itérative contractée qui pallie aux problèmes de ces deux études approximatives des états métastables du vinylidène. D'abord, un ensemble de coordonnées qui permettent l'exploitation de la symétrie complète du systéme est utilisée. Ce point est très important car il permet de calculer des valeurs propres séparément pour chacun des huit blocs de symétrie de l'acétylène-vinylidène [23–25], ce qui diminue la densité des états par un facteur d'environ 8. Il est généralement préférable de choisir des coordonnées qui minimisent le couplage entre elles afin de faciliter leur séparation pour la construction d'une base contractée. Toutefois, puisque la convergence des méthodes itératives dépend inversement de la densité spectrale, il convient de tenir compte de ces deux aspects simultanément pour faire un choix éclairé. Dans le cas présent, de meilleurs systèmes de coordonnées du point de vue du couplage ont aussi été considérés mais il apparaît que la densité soit le facteur dominant. Notre choix s'est donc porté sur un ensemble de coordonnées orthogonales, dites de Jacobi, composées de 2 fragments diatomiques (r_{CC} et r_{HH}) reliés par leur centre de masse par un troisième vecteur (R) ainsi que des angles associés. Afin de générer une base contractée dont

la structure puisse être exploitée par une méthode itérative, nous optons pour une stratégie de contraction dite "simple", fortement inspirée de la littérature [27, 28]. Le schéma de contraction se fait, dans un premier temps, par la résolution d'un modèle à 4D de la réaction d'isomérisation incluant les angles ainsi que la coordonnée R. Les fonctions sont obtenues à l'aide de l'algorithme Lanczos symétrique et peuvent être divisées en deux groupes : celles délocalisées, possédant un caractère "acétylénique", et celle localisées, possédant un caractère "vinylidénique". Nous avons effectué les tests de convergence de la base primitive utilisée pour résoudre le problème à 4D et toutes les fonctions 4D possédant le caractére du vinylidène sont apparues stabilisées à moins de 1cm^{-1}. L'utilisation d'une méthode itérative nous a permis de conserver *toutes* les fonctions 4D situées sous le niveau de vinylidène en plus d'en conserver un très grand nombre au-dessus de ce niveau. Les autres degrés de libertés sont représentés à l'aide de bases DVR, dont le nombre a été optimisé indépendamment afin d'obtenir le même niveau de précision que pour les fonctions à 4D. Nous pouvons affirmer posséder à ce jour la base la plus complète pour la caractérisation des états du vinylidène.

Puisque notre base est de dimension appréciable, un ensemble de raffinements ont dû être développés afin de rendre la méthode viable. Dans un premier temps, l'algorithme de Lanczos symétrique a été remplacé par sa variante plus stable "coupled two-term", reconnue pour ses propriétés de convergence légèrement supérieures [29–31]. Toutefois, la densité d'états dans la région de vinylidène a rendu la convergence de ces états extrêmement longue à cause, entre autres, de la perte d'orthogonalité des vecteurs de Lanczos au cours de la récursion. Il est bien connu que cette perte d'orthogonalité cause l'apparition de copies des valeurs propres déjà convergées au détriment d'autres à énergies plus élevées (dans le cas présent, ce sont celles désirées). Nous avons donc opté pour une réorthogonalisation *locale* de chaque nouveau vecteur de Lanczos par rapport aux quelques précédents [32]. Cette stratégie s'est avérée payante et a réduit le temps de calcul de façon significative. Nous

avons ainsi demontré qu'il est possible de contourner simplement et efficacement le problème de convergence des valeurs propres dans les zones du spectre dont la densité locale est élevée. Tous les raffinements proposés ont été implémentés sur un ordinateur multiprocesseur à mémoire partagée. Pour ce faire, nous avons proposé une nouvelle stratégie de parallélisation de l'algorithme de Lanczos avec une base contractée qui, tenant compte des ressources disponibles, s'est avérée très efficace. Il est important de noter que la méthode est excessivement exigeante du point de vue de la mémoire et du temps de calcul. Notre nouvelle stratégie de parallélisation est robuste et générale.

L'analyse des fonctions d'onde à six dimensions s'est avérée un exercice fort intéressant. Dans un premier temps, nous avons étudié les valeurs attendues des positions r_{HH} et R ainsi que d'un opérateur de localisation X_{viny}, que nous avons spécialement conçu pour évaluer qualitativement le degré de localisation d'une fonction propre dans le puits de vinylidène. Par exemple, les états du vinylidène présentent généralement des valeurs attendues autour de $2a_0$ et $4a_0$ pour R et r_{HH} respectivement contre $0.5a_0$ et $6a_0$ pour les états de l'acétylène. Ceci nous a permis de filtrer grossièrement une majorité de fonctions qui ne possédaient aucun caractère "vinylidénique". Il est à noter que le nouvel opérateur de localisation s'est montré très efficace pour trier les fonctions propres, même dans les cas où les valeurs attendues des coordonnées prenaient des valeurs qui laissaient planer un doute quant au caractère de ces fonctions. Dans un second temps, nous avons observé et caractérisé la structure nodale des fonctions d'onde selon le plan défini par R et l'angle de déformation θ_2, ce qui nous a permis de déterminer les états possédant un degré de localisation assez grand pour être attribués au vinylidène. L'analyse des modes normaux de la molécule de vinylidène permet d'identifier six vibrations attribuables à cette espèce : l'élongation symétrique C-H (ν_1), l'élongation symétrique C-C (ν_2), la déformation symétrique H-C-H (ν_3), la déformation hors plan (ν_4), l'élongation non symétrique C-H (ν_5) et la déformation non symétrique dans

le plan (ν_6). Puisque le calcul reporté traite uniquement des états totalement symétriques du système, seuls les modes ν_1, ν_2 et ν_3 ainsi que les harmoniques paires des autres modes peuvent être observés.

Ainsi, cinq états ont été assignés à l'espèce vinylidène. Il est à noter que l'état fondemental de vinylidène se trouve 9cm^{-1} sous le niveau précédemment reporté [25]. Ce résultat démontre que notre base est variationnellement supérieure à celle utilisée par Zou et Bowman pour leur approche approximative. Afin de confirmer le comportement variationnel de notre base, nous avons étudié l'effet de l'augmentation de sa taille sur les niveaux d'énergie du vinylidène. Nous avons remarqué que les états les plus localisés étaient très stables et nous sommes confiants qu'ils sont convergés à environ 1cm^{-1}. Dans le cas des états moins localisés, nous avons remarqué que les énergies associées variaient encore de quelques centimètres réciproques. Ceci est en contradiction avec les observations des études approximatives précédemment publiées, qui faisaient état de fonctions d'onde très stables et localisées pour l'espèce vinylidène [22, 25]. Nous avons pu démontrer que la troncature de la base par l'élimination de fonctions 4D associées à l'acétylène à basse énergie causait une surestimation de la localisation des fonctions du vinylidène. Ainsi, nous pouvons affirmer que notre approche est la première à avoir considéré globalement le comportement des fonctions d'onde du vinylidène. De plus, nous avons proposé une nouvelle assignation d'une harmonique du mode vibrationnel de déformation hors plan ν_4 en approfondissant l'étude de sa structure nodale selon les différents degrés de liberté de la molécule. De façon générale, il ressort de cette étude que le système possède certains états qui sont bien localisés près de la géométrie de l'espèce vinylidène et qui ont, par le fait même, une durée de vie assez longue. Toutefois, il a été démontré que le degré de localisation est moindre que précédemment reporté.

6.3 Une nouvelle méthode pour l'étude des résonances et sa généralisation

Le potentiel de l'état fondamental de la molécule de HCO admet un ensemble d'états résonants comme solution. Ceux-ci, on le rappelle, sont très similaires aux états liés dans une petite région de l'espace, appelée région d'interaction, mais sont intrinsèquement instables et se comportent comme des ondes planes dans la limite de dissociation [33–35]. Afin d'imposer les bonnes conditions limites aux ondes sortantes, on utilise généralement un potentiel absorbant complexe (CAP) dont les paramètres sont ajustés de sorte que la perturbation causée par ce potentiel soit minimale [36,37]. La partie imaginaire de la valeur propre de l'hamiltonien perturbé décrit la largeur de la résonance, qui est inversement proportionnelle à la durée de vie. Il a été proposé par Mandelshtam et Neumaier de transformer le problème complexe aux valeurs propres en un problème quadratique aux valeurs propres en arithmétique réelle [38, 39]. En remaniant de la façon standard le probléme quadratique sous forme linéaire, on doit ainsi résoudre un problème non symétrique de double dimension. Nous avons proposé au chapitre 4 l'utilisation de l'algorithme de Lanczos pour le calcul des valeurs et vecteurs propres de cette matrice non symétrique. Nous avons remarqué que l'algorithme dans sa forme primitive est instable et que la rebiorthogonalisation des vecteurs de Lanczos ne semblait pas améliorer les résultats de façon significative. Nous avons donc proposé d'utiliser la variante "coupled two-term Lanczos" [29–31], qui a su améliorer la stabilité de l'algorithme sans toutefois nous permettre d'obtenir la précision désirée. Il faut comprendre que la précision nécessaire pour le calcul des durées de vie des résonances doit être extrêmement grande. À titre d'exemple, une résonance très étroite existe à environ 1098,79cm^{-1}. Sa durée de vie est très longue et sa partie imaginaire est donc très petite, en l'occurrence $< 10^{-7}$cm^{-1}. Il faut donc s'assurer que la méthode donne des résultats précis à 10 chiffres significatifs afin d'extraire cette information, ce qui

n'est pas le cas de l'algorithme de Lanczos non symétrique, même dans sa variante la plus stable.

Ainsi, nous avons développé un schéma exploitant les informations approximatives obtenues à l'aide de l'algorithme de Lanczos pour extraire des informations précises de la matrice représentant le système perturbé. Dans un premier temps, nous avons démontré qu'il est possible de réécrire l'algorithme de Lanczos afin d'exploiter la symétrie inhérente au système. Sous cette forme, il n'est nécessaire que d'effectuer un seul produit matrice-vecteur par itération Lanczos, ce qui représente une amélioration d'un facteur de 2 par rapport à l'algorithme standard. On a ainsi montré comment il est possible d'obtenir des valeurs propres et vecteurs propres (gauches et droits) approximatifs à partir d'un seul ensemble de produits matrice-vecteur définissant deux espaces de Krylov biorthogonaux. En utilisant le concept de profondeur d'itération optimale [40], nous avons réussi à réduire l'effort associé au calcul des vecteurs propres approximatifs en limitant la taille de l'espace de Krylov utilisé pour définir lesdits vecteurs. Notre contribution la plus importante a été d'utiliser ces vecteurs approximatifs à des fins de projection en séparant les valeurs propres par groupe pour limiter les besoins de stockage. La plus grande victoire de cette approche, c'est qu'elle permet de stabiliser l'algorithme de Lanczos et d'en extraire des valeurs popres exactes.

Il y a cependant plus dans le nouveau schéma numérique encore que la stabilité et l'exactitude de ses résultats. On sait qu'il faut, pour le calcul des résonances à l'aide d'un hamiltonien perturbé par un CAP, répéter le calcul à plusieurs reprises (typiquement 10 à 20 fois) pour minimiser la perturbation [36, 37]. Nous avons démontré à l'aide d'exemples numériques qu'il n'était pas nécessaire de procéder ainsi. En choisissant les paramètres du potentiel absorbant de façon appropriée, on peut générer à l'aide de l'algorithme un ensemble de fonctions propres approximatives qui possèdent des conditions limites qui se rapprochent grossièrement de celles qui minimisent la perturbation [41–46]. Notons que ces conditions sont différentes

pour chacune des valeurs propres et le choix des paramètres du potentiel absorbant est critique. Heureusement, il existe de très bonnes approximations disponibles dans la littérature, notamment celle développée par Poirier et Carrington [47, 48]. Ainsi, nous avons démontré que les fonctions approximatives pour une CAP-guide pouvaient servir de base pour la projection de l'hamiltonien *non perturbé* afin d'obtenir les énergies et les largeurs des résonances directement sans répéter le calcul. Puisque les fonctions de base sont générées à l'aide d'un opérateur perturbé spécialement conçu pour imposer de bonnes conditions limites aux états résonants, ces fonctions imposent le bon comportement aux fonctions propres de l'opérateur non perturbé. En quelque sorte, nous proposons d'incorporer les conditions limites directement dans les fonctions de base plutôt que de modifier l'opérateur. La stratégie est payante puisqu'elle permet de réduire significativement le nombre d'opérations nécessaires à la caractérisation des résonances. Pour une discussion plus approfondie des conditions nécessaires à la formation d'une bonne base, nous référons le lecteur à l'annexe II. Le principal désavantage de la méthode est que le calcul des vecteurs propres est obligatoire et ceci représente du travail excédentaire si l'on ne veut extraire que les valeurs propres. Toutefois, ce travail n'est pas vain car les fonctions d'onde contiennent beaucoup d'informations très utiles, par exemple pour l'assignation des modes vibrationnels associés à chaque valeur propre.

Ayant remarqué que l'algorithme de Lanczos pour les matrices non symétriques est instable et très souvent inexact [49–52], nous nous sommes intéressés à la généralisation de l'algorithme proposé au chapitre 4 pour la caractérisation des états résonants. Ainsi, nous avons proposé au chapitre 5 une méthode de type "boîte noire" qui contenait les éléments essentiels de la méthode en éliminant les raffinements spécifiques au problème des résonances. Il existe certes des méthodes itératives très efficaces basées sur la projection de la matrice étudiée dans un espace de Krylov *orthogonal* mais les méthodes de projection *biorthogonale* offrent l'avantage de ne nécessiter que très peu de stockage en mémoire [51,53,54]. De plus, il est connu que

la convergence des méthodes de projection biorthogonale est supérieure à celles de projection orthogonale [50, 54]. Nous avons choisi d'éliminer le recours à la variante "coupled two-term Lanczos" qui, quoique favorisant la convergence, n'est pas nécessaire pour illustrer l'essence de notre nouvelle approche. Ainsi, nous sommes arrivés à un schéma raffiné faisant appel, dans un premier temps, à l'algorithme de Lanczos non symétrique et ses propriétés de convergence favorables pour extraire d'une matrice générale un ensemble de valeurs propres approximatives. Il est bien connu que l'algorithme utilisé sans réorthogonalisation génère plusieurs copies inexactes des vraies valeurs propres en plus d'autres valeurs propres non physiques [55, 56]. Nous avons donc défini un critère numérique pour regrouper les valeurs propres copiées en agrégats et proposé l'utilisation d'un filtre, développé par Cullum et Willoughby pour les problèmes symétriques [40], afin de se débarrasser des valeurs propres non physiques. Les valeurs satisfaisant ces deux critères ont été utilisées pour le calcul de vecteurs propres gauches et droits approximatifs. Nous avons ensuite montré qu'il était possible d'utiliser efficacement ces vecteurs pour projeter la matrice originale et ensuite en extraire les valeurs propres numériquement très précises. Cette méthode peut être alternativement vue comme une forme dérivé de la méthode de Ritz pour extraire les valeurs et vecteurs propres en utilisant une base particulière, générée à l'aide de l'algorithme de Lanczos [15].

Plusieurs tests numériques provenant de différents domaines ont été étudiés pour démontrer la stabilité et l'exactitude du schéma numérique proposé. Ainsi, nous avons éprouvé la nouvelle méthode, baptisée RULE ("Refined Unsymmetric Lanczos Eigensolver") à l'aide d'exemples allant de la modélisation de la stabilité d'une aile d'avion en vol à la résolution d'une équation aux dérivées partielles, en passant par une reformulation du problème des résonances discuté plus haut [57–59]. Ainsi, nous avons démontré qu'il était possible, grâce à RULE, d'extraire des valeurs propres exactes pour des matrices de petite, moyenne et grande taille, tant pour les valeurs propres extrêmes que pour les valeurs propres situées un peu à

l'intérieur du spectre pour lesquelles la précision est généralement moins bonne. Nous avons pu constater que le coût de la présente méthode se compare avantageusement à l'implémentation la plus populaire de l'algorithme d'Arnoldi, contenue dans ARPACK [60]. Un des principaux avantages de RULE sur ARPACK vient de l'exploitation de l'information contenue dans un très grand espace de Krylov biorthogonal. ARPACK utilise une méthode à faible stockage qui tente de raffiner un très petit espace de Krylov orthogonal selon les propriétés des valeurs propres désirées (plus grande norme, plus petite partie réelle, etc.). De plus, contrairement à ARPACK, RULE ne nécessite pas de réorthogonalisation des vecteurs au fil des itérations, ce qui représente une opération excessivement coûteuse quant au nombre de flops et au stockage en mémoire [15,53]. Le schéma que nous avons proposé présente toutefois certaines limites qu'il convient ici de rappeler. D'abord, la qualité des résultats obtenus est grandement influencée par la présence de vecteurs de base associés à des valeurs propres non physiques. Le filtre utilisé dépend d'un paramètre qui doit être choisi par l'utilisateur, la tolérance relative. Une grande attention doit donc être portée pour sa sélection, quoique presque tous les exemples qui ont été reportés au chapitre 5 se soient montrés particulièrement robustes à cet égard. Finalement, malgré qu'il soit possible d'extraire efficacement des valeurs propres non extrêmes à l'aide de RULE, ses propriétés de convergence ne permettent pas de prétendre que les valeurs situées dans des régions très denses du spectre pourront être facilement obtenues. Ainsi, nous croyons que le recours à une transformation spectrale serait nécessaire dans ce cas [51,53]. Heureusement, cette limite est commune à toutes les méthodes itératives.

Bibliographie

[1] S. Chelkowski, A. D. Bandrauk, and P. B. Corkum. Efficient molecular dissociation by a chirped ultrashort infrared laser pulse. *Phys. Rev. Lett.*, 65 :2355, 1990.

[2] Claude Cohen-Tannoudji, Bernard Diu, and Franck Laloë. *Mécanique Quantique.* Hermann, éditeur des Sciences et des Arts, 1973.

[3] P. W. Atkins and R. S. Friedman. *Molecular Quantum Mechanics.* Oxford University Press Inc., New York, third edition, 1997.

[4] D. A. McQuarrie. *Quantum Chemistry.* University Science Books, Sausalito, California, 1983.

[5] J. M. Hollas. *Modern Spectroscopy.* John Wiley & Sons, Chichester, West Sussex, England, third edition, 1996.

[6] W. S. Struve. *Fundamentals of molecular spectroscopy.* John Wiley & Sons, New York, 1989.

[7] J. D. Graybeal. *Molecular Spectroscopy.* Mcgraw-Hill, 1993.

[8] J. Z. H. Zhang. New method in time-dependent quantum scattering theory : Integrating the wave function in the interaction picture. *J. Chem. Phys.*, 92 :324, 1990.

[9] J. Z. H. Zhang. Multichannel quantum wave packet propagation in the interaction picture : application to gas-surface scattering. *Comp. Phys. Comm.*, 63 :28, 1991.

[10] D. J. Tannor, A. Besprozvannaya, and C. J. Williams. Nested interaction representations in time dependent quantum mechanics. *J. Chem. Phys.*, 96 :2998, 1992.

[11] M.D. Feit and J.A. Fleck. Wave packet dynamics and chaos in the hénon-heiles system. *J. Chem. Phys.*, 80 :2578, 1984.

[12] C. Leforestier, R. Bisseling, C. Cerjan, M.D. Feit, R. Friesner, A. Guldberg, A. Hammerich, W. Jolicard, G. Karrlein, H.-D. Meyer, N. Lipkin, O. Roncero, and R. Kosloff. A comparison of different propagation schemes for the time dependent Schrödinger equation. *J. Comp. Phys.*, 94 :59, 1991.

[13] W. H. Press, S. A. S.A. Teukolsky, W. T. Vetterling, and B. P. Flannery. *Numerical Recipes in FORTRAN 77 The Art of Scientific Programming.* Cambridge University Press, 1986.

[14] P. Castillo and Y. Saad. Preconditioning the matrix exponential operator with applications. *J. of Sci. Computing*, 13 :275, 1998.

[15] G. H. Golub and C. F. Van Loan. *Matrix Computations.* John Hopkins University Press, Baltimore, 1989.

[16] R. E. Wyatt. Matrix spectroscopy : Computation of interior eigenstates of large matrices using layered iteration. *Phys. Rev. E*, 51 :3643, 1995.

[17] B. Poirier and W. H. Miller. Optimized preconditioners for green function evaluation in quantum reactive scattering calculations. *Chem. Phys. Lett.*, 265 :77, 1997.

[18] B. Poirier. Efficient preconditioning scheme for block partitioned matrices with structured sparsity. *Numer. Linear Algebra Appl.*, 7 :715, 2000.

[19] P. Arbenz, U. L. Hetmaniuk, R. B. Lehoucq, and R. S. S. Tuminaro. A comparison of eigensolvers for large-scale 3d modal analysis using AMG-preconditioned iterative methods. *Internat. J. Numer. Methods Engrg.*, 64 :204–236, 2005.

[20] T. Carrington Jr., L. M. Hubbard, H. F. Schaefer III, and W. H. Miller. Vinylidene : Potential energy surface and unimolecular reaction dynamics. *Chem. Phys.*, 80 :4347, 1984.

[21] T. C. Germann and W. H. Miller. Quantum mechanical calculation of resonance tunneling in acetylene isomerization via the vinylidene intermediate. *J. Chem. Phys.*, 109 :94, 1998.

[22] R. Schork and H. Köppel. Barrier recrossing in the vinylidene-acetylene isomerization reaction : A five-dimensional ab initio quantum dynamical investigation. *J. Chem. Phys.*, 115 :7907, 2001.

[23] S. Zou and J. M. Bowman. Reduced dimensionality quantum calculations of acetylene $< -- >$ vinylidene isomerization. *J. Chem. Phys.*, 116 :6667, 2002.

[24] S. Zou and J. M. Bowman. Full dimensionality quantum calculations of acetylene/vinylidene isomerization. *J. Chem. Phys.*, 117 :5507, 2002.

[25] S. Zou, J. M. Bowman, and A. Brown. Full-dimensionality quantum calculations of acetylene–vinylidene isomerization. *J. Chem. Phys.*, 118 :10012, 2003.

[26] I. N. Kozin, M. M. Law, J. Tennyson, and J. M. Hutson. Calculating energy levels of isomerizing tetraatomic molecules : II. the vibrational states of acetylene and vinylidene. *J. Chem. Phys.*, 122 :064309, 2005.

[27] X. Wang and T. Carrington Jr. New ideas for using contracted basis functions with a Lanczos eigensolver for computing vibrational spectra of molecules with four or more atoms. *J. Chem. Phys.*, 117 :6923, 2002.

[28] H.-G. Yu. Full-dimensional quantum calculations of vibrational spectra of six-atom molecules. I. theory and numerical results. *J. Chem. Phys.*, 120 :2270, 2004.

[29] R. W. Freund and N. M. Nachtigal. *Linear Algebra for Large Scale and Real-Time Applications.* Kluwer Academic Publishers, 1993.

[30] R. W. Freund and N. M. Nachtigal. Implementation details of the coupled QMR algorithm. *SIAM J. Sci. Stat. Comp.*, 15 :313, 1994.

[31] H. O. Karlsson and S. Holmgren. Cross correlation functions $c_{nm}(e)$ via lanczos algorithms without diagonalization. *J. Chem. Phys.*, 117 :9116, 2002.

[32] Beresford N. Parlett. *The Symmetric Eigenvalue Problem.* Society for Industrial and Applied Mathematics, Philadelphia, 1998.

[33] A. F. J. Siegert. On the derivation of the dispersion formula for nuclear reactions. *Phys. Rev.*, 56 :750, 939.

[34] D.G. Truhlar, editor. *Resonances in Electron-Molecule Scattering, Van der Waals Complexes, and Reactive Chemical Dynamics.* Number 263 in Symposium Series. American Chemical Society, Washington, 1984.

[35] R. Schinke. *Photodissociation Dynamics.* Cambridge University Press, Cambridge, 1993.

[36] G. Jolicard and E. Austin. Optical potential stabilisation method for predicting resonance levels. *Chem. Phys. Lett.*, 121 :106, 1985.

[37] G. Jolicard and E. Austin. Optical potential method of calculating resonance energies and widths. *Chemical physics*, 103 :295, 1986.

[38] V. A. Mandelshtam and A. Neumaier. Pseudotime Schrödinger equation with absorbing potential for quantum scattering calculations. *Phys. Rev. Lett.*, 86 :5031–5034, 2001.

[39] V. A. Mandelshtam and A. Neumaier. Further generalization and numerical implementation of pseudotime Schrödinger equations for quantum scattering calculations. *J. Theor. Comput. Chem.*, 1 :1, 2002.

[40] J. K. Cullum and R. A. Willoughby. *Lanczos algorithms for large symmetric eigenvalue computations.* Birkhäuser, Boston, 1985.

[41] U.V. Riss and H.-D. Meyer. Investigation on the reflection and transmission properties of complex absorbing potentials. *J. Chem. Phys.*, 105 :1409, 1996.

[42] T. Seideman and W.H. Miller. Calculation of the cumulative reaction probability via a discrete variable representation with absorbing boundary conditions. *J. Chem. Phys.*, 96 :4412, 1992.

[43] A. Vibok and G. G. Balint-Kurti. Parametrization of complex absorbing potentials for time-dependent quantum dynamics. *J. Phys. Chem.*, 96 :8712, 1992.

[44] D. Neuhauser and M. Baer. The time-dependent Schrödinger equation : Application of absorbing boundary conditions. *J. Chem. Phys.*, 90 :4351, 1989.

[45] M. S. Child. Analysis of a complex absorbing barrier. *Mol. Phys.*, 72 :89, 1991.

[46] D. E. Manolopoulos. Derivation and reflection properties of a transmission-free absorbing potential. *J. Chem. Phys.*, 117 :9552, 2002.

[47] B. Poirier and T. Carrington Jr. Semiclassically optimized complex absorbing potentials of polynomial form. I. pure imaginary case. *J. Chem. Phys.*, 118 :17, 2003.

[48] B. Poirier and T. Carrington Jr. Semiclassically optimized complex absorbing potentials of polynomial form. II. complex case. *J. Chem. Phys.*, 119 :77, 2003.

[49] Z. Bai. Error analysis of the lanczos algorithm for the nonsymmetric eigenvalue problem. *Math. Comp.*, 62 :209–226, 1994.

[50] Z. Bai, D. Day, and Q. Ye. ABLE : An adaptive block-lanczos method for non-hermitian eigenvalue problems. *SIAM J. Matrix Anal. Appl.*, 20 :1060–1082, 1999.

[51] Z. Bai, J. Demmel, J. Dongarra, A. Ruhe, and H. van der Vorst, editors. *Templates for the Solution of Algebraic Eigenvalue Problems : A Practical Guide.* Society for Industrial and Applied Mathematics, Philadelphia, 2000.

[52] H. I. van der Veen and K. Vuik. Bi-Lanczos with partial orthogonalization. *Comput. & Structures*, 56 :605, 1995.

[53] L. N. Trefethen and D. Bau III. *Numerical Linear Algebra.* Society for Industrial and Applied Mathematics, Philadelphia, 1997.

[54] D. Day. An efficient implementation of the nonsymmetric Lanczos algorithm. *SIAM J. Matrix Anal. Appl.*, 18 :566–589, 1997.

[55] J. K. Cullum and R. A. Willoughby. Computing eigenvalues of very large symmetric matrices-an implementation of a lanczos algorithm with no reorthogonalization. *J. Comput. Phys.*, 44 :329–358, 1981.

[56] Jane K. Cullum and Ralph A. Willoughby. *Large Scale Eigenvalue Problems*, chapter A practical procedure for computing eigenvalues of large sparse nonsymmetric matrices. North-Holland, Amsterdam, 1986.

[57] H.-M. Keller, A. J Floethmann, H. and. Dobbyn, R. Schinke, and H. J. Werner. The unimolecular dissociation of HCO. II. comparison of calculated resonance energies and widths with high-resolution spectroscopic data. *J. Chem. Phys.*, 105 :4983, 1996.

[58] http ://math.nist.gov/MatrixMarket/.

[59] http ://www.ma.man.ac.uk/~higham/mctoolbox/.

[60] http ://www.caam.rice.edu/software/ARPACK/.

CHAPITRE 7

CONCLUSION

Le but de la présente thèse visait le développement de nouvelles méthodes numériques pour la résolution de problèmes de dynamique moléculaire. Plus spécifiquement, nous nous sommes concentrés sur l'étude théorique de propriétés spectroscopiques d'états métastables afin de pouvoir les interpréter en termes moléculaires et de les caractériser tant de façon quantitative que qualitative. Rappelons qu'un état métastable est défini comme un état qui possède une durée de vie finie. Ainsi, nous avons développé un nouvel intégrateur pour étudier la photodissociation d'une molécule en phase gazeuse soumise à une forte radiation électromagnétique. De plus, nous avons proposé l'utilisation d'une méthode itérative contractée pour l'étude de la réaction d'isomérisation du système acétylène-vinylidène. Finalement, nous avons établi une nouvelle approche pour le calcul des énergies et durées de vie des états résonants de petites molécules. Toutes ces études sont regroupées sous un même thème unificateur : le développement de nouvelles méthodes pour le calcul et la caractérisation des états métastables dans l'espoir de mieux comprendre les mécanismes régissant les réactions chimiques à l'état moléculaire. La dernière méthode proposée (RULE) se situe un peu en marge des autres en ce qui concerne le domaine d'application mais s'inscrit néanmoins dans la même lignée, soit le développement d'outils numériques plus efficaces.

Dans leur ensemble, les quatre nouveaux schémas numériques se sont montrés à la hauteur des attentes que nous avions du point de vue de l'efficacité. En l'occurrence, l'idée promue au chapitre 2 est excessivement efficace tout en gardant la simplicité essentielle pour une application à grande échelle. L'avantage que présente la structure "boîte noire" de la nouvelle approche est très important pour motiver l'application d'une méthode à une variété de problèmes. La supériorité de

l'intégration directe dans la représentation d'interaction, des points de vue de la stabilité et de l'efficacité, n'est plus à démontrer et nous avons d'ores et déjà présenté les conditions nécessaires à son bon fonctionnement. À l'opposé, l'efficacité de la stratégie employée pour la caractérisation du système acétylène-vinylidène ne représentait pas le point clé de la méthode. Néanmoins, nous avons démontré que l'utilisation d'une base contractée en conjonction avec une méthode itérative pouvait être suffisamment efficace pour extraire des niveaux vibrationnels situés à énergie extrêmement élevée. La structure complexe de la base contractée ainsi que sa grande taille nous ont forcés à développer une nouvelle stratégie de parallélisation dont les performances en termes de temps CPU se sont montrées excessivement satisfaisantes. Pour ce qui est de la caractérisation des résonances de HCO à l'aide d'un potentiel absorbant, nous avons amélioré l'efficacité de la méthode standard en éliminant le recours à une minimisation paramétrique de la perturbation qui imposait qu'on répète plusieurs fois le calcul. Notre schéma numérique est basé sur la méthode de Lanczos et tire avantage d'une stratégie récemment développée pour éviter l'utilisation de l'arithmétique complexe, ce qui réduit encore la charge de travail. Par la généralisation de cette approche, nous obtenons une méthode alternative pour l'extraction des valeurs propres et vecteurs propres de toute matrice non symétrique réelle. Cette nouvelle méthode a démontré sa grande efficacité par la comparaison avec la méthode de référence et nous avons observé que ses besoins en mémoire et en temps CPU sont très faibles à cause de l'absence de toute forme de réorthogonalisation. Somme toute, les nombreux tests numériques des méthodes introduites dans les chapitres précédents montrent clairement que les nouvelles approches proposées dans la présente thèse sont très efficaces.

Les travaux de la présente thèse ont aussi proposé un certain nombre de solutions aux problémes numériques reliés aux erreurs d'arrondissement. Dans le cas des problèmes symétriques comme celui associé au vinylidène, il est bien connu que ces erreurs d'arrondissement sont responsables de la perte d'orthogonalité des vecteurs

de Lanczos. Ceci cause un ralentissement de la convergence des états situées à haute énergie sans toutefois rendre la méthode instable. Dans ce cas, nous avons opté pour une simple stratégie de réorthogonalisation locale qui s'est montrée trés robuste et facile à implémenter. Pour les problèmes non symétriques, il se trouve que les erreurs d'arrondissement entraînent une instabilité qu'il nous a été impossible de contourner à l'aide de la réorthogonalisation locale. Une stratégie différente a donc été proposée, soit l'utilisation de l'information approximative, c'est-à-dire polluée numériquement, à des fins de raffinement pour extraire des valeurs et vecteurs propres numériquement exacts. Nous avons éprouvé cette idée à l'aide de nombreux tests provenant de différents domaines et présentant des défis intéressants. De façon globale, les stratégies que nous avons employées pour la résolution de nos problèmes ont permis de bien contenir les effets néfastes des erreurs d'arrondissement et de maintenir la stabilité de l'algorithme.

7.1 Perspectives futures

Les applications potentielles des méthodes précédemment discutées sont multiples. Dans un premier temps, la stratégie de parallélisation couplée à la méthode itérative contractée et ses raffinements s'est avérée très robuste, ce qui indique que l'approche pourrait être utilisée pour étudier d'autres systèmes de taille similaire ou légèrement supérieure. Notamment, nos idées pourraient être applicables à l'étude de l'isomérisation entre les formes *cis* et *trans* de la molécule de HONO. Les niveaux vibrationnels associés aux deux espèces calculés à l'aide d'une méthode iteŕative approximative ont été reportés récemment [1] et reproduisent les données expérimentales avec une précision d'environ 10cm^{-1}. L'utilisation de notre méthode exacte permettrait de déterminer si l'écart entre les valeurs théoriques et expérimentales est dû à l'utilisation d'une méthode approximative ou représente une limite du potentiel *ab initio* proposé par les auteurs. De plus, des calculs préli-

minaires étudiant les vibrations associées aux degrés de liberté de déformation de la molécule de CH_3F ont été récemment publiés [2]. Il serait intéressant de savoir s'il est possible, à l'aide de notre nouvelle méthode contractée, d'utiliser cette information pour calculer les niveaux vibrationnels de la molécule en 9 dimensions. Ceci permettrait une analyse des fréquences vibrationnelles observées expérimentalement.

Dans un second temps, la méthode de propagation proposée au chapitre 2 pourrait être utilisée pour améliorer les performances de la méthode connue sous le nom de "Multi Configuration Time-Depend Hartree" (MCTDH). C'est une méthode approximative très puissante qui permet de résoudre l'équation de Schrödinger dépendante du temps pour des systèmes de taille moyenne. Les analyses de certaines propriétés du pyrazine [3], de l'allène [4], du butatriène [5] , du benzène [6] et du furane [7] ont été reportées. L'efficacité de MCTDH dépend de plusieurs facteurs, notamment de la résolution d'un système d'équations du mouvement couplées dont une partie est linéaire et une autre partie non linéaire. La solution des équations linéaires est faite à l'aide d'une méthode conventionnelle en dynamique moléculaire (SIL) et l'intégration des équations non linéaires se fait normalement à l'aide d'un intégrateur de Runge-Kutta non préconditionné [8]. Il est anticipé que l'utilisation de notre schéma d'intégration dans la représentation d'interaction pourrait entraîner des gains de performance significatifs et donc permettre l'étude de systèmes de taille encore plus importante. Notons toutefois que la forme des équations couplées dans la représentation d'interaction ainsi que la composition du préconditionneur nécessaire à cette fin ne sont pas encore connues.

Finalement, la méthode proposée pour l'étude des résonances de HCO pourrait être appliquée à de nombreux autres systèmes du même type. En l'occurrence, il existe plusieurs molécules de taille similaire, dont le potentiel de l'état fondamental admet des résonances bien isolées comme solution, qui ont été étudiées expérimentalement (DCO [9], HOCl [10], D_2CO [11], HFCO [12], CH_3O [13], HN_3 [14]

et HONO [15]). La caractérisation théorique des états résonants de ces molécules pourrait ainsi être faite efficacement grâce à notre nouvelle approche. De plus, la généralisation de la méthode présentée au chapitre 5, RULE, pourrait être utile à la résolution d'un certain nombre de problèmes de chimie théorique ainsi que de physique numérique. Notamment, le calcul de la probabilité réactionnelle cumulative (CRP), directement lié à la constante de vitesse réactionnelle, peut être reformulé en termes de fonctions de Green et d'opérateurs d'absorption [16,17]. Selon cette reformulation, on doit résoudre un problème non symétrique aux valeurs propres. La méthode RULE pourrait être utilisée à cet effet, quoique la viabilité de l'approche reste à démontrer. Il faudrait notamment développer une stratégie pour évaluer efficacement l'effet d'une fonction de Green sur un vecteur. Il est bien connu que la singularité des fonctions de Green en rend l'inversion et l'application sur un vecteur ardues.

Bibliographie

[1] I. N. Kozin, M. M. Law, J. Tennyson, and J. M. Hutson. Calculating energy levels of isomerizing tetraatomic molecules : II. the vibrational states of acetylene and vinylidene. *J. Chem. Phys.*, 122 :064309, 2005.

[2] S. A. Manson, M. M. Law, I. A. Atkinson, and G. A. Thomson. The molecular potential energy surface and vibrational energy levels of methyl fluoride. *Phys. Chem. Chem. Phys.*, 8 :2855, 2006.

[3] G. Worth, H.-D. Meyer, and L.S. Cederbaum. The effect of a model environment on the s_2 absorption spectrum of pyrazine : A wavepacket study treating all 24 vibrational modes. *J.Chem.Phys.*, 105 :4412, 1996.

[4] S. Mahapatra, G. Worth, H.-D. Meyer, L.S. Cederbaum, and H. Köppel. The A^2E B^2B_2 photoelectron bands of allene beyond the linear coupling scheme : An ab initio dynamical study including all fifteen vibrational modes. *J.Phys.Chem A.*, 105 :5567, 2001.

[5] C. Cattarius, G. A. Worth, H.-D. Meyer, and L. S. Cederbaum. All mode dynamics at the conical intersection of an octa-atomic molecule : Multiconfiguration time-dependent hartree (MCTDH) investigation on the butatriene cation. *J. Chem. Phys.*, 115 :2088, 2001.

[6] H. Köppel, M. Döscher, I. Baldea, H.-D. Meyer, and P.G. Szalay. Multistate vibronic interactions in the benzene radical cation. II : Quantum dynamical simulations. *J. Chem. Phys.*, 117 :2657, 2002.

[7] E.V. Gromov, A. B. Trofimov, N. M. Vitkovskaya, H. Köppel, J. Schirmer, H.-D. Meyer, and L. S. Cederbaum. Theoretical study of excitations in furan : Spectra and molecular dynamics. *J. Chem. Phys.*, 121 :4525, 2004.

[8] H.-D. Meyer and G. Worth. Quantum molecular dynamics : Propagating wavepackets and density operators using the multi-configuration time-dependent hartree (MCTDH) method. *Theor. Chem. Acc.*, 109 :251, 2003.

[9] C. Stöck, X. Li, H.-M. Keller, R. Schinke, and F. Temps. Unimolecular dissociation dynamics of highly vibrationally excited DCO ($\tilde{X}^2$A). I. investigation of dissociative resonance states by stimulated emission pumping spectroscopy. *J.Chem.Phys.*, 106 :5333, 1997.

[10] G. Dutton, R. J. Barnes, and A. Sinha. State selected unimolecular dissociation of HOCL near threshold : The $6\nu_{OH}$ vibrational state. *J. Chem. Phys.*, 111 :4976, 1999.

[11] W. F. Polik, D. R. Guyer, and C. B. Moore. Stark level-crossing spectroscopy of S_0 formaldehyde eigenstates at the dissociation threshold. *J. Chem. Phys.*, 92 :3453, 1990.

[12] Y. S. Choi and C.B. Moore. State-specific unimolecular reaction dynamics of HFCO. I. dissociation rates. *J. Chem. Phys.*, 97 :1010, 1992.

[13] A. Geers, J. Kappert, and F. Temps. Rotation-vibration state resolved unimolecular dynamics of highly vibrationally excited CH_3O ($\tilde{X}^2$E). I. observed stimulated emission pumping spectra. *J. Chem. Phys.*, 101 :3618, 1994.

[14] B.R. B. R. Foy, M. P. Casassa, J. C. Stephenson, and D. S. King. Dissociation lifetimes and level mixing in overtone-excited $HN_3(\tilde{X}^1A)$. *J. Chem. Phys.*, 90 :7037, 1989.

[15] F. Reiche, B. Abel, R.D. Beck, and T.R. Rizzo. Double-resonance overtone photofragment spectroscopy of trans-HONO. I. spectroscopy and intramolecular dynamics. *J. Chem. Phys.*, 112 :8885, 2000.

[16] T. Seideman and W. H. Miller. Calculation of the cumulative reaction probability via a discrete variable representation with absorbing boundary conditions. *J. Chem. Phys.*, 96 :4412–4422, 1992.

[17] U. Manthe and W. H. Miller. The cumulative reaction probability as an eigenvalue problem. *J. Chem. Phys.*, 99 :3411, 1993.

Annexe I

Coordonnées de Jacobi pour représenter le système acétylène-vinylidène

FIG. I.1 – Coordonnées de Jacobi choisies pour représenter les six degrés de libertés de la molécule de C_2H_2

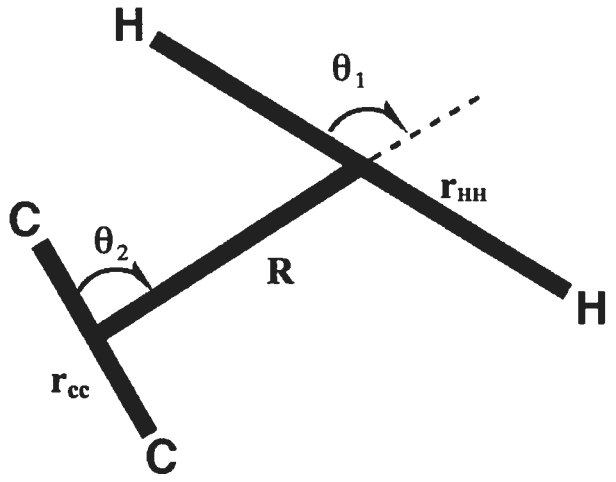

Annexe II

Analyse du comportement des fonctions de bases amorties utilisées pour le calcul des états résonants

Dans cette annexe, nous proposons une analyse du comportement des fonctions de bases utilisées au chapitre 4 pour le calcul des états résonants. Les conditions *nécessaires mais non suffisantes* que celles-ci doivent remplir sont ici décrites en termes de perturbation à la fonction d'onde exacte du système. Ainsi, notre but ultime est de résoudre l'équation

$$\hat{H}(r)\psi(r) = E\psi(r) \quad , \tag{II.1}$$

où r est la coordonnée de dissociation et E est l'énergie associée à une solution particulière du problème, $\psi(r)$. Cette solution doit respecter la condition limite $\lim_{r\to\infty} \psi(r) = e^{ikr}$ dans la limite de dissociation de la molécule considérée. L'énergie associée devient donc complexe et sa fonction d'onde diverge asymptotiquement. Considérons maintenant le développement de cette fonction d'onde divergente dans une base de fonctions complexes de carré intégrable, c'est-à-dire des fonctions convergentes dans la limite de dissociation. Ces fonctions de bases seront définies par l'équation

$$\left(\hat{H}(r) - i\eta\hat{W}(r)\right)\phi_k(r) = \epsilon_k\phi_k(r) \quad , \tag{II.2}$$

où $\hat{W}(r)$ est un potentiel absorbant complexe (CAP) et η est le paramètre de force du CAP. Rappelons que le CAP doit être 0 dans la région d'interaction, c'est-à-dire qui décrit les états liés du système, et doit ensuite augmenter doucement afin d'absorber la queue de la fonction d'onde sans causer de réflexion. Puisque

la fonction $\psi(r)$ est divergente, son développement dans une base de fonctions convergente sera entaché d'erreur. On peut représenter de façon exacte $\psi(r)$ sous cette forme

$$\psi(r) = \psi_{fb}(r) + O_E(r) \quad , \tag{II.3}$$

où $\psi_{fb}(r) = \sum_{k=1}^{N} c_k \phi_k(r)$ est l'expansion de la fonction d'onde dans la base et O_E est l'erreur associée à l'utilisation d'une base de fonctions convergentes. En substituant dans Eq. (II.1), on obtient ainsi

$$\hat{H}(r)\psi_{fb}(r) + \hat{H}(r)O_E(r) = E\psi_{fb}(r) + EO_E(r) \quad . \tag{II.4}$$

En multipliant par $\psi_{fb}(r)$ à gauche et en intégrant sur tout l'espace, on a

$$\langle \psi^*_{fb}|\hat{H}|\psi_{fb}\rangle + \langle \psi^*_{fb}|\hat{H}|O_E\rangle = E\langle \psi^*_{fb}|\psi_{fb}\rangle + E\langle \psi^*_{fb}|O_E\rangle \quad . \tag{II.5}$$

En réarrangeant les termes, on obtient une expression exacte pour l'énergie

$$E = \frac{\langle \psi^*_{fb}|\hat{H}|\psi_{fb}\rangle}{\langle \psi^*_{fb}|\psi_{fb}\rangle} \quad , \tag{II.6}$$

advenant que

$$\begin{aligned} 0 &= \langle \psi^*_{fb}|E - \hat{H}|O_E\rangle \\ &= \sum_{k=1}^{N} c_k \langle \phi^*_k|E - \hat{H}|O_E\rangle \quad . \end{aligned} \tag{II.7}$$

L'équation II.7 permet de définir les conditions auxquelles doivent satisfaire nos fonctions de base afin de minimiser l'erreur dans l'équation II.6. Réarrangeons dans un premier temps Eq. (II.2) de sorte que

$$\hat{H}(r)\phi_k(r) = \left(\epsilon_k + i\eta\hat{W}(r)\right)\phi_k(r) \tag{II.8}$$

et substituons ensuite ce résultat dans l'équation II.7. Donc,

$$\sum_{k=1}^{N} c_k E\langle\phi_k^*|O_E\rangle = \sum_{k=1}^{N} c_k\langle\phi_k^*|\epsilon_k + i\eta\hat{W}(r)|O_E\rangle \tag{II.9}$$

$$\sum_{k=1}^{N} c_k(E-\epsilon_k)\langle\phi_k^*|O_E > = \sum_{k=1}^{N} i\eta c_k\langle\phi_k^*|\hat{W}(r)|O_E\rangle \tag{II.10}$$

$$\sum_{k=1}^{N} c_k\langle\phi_k^*|O_E\rangle = \sum_{k=1}^{N} i\eta c_k\frac{\langle\phi_k^*|\hat{W}(r)|O_E\rangle}{(E-\epsilon_k)} \quad . \tag{II.11}$$

Puisque la quantité O_E est inconnue et peut être excessivement grande à l'extérieur de la région d'interaction, là où le potentiel absorbant devient lui aussi très grand, nous cherchons des fonctions de base qui satisfont simultanément aux conditions $\langle\phi_k^*|O_E\rangle \rightarrow 0$ et $\langle\phi_k^*|\hat{W}(r)|O_E\rangle \rightarrow 0$. En termes plus physiques, nous imposons que *toutes* les fonctions de base décroissent et tendent vers 0 dans la région où le potentiel absorbant croît.